TUM School of Life Sciences

MAPT exon 10 alternative splicing modulation in an hiPSC $MAPT^{\text{EXSISERS}}$ model

Bianca Eßwein

Vollständiger Abdruck der von der TUM School of Life Sciences der Technischen Universität München zur Erlangung des akademischen Grades einer

Doktorin der Naturwissenschaften
(Dr. rer. nat.)

genehmigten Dissertation.

Vorsitz:
Prof. Angelika Schnieke, PhD

Prüfende der Dissertation:
1. Prof. Dr. Wolfgang Wurst
2. Prof. Dr. Nina Henriette Uhlenhaut

Die Dissertation wurde am 29.03.2022 bei der Technischen Universität München eingereicht und durch die TUM School of Life Sciences am 11.10.2022 angenommen.

Qui audet adipiscitur

I solemnly swear that I am up to no good!

Publications

Parts of this thesis work was previously published in Nature Cell Biology. Hereby, published work was adapted and modified in appearance for thesis purposes. Please refer to Figure 3 [1] for already published data, prior to submission of this Doctoral dissertation, also shown in Figure 2.3a and 2.6c of this dissertation.

Truong, D.-J. J. *et al.* Non-invasive and high-throughput interrogation of exon-specific isoform expression. en. Nature Cell Biology, 1–12. ISSN: 1476-4679. `https://www.nature.com/articles/s41556-021-00678-x` (2021) (June 2021).

Abstract

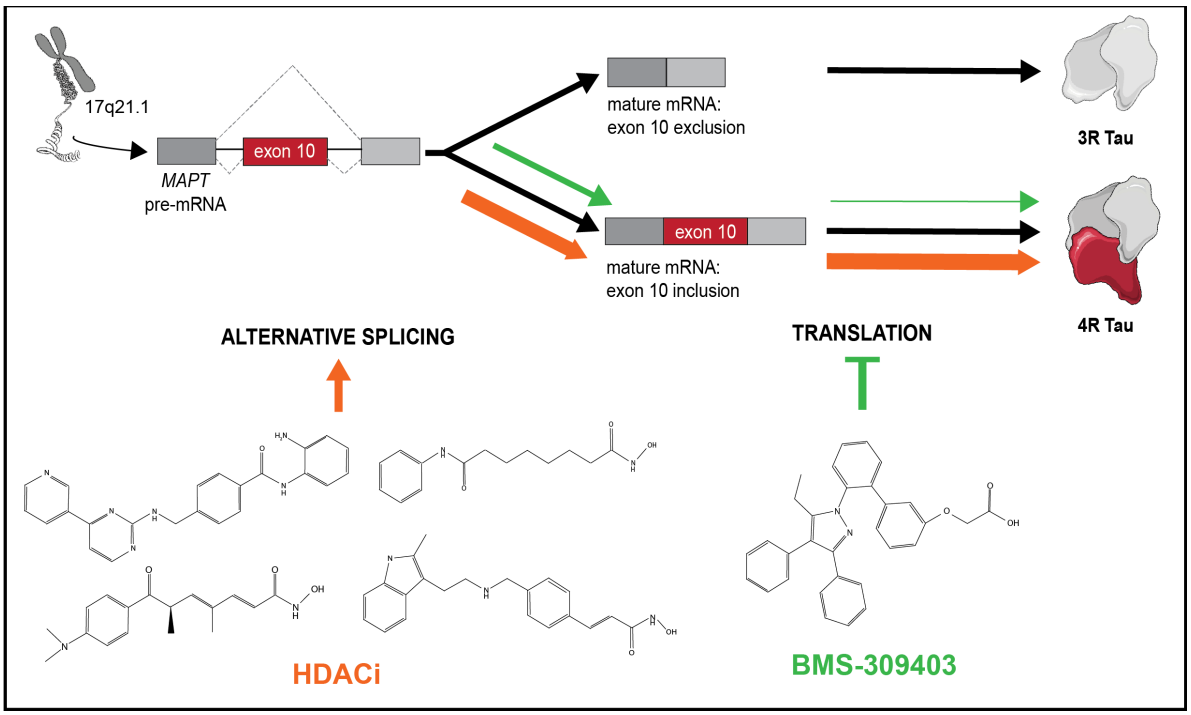

Tauopathies are a group of neurodegenerative diseases characterised by hyperphosphorylation and aggregation of Tau. Six Tau isoforms are expressed in the mature human central nervous system (CNS), due to alternative splicing of exon 2, 3 and 10. Ex- and inclusion of exon 10 results in Tau isoforms differing in the presence of three repeat (3R) or four repeat (4R) microtubules binding domains (MBDs), respectively. Physiologically, 3R and 4R isoforms are expressed equally, while 3R/4R ratio alterations are prone to result in an excess of 4R Tau. The well established intronic point mutation IVS10+16 c > t, associated with several tauopathies, inherits an increase in 4R Tau expression. A major limitation in understanding the molecular mechanisms connecting Tau to neurodegeneration has been the availability of disease models as alternative splicing is species-specific.

The novel Exon Specific Isoform Expression Reporter System (EXSISERS) was adapted to generate *microtubule associated protein Tau (MAPT)*$^{\text{EXSISERS}}$ human induced pluripotent stem cell (hiPSC) models with application of isoform modulation studies in a high throughput screening (HTS) manner. Longitudinal isoform monitoring was possible using the EXSISERS over the time course of hiPSC derived neuron differentiation, with higher sensitivity than commonly used methods for protein expression investigation. Morphological investigation showed greater neuron complexity upon higher 3R/4R Tau imbalance, shifting to increased 4R Tau expression. Pharmacological HTS in *MAPT*$^{\text{EXSISERS}}$ hiPSC derived small molecule

neuronal precursor cells (smNPCs) identified several histone deacetylase (HDAC) inhibitors and a fatty acid binding protein (FABP) inhibitor, BMS-309403, modulating 4R Tau expression. HDAC inhibition (HDACi) was shown to alternate the alternative splicing of *MAPT*, shifting the alternative splicing process towards exon 10 inclusion, whereby, BMS-309403 showed inhibition of *MAPT* exon 10 including mRNA translation exclusively in physiological and pathological conditions. Alterations in spliceosome recruitment were observed under pathological conditions based on the intronic point mutation IVS10+16 c > t.

In this work I present the successful generation and application of hiPSC based disease models for isoform studies using the EXSISERS, building the basis of further use of the model for disease related investigation in a human genetic background. We show evidence implicating Class I and IV HDAC involvement in *MAPT* alternative splicing under physiological conditions. Furthermore, a novel regulation of *MAPT* exon 10 mRNA translation was shown indicating a FABP involvement in translational regulation.

Zusammenfassung

Tauopathien sind eine Gruppe neurodegenerativer Erkrankungen, die durch eine Hyperphosphorylierung und Aggregation des Mikrotubuli assoziierten Proteins Tau gekennzeichnet sind. Im reifen menschlichen Zentralnervensystem (CNS) werden sechs Tau-Isoformen exprimiert, die durch alternatives Spleißen von Exon 2, 3 und 10 entstehen. Die Ex- und Inklusion von Exon 10 führt zu Tau-Isoformen, die sich durch das Vorhandensein von Mikrotubuli-Bindungsdomänen (MBDs) mit drei Repeats (3R) bzw. vier Repeats (4R) unterscheiden. Physiologisch gesehen werden die 3R- und 4R-Isoformen gleichermaßen exprimiert, während Veränderungen des 3R/4R-Verhältnisses zu einem Überschuss an 4R-Tau führen können. Die gut etablierte intronische Punktmutation IVS10+16 c > t, die mit mehreren Tauopathien in Verbindung gebracht wird, führt zu einer erhöhten Expression von 4R-Tau. Eine große Einschränkung beim Verständnis der molekularen Mechanismen, die Tau mit Neurodegeneration verbinden, ist die Verfügbarkeit von Krankheitsmodellen, da alternatives Spleißen artspezifisch ist.
Das neuartige Exon Specific Isoform Expression Reporter System (EXSISERS) wurde angepasst, um *MAPT*$^{\text{EXSISERS}}$-Modelle menschlicher induzierter pluripotenter Stammzellen (hiPSC) für Isoform-Modulationsstudien in einem Hochdurchsatz-Screening (HTS) zu generieren. Mit Hilfe des EXSISERS war es möglich, die Isoformen im Zeitverlauf der Differenzierung von hiPSC abgeleiteten Neuronen zu verfolgen, und zwar mit einer höheren Empfindlichkeit als bei den üblicherweise verwendeten Methoden zur Untersuchung der Proteinexpression. Morphologische Untersuchungen zeigten eine größere Komplexität der Neuronen bei einem höheren Ungleichgewicht zwischen 3R und 4R Tau, das sich zu einer erhöhten 4R Tau-Expression verschiebt. Pharmakologisches HTS in *MAPT*$^{\text{EXSISERS}}$ hiPSC-abgeleiteten neuronalen Vorläuferzellen (smNPCs) identifizierte mehrere Histon-Deacetylase (HDAC)-Inhibitoren und einen Fettsäure-bindenden Protein (FABP)-Inhibitor, BMS-309403, welche 4R-Tau-Expression modulieren. Es wurde gezeigt, dass HDAC-Inhibition (HDACi) das alternative Spleißen von *MAPT* verändert und den alternativen Spleißprozess in Richtung Exon 10-Inklusion verschiebt, wobei BMS-309403 unter physiologischen und athologischen Bedingungen ausschließlich die Translation von *MAPT* Exon 10 einschließlich der mRNA hemmt. Unter pathologischen Bedingungen wurden Veränderungen bei der Rekrutierung von Spleißosomen beobachtet, die auf der intronischen Punktmutation IVS10+16 c > t beruhen. In dieser Arbeit stelle ich die erfolgreiche Generierung und Anwendung von hiPSC-basierten Krankheitsmodellen für Isoformstudien unter Verwendung des EXSISERS vor und schaffen damit die Grundlage für die weitere Nutzung des Modells für krankheitsbezogene Untersuchungen mit menschlichem genetischem Hintergrund. Ich zeige Hinweise für eine Beteiligung von HDACs der Klassen I und IV am alternativen *MAPT* Spleißen unter physiologischen Bedingungen auf. Darüber hinaus wurde eine neuartige Regulation der *MAPT* Exon 10 mRNA-Translation gezeigt, die auf eine Beteiligung von FABP an der Translationsregulation hinweist.

Contents

1 Introduction

Neurodegenerative diseases affect millions of people worldwide [2]. Being a very heterogeneous group of disorders, neurodegenerative diseases are characterised by the progressive degeneration of the central nervous system (CNS) or peripheral nervous system (PNS) in structure and function. Onset of disease are causes upon the functional loss of neurons and ultimately neuronal death. To this day, the process of neuronal death is irreversible, declaring neurodegenerative diseases as incurable, emphasising the importance of understanding the underlying mechanisms to develop novel therapy strategies. A hallmark of neurodegenerative diseases is the misfolding, aggregation and accumulation of proteins, leading to cellular dysregulation, loss of synaptic connections and brain damage. Notwithstanding their large differences in clinical manifestation and prevalence, neurodegenerative diseases have similar attributes, including their progressive and chronic nature, increased prevalence with age, brain area specific destruction of neurons, damages in the synaptic connection network and brain mass loss [3]. The protein aggregates involved in the development of neurodegenerative diseases are distinct and exhibit no similarities in sequence, size, structure, expression level or function, however the protein folding process, its intermediates, end-products and main features are similar [4]. In the pathological state, all undergo misfolding by forming β-sheet-rich structures, ranging from small oligomers to large fibrillar aggregates [3, 4]. Protein misfolding, oligomerisation and accumulation in the brain trigger pathological responses resulting in disease [3–5]. Most commonly implicated proteins are α-synuclein in Parkinson's Disease (PD), multiple system atrophy and dementia with Lewy bodies, TAR DNA-binding protein 43 in amyotrophic lateral sclerosis (ALS) and frontotemporal dementia (FTD), prion proteins in Prion diseases, amyloid β (Aβ) in Alzheimer's Disease (AD) and Tau in AD and FTD, corticobasal degeneration (CBD), progressive supranuclear palsy (PSP), argyrophilic grain disease, and chronic traumatic encephalopathy [6].

1.1 Alzheimer's Disease

AD is the most common neurodegenerative dementia. Several risk factors as increasing age, genetic factors, head injuries, vascular disease, infections and environmental factors contribute to the onset of AD. From the early stages axonopathy and white matter alterations are observed, with progression the axonal damage is correlated with cognitive dysfunction and Tau pathology [7–9]. While the pathophysiology is not yet fully understood, several genes and pathways are implicated in AD pathology, including the Aβ cascade, Tau, inflammation, as much as cholinergic and oxidative stress [10]. With this, AD is characterised by its pathological changes of deposition of extracellular Aβ plaques, formation of intracellular neurofibrillary tangles (NFTs) and synaptic loss [11–13]. The Aβ cascade, the proteolytic enzymes β-secretase and γ-secretase mediate the deposition of Aβ from the transmembrane protein amyloid precursor protein (APP) [14–16]. Whereby, β-secretase is the rate-limiting step in the APP cleaving process, hence, interest of regulation. Post-translational acetylation of β-secretase, as much as for Tau, contribute to the stability of the enzyme [17]. Ubiquitination on the other hand promotes the degradation of β-secretase by lysosomes, a process impaired in AD [18, 19]. Several amino acid fragments of cleaved APP form the final forms Aβ40 and Aβ42, for simplification in

the following referred to as Aβ. Aβ monomers, can accumulate, forming Aβ plaques, whereby accumulation preferentially occurs in brain regions of high metabolic demand [20, 21]. The disposition of Aβ triggers neuroinflammation and oxidative damage [16, 22, 23]. The deposition and subsequent spread of Tau arises secondarily to the Aβ pathology. While Aβ accumulation already occurs 10-20 years prior to clinical AD onset, Tau pathology correlates strongly with neurodegeneration and cognitive impairment [24]. Moreover, NFTs composed of acetylated and hyperphosphorylated Tau can accumulate in neuralperikaryal cytoplasm, axons, and dendrites, resulting in a loss of cytoskeletal microtubules and tubulin-associated proteins [25, 26]. Synaptic loss in the neocortex and limbic system are associated with memory impairment already observed in early stages of AD. Defects including axonal transport, mitochondrial damage and oxidative stress contribute to the synaptic loss as much as accumulation of Tau and Aβ at the synaptic sites. All combined, those processes inevitably lead to the loss of dendritic spines, pre-synaptic terminals and axonal dystrophy [13].

1.2 Microtubule associated protein Tau

In neurons, the stable dynamics of microtubule bundles are pivotal for axon outgrowth, guidance, branching and regeneration [27, 28]. The specific organisation is determined by several microtubule associated proteins (MAPs), controlling assembly, dynamics, bundling and interaction with organelles [29–31]. The human *MAPT* gene, located on the q-arm of chromosome 17 at band position 17q21.1, encodes for the protein microtubule associated protein Tau, a protein of the MAP family, highly conserved and exclusively found in higher eukaryotes. Tau was first described by Weinberg *et al.* [32], identifying Tau as essential for microtubules formation. Since then, Tau has been a major focus of research, expanding its physiological role from the initial microtubules dynamics regulation to synaptic function regulation, axonal extension, microtubules transport and mitogen-activated protein kinase activation. In addition to its many physiological roles, Tau has a pivotal role in a group of neurodegenerative diseases, known as tauopathies.
The human *MAPT* gene comprises 16 exons. Whereby, exons 1, 4, 5, 7, 9, 11, 12 and 13 are constitutively expressed in the CNS and PNS, the remaining exons are subject of alternative splicing. Exon 1 as part of the promoter, is transcribed, but not translated, exon 14 builds part of the 3'-untranslated region (UTR) and exon 4A and 8 are present in the mRNA of peripheral tissue, but never in the human brain (Figure 1.1a) [33, 34]. *MAPT* mRNA expressing exon 6 is present in the CNS and PNS but with low abundance. Due to alternative splicing of exon 2, 3 and 10, six Tau isoforms are expressed in the mature human CNS (Figure 1.1a) [35]. Isoforms comprising exon 2, exon 2 and 3 or neither are referred to as 1N, 2N and 0N isoforms, respectively. Exon 9, 10, 11 and 12 span the microtubules binding repeats of Tau. Whereby, exon 10 is subject of alternative splicing in the CNS. Ex- and inclusion of exon 10 result in Tau isoforms differing in the presence of three (three repeat (3R)) or four (four repeat (4R)) microtubules binding domains (MBDs), respectively [35–40]. Hence, the 2N4R isoform being the longest isoform expressed in the mature human brain. Moreover, the Tau protein is subdivided into four regions: (1) an acidic part in the N-terminal part, encoded by exon 1-5; (2) a proline-rich region, encoded by exon 7 and parts of exon 9; (3) the MBDs, four repeats (R1-R4), encoded by exon 9-12, mediating Tau binding to the microtubules and (4) a C-terminal part, encoded by exon 13 [41, 42]. Next to the alternative splicing events, determining the Tau isoform expression, a 900 kilo base pairs (kbp) inversion on chromosome 17q21 including *MAPT*

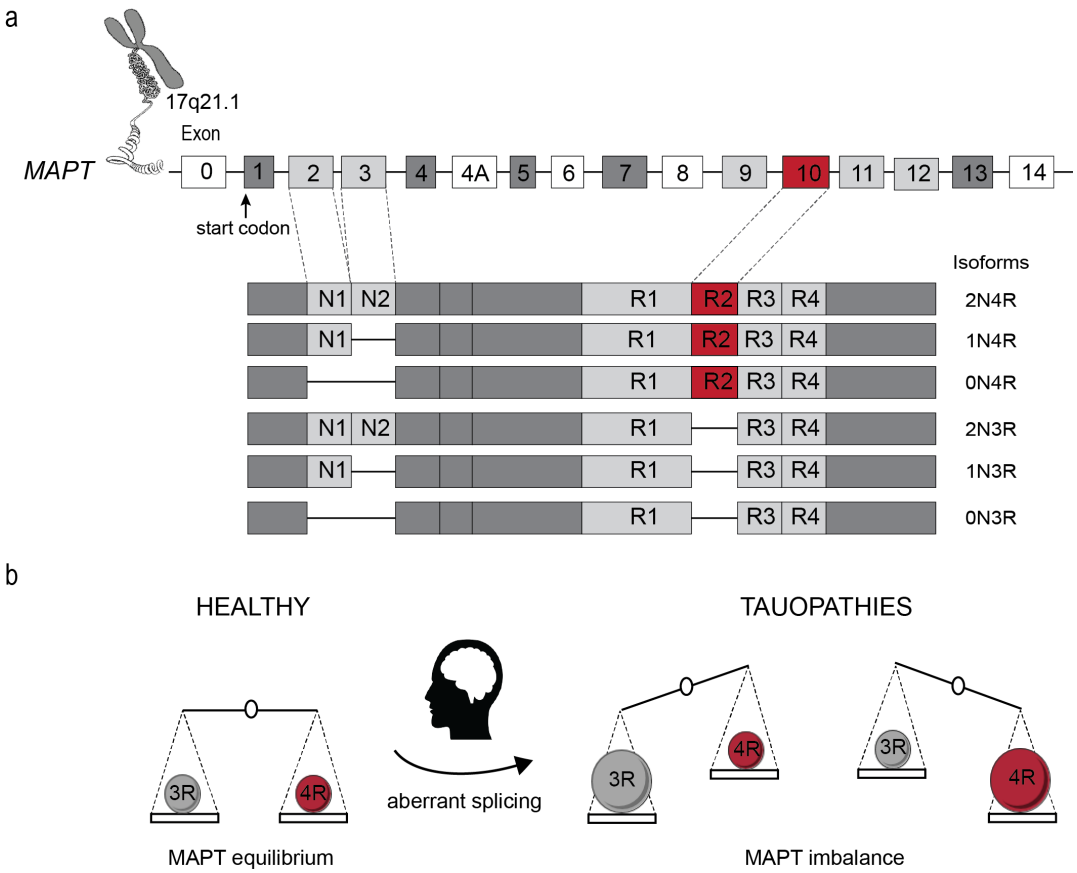

Figure 1.1: Physiological and pathological Tau. (a) *MAPT* is located on chromosome 17, due to alternative splicing of exon 2, 3 (N, bright grey) and 10 (R, red), six Tau isoforms are expressed in the mature human brain, with either three microtubules binding domains (MBDs) (three repeat (3R)) or four MBDs (four repeat (4R)). Exons 4A, 6, 8 and 14 are not present in *MAPT* mRNA transcripts in the human brain. (b) Existing isoform equilibrium of 3R and 4R MAPT isoforms is disturbed due to aberrant splicing resulting an imbalance in 3R to 4R Tau isoform expression. Imbalance leads to development of tauopathies. Modified, based on [35, 43, 44].

stands out, resulting in two haplotypes, H1 (direct orientation) and H2 (indirect orientation) [45, 46]. H1 is the risk haplotype based on its connection to familial and sporadic neurodegenerative disorders as PSP, AD, CBD, PD and FTD [47–52]. The H1 haplotype shows considerable diversity. Sub-haplotype H1c is largely responsible for the association of H1 to sporadic tauopathies by promoting an increase in total MAPT transcript expression, but especially exon 10 including transcripts [52–54]. To the contrary, haplotype H2 is associated with a lower risk for AD and other neurodegenerative diseases [55, 56].

1.2.1 Alternative splicing of *MAPT*

Constitutive splicing refers to the process of intron removal and subsequent exon ligation. Alternative splicing on the other hand, is a process, diverting from this process by skipping certain exons resulting in a variety of mature mRNAs. It is a central genetic regulation mechanism, occurring in over 95% of multi-exon genes of higher eukaryotes, leading to a variety of mRNAs and subsequently protein diversity [57–59]. A dynamic and flexible multi-protein complex, the spliceosome, mediates the complex process. Multiple interacting components, as

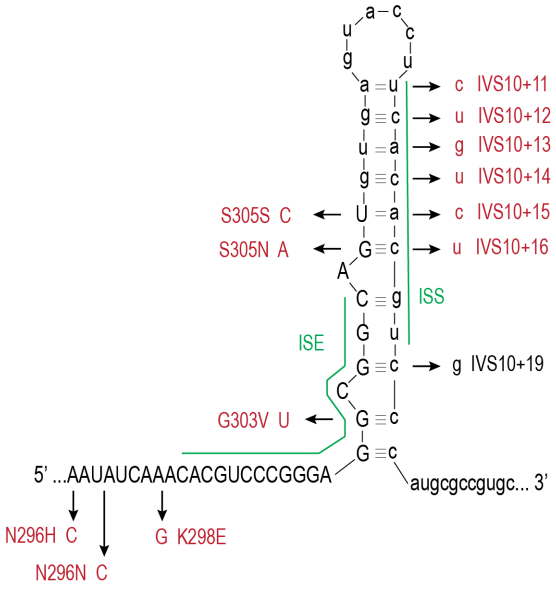

Figure 1.2: *MAPT* exon 10 stem loop. The 3'-end of exon 10 in combination with the 5'-end of intron 10 form a highly self-complimentary stem loop. Pathogenic mutations in the exon and intron with their corresponding amino acid changes are shown. Boundary between exon 10 and intron 10 is indicated by upper and lower case letters. Mutations known to increase exon 10 inclusion are shown in red, mutations known to exclude exon 10 in black. The intron splicing silencer (ISS) and intron splicing enhancer (ISE) important for alternative splicing regulation are shown in green. Modified, based on [44]

cis-acting elements and *trans*-acting factors are involved. Whereby, spliceosome assembly to the *cis*-acting element is an essential part of the splicing process. Depending on their influence on the splicing process, *cis*-acting elements are classified as splicing enhancers, silencers, or modulators, located in the intron or exon of a gene. Regulation and the resulting distinct splicing patterns are dependent on the cellular environment, e.g. tissue, developmental state or differentiation-specific cues [60–62]. The basic alternative splice patterns include exon skipping, accounting for 40% of all alternative splicing events, and alternative 5'- and 3' splice sites, a process selected in pre-mRNA transcripts to produce different mRNA transcripts [63, 64]. Alternative exons share similar splice donors and acceptors, weaker in their binding affinity to the spliceosome than consensus exons [65]. Splicing factors play another major part in the process of alternative splicing. Serine (Ser) and arginin (Arg)-rich (SR) proteins usually enhance the recognition of the alternatively spliced exon, while, heterogeneous nuclear ribonucleoproteins (hnRNPs) facilitate the exclusion of the exon. Combination of multiple alternatively spliced regions can give rise to several unique mRNA transcripts from a single gene [66]. The specific mRNA transcripts may have individual regulatory properties, as stability, localisation and transcriptional efficiency. When translated into distinct protein isoforms, these show diverge structure and functions throughout their different isoforms [64, 67].
Disruption of this delicate mechanism is associated with several diseases, including tauopathies [58, 59, 68]. Focusing on the in- and exclusion of exon 10, several factors are involved influencing the ratio between 3R and 4R Tau in the brain. Tau exon 10, in particular, is flanked by an unusually large intron 9 and weak 5'- and 3'- splice sites. Many SR proteins possess a specific affinity to the *MAPT* *cis*-acting elements, regulating the alternative splicing of exon 10 (thoroughly discussed in [35]). In addition, the 3'-end of exon 10 in combination with the 5'-end of intron 10 form a highly self-complimentary stem loop, which inhibits the U1 small nuclear

RNA (snRNA) binding. U1 being a part of a small nuclear ribonucleoprotein (RNP) (snRNP), functioning as a catalyser for intron removal [69]. The stem loop itself bears several splicing elements, including an intron splicing silencer (ISS) and intron splicing enhancer (ISE) (Fig. 1.2). Several splice factors and hnRNPs are known to bind to these sequences, either promoting or prohibiting *MAPT* exon 10 inclusion. hnRNPE2 and hnRNPE3 are known to bind to the ISE to enhance *MAPT* exon 10 inclusion [70, 71]. Disruption of the stem loop, e.g. by intronic mutations, enhances binding of the snRNP leading to higher levels of exon 10 inclusion [72]. One intronic point mutation, well known for its impact on exon 10 splicing, is IVS10+16 c > t, 16 base pairs (bps) downstream of exon 10 [44, 73]. This mutation not only disrupts the stem loop, but with its location also alters the ISS [74]. Thus, specific mutations in specific *cis*-elements may alter the splicing pattern, promoting or suppressing the inclusion of exon 10, whereby, mutations within the stem loop tend to promote the inclusion [69]. Regulation of the alternative splicing process is further complicated by altered expression and activity of splicing factors based on modifications at a transcriptional, post-transcriptional and post-translational level. Various kinases, including protein kinase A (PKA), dual specificity tyrosine phosphorylation regulated kinase 1A (DYRK1A) and glykogensynthasekinase-3 β (GSK3β), regulate the activity of splicing factors through phosphorylation, also relevant in exon 10 alternative splicing [74–79]. The process of *MAPT* alternative splicing plays a crucial role in the physiology of Tau, allowing for diverse regulatory properties. Disruption of the splicing pattern of *MAPT* exon 10, as mutations in the stem loop downstream of exon 10, are prone to result in pathological Tau, emphasising the need to decipher the alternative splice machinery.

1.2.2 Post-translational modifications of Tau

Post-translational modifications are essential processes to diversify the protein function and coordinate the dynamic signalling network of eukaryotes. As a highly reversible event, post-translational modifications are particular reliable for rapid massages in the cell. Therefore, they play a role in gene expression, signal transduction, protein-protein interaction, cell-cell interaction and communication between the intra- and extracellular environment [80].
The post-translational modifications of Tau have been extensively studied in the context of pathological impact, but contribute just as much to the function of Tau in a physiological state. Phosphorylation of Tau is the most studied post-translational modification of Tau. Whereby, protein phosphorylation refers to the addition of a phosphate group by esterification at three amino acids: Ser, threonine (Thr) or tyrosine (Tyr). The Tau amino acid sequence comprises 85 putative phosphorylation sites, 53% Ser, 41% Thr and 6% Tyr [81–83]. Among those, 31 different phosphorylation sites influencing the physiological function [84–88] and 16 sites associated with the physiological and pathological condition [89], have been reported. Physiological functions influenced by site specific Tau phosphorylation being among others microtubules binding and subcellular localisation. For example, phosphorylation of Sers, located in the conserved consensus K259Q, K290Q, K321Q, K353Q (KXGS) motif of the MBDs, decrease Tau binding to microtubules [90], subsequently, leading to the destabilisation of the neuronal cytoskeleton, while phosphorylation of Ser/Thr motifs proximal to the microtubules binding domains prohibit neuritic outgrowth [91]. Next to the most common and extensively studied phosphorylation of Tau, other post-translational modifications of Tau include methylation, acetylation, sumoylation, nitration, glycolysation, glycation, prolyl-isomerisation and ubiquitination, influencing the function and stability of Tau. Whereby, methylation regulates Tau metabolism and directly competes with ubiquitination and acetylation. Tau acetylation may control the ubiquitination

and subsequently indirectly degradation of Tau [92]. Moreover, by acetylation the charges of the microtubules binding domain are neutralised, interfering with microtubules binding and subsequent Tau dysfunction [93, 94]. The impaired microtubule binding capacity generates an increase in cytosolic Tau, which is considered to be an initiating step in NFT formation [92, 93]. Sumoylation stimulates Tau phosphorylation and inhibits its degradation by proteasomes. Nitration decreases the binding strength of Tau to microtubules and modulates its propensity to aggregate. Similarly, glycation favours polymerisation and aggregation of Tau, while preventing its degradation. Glycolysation reduces the degradation rate of Tau as much as the propensity of aggregation. Besides all other post-translational modifications, prolyl-isomerisation favours the dephosphorylation of Tau, while restoring its ability to bind the microtubules (extensively reviewed in [95]).
Post-translational regulation influences the function of Tau greatly. Disruption by hyperphosphorylation on the other hand results in pathological Tau.

1.3 Pathological Tau - Tauopathy

Pathological Tau has been observed in a wide range of neurodegenerative diseases and is the defining factor of a heterogeneous class of diseases, tauopathies. Despite intense investigation the pathology of Tau-mediated neurodegeneration is still elusive. Loss of function, gain of function and mislocalisation of Tau have all been implicated to cause the Tau-mediated neurodegenerative diseases [96–98]. Tauopathies, characterised as sporadic or familial neurodegenerative diseases involve hyperphosphorylation and aggregation of Tau protein in NFTs. They were first recognised by Alois Alzheimer describing the case study of Auguste Dete, connecting Tau to the pathology of AD [99–102]. Subsequent studies identified Tau as the primary pathological feature of several other neurodegenerative diseases, among others frontotemporal lobar degeneration (FTLD) and Pick's Disease (PiD), emphasising the necessity to understand physiological and pathological Tau. Based on the general pathology, tauopathies can be distinguished as primary and secondary tauopathies. PSP, PiD and FTLD-Tau (FTLD-Tau) are primary tauopathies, where Tau is the first lesion of disease onset. AD and Down syndrome show association with other pathologies and therefore are classified as secondary tauopathies [103]. While the most well-described role of physiological Tau is its entity to bind and stabilise microtubules, particularly microtubules of neuronal axons [104], pathological Tau implies several different traits, including aberrant post-translational modifications [105], truncation [106], and aggregation into oligomers and larger insoluble filaments [104]. Hereby, pathological Tau forms common hallmarks of tauopathy: (1) hyperphosphorylation of Tau [96], (2) re-distribution of Tau from the axonal to the somatodendritic compartments of neurons [97] and (3) aggregation of Tau into fibrils, NFTs, in neurons and glial cells. Despite comparable hallmarks, tauopathies differ in respect to changes in the isoform pattern, phosphorylation and filament formation, as well as in cellular Tau distribution. Physiologically, 3R and 4R isoforms are expressed equally, while 3R/4R ratio alterations are prone to result in an access of either 3R or 4R Tau (Fig. 1.1b). Based on their predominant isoform patterns, tauopathies can be clustered into four different classes: Class I, 3R and 4R; Class II, predominantly 4R; Class III, predominantly 3R and Class IV, with a short 0N3R isoform. The most prominent Class II tauopathy is AD. AD is characterised not only by the presence of Aβ plaques, but also by NFTs of hyperphosphorylated Tau. Aberrant phosphorylation prohibits Tau binding to microtubules and its promotion of microtubule assembly, leading to self-aggregation into NFTs [98, 107, 108]. Whereby, 4R Tau is generally more likely to be hyperphosphorylated [36, 37, 109].

The aberrant alternative splicing of *MAPT* and the aggregation hyperphosphorylated Tau in NFTs are the drivers of tauopathy pathology. Thus, understanding Tau pathology will pave the way for therapeutical approaches.

1.4 Therapeutic potential for tauopathies

Identification and understanding of pathological mechanisms of human diseases is necessary for discovery of novel therapeutic approaches. Animal models, and mainly mouse models, build a valuable tool in *in vivo* studies, enabling the investigation of diseases progression in distinct developmental stages. But often substantial species differences prohibit the recapitulation of the full human disease phenotype. Based on the high involvement of Tau in development of neurodegenerative diseases, it comes of no surprise, that Tau is the therapeutic focus to treat tauopathies. Nevertheless, targeting of Tau for therapy modifying approaches have been challenging, resulting in no approved and established pharmacologic treatment options. Available therapeutics strategies are limited and focus on the symptomatology, as delaying the underlying process of neuronal loss is not possible. Hence, the need to understand processes underlying the neuronal death and risk factors, already aberrantly expressed before any clinical symptoms, is urgent. Several converging pathological mechanisms have emerged, including oxidative stress, immuno-inflammation and alteration in the metabolic pathway, e.g. lipid metabolism. Disease related research investigating the therapeutic potential are mainly focused on AD. Therefore, the following subsections will give an overview over the findings made in the process, as a foundation for future research focusing on Tau pathology.

1.4.1 Fatty acid signalling regulation for neurodegenerative disease therapy

In the brain, lipids have multiple structural, developmental, signalling and metabolic functions. Fatty acids function as energy source and signals for metabolic regulation. Their mode of action is either through enzymatic and transcriptional networks to modulate gene expression or growth and survival pathways as inflammatory and metabolic response [110, 111]. Therefore, fatty acid trafficking is a very complex and dynamic process, relying on complex processing, shuttling, lipid availability and removal to keep a delicate balance between the different lipid species at the target compartments and to regulate their contribution to signalling targets. As of today, three protein families are known to sense the presence and type of fatty acids, in the extracellular matrix, cytosol or the nuclear matrix. At the plasma membrane, fatty acids activate G-protein coupled free fatty acid receptors (FFARs) [112]. In the cytosol, fatty acids can be bound by fatty acid binding proteins (FABPs), targeting specific subcellular structures or metabolic pathways [113]. Peroxisome proliferator-activated receptors (PPARs) regulate fatty acid signalling in the nucleus. They can be stored as triglycerides, degraded by β-oxidation or used in phospholipids' synthesis, being the main components of biological membranes.

1.4.1.1 Fatty acid binding proteins

Fatty acids have a low solubility, making it difficult to diffuse through the aqueous medium of the cytosol. Hence, to circumvent the problem, FABP, as intracellular lipid chaperones, bind free fatty acids for efficient navigation through the cytosol, to coordinate the lipid response in the cell, linking them to metabolic and inflammatory pathways [114, 115]. FABPs are 15 kDa small intracellular soluble proteins, reversely binding fatty acids and other hydrophobic ligands. Upon binding, FABPs traffic their ligands to different intercellular compartments, such as

mitochondria, peroxisome, endoplasmic reticulum or the nucleus.
As small intracellular proteins, FABPs can enter the nucleus under certain conditions, targeting fatty acids to a specific group of nuclear receptors (NRs), PPARs, in the nuclear lumen. Whereby, those transcription factors control the expression of FABPs, upon fatty acids or other hydrophobic agonists activation [116–118]. In the physiological CNS, brain lipids play a crucial role, embodying a range of functions: formation and remodelling of cellular membranes; regulation of synaptic functions, modulation of intracellular signalling and reporter-ligand interactions [119, 120]. Polyunsaturated fatty acids (PUFA), as ω-3 and ω-6, build essential fatty acids in the mammalian brain [121]. By inclusion of PUFAs in the membrane phospholipids, the fluidity as much as the permeability of cell membranes is modulated, contributing to the dynamics of the bilayer and neurite growth [122]. Moreover, PUFAs regulate the formation of lipid rafts, playing a huge role in neurotransmission, ion channel formation and synaptic plasticity [123]. There are three FABP isoforms, with relevant expression in the brain: FABP3, FABP5 and FABP7. FABP3 preferably binds ω-3 PUFA, FABP5 binds saturated fatty acids and FABP7 has a preference in binding ω-3 fatty acids [124]. Their specific role of FABPs to transport PUFAs may link their function as lipid transporters to the regulation of membrane composition and fluidity. FABP7 shows high expression in the neuronal stem cells of astrocytes, while expression decreases over the time of development, suggesting a role in the migration and differentiation of nerve cells [125, 126]. FABP5 is the most ubiquitously expressed FABP. While highly expressed during the midterm embryonic stages, expression decreases progressively after birth. In the adult brain, FABP5 shows only moderate expression in neurons and astrocytes [127]. Expression is induced in the adult brain upon necessity of stress or pathological condition adaptation [128, 129]. FABP3 on the other hand is not expressed in embryonic stages, but in neurons of the mature brain [127]. FABP3 consolidates and maintains the differentiated status of neurons, through the utilisation of PUFAs [130]. Interestingly, FABP3 shows elevated expression in patients of neurodegenerative diseases, including AD and PD [129, 131, 132]. Interestingly, Harari *et al.*, 2014 [133], demonstrated similar ratio dependency between FABP3/Aβ42 akin to p-Tau/Aβ42 [133, 134]. Despite the known interference of FABP3 in lipid composition, fluidity and function of the cell membrane in relation to Aβ and α-synuclein pathology alterations in neurodegenerative diseases, the functional interactions between FABP3 and Tau is yet elusive [135].

1.4.1.2 PPARi as an AD therapy approach

Association between neurodegenerative diseases and type II NRs, have been established. NRs, including Retinoid X receptor α (RXR) and PPARs, belong to a superfamily of ligand-activated transcription factors, known to regulate a wide range of genes [136].
PPARs in their crucial biological role as governors of gene expression, responsible for lipid metabolism, energy balance and anti-inflammation dictate the scientific interest in those receptors as pharmacological targets. PPARs, as nuclear hormone receptors, serve as ligand-activated transcription factors, with three isoforms showing structural homology: PPARα, PPARβ/δ and PPARγ [137, 138]. Once activated in the cytoplasm, PPARs build heterodimers with the RXR. Subsequently, in the nucleus consensus DNA sequences are bound by the PPAR-RXR-complex to regulate transcription. Specific ligand binding results in a conformational change in the PPAR to promote either co-repressor release or co-activator recruitment [139–141]. Fatty acids, oligosaccharides, polyphenols, and numerous synthetic ligands target the PPARs to mediate their binding and transport. Moreover, they are involved in several molecular processes, including

peroxisomal regulation, mitochondrial β-oxidation, thermogenesis and lipoprotein metabolism [142]. Within their ubiquitous mRNA and protein expression in the CNS, PPARs are suggested to play a role in the regulation of neuronal and glial metabolism and energy balance. Different brain disorders, ranging from neurological to neuropsychological and neurodegenerative diseases share general etiopathogenic factors, such as altered cellular metabolism, modification in synaptic activity and concurrent inflammatory processes. Remarkably, PPARs showed a direct regulation of a sum of target genes involved in these processes within the periphery and the CNS, including fatty acid binding protein 4 (FABP4) [143]. Moreover, PPAR pathways have also been identified as risk factors in various neurodegenerative diseases, as AD, multiple sclerosis (MS) and PD [144–147]. While, PPARα and PPARβ/δ show reduction in expression in the association with AD, PPARγ selectively increases with the progression of disease.
Even though, PPARα and PPARγ endogenous and synthetic ligands have been thoroughly characterised to treat diabetes and cardiovascular disease, the effect on the CNS and subsequent impact on neuropathological treatment relevance has only emerged recently [148]. Evidence showing dysregulation of PPARγ in several different neurodegenerative diseases, classifying two categories of neurodegenerative diseases. ALS, PD, Huntington's disease (HD), MS and Friedreich's ataxia, with downregulated PPARγ, AD, bipolar disorder and schizophrenia on the other hand, classified as neurodegenerative diseases with upregulated PPARγ [149–151]. Furthermore, PPARα and PPARβ/δ expression are significantly reduced in AD, suggesting a contribution of an aberrant PPAR system to AD progression [152]. Despite an elevated PPARγ expression in AD patients, numerous PPARγ antagonists have been used in humans and animal model to treat AD with induced beneficial effects [144, 153–157]. For example, a pilot phase II clinical trial with the PPARγ antagonist rosiglitazone improved clinical outcomes based on better delayed recall, selective attention and stable plasma levels of Aβ-42 peptide [144].

1.4.2 Epigenetic regulation for neurodegenerative disease therapy

Epigenetic modification can serve as a marker of chromatin identification, whereby, heterochromatin is characterised by low acetylation levels, euchromatin on the other hand show a high level of acetylation [158]. Histones are a critical component of the nucleosome. By post-translational modification of the histones, chromatin structure and gene expression can be regulated [159]. Tightly coiled by DNA, histones form nucleosomes, contributing to the compact packaging of the eukaryote genome [160]. The highly compact structures of the histone-DNA, chromatin, are highly dynamic. Hence, histone acetylation is a highly regulated process, mediated by the balance between histone acetyltransferases (HATs) and histone deacetylases (HDACs) activity. Besides their action of histone modulation, HATs and HDACs as epigenetic modifiers are direct or indirect regulators of neuronal-specific, immune-specific, and other tissue-specific gene expression in the CNS [161].

1.4.2.1 Histone deacetylases

Human HDACs can be clustered into two families based on their conserved deacetylase domain and their dependence on specific cofactors: the deacetylase family and sirtuin proteins. The deacetylase family is subdivided into Class I (HDAC1, 2, 3 and 8), Class IIa (HDAC4, 5, 7, 9), IIb (HDAC6, 10) and Class IV (HDAC11), based on their sequence similarity to the primary deacetylase in yeast. The sirtuin proteins are classified within Class III, characterised by the need of nicotinamide adenine dinucleotide (NAD) for their catalytic function. Class I HDACs are ubiquitously expressed and predominantly located in the nucleus. Next to their high activity in

histone deacetylation, Class I HDACs act as catalytic subunits to suppress target genes. Target gene repression is mediated by building a complex with their cognate corepressor, regulated by inositol phosphate [162]. Moreover, Class I HDACs show deacetylation activity on non-histone proteins as AMP-activated protein kinase (AMPK), cohesin subunit structural maintenance of chromosomes 3 (SMC3) and transcriptional regulators to regulate their activity [163]. Whereby, the cohesin complex as a chromosome-associated multi-subunit protein complex is required for efficient DNA repair and regulation of gene expression in proliferating and post-mitotic cells [164, 165]. HDAC1 and HDAC2 build a complex with nucleosome remodeling and deacetylase complex (NuRD), transcriptional regulatory protein SIN3 transcriptional regulator family member A (SIN3A), corepressor of REST (CoREST) and mitotic deacetylase complex (MiDAC) [166]. HDAC3 interacts with two closely related co-repressors: retinoid and thyroid receptors (SMRT) and nuclear receptor corepressor (NCoR). HDAC3 is inactive in its solitary state, but upon SMRT/NCoR binding HDAC3 becomes enzymatically active [167, 168]. In its physiologically active state, HDAC3 regulates the metabolism by increasing fatty acid oxidation. Additionally, HDAC3 actively impacts fatty acid synthesis and oxidation by deacetylation in the enhancer region of *uncoupling protein 1 (Ucp1)* and *PPAR*γ [169].
Few indications emerged connecting histone modification to alternative splicing, seemingly two unrelated processes [170–174]. Treatment of Henrietta Lacks (HeLa) cells with a pan-HDAC inhibitor showed changes in over 700 genes alternative splicing pattern, with no impact on the phosphorylation state of SRs splice factors (SRSFs). *MAPT* showed an decrease in exon 10 inclusion upon pan-HDAC inhibition (HDACi) [170]. Khan *et al.* [171], showed protein-protein interaction of HDAC1 and hypophosphorylated HDAC2 with several SRSF, involved in alternative splicing. HDACi, or knock down (KD) of SRSF1 showed clear involvement in alternative splicing. Human hnRNP F and hnRNP H increased in their stability upon HDACi by pan-HDAC inhibitor Trichostatin A (TSA), indicating a protein stabilisation control of HDACs through the acetylation/ubiquitination pathway [172].

1.4.2.2 HDACi as an AD therapy approach

HDACi was mainly in focus as anticancer agents and remain to be with clinically proven activity for epigenetic modifications. In 2008, Hahnen *et al.* [175] brought attention to the potential of HDACi as neurodegenerative disease therapy approach. Identification of two major neuroprotective mechanisms, including the transcriptional activation of disease modifying genes and the rectification of destabilization in histone acetylation homeostasis, emphasised the potential of HDACi for neurodegenerative disease treatment [175]. Histone acetylation homeostasis is greatly impaired in neurodegenerative diseases, shifting to hypoacetylation [176–178]. In this context, HDACi, transforming hypo- to hyperacetylation, results in neuroprotection [179–182]. Besides hyperacetylation, HDACi may also involve activation of the kinase pathway by extrinsic signals, suppression of pro-apoptotic factors or microglial-mediated inflammation in the process of neuroprotection [179, 180, 183].
Hundreds of failed clinical trials with AD patients demonstrate the necessity to explore new avenues to develop treatments away from the one-target–one-disease approach. Impairment of HDAC function has been implicated in the pathology of AD. Over the last few decades several compounds were designed to reduce the formation of Aβ plaques or increase clearance efficiency. Among the diverse targets for the yet often unknown cause of neurodegenerative diseases epigenetic remodelling has emerged as a therapeutic approach. Especially, HDAC inhibitors have shown a beneficial impact on cognitive ability of impaired AD mouse models, exhibiting

neuroprotective properties, while rescuing learning and memory abilities [184–191]. For example, treatment with TSA rescued fear memory and learning behaviours, also showing a clearance of Aβ plaques and soluble Aβ oligomers, attributing the improvement of Aβ pathology to the phagocytosis of Aβ by microglia and endocytosis and transport by microvascular endothelial cells [186, 191]. Age-dependent memory loss was improved by treatment with the pan-HDAC inhibitor suberoylanilide hydroxamic acid (SAHA) [184]. Both effects mediated through increased histone H4 acetylation. Furthermore, Aβ degrading enzyme neprilysin (NEP) expression was significantly increased upon HDACi by TSA, also implicating a direct regulation of NEP by APP [192]. Microglia activation improved, in combination with degressive Aβ deposition and attenuated inflammation upon Class I HDAC inhibition [193]. Pan-HDACi by M344 reduced Aβ accumulation and the phosphorylation of Tau Ser^{398}, as much as decreased the gene expression of *β-site amyloid precursor protein-cleaving enzyme-1 (BACE)*, encoding for β-secretase and apolipoprotein ϵ 4 (APOEϵ4). On the other hand, gene expression of several other genes, relevant in AD progression were increased, including, but not restricted to *brain-derived neurotrophic factor (BDNF)*, *REST* and *a disintegrin and metalloproteinase 10 (ADAM10)* [185]. Similar effects were shown in accumulating studies of several different other HDAC inhibitors [187, 189, 194–196]. Several studies also indicated Tau as a substrate of HDACs. Tau acetylation was increased upon selective HDAC6 inhibition as much as pan-HDACi enhances Tau aggregation [92, 197, 198].
AD therapy approaches relying on HDACi show a positive influence on Aβ pathology. The impact of HDACi on *MAPT* alternative splicing and Tau aggregation on the other hand is loosely investigated. Sparse data indicate a contradictory effect by HDACi enhancing Tau pathology, emphasising the need to push the limits to establish a disease model resembling human physiology and Tau pathology.

1.5 Challenges in tauopathy research

For the last decades extensive effort was put into deciphering the molecular mechanisms underlying physiological and pathological Tau. Despite great progress, investigation of Tau still faces several limitations, including applicable animal models with pronounced Tau pathology or species-specific alternative splicing machineries. Hence, emphasising the need for more accurate disease modelling to tackle the challenges of decoding of the molecular mechanisms of Tau.

1.5.1 Animal disease models

A major limitation in understanding the molecular mechanisms connecting Tau to neurodegeneration has been the availability of disease models exhibiting key features of disease. Several rodent models have been generated, but failed to reliably recapitulate Tau tangles and neuronal loss as much as some key aspects of physiological Tau important for neuronal health [199, 200]. Despite the humanisation of the entire murine *MAPT* gene in a *MAPT* knock-in (KI) mouse model expressing all six Tau isoforms, this model is limited in its application. As this mouse model exhibits a relatively high 3R Tau expression, the *MAPT* KI mouse may only be applicable for pathological Tau investigations in context of Class III tauopathies [201, 202]. However, advancement of imaging, genomic and genetic technologies has more and more shown human-specific aspects of neural development, genetics, pathology and disease mechanisms. Fundamental differences between humans and common animal models raise questions about the information of disease development which was primarily gained from animal models. Notably,

alternative splicing, a crucial key feature of Tau biology, is species-specific and experimental animal models do not recapitulate patterns observed in the adult human CNS. Murine Tau (mtau) is spliced only into the 4R isoforms in the murine adult brain, setting limits to the animal models not able to be circumvented by generation of transgenic animal models, expressing human Tau [203, 204]. In addition, failed translation of treatments into clinical trials strengthens the need in human based research for therapy development. Tau dysfunction and aggregation is known to occur decades prior to clinical symptom onset of common tauopathies. To prevent substantial cell loss already present at the stage of clinical symptom manifestation, therapeutic strategies addressing pre-symptomatic stages may be most successful [205]. Dissecting the earlier stages of tauopathy on a molecular level will be a great addition to understand the pathology and potentially identify targets for tauopathy therapy.

1.5.2 hiPSCs as a disease model

The achievement of reprogramming adult human fibroblasts into pluripotent cells elevated the stem cell research, opening up opportunities hitherto restrained by ethical factors and feasibility. In 2007, Yamanaka and co-workers successfully reprogrammed fibroblasts into pluripotent cells, so called induced pluripotent stem cells by retroviral delivery of four factors: octamer binding transcription factor 4 (Oct3/4), sex determining region Y-box 2 (SOX2), c-MYC and kruppel-like factor 4 (KLF4), termed Oct3/4-SOX2-KLF4-c-Myc (OSKM) factors [206, 207]. Fast forward to today human induced pluripotent stem cells (hiPSCs) are the preferred option for human disease modelling, circumventing the ethical concerns associated with human embryonic stem cells (ESCs). Whereby, hiPSCs and ESCs show great similarity by both expressing human pluripotent markers and ESCs specific surface markers as much as holding the potential to differentiate in all three germ layers [207, 208]. Even though, hiPSCs may exhibit a residual epigenetic memory of the parental cells, similar observations were made in human ESCs, strong arming the use of patient-derived hiPSCs for disease modelling [209–211].
Prior to the successful reprogramming of patient derived fibroblasts into hiPSCs, knowledge of diseases was gained by primary cultures of patients derived cells. Those gave great access to study individual therapeutic approaches of treatment as much as the aetiology of human diseases. Hard to access materials, e.g. brain cells or heart cells, restrict this method to be applicable to a variety of different diseases. Patient derived hiPSCs lifted these limitations by opening up a way of precision medicine design by easily accessible cell types as a source for disease modelling of genetic cause. Disease modelling starts of with patient-derived hiPSCs carrying the disease causing aberration/mutation, which in the following will be differentiated into the affected cell type to identify disease aetiology and uncover pathological processes during development. In the beginning, hiPSCs unaffected by disease were used as study controls. Similar to other cell lines, hiPSCs exhibit line-to-line differences making distinguishing between line-to-line variation and disease-relevant phenotype difficult to interpret. Site-specific genome editing by, e.g. clustered regularly interspaced short palindromic repeats (CRISPR)/CRISPR-associated protein 9 (Cas9), allow the correction of disease relevant mutations in patient derived hiPSCs, with identical genomic background except for the mutation of interest, circumventing the issue of line-to-line variation. This approach enables confident interpretation of obtained data excluding line-to-line effects as much as potential relevance of other single nucleotide polymorphisms (SNPs) in disease pathology. Several groups demonstrated the value of hiPSCs for tauopathy studies. However, one major challenge remains. *In vitro* recapitulation of Tau pathology is hard, due to the relative immaturity of hiPSC derived neurons. Numerous studies showed predominantly fetal

0N3R Tau isoform expression in disease unrelated hiPSC derived cortical neurons. Despite a shift in alternative splicing to 4R and 3R isoform expression, the shortest Tau isoform remains predominantly expressed [212–219]. Common knowledge in working with hiPSCs and derivatives for Tau studies is the necessity of long-term culturing. 365 days of neuron culture is needed for a start in 4R Tau isoform expression. Extensive culture time allows for the detection of 0N3R, 0N4R, 1N3R and 1N4R, with remaining predominant fetal 0N3R expression [215, 220]. Despite the detection of all adult Tau isoforms on a post-transcriptional level in hiPSC derived cortical neurons, detection of those on a protein level was not reported [221], making studying exon 10 related alternative splicing challenging. Hence, hiPSC derived neurons have been investigated under pathological conditions by introduction of different intronic and exonic Tau mutations associated with tauopathy. Pathogenic intronic point mutation IVS10+16 c > t shows inclusion of exon 10 in hiPSC of healthy donors, directly linking the mutation with alternative splicing alteration associated with tauopathy [218, 220]. Furthermore, introduction of *MAPT* IVS10+16 c > t showed hyperphosphorylation, similar to patient derived hiPSCs exhibiting the *MAPT* IVS10+16 c > t mutation [218].
Thus, increasing the maturity of hiPSC derived neuron cultures for physiological Tau studies, more sensitive methods for isoform detection and pathological recapitulation of tauopathy pathology remain a challenge and need further investigation.

1.6 Alternative splicing monitoring

Different spliced isoforms not only contribute to an essential resource of protein diversity, but their imbalance can also be a reason of disease development. Besides disease association, alternatively spliced isoforms comprise distinct biological functions, emphasising the need to explore a way of accurate quantification of certain splice isoforms, in healthy and disease state. Several analyses for alternative splicing investigation are established, but have their limits. Measurement of mRNA by endpoint labelling, as quantitative real-time PCR (qRT-PCR), single-molecule fluorescent *in situ* hybridization (smFISH) and RNA sequencing, neglect post-transcriptional, co- and post-translational modifications [222–224]. Translational arrest, ribosomal frame-shift regulation and locally translated mRNA will be undetected by these methods, therefore mRNA based analyses may be misleading [225–228]. Alternative splice isoform analyses on protein level as single time point immunochemistry, like immunoblot chemistry or immunofluorescence stainings are highly reliant on protein and isoform specific antibodies. Also, detection of low expressed proteins may be restrained by the sensitivity of the method autonomous of isoform specific antibodies. Mimicry of the endogenous environment is usually accomplished by minigenes. As the whole splicing process is a very delicate mechanism, minigenes may overexpress partial intron/exon regions, as much as truncate or excluding other relevant regions for representation of the physiological splicing events [229, 230]. Indications have been made, that transient overexpression of minigenes competitively bind splice factors oppressing the endogenous binding resulting in altered splicing of collateral genes, disrupting overall physiological splicing [231].

1.6.1 Exon Specific Isoform Expression Reporter System

We recently published a novel method for alternative spliced isoform analysis, the Exon Specific Isoform Expression Reporter System (EXSISERS) [1]. With its non-invasive, scarless post-translational excision of an exon present reporter domain, the EXSISERS circumvents named

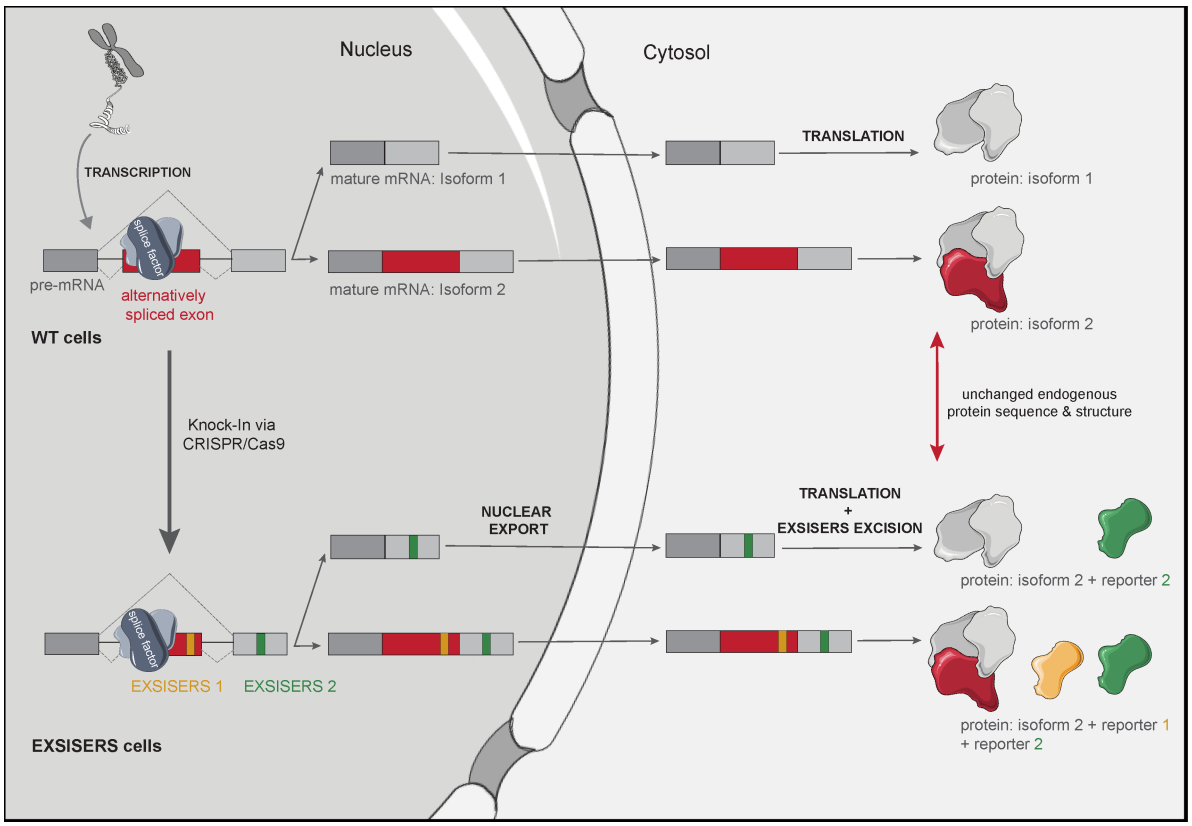

Figure 1.3: Exon Specific Isoform Expression Reporter System. Schematic description of mRNA processing and subcellular trafficking in mammalian cells. After transcription of the pre-mRNA, alternative spicing in the nucleus can lead to different mature mRNA variants by inclusion or exclusion of an alternatively spliced exon (red). Via nuclear transport, the mature mRNAs are transported into the cytosol, the place of translation. The different mature mRNAs lead to different protein isoforms (wild type (WT) cells). Clustered regularly interspaced short palindromic repeats (CRISPR)/clustered regularly interspaced short palindromic repeats (CRISPR)-associated protein 9 (Cas9) based knock-in (KI) approach of the Exon Specific Isoform Expression Reporter System (EXSISERS) into the alternatively splices exon, enables the detection of different splicing events, whereby, reporter 1 (yellow) KI in the alternatively spliced exon (EXSISERS 1) is specific for the isoform of interest, reporter 2 (green) KI (EXSISERS 2) represents an universal exon (bright grey). Post-translational intein-mediated, scarless self-excision of the exon-specific reporters from the protein of interest, allows reporter based detection of isoforms 1 and 2 with unchanged endogenous protein sequence and structure (EXSISERS cells).

limits of established methods. Inclusion of a luciferase reporter in an alternative spliced exon of interest (EOI) and a second luciferase reporter in an universally expressed exon, present in any protein isoform, enables non-invasive quantification of exon usage on a protein level without disruption of the endogenous protein sequence nor structure (Fig. 1.3). The reporters are co-translated and rapidly released by a protein splicing event, mediated by inteins, preserving the original isoform ratios. The EXSISERS takes advantage of the distinct substrates of the nano luciferase (NLuc) and firefly luciferase (FLuc), building the reporter for the EOI and the universally expressed exon, respectively. Bioluminescence in itself has been greatly used due to its high sensitivity, broad dynamic range and operational simplicity. Using the 19 kDa small luciferase subunit of *Oplophorus gracilirostris* improved the field of biotechnological usage of luciferases greatly by higher expression in mammalian cells [232]. By extensive modulation of this subunit a new system was created, known as NLuc [233]. NLuc utilises furimazine

to furimamide in an ATP independent reaction. High-intensity bioluminescence is produced, centred at 470 nm. *Photinus pyralis* FLuc has also been greatly studied. As a 62 kDa luciferase, FLuc catalyses D-luciferin oxidation ATP dependent to oxyluciferin, while producing high emission centred at 560 nm.

1.6.2 Protein Splicing

Inteins as a parasitic element present in all kingdoms of life, are usually integrated within essential protein coding gene sequences, not disrupting protein production, due to post-translational traceless excision [234, 235]. Hereby, the inteins carry out an unique process of self-excising out from a larger precursor peptide by cleavage of two peptide bonds and subsequent ligation of the downstream and upstream located polypeptide sequences (exteins) by forming two new peptide bonds, a mechanism known as protein splicing. Intein-mediated protein splicing is a spontaneous process, independent of any external factors or energy sources. Requirement of intein self-excision is exclusively the folding of the intein domains (reviewed in [236]). Less than 5% of all inteins are split inteins. Split inteins are transcribed and translated as two separate polypeptides, the N-intein and the C-intein. Both of these inteins are fused to an extein, the N-extein and C-extein, respectively. Post-translation, the split inteins assemble spontaneously and non-covalently into the canonical intein structure for *trans* protein splicing. Protein splicing or *trans* splicing found many uses including segmental isotope labelling of proteins for nuclear magnetic resonance (NMR) studies, gene editing procedures using split genes, protein two-hybrid methods to identify protein-protein interactions and sub-cellular protein location, side specific labelling and modification [237–241].

1.7 Objective

MAPT alternative splicing and the Tau isoforms are well studied, but an efficient therapy tackling the aggregation of Tau is still unexplored and restrained by the lack of human based disease models. *In vitro* hiPSC models based alternative splicing investigations are so far restricted by laborious and vulnerable neuronal long-term cultures.
This work is sought to

(1) close the gap of missing human based models for *MAPT* exon 10 alternative splicing investigation in a biotechnological approach, by introducing the novel EXSISERS in hiPSCs;

(2) establish a model to investigate the *MAPT* exon 10 alternative splicing pattern in diverse sets of cell types under physiological and pathological conditions, circumventing vulnerable neuronal long-term culture; and

(3) investigate the *MAPT* exon 10 alternative splicing modulation in a pharmacological HTS platform to further decipher the mechanisms involved.

In the long run, this work aims to build the bases to help highlight targets for early pharmacological interference in Tau pathology.

2 Results

2.1 *MAPT*$^{\text{EXSISERS}}$ hiPSC model

In order to establish an hiPSC based *MAPT* alternative splicing model, I exploited the novel EXSISERS by generating a *MAPT*$^{\text{EXSISERS}}$ hiPSC model. Focusing on the regulation of the alternatively spliced exon 10, I adapted the novel EXSISERS to report on the 4R isoforms and total Tau expression (Fig. 2.1).
An experimental EXSISERS was introduced in the alternative spliced exon 10, for 4R isoform monitoring. A control EXSISERS was included in the universally expressed exon 11 for total Tau expression monitoring (Fig. 2.1a). In general, the EXSISERS cassettes are comprised of:

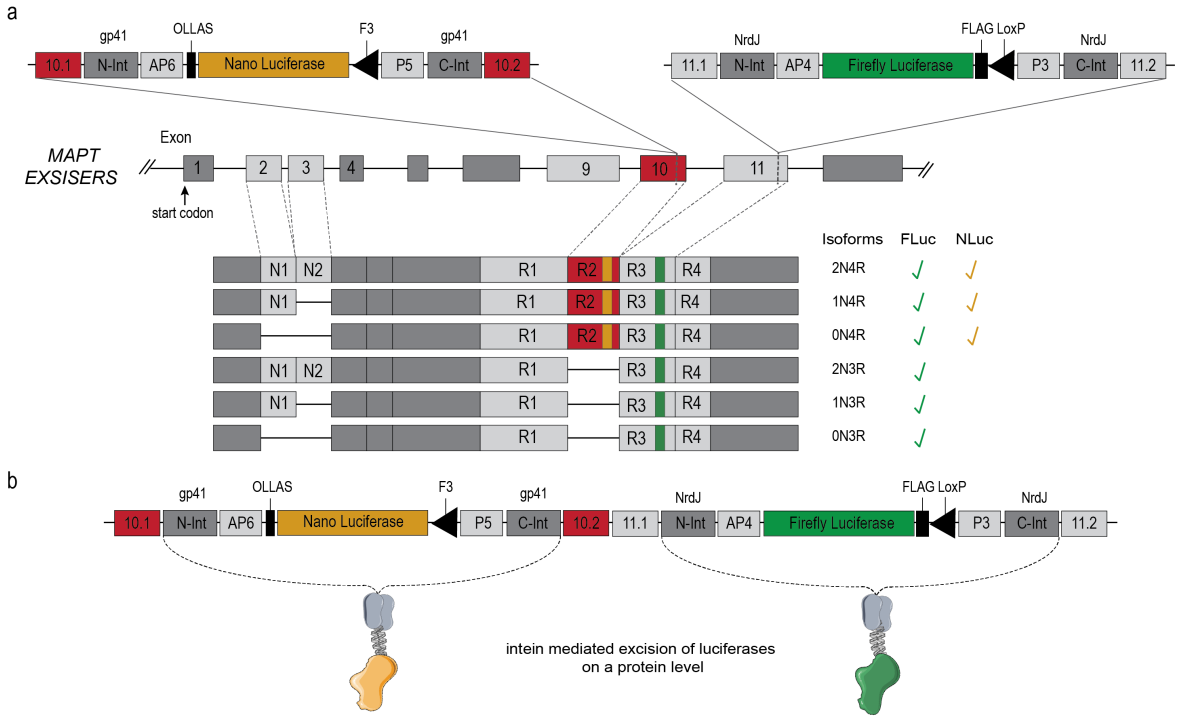

Figure 2.1: Scheme and mechanism of *MAPT*$^{\text{EXSISERS}}$. (a) Schematic description of the CRISPR/Cas9 mediated knock-in (KI) of the experimental Exon Specific Isoform Expression Reporter System (EXSISERS) (nano luciferase (NLuc), yellow) and control EXSISERS (firefly luciferase (FLuc), green) cassettes for Tau 4R isoform monitoring. KI of the experimental EXSISERS into *MAPT* exon 10 (red), enabling detection of the inclusion and exclusion of exon 10 by NLuc (yellow). Total Tau is monitored by control EXSISERS (FLuc, green) KI in *MAPT* exon 11, an universal exon (light grey). The cassettes are introduced into exon 10 (10.1, 10.2), or exon 11 (11.1, 11.2) upstream of Ser for efficient intein mediated excision of the luciferase on a protein level. N- and C-terminal split inteins (N-Int, C-Int) mediated excision of the NLuc (gp41 split-inteins) and FLuc (NrdJ split-inteins) is increased by flanking α-helices (AP6, P5, AP4, P3). (b) Post-translational intein-mediated scarless self-excision of the exon-specific reporters from the protein of interest allows reporter based detection of the 4R Tau isoforms (NLuc, yellow) and Total Tau (FLuc, green) with unchanged endogenous protein sequence and structure. Modified, based on [1].

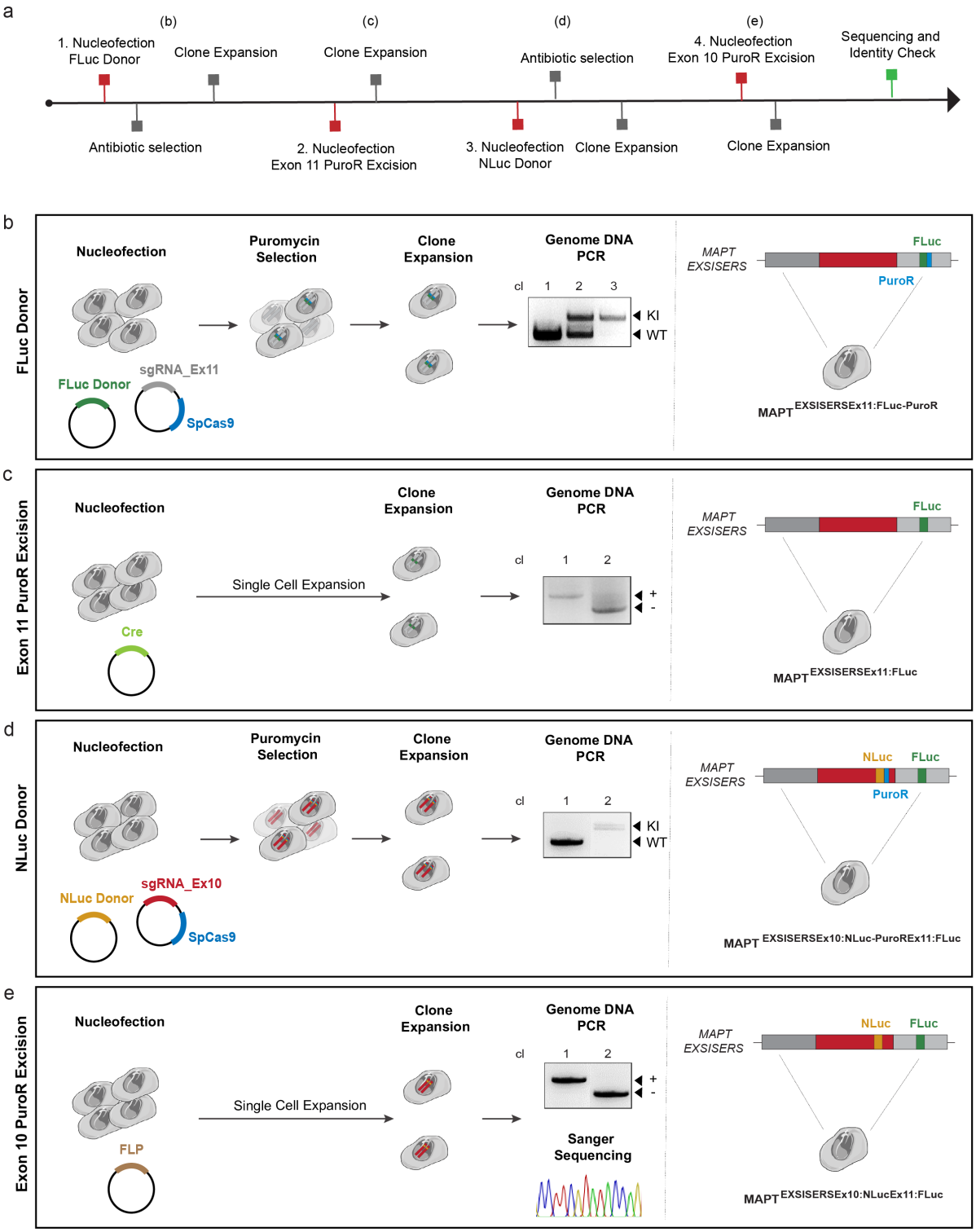

Figure 2.2: CRISPR/Cas9 mediated genome editing in hiPSCs. (a) Knock-in (KI) strategy to establish a CRISPR/Cas9 mediated $MAPT^{EXSISERS}$ hiPSC model. (b) $EXSISERS^{FLuc}$ targeting of *MAPT* exon 11. Donor vector (firefly luciferase (FLuc) donor, green) and sgRNA (sgRNA_Ex11, grey)-SpCas9 (blue) expression vector were co-delivered. KI was selected by puromycin and confirmed by gDNA based PCR, distinguishing between KI (+) and wild type (WT) (-) by size. (c) The puromycin resistance (PuroR) cassette (light blue) was excised by transient Cre recombinase (Cre) (light green) expression. (d) *MAPT* exon 10 was targeted for $EXSISERS^{NLuc}$ KI (nano luciferase (NLuc) donor, yellow). The CRISPR/Cas9 system is co-delivered by a sg-

Figure 2.2 *(continued)*: RNA (sgRNA_Ex10, red)-SpCas9 (blue) expression vector. Successful KI is confirmed by gDNA PCR after antibiotic selection, distinguishing between KI and WT by size. (e) Excision of the PuroR in the EXSISERS^{NLuc} cassette by transient flippase (FLP) (brown) expression. Cells were subsequently clonalised by single cell expansion and successful PuroR excision checked by gDNA PCR, distinguishing between excised (-) and remaining (+) PuroR by size and sequenced by Sanger sequencing.

a N-terminal split-intein (N-Int), α-helices, a luciferase-reporter, an epitope tag and a C-terminal split-intein (C-Int). The experimental EXSISERS cassette, include gp41 split-inteins, *E.coli* OmpF linker and mouse langerin fusion sequence (OLLAS) as an epitope tag and NLuc as a reporter for 4R Tau isoform expression. In case of the control EXSISERS cassette, NrdJ split-inteins, FLAG as an epitope tag and FLuc as a reporter for total Tau expression are included (Fig. 2.1a). Using split-inteins of different origin ensured precise protein-splicing of the EXSISERS cassettes, eliminating cross-splicing between the two cassettes (Fig. 2.1b). Intein mediated protein-splicing efficiency was enhanced by α-helices adjacent to the split inteins, enabling a faster excision by bringing the two splice-inteins in close proximity to each other. Using NLuc and FLuc as reporters enables an assessment of the 4R isoforms and total Tau expression within the same sample at the same time.

2.1.1 Gene targeting in hiPSC

HiPSC with their multiple possibilities of differentiation into several distinct cell types bring research closer to identifying key factors in disease regulation. To apply our novel EXSISERS for precise *MAPT* alternative splicing studies in a pharmacological manner, I tackled the obstacle of gene targeting several hiPSC lines without losing their pluripotency, establishing a targeting pipeline (Fig. 2.2a). Several recovery phases interposed the four precise gene targeting steps to keep the hiPSC identity. In general, introduction of the experimental and control EXSISERS, including a puromycin resistance (PuroR) cassette for positive selection, was mediated using the established CRISPR/Cas9 system. Donor vectors carrying the respective EXSISERS with flanking asymmetric homology arms for exon 10 and exon 11 were co-delivered into the parental hiPSC line with a vector carrying the CRISPR/Cas9 system (Fig. 2.2b, d). Selection was applied after a three day recovery phase, ensuring a steady pluripotency of the targeted hiPSCs. Entering a second recovery phase, colonies were manually picked under sterile conditions, expanded and genotyped for successful KI of the referring EXSISERS. *MAPT*$^{\text{EXSISERSEx11:FLuc\_PuroR}}$ and *MAPT*$^{\text{EXSISERSEx10:NLuc\_PuroREx11:FLuc}}$ positive cells were targeted for PuroR excision. In case of *MAPT*$^{\text{EXSISERSEx11:FLuc\_PuroR}}$, the PuroR cassette, flanked by LoxP sites, was mediated by Cre recombinase (Cre) transiently expressed upon plasmid delivery in a second targeting step. Targeted EXSISERS$^{MAPT\text{Ex11:FLuc_PuroR}}$ hiPSCs were expanded and clonalised. Clones were verified for successful excision of the PuroR cassette by negative selection. Excision of the selection cassette of *MAPT*$^{\text{EXSISERSEx10:NLuc\_PuroREx11:FLuc}}$, flanked by flippase (FLP) recognition target (FRT) sites, was mediated by FLP delivery. Successful excision of the PuroR cassette from the *MAPT*$^{\text{EXSISERSEx10:NLuc\_PuroREx11:FLuc}}$ hiPSC was verified by genotyping and Sanger sequencing.
Establishing this pipeline turned out to be successful, nevertheless, I met several issues in the process. Generally, one colony was considered to be emerged from one single cell. Therefore, clonalisation between every targeting step was performed by manual colony picking under sterile conditions. Five parental hiPSC lines were targeted for generation of a *MAPT*$^{\text{EXSISERS}}$ hiPSC

Table 2.1: hiPSC $MAPT^{EXSISERS}$ KI statistics. Selectional pressure was applied for knock-in (KI) targeting steps of exon 10 nano luciferase (NLuc) (Ex10 NLuc) and exon 11 firefly luciferase (FLuc) (Ex11 FLuc) (grey), by included puromycin resistance (PuroR) cassette. Resistance cassette was excised by either flippase (FLP) or Cre recombinase (Cre).

Cell line	Editing	Clones [#]	hom [#]	het [#]	WT [#]	hom [%]	targeted [%]
uilk_2	Ex10 NLuc [3.5 kbp]	49	16	0	0	32.65	32.65
	FLP [-2.3 kbp]	3	3	0	0	100.00	100.00
	Ex11 FLuc [4.7 kbp]	23	15	3	5	65.22	78.26
	Cre [-2.3 kbp]	30	3	0	0	10.00	10.00
vuna_3	**IVS10+16** Ex10 NLuc [3.5 kbp]	21	2	14	5	9.52	76.19
	FLP [-2.3 kbp]	53	3	0	0	5.66	5.66
	Ex11 FLuc [4.7 kbp]	15	3	11	1	20.00	93.33
	Cre [-2.3 kbp]	34	1	0	0	2.94	2.94
vuna_3	Ex10 NLuc [3.5 kbp]	20	3	14	5	15.00	85.00
	FLP [-2.3 kbp]	24	0	0	0	0.00	0.00
	Ex11 FLuc [4.7 kbp]	4	1	1	2	25.00	50.00
	Cre [-2.3 kbp]	44	0	0	0	0.00	0.00

model. These cell lines showed different targeting efficiencies in KI efficiency undergoing the targeting pipeline (Tab. 2.1). In this process, the parental hiPSCs HPSI0913i-diku_1, HPSI1013i-yemz_1, and HPSI1113i-qolg_1 did not yield any EXSISERS KI, either by toxicity of the DNA delivery or inefficient editing efficiency. We did not consider pursuing establishing the EXSISERS in those parental hiPSCs further, based on the cell line dependent DNA delivery toxicity. Issues with the targeting of HPSI0514i-vuna_3 were revealed by checking the intein-mediated excision of the control and experimental EXSISERS by immunoblotting, observing an abolished Tau expression (data not shown). Despite successful KI of the control and experimental EXSISERS in HPSI0514i-vuna_3, genome DNA PCR spanning the whole locus identified a unsuccessful excision of the eukaryotic translation elongation factor 1 α (EF1α) promoter regulated PuroR cassettes from both loci. Repeated targeting with Cre and FLP was not successful, respectively. Hence, one step of the pipeline seemed to cause a false positive. Initially, successful PuroR was verified by negative selection. However, targeting of HPSI0514i-vuna_3 did not give any indication of remaining PuroR cassette, as negative selection worked as expected. Moreover, remaining selection cassette is suspected to lower the KI efficiency of the experimental EXSISERS. Yet, targeting the EXSISERS$^{MAPT\text{Ex11:FLuc_PuroR}}$ clones for

EXSISERS$^{MAPT\text{Ex10:NLuc_PuroR}}$ KI yielded a targeting efficiency of 85%, with a homozygous KI in 15% of cases (Tab. 2.1). We concluded, that potential silencing of the EF1α promoter may cause observed results. The pipeline was adjusted accordingly to account for potential silencing of the EF1α promoter resulting in false positive indications of PuroR excision. Therefore, negative selection as PuroR excision verification was replaced by genotyping expanding to a locus spanning PCR of the respective clones and limited dilution substituted for manual colony picking for clonalisation after PuroR excision targeting. Considering the changes, I established a new pipeline (Fig. 2.2).
In the scope of this thesis two *MAPT* EXSISERS hiPSC models were successfully generated, in the following referred to as *MAPT*$^{\text{EXSISERS}}$ and *MAPT*$^{\text{IVS10+16EXSISERS}}$. KI of EXSISERS$^{MAPT\text{Ex11:FLuc_PuroR}}$ in *MAPT*$^{\text{EXSISERS}}$ had a targeting efficiency of 78.26% (homozygous KI: 65.22%), while PuroR cassette excision from the control EXSISERS resulted in an efficiency of 10%. Experimental EXSISERS KI yielded a targeting efficiency of 32.65% homozygous KI, while excision of the PuroR cassette yielded a 100% targeting efficiency (HPSI0614i-uilk_2, Tab. 2.1). For *MAPT*$^{\text{IVS10+16EXSISERS}}$, efficiency targeting exon 11 was 93.33%, 20% accounting for a homozygous KI. The IVS10+16 c > t point mutation to generate the *MAPT*$^{\text{IVS10+16EXSISERS}}$ hiPSC model was introduced in the third targeting step of the pipeline. Hereby, the donor vector carrying the experimental EXSISERS included the point mutation in its 3'-homology arm, introducing not only the EXSISERS but also the mutation of interest by homology directed repair (HDR). This KI showed a targeting efficiency of 76.19%, whereby, 9.52% account for a homozygous KI (HPSI0514i-vuna_3, Tab. 2.1). PuroR excision showed a 5.66% efficiency in all tested clones. Final verification of successful generation of *MAPT*$^{\text{EXSISERS}}$ hiPSCs was performed by Sanger sequencing (App. Fig. A.1b, c, e). Subsequently, generated *MAPT* EXSISERS hiPSC cell models underwent quality control, checking for pluripotency, the capacity to differentiate into all three germ layers and a undisturbed karyotype. Pluripotency and a normal karyotype was observed for both cell lines (App. Fig. A.3, App. Fig. A.2).

2.1.2 Longitudinal Tau monitoring

Technical evaluation of the *MAPT*$^{\text{EXSISERS}}$ system was published recently [1]. Human embryonic kidney cells (HEK293T) show very low endogenous *MAPT* expression. EXSISERS mediated alternative splicing monitoring upon CRISPR activation in HEK293T was shown. Verifying the general applicability of the system for alternative splicing studies. We used our generated hiPSC *MAPT*$^{\text{EXSISERS}}$ and *MAPT*$^{\text{IVS10+16EXSISERS}}$ models to establish *MAPT* alternative splicing monitoring on an endogenous level. Although, expression of 4R Tau expression is minor in hiPSC, the fetal 0N3R isoform shall already be detectable in hiPSC. To draw on the full potential of our hiPSC based EXSISERS models, I foremost adapted the bioluminescence measurement protocol. Bioluminescence measurements were adapted for stable isoform assessment. Inclusion time was increased compared to HEK293T cells to be able to detect a reliable FLuc (total Tau) expression. Surprisingly, the sensitivity of the luciferase mediated EXSISERS system allowed detection of NLuc signal (4R Tau expression) already in hiPSC state. 4R isoforms previously thought to be unexpressed in hiPSC (Fig. 2.3a). Based on the requirements in hiPSCs and subsequent hiPSC derivates, I assessed the correlation between the two luciferase reporters under the newly set measurement conditions. Based on simplicity, luciferase correlation was assessed by transient expression of NLuc and FLuc from the same plasmid, in HEK293T cells. Subsequent bioluminescence measurements under newly set conditions indicated a brighter

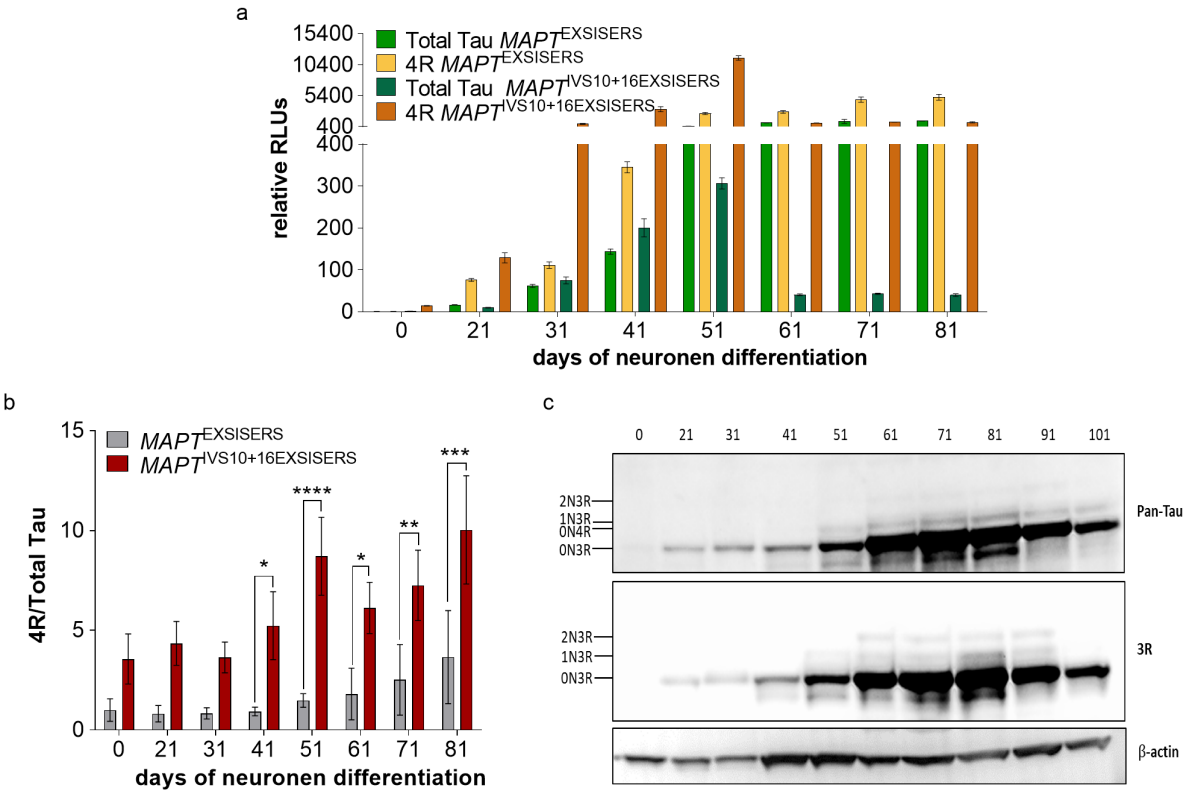

Figure 2.3: Longitudinal 4R isoform monitoring. (a) Total Tau (relative FLuc RLUs) and 4R Tau (relative NLuc RLUs) expression in $MAPT^{EXSISERS}$ (light green, yellow) and $MAPT^{IVS10+16EXSISERS}$ (dark green, orange) hiPSC derived neurons over a time period of 81 days of differentiation relative to d0 of $MAPT^{EXSISERS}$. (b) Longitudinal 4R/Total Tau ratio for EXSISERS based Tau isoform expression in $MAPT^{EXSISERS}$ (grey) and $MAPT^{IVS10+16EXSISERS}$ (red) hiPSC derived neurons over a time period of 81 days of differentiation. (c) Representative immunoblots of pan-Tau, 3R and β-actin as housekeeping gene in $MAPT^{EXSISERS}$ hiPSC derived neurons. Bioluminescence was measured every 10 days. Data represent the mean ± SD of three independent experiments. Statistical significance of selected ANOVA Bonferroni MCT results are shown, p-values: * < 0.1, ** < 0.01, *** < 0.001, **** < 0.0001, respectively (detailed statistical results are provided in Supp. Tab. A.1).

NLuc signal compared to FLuc, concluding that 57 FLuc molecules are needed to match the brightness of one NLuc molecule (App. Fig. A.4).
To demonstrate non-invasive monitoring of *MAPT* exon 10 under endogenous Tau expression, I differentiated $MAPT^{EXSISERS}$ and $MAPT^{IVS10+16EXSISERS}$ hiPSC into hiPSC derived neurons while monitoring the 4R Tau and total Tau expression through NLuc and FLuc over a period of three months (Fig. 2.3). Neural differentiation was initiated by differentiating the hiPSCs (d0) to hiPSC derived smNPCs, following the adherent smNPC differentiation protocol. On day 21, cells show characteristics of smNPC (App. Fig. A.5). $MAPT^{EXSISERS}$ showed a graduate increase in the fractional of 4R Tau expression (Fig. 2.3a, b). 4R Tau expression reached a plateau at d51 of differentiation, which remained similar from that day forward (relative NLuc RLU 2528.76 ± 194.8, Fig. 2.3a). Total Tau, on the contrary, increased in expression over the complete time course of three month in $MAPT^{EXSISERS}$ hiPSC derived neurons (Fig. 2.3a). Intriguingly, $MAPT^{IVS10+16EXSISERS}$ hiPSC derived neurons showed an elevated 4R/Total Tau ratio already in the undifferentiated hiPSCs compared to $MAPT^{EXSISERS}$ (relative NLuc RLU 14.38 ± 0.98, Fig. 2.3b). Elevated 4R Tau isoform expression stably detected by bioluminescence measurement was not detected by immunoblotting (Fig. 2.3c, App. Fig. A.6). Subsequently,

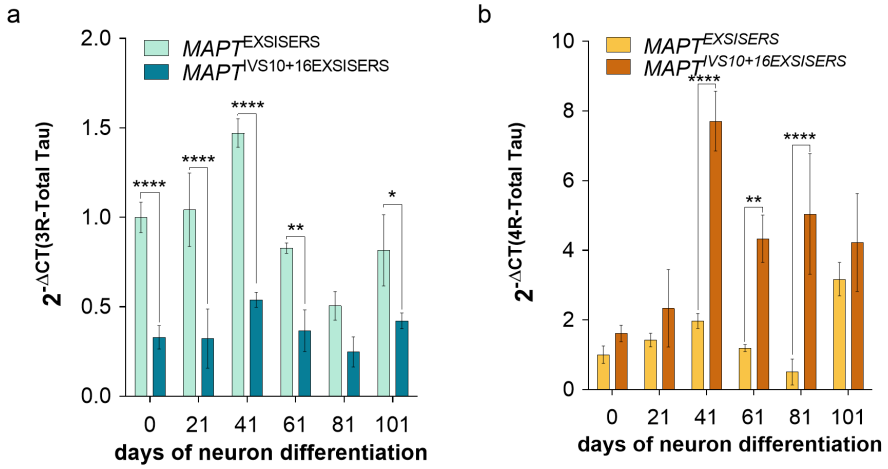

Figure 2.4: Longitudinal *MAPT* expression. (a) mRNA expression of *MAPT* excluding exon 10 (corresponding to the 3R isoforms) mRNA in $MAPT^{\text{EXSISERS}}$ (light blue) and $MAPT^{\text{IVS10+16EXSISERS}}$ (dark blue) hiPSC derived neurons relative to total *MAPT* mRNA (Total Tau) expression. (b) mRNA expression of *MAPT* including exon 10 mRNA (corresponding to the 4R isoforms) in $MAPT^{\text{EXSISERS}}$ (yellow) and $MAPT^{\text{IVS10+16EXSISERS}}$ (orange) relative to total *MAPT* mRNA (Total Tau) expression. Data represent the mean ± SD of three independent experiments. Statistical significance of selected ANOVA Bonferroni MCT results are shown, *p*-values: * < 0.1, ** < 0.01, *** < 0.001, **** < 0.0001, respectively (detailed statistical results are provided in Supp. Tab. A.1).

the isoform expression increased non-monotonically, with peaks at day 51 and day 81 of neuron differentiation. Relative NLuc RLUs clearly show a steady increase of 4R Tau expression up to day 51 of neuron differentiation (relative NLuc RLU 11488.01 ± 352.38, Fig. 2.3a). In contrast, total Tau expression increased only slightly over the time course of 51 days of differentiation (Fig. 2.3a). Overall, total Tau expression was significantly lower in $MAPT^{\text{IVS10+16EXSISERS}}$ compared to $MAPT^{\text{EXSISERS}}$. 4R Tau and total Tau expression were significantly reduced after that in $MAPT^{\text{IVS10+16EXSISERS}}$ hiPSC derived neurons older than 51 days, falling under the expression level observed in $MAPT^{\text{EXSISERS}}$ hiPSC derived neurons (Fig. 2.3a).
Successful monitoring of *MAPT* alternative splicing by the EXSISERS made us confident in using our two hiPSC models for further alternative splicing studies. Nevertheless, our system detects alternative splicing processes on a protein level. Reporter based detection is allowing the distinction between the 4R Tau isoforms, by NLuc and the overall total Tau expression, by FLuc. Total Tau expression is therefore including all isoforms expressed at the time point of measurement. Thus, EXSISERS do not report on the 3R Tau expression by a reporter. To enable the analysis of 3R to 4R Tau expression in our longitudinal monitoring, I sought to investigate the $MAPT^{\text{EXSISERS}}$ and $MAPT^{\text{IVS10+16EXSISERS}}$ hiPSC derived neurons on an mRNA level. Specific probes targeting the exon junctions for *MAPT* exon 10 in- and exclusion allowed us to distinguish 3R and 4R Tau corresponding RNA expression over the time course of the differentiation. Expression of the mRNA corresponding to the 3R isoform was increased in the $MAPT^{\text{EXSISERS}}$ between day 0-41 of differentiation (relative *MAPT* exon 10 excluding mRNA expression 1.48 ± 0.08, *p*-value: **** < 0.0001, two-way analysis of variance (ANOVA) with Bonferroni multiple comparison test (MCT), Fig. 2.4a). In contrast, $MAPT^{\text{IVS10+16EXSISERS}}$ showed an overall lower *MAPT* exon 10 excluding mRNA expression compared to $MAPT^{\text{EXSISERS}}$ (Fig. 2.4a). *MAPT* exon 10 including mRNA expression elevated

over time of differentiation in $MAPT^{EXSISERS}$ up to day 41. Expression decreased after that until day 101, showing the highest expression of *MAPT* exon 10 including mRNA (relative *MAPT* exon 10 including mRNA expression 3.17 ± 0.48, Fig. 2.4b). Contrary to *MAPT* exon 10 excluding mRNA, mRNA corresponding to the 4R isoforms showed significant increase in $MAPT^{IVS10+16EXSISERS}$ hiPSC derived neurons, with highest expression on day 41 (relative *MAPT* exon 10 including mRNA expression 7.71 ± 0.86, p-value: **** < 0.0001, two-way ANOVA with Bonferroni MCT, Fig. 2.4b). A lower but steady elevated expression was observed at later time points of differentiation (Fig. 2.4b). Notably, 4R/Total Tau expression on posttranscriptional and posttranslational level was matching in both $MAPT^{EXSISERS}$ and $MAPT^{IVS10+16EXSISERS}$ (Fig. 2.3b, Fig. 2.4b).
We showed successful non-invasive monitoring of 4R Tau isoform expression over several weeks of neuron differentiation by the EXSISERS, allowing specific 4R Tau detection starting from the hiPSC state not possible by commonly used methods.

2.2 Increased neuron complexity in $MAPT^{IVS10+16EXSISERS}$

Coinciding with application of our generated EXSISERS cell models for *MAPT* alternative splicing investigation, I sought to investigate our two EXSISERS cell models, one with the 4R Tau isoforms increasing intronic point mutation IVS10+16 c > t, based on neuron complexity. Sholl analysis of $MAPT^{EXSISERS}$ and $MAPT^{IVS10+16EXSISERS}$ hiPSC derived neurons showed an highly significant difference in neuritic tree complexity of the two cell models. We observed a greater number of intersections in the Sholl analysis of 41 days old $MAPT^{IVS10+16EXSISERS}$ hiPSC derived neurons compared to $MAPT^{EXSISERS}$ hiPSC derived neurons (p-value: **** < 0.0001, Kolmogorov-Smirnov-Test, Fig. 2.5a). While the total length between the parental cell lines HPSI0614i-uilk_2 ($MAPT^{EXSISERS}$) and HPSI0514i-vuna_3 ($MAPT^{IVS10+16EXSISERS}$) was indifferent, total length of the neuritic tree between both EXSISERS cell models was significantly different (Fig. 2.5b, c). $MAPT^{IVS10+16EXSISERS}$ showed significantly greater total length (two-tailed p-value: **** < 0.0001, unpaired parametric t-test, Fig. 2.5b). To exclude any KI and genotype effect, considering the different parental cell lines of both EXSISERS cell models, I also investigated the parental cell lines concerning their neuritic tree complexity (App. Fig. A.7). hiPSC derived neurons of the parental cell line HPSI0514i-vuna_3 showed higher efficiency in neuron differentiation compared to neurons derived from the parental cell line HPSI0614i-uilk_2 and $MAPT^{EXSISERS}$. Interestingly, comparing HPSI0514i-vuna_3 derived neurons with $MAPT^{IVS10+16EXSISERS}$ showed a significant increase in neuron differentiation efficiency by the EXSISERS KI (App. Fig. A.7a). Number of intersections in the Sholl analysis of day 41 old neurons was significantly increased in HPSI0514i-vuna_3 compared to HPSI0614i-uilk_2 (p-value: **** < 0.0001, Kolmogorov-Smirnov-Test, App. Fig. A.7b). Comparison of parental HPSI0614i-uilk_2 hiPSC derived neurons with $MAPT^{EXSISERS}$, $MAPT^{EXSISERS}$ showed an overall shorter neuritic tree total length (p-value: ** < 0.01, Kolmogorov-Smirnov-Test, App. Fig. A.7c). Complexity was slightly increased in the parental neurons compared to the EXSISERS KI neurons (p-value: * < 0.05, Kolmogorov-Smirnov-Test, App. Fig. A.7c), greater difference in total length and complexity of the neuritic tree was apparent by comparing the hiPSC derived neurons of the parental cell line HPSI0514i-vuna_3 and $MAPT^{IVS10+16EXSISERS}$. Total neuritic tree length was three times longer in $MAPT^{IVS10+16EXSISERS}$ compared to HPSI0514i-vuna_3 hiPSC derived neurons (p-value: **** < 0.0001, Kolmogorov-Smirnov-Test, App. Fig. A.7e). Results were similar when comparing both based on their complexity.

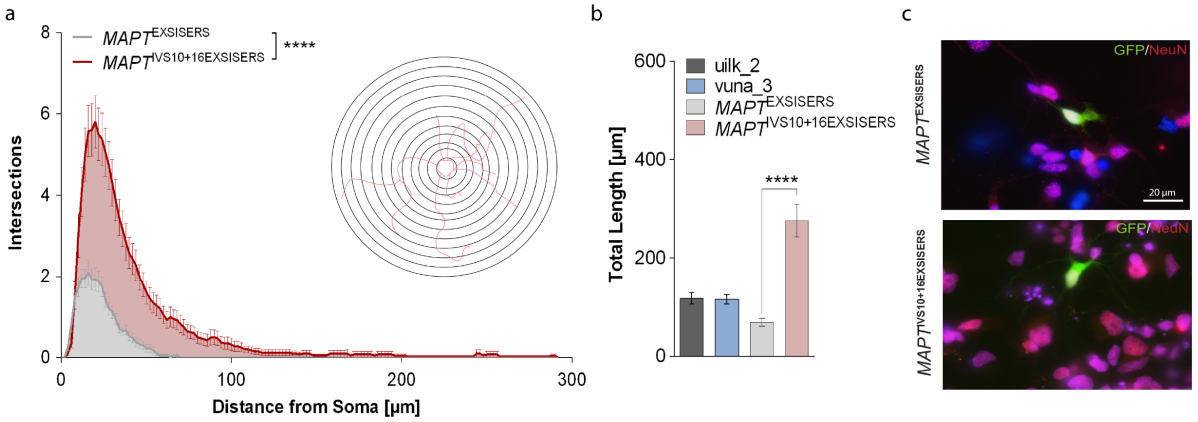

Figure 2.5: Maturation effect in hiPSC *MAPT*$^{\text{IVS10+16EXSISERS}}$ derived neurons. (a) Sholl analysis of the number of intersections with respect of their distance from the soma of 41 day old *MAPT*$^{\text{EXSISERS}}$ (bright grey) and *MAPT*$^{\text{IVS10+16EXSISERS}}$ (red) hiPSC derived neurons. Intersections of Sholl analysis were counted at a 2 µm interval. (b) Total neuritic length of parental HPSI0614i-uilk_2 (dark grey) and HPSI0514i-vuna_3 (blue) and EXSISERS KI *MAPT*$^{\text{EXSISERS}}$ (bright grey) and *MAPT*$^{\text{IVS10+16EXSISERS}}$ (red) hiPSC derived neurons. (c) Exemplary fluorescence images of *MAPT*$^{\text{EXSISERS}}$ and *MAPT*$^{\text{EXSISERS}}$ transiently expressing GFP (green) and immunofluorescently stained for the neuronal marker NeuN (red) and DAPI (blue). Data show the mean ± SEM of 40 measured neurons per cell line. Selected statistical tests (Kolmogorov-Smirnov-Test (a), unpaired two-tailed t-test (b)) are shown: p-value: * < 0.05, ** < 0.01, *** < 0.001, **** < 0.0001 (detailed statistical results are provided in Supp. Tab. A.5 and Supp. Tab. A.6.)

Complexity was significantly greater in *MAPT*$^{\text{IVS10+16EXSISERS}}$ (p-value: **** < 0.0001, Kolmogorov-Smirnov-Test, App. Fig. A.7f).
Increased neuron complexity was observed in *MAPT*$^{\text{IVS10+16EXSISERS}}$ hiPSC derived neurons with increased 4R Tau expression, compared to parental cells and the EXSISERS KI counterpart *MAPT*$^{\text{EXSISERS}}$.

2.3 *MAPT*$^{\text{EXSISERS}}$ for pharmacological HTS

Stoilov *et al.*, 2008 [242] previously investigated *MAPT* alternative splicing modulators using minigenes. In this context the DYRK1A/GSK3β inhibitor 5-Iodotubercidin (5-ITU) was identified as a compound with 4R Tau upregulating properties. To test, whether our system not only is applicable for pharmacological HTS for *MAPT* alternative splicing modulation, but also to evaluate whether our system has a cell type independent responsiveness, I differentiated the *MAPT*$^{\text{EXSISERS}}$ into hiPSC derived small molecule neuronal precursor cells (smNPCs) and forebrain organoids (FBOs). Both were treated with increasing concentration of 5-ITU (Fig. 2.6a). Cell viability upon 5-ITU treatment of different concentration, over the time course of 72 h, was assessed to confirm a Tau dependent upregulation of the relative values. Treatment with concentrations lower than 1 µM had no significant impact on cell viability in *MAPT*$^{\text{EXSISERS}}$ and *MAPT*$^{\text{IVS10+16EXSISERS}}$ hiPSC derived smNPCs. 5-ITU treatment with concentrations of 1 µM or 10 µM showed a reduction of cell viability in both hiPSC derived smNPC lines up to 50% (Fig. 2.6b). In case of hiPSC derived smNPCs, a treatment with 1 µM 5-ITU over the time course of 48 h showed a significant increase in the 4R/Total Tau ratio compared to vehicle control (2.93 ± 0.78, p-value: **** < 0.0001, two-way ANOVA with Bonferroni MCT). Treatment over a period of 72 h increased the 4R/Total Tau ratio even more (3.40 ± 0.89, p-value: **** < 0.0001, two-way ANOVA with Bonferroni MCT, Fig. 2.6c, d). Unravelling the

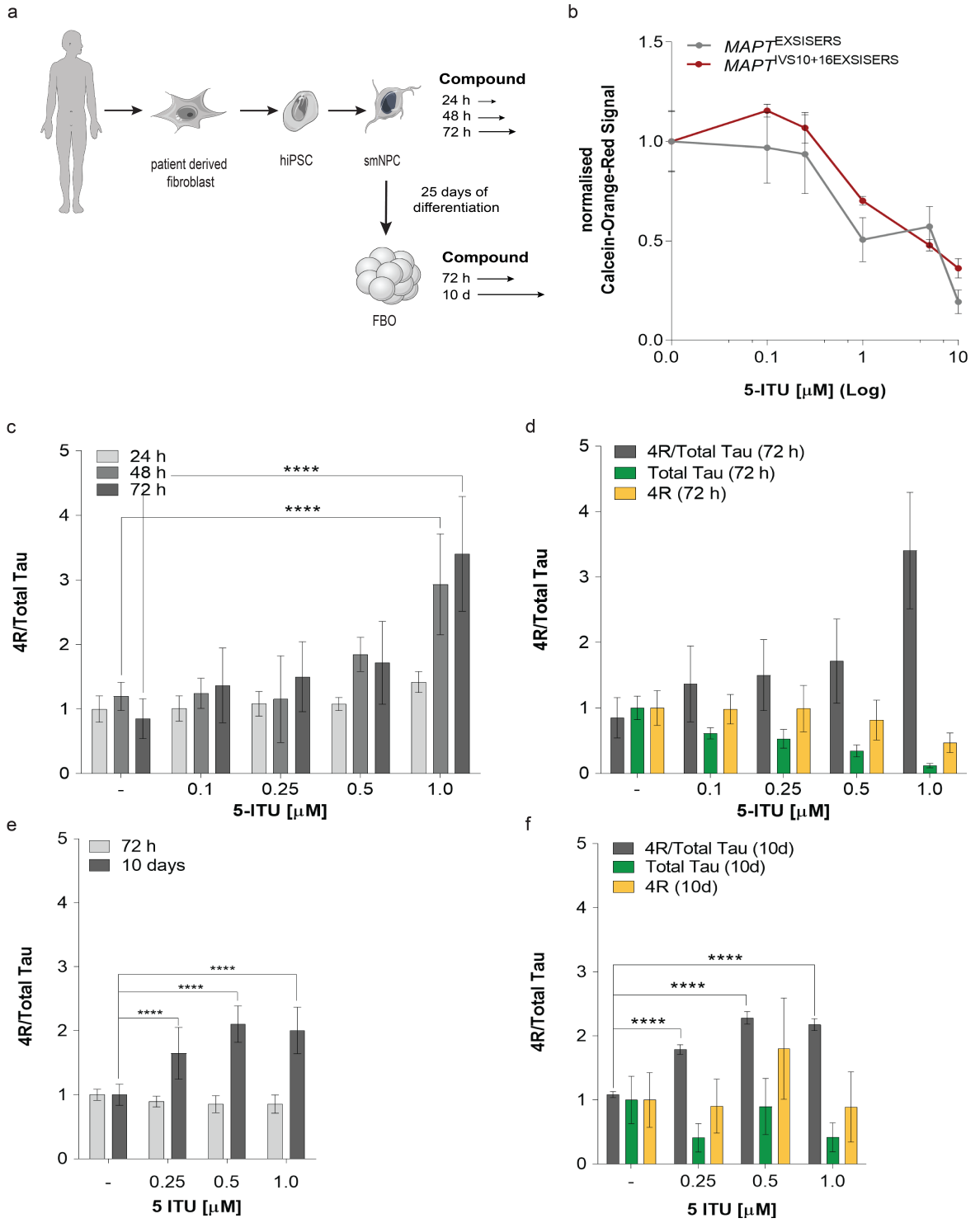

Figure 2.6: Cell type independent EXSISERS response. (a) Scheme of compound treatment of human induced pluripotent stem cell (hiPSC) derived small molecule neuronal precursor cells (smNPCs) and forebrain organoids (FBOs). (b) Linear-log-plot of cell viability of hiPSC $MAPT^{EXSISERS}$ (grey) and $MAPT^{IVS10+16EXSISERS}$ (red) derived smNPCs upon exposure to increasing concentrations of 5-Iodotubercidin (5-ITU) over 72 h. (c) 4R/Total Tau ratio of relative nano luciferase (NLuc) (4R Tau) and firefly luciferase (FLuc) (Total Tau) RLUs normalised to vehicle, as a function of increasing DYRK1A/GSK3β inhibitor 5-ITU concentration after 24 h, 48 h and 72 h in $MAPT^{EXSISERS}$ hiPSC derived smNPCs. (d) 4R/Total Tau ratio, Total

Figure 2.6 ***(continued)*:** Tau and 4R of the RLUs of NLuc and FLuc normalised to vehicle, as a function of increased 5-ITU concentration after 72 h in $MAPT^{\text{EXSISERS}}$ hiPSC derived smNPCs. (e) 4R/Total Tau ratio of the RLUs of NLuc and FLuc normalised to vehicle, as a function of increased 5-ITU concentration after 72 h (light grey) and 10 days (dark grey) in $MAPT^{\text{EXSISERS}}$ hiPSC derived FBOs (f) 4R/Total Tau (dark grey), Total Tau (green) and 4R Tau (yellow) of the RLUs of NLuc (4R Tau) and FLuc (Total Tau) normalised to vehicle, as a function of increased 5-ITU concentration after 10 days in $MAPT^{\text{EXSISERS}}$ hiPSC derived FBOs. All values are normalised to the vehicle control after 24 h. Data are the mean ± SD of three biological and technical replica. (d) Selected ANOVA analysis results of Bonferroni MCT are shown: p-value: * < 0.05, ** < 0.01, *** < 0.001, **** < 0.0001 (full statistical results are provided in Supp. Tab. A.2 and Supp. Tab. A.4).

4R/Total Tau ratio illustrates that the ratio increase is rather by total Tau decrease than 4R Tau increase (Fig. 2.6d).
HiPSC derived FBOs were treated with increasing concentrations of 5-ITU over a time period of 72 h or 10 days. 5-ITU treatment over 72 h showed no impact on Tau expression (Fig. 2.6e). Similar Tau regulation upon 5-ITU treatment was observed in hiPSC derived FBOs compared to smNPCs, when treated with 0.25, 0.5 or 1 µM 5-ITU over a time course of 10 days (Fig. 2.6e, f). Whereby, 0.5 µM 5-ITU treatment showed the greatest increase in 4R/Total Tau ratio with 2.28 ± 0.10 fold normalised to vehicle control (p-value: **** < 0.0001, two-way ANOVA with Bonferroni MCT, Fig. 2.6e). Coinciding with the effect of 5-ITU on total Tau expression in hiPSC derived smNPCs, total Tau expression was rather reduced by 5-ITU in hiPSC derived FBOs than 4R Tau increased (Fig 2.6f).
Despite a cell type independent reliable detection of 4R/Total Tau ratio modulation by 5-ITU in hiPSC derived smNPCs and FBOs, I decided based on the obtained reliable signal of *MAPT* alternative splicing modulation in hiPSC derived smNPCs, on those, for further conduction of pharmacological HTSs. HiPSC derived smNPCs are more cost efficient and convenient to handle and therefore qualify as a suitable cell type to perform pharmacological HTSs, with the possibility of time-point quantification of isoform expression.

2.3.1 FDA approved compound screen

Confident in the parameters for *MAPT* alternative splicing modulator studies in $MAPT^{EXSISERS}$ hiPSC derived smNPCs, I exploited this system by conducting a primary library screen of 1,230 FDA approved compounds in an HTS manner. Prior to the screen, I assessed the stability of our system by calculating the Z'-factor (Equation 5.6). We established 5-ITU as a positive control, previously shown as a compound with 4R Tau upregulating properties, and dimethyl sulfoxide (DMSO) as a vehicle control. We exposed $MAPT^{EXSISERS}$ hiPSC derived smNPCs to 5-ITU in concentrations of 0.5 µM, 1 µM and 10 µM for either 24 h, 48 h or 72 h, prior to bioluminescence measurements (App. Fig. A.10). 4R isoform expression was significantly increased upon 1 µM 5-ITU exposure over 48 h and 72 h. Whereby, the Z'-factor, with acceptance criteria for an excellent assay being ≥ 0.5, was Z'-factor (48 h) = 0.26 and Z'-factor (72 h) = 0.87 for 1 µM 5-ITU treatment (App. Fig. A.10). Hence, setting the conditions for the primary FDA approved compound screen, exposing $MAPT^{EXSISERS}$ hiPSC derived smNPCs to the Prestwick Library in a concentration of 1 µM over a time course of 72 h (Fig. 2.7, App. Fig. A.11). Out of 1,230 FDA approved compounds, I identified 25 potential hits in the primary screen, sought to be verified in $MAPT^{EXSISERS}$ hiPSC derived smNPCs (App. Fig. A.8). As a first step, all potential hits were analysed by reproduction of the primary screen conditions (App. Fig. A.9). Two, Digoxin and Digitoxigenin showed a reduction of 4R and total Tau expression, further investigated in a response curve (Fig. 2.8). Treatment of $MAPT^{EXSISERS}$ hiPSC derived smNPCs with increasing Digoxin concentration showed a peak of 4R isoform expression at the lowest concentration tested (normalised NLuc RLU 1.27 ± 0.05, Fig. 2.8a). Higher Digoxin concentrations resulted in a declining 4R and total Tau expression, coinciding with a decreasing cell viability with increasing Digoxin concentration (Fig. 2.8c). Cell viability

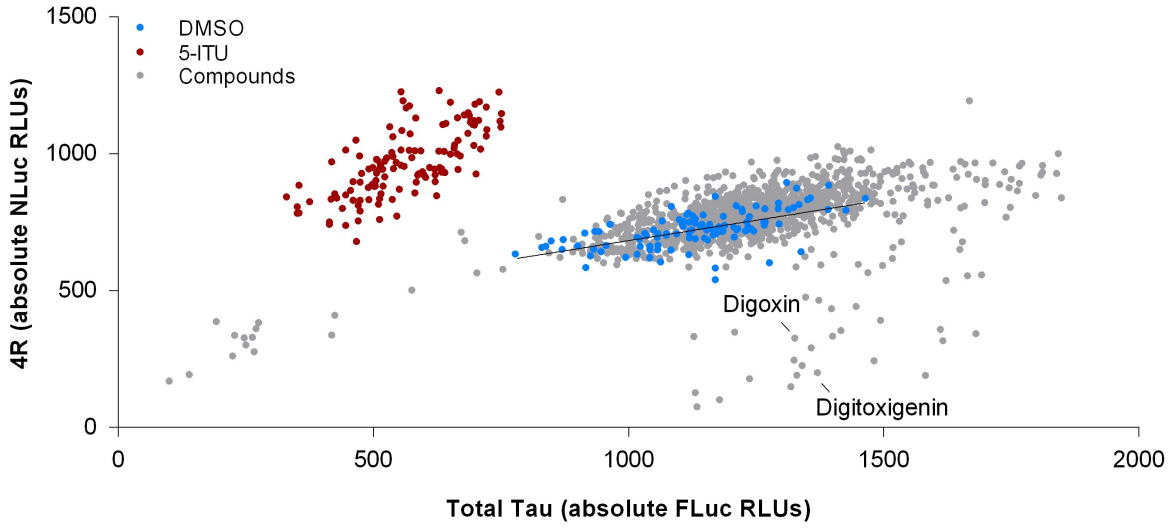

Figure 2.7: Primary Prestwick Library screen. (a) Scatter plot of 4R Tau (absolute nano luciferase (NLuc) RLUs) and Total Tau (absolute firefly luciferase (FLuc) RLUs) values of screened Prestwick Library, comprised of 1,280 FDA approved compounds (grey), screened in $MAPT^{EXSISERS}$ hiPSC derived smNPCs. SmNPCs were exposed to the library for 72 h prior to bioluminescence imaging. 5-ITU (red), a DYRK1A/GSK3β inhibitor, served as a positive control for 4R Tau upregulation, DMSO as vehicle (blue). The linear regression of the vehicle is shown by a black line.

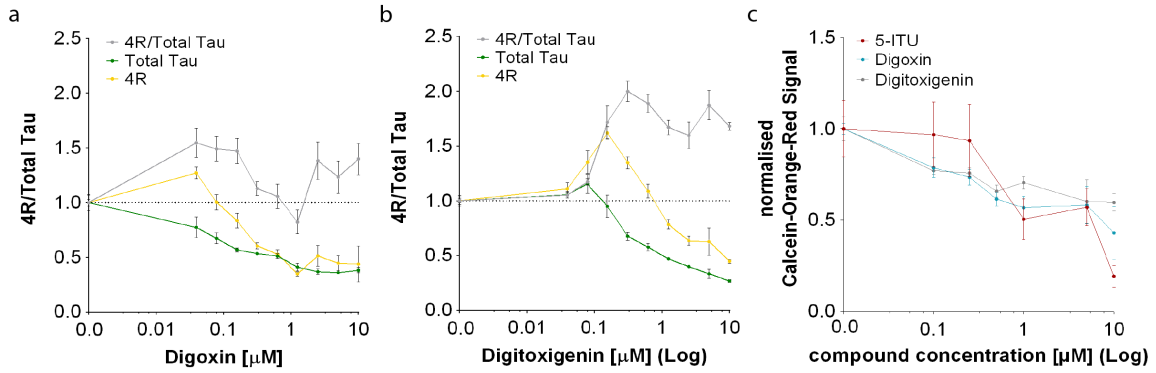

Figure 2.8: Prestwick Library validation - 4R Tau modulation. Dose response curves as linear log-plots of relative NLuc (4R Tau) and FLuc (Total Tau) RLUs shown as 4R/Total Tau ratio (grey), Total Tau (green) and 4R Tau (yellow) as a function of increased (a) Digoxin and (b) Digitoxigen concentration in *MAPT*$^{\text{EXSISERS}}$ hiPSC derived smNPCs after 72 h of compound treatment normalised to vehicle. (c) Cell viability as relative calcein-orange-red signal as a function of increased 5-ITU (red), Digoxin (blue) and Digitoxigenin (grey) concentration in *MAPT*$^{\text{EXSISERS}}$ hiPSC derived smNPCs after 72 h of compound exposure, normalised to vehicle. The black dashed line indicates the vehicle control, all values are normalised to. Data are the mean ± SD of three technical and biological replica.

was already reduced by 43% compared to vehicle control at a concentration of 1 µM (relative calcein-orange-red signal 0.57 ± 0.06, Fig. 2.8d). Treatment of *MAPT*$^{\text{EXSISERS}}$ hiPSC derived smNPCs with increasing Digitoxigenin concentration showed a peak of 4R Tau expression at a concentration of 0.156 µM (normalised NLuc RLU 1.62 ± 0.05, Fig. 2.8b) with a cell viability decrease by 23% (relative calcein-orange-red signal 0.77 ± 0.02, Fig. 2.8c). Despite the fact, that I was able to find two out of 25 potential *MAPT* alternative splicing modulators, I discovered a discrepancy between the primary screen results and our hit verification attempt. Treatment of *MAPT*$^{\text{EXSISERS}}$ hiPSC derived smNPCs with Digoxin and Digitoxigenin showed a 4R Tau downregulation in the initial screening results, but 4R Tau upregulation in the following verification steps (Fig. 2.7, Fig. 2.8). Non of the other potential hits showed any producible *MAPT* alternative splicing modulation. Hence, I explored whether primary screening data was reproducible using the initial library. To reproduce our primary screening data, I selectively re-screened 320 compounds, including Digoxin and Digitoxigenin (App. Fig. A.12). Comparing the 4R and total Tau values of the initial screen and the rerun of the selected 320 compounds stroke with a clear difference in *MAPT* alternative splicing modulators. Contrary to the initial screen, Digoxin and Digitoxigenin showed an upregulation of 4R Tau upon treatment over a time course of 72 h (App. Fig. A.12b). Furthermore, initially identified potential hits, some contained within the retested 320 compounds, were not renominated as potential *MAPT* alternative splicing modulators. We concluded, that the EXSISERS bares the hypothesised potential for HTS to identify pharmacological isoform modulators, but also recognise the further need of investigation to nominate those.

2.3.2 Broad Repurposing Library screen

Considering the potential of the $MAPT^{EXSISERS}$ for 4R modulation factor screening, I sought to expand the screening platform for potential identification of pharmacological *MAPT* alternative splicing modulators. Therefore, I used the Broad Repurposing Library, comprised of 5,040 compounds in $MAPT^{EXSISERS}$ hiPSC derived smNPCs, with a final concentration of 1 µM and a 72 h incubation time, prior to bioluminescence mediated 4R Tau and total Tau expression assessment. The total of all compounds was measured in four consecutively days, every screening day entailing a quarter of the total library (Fig. 2.9). We included the DYRK1A/GSK3β inhibitor 5-ITU in the same concentration as a control for 4R Tau isoform upregulation on every plate. 1% (v/v) DMSO as vehicle control was also included on every plate to account for any plate effect. Plotting of respective absolute FLuc (Total Tau) and NLuc (4R Tau) RLUs showed a clear cluster of the vehicle control over mostly all plates. Clustering of the vehicle control excludes a plate and batch effect. 5-ITU showed expected 4R isoform upregulation by increased absolute NLuc RLUs. Exceptions in the overall similar clustering of 5-ITU and vehicle control were attributed to three plates of different screening days, showing double in absolute NLuc and FLuc RLUs (Fig. 2.9). Considering the 4R/Total Tau ratio an internal control of cell density in

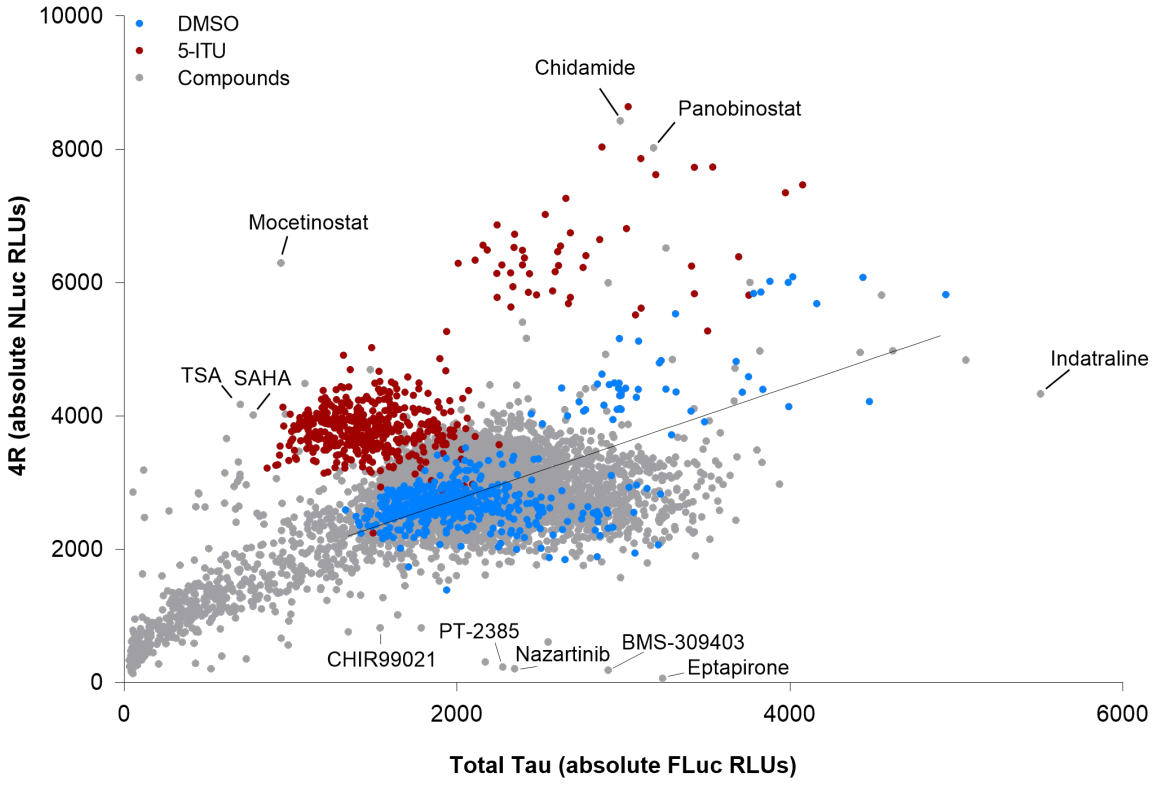

Figure 2.9: Broad Repurposing Library screen. Scatter plot of absolute NLuc RLUs (4R) and FLuc RLUs (Total Tau). The Broad Repurposing Library, comprised of 5,040 compounds, was screened in $MAPT^{EXSISERS}$ hiPSC derived smNPCs, with a final concentration of 1 µM and a 72 h incubation time, prior to bioluminescence mediated 4R and Total Tau assessment (grey). The DYRK1A/GSK3β inhibitor 5-ITU was included in the screen as a positive control (red), DMSO as a vehicle control (blue). Linear regression of the vehicle is shown by a black line.

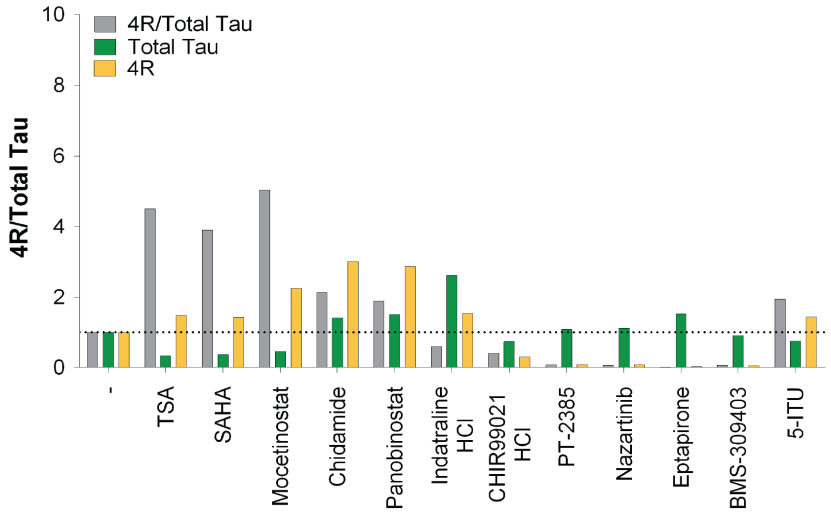

Figure 2.10: Broad Repurposing Library screen. Bar chart of the 11 nominated primary screening hits normalised to the mean of all vehicle controls. 4R/Total Tau ratio (grey), Total Tau (green) and 4R (yellow) of relative NLuc (4R Tau) and FLuc (Total Tau) RLUs of the Broad Repurposing Library. 5-ITU values are the mean of all values of the positive control in the initial Broad Repurposing Library screen. The black dashed line indicates the vehicle control all values are normalised to.

each well, the ratios of the absolute values were comparable. Higher cell density rather than a plate effect may be cause of the elevated NLuc and FLuc RLUs. Additionally, I looked at the overall mean of all library compound treated wells, noticing no differences between plates. Hence, the three plates were not considered to be neglected nor excluded from analysis. Under the consideration of the Signal Window (SW) (Equation 5.2), the coefficient of variation (C_V) (Equation 5.3), the Hit threshold (HT) (Equation 5.4), the %Activity (Equation 5.5) and the absolute NLuc and FLuc RLUs (Fig. 2.9a, App. Table A.7), I nominated 11 compounds for further investigation. TSA, SAHA and Mocetinostat showed a clear downregulation of total Tau expression (normalised FLuc RLUs 0.33, 0.37 and 0.45, respectively), with elevated 4R Tau expression relative to vehicle control (normalised NLuc RLUs 1.49, 1.44 and 2.25, respectively), resulting in an elevation of the 4R/Total Tau ratio (Fig. 2.10). Chidamide, Panobinostat and Indatraline HCl showed an elevation in total Tau expression with normalised FLuc RLUs of 1.41, 1.51 and 2.61 relative to vehicle control, respectively. Furthermore, all three showed a clear increase in 4R Tau expression with normalised NLuc RLUs of 3.02, 2.87 and 1.55 relative to vehicle control, respectively (Fig. 2.10). Noticeably, Indatraline HCl showed the greatest increase in total Tau expression, with only slight increase of 4R Tau expression compared to TSA, SAHA, Mocetinostat, Chidamide and Panobinostat, resulting in a decrease of the 4R/Total Tau ratio to 0.59 normalised to vehicle control. We nominated five compounds, indicating a specific 4R downregulation: CHIR99021 (normalised NLuc RLU 0.29), PT-2385 (normalised NLuc RLU 0.08), Nazartinib (normalised NLuc RLU 0.07), Eptapirone (normalised NLuc RLU 0.02) and BMS-309403 (normalised NLuc RLU 0.04). Treatment with CHIR99021 showed a decrease in Total Tau expression compared to vehicle control, with normalised FLuc RLU of 0.73. PT-2385, Nazartinib and BMS-309403 treatment showed no change in total Tau expression compared to vehicle control (normalised FLuc RLUs 1.08, 1.11 and 0.90, respectively). In case of Eptapirone, total Tau expression was elevated with normalised FLuc RLU of 1.54. Targets of the positively tested compounds are listed in Tab. 2.2. Their chemical structure in App. Fig. A.13. Positive hits with 4R Tau upregulation properties cluster as HDAC inhibitors. All are pan-HDAC inhib-

Table 2.2: Targets of nominated primary screening hits. Nominated primary hit targets, also successively verified for their 4R Tau isoform modulation potential. Cluster of pan-HDAC inhibitors for 4R Tau isoform upregulation (>), combined with either decreasing (<) or steady (=) Total Tau expression relative to vehicle.

Compound	Isoform regulation		Target
	4R Tau	Total Tau	
TSA	> 4R	< Total Tau	pan-HDAC inhibitor
SAHA	> 4R	= Total Tau	pan-HDAC inhibitor
Mocetinostat	> 4R	< Total Tau	HDAC (Class I/IV) inhibitor
Panobinostat	> 4R	< Total Tau	pan-HDAC inhibitor
BMS-309403	< 4R	= Total Tau	FABP3, 4, 5 inhibitor
5-ITU	> 4R	< Total Tau	DYRK1A/GSK3β inhibitor

itors, except for Mocetinostat, with Class I/IV HDACi specificity.
Conducted HTS to investigate *MAPT* exon 10 alternative splicing modulation identified several HDAC inhibitors involved in the process of 4R Tau upregulation. Selective 4R Tau downregulation was contributed to the FABP inhibitor BMS-309403.

2.4 4R Tau expression elevation by HDACi

For verification of nominated hits, I screened selected compounds again under resembling screening conditions. Hence, $MAPT^{\text{EXSISERS}}$ hiPSC derived smNPCs were treated with 1 µM compound over the time course of 72 h. Nominated compounds TSA, SAHA, Mocetinostat and Panobinostat for 4R Tau upregulation properties showed a significant increase in 4R Tau expression relative to vehicle control, as indicated by the initial screening results (App. Fig. A.14). Noticeably, increase in 4R Tau expression was even greater compared to the initial screen, for TSA (normalised NLuc RLU 1.89 ± 0.43), SAHA (normalised NLuc RLU 3.26 ± 0.49) and Mocetinostat (normalised NLuc RLU 2.68 ± 0.20). Panobinostat showed similar increase in 4R Tau expression (normalised NLuc RLU 1.46 ± 0.13), combined with a decrease in total Tau expression (normalised FLuc RLU 0.19 ± 0.02), not seen in the initial screen (Fig. 2.10, App. Fig. A.14). Indatraline, nominated for its potential to increase overall Tau expression, did not show any regulation in Tau upon resembling compound screen (normalised NLuc RLU 0.90 ± 0.04, normalised FLuc RLU 0.90 ± 0.02, Fig. A.14). Hence, Indatraline was not included in any further characterisation.
For further characterisation of the compound with 4R Tau upregulating properties I conducted bioluminescence measurements and cell viability assays to evaluate the response optimum of each individual compound (Fig. 2.11). Greatest 4R Tau upregulation by TSA was shown upon a treatment of a concentration of 0.1 µM (normalised NLuc RLU 2.54 ± 0.07, p-value: ** < 0.01, one-way ANOVA with Bonferroni MCT). Total Tau expression was slightly elevated compared to vehicle control upon 0.01 µM TSA exposure (normalised FLuc RLU 1.57 ± 0.06, p-value: ** < 0.01, one-way ANOVA with Bonferroni MCT, Fig. 2.11a), but was lower than the vehicle control upon treatment with higher concentrations. 4R Tau expression increased with increasing SAHA concentration, whereby, 4R Tau expression was significantly increased upon 0.2 µM SAHA exposure (normalised NLuc RLU 2.29 ± 0.06, p-value: ** < 0.01, one-way ANOVA with Bonferroni MCT, Fig. 2.11b). Total Tau expression was significantly increased

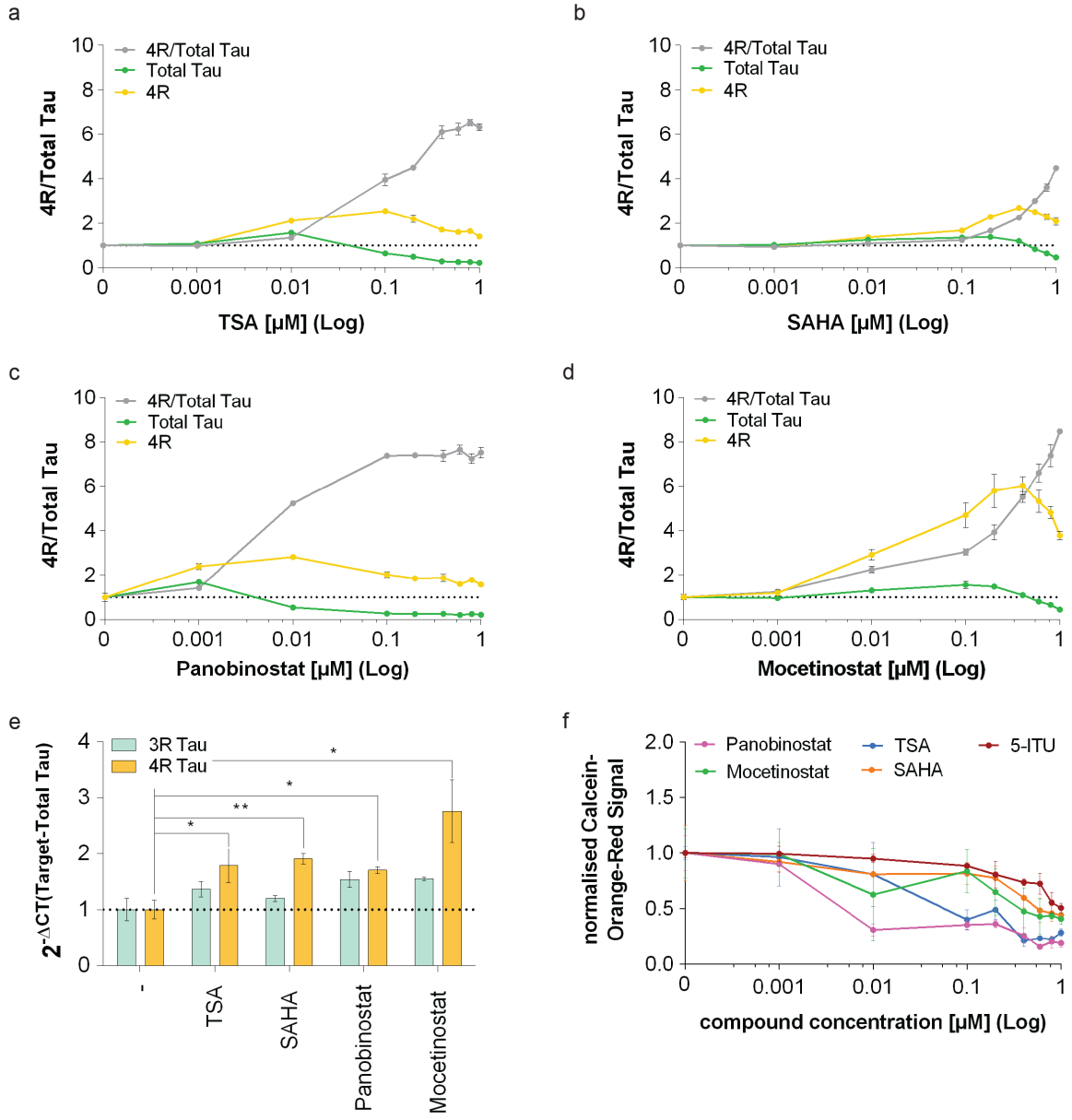

Figure 2.11: *MAPT* alternative splicing modulators. Dose response as a linear-log plot of (a) TSA, (b) SAHA, (c) Panobinostat and (d) Mocetinostat in $MAPT^{\text{EXSISERS}}$ hiPSC derived smNPCs. (a-d) Relative 4R/Total Tau ratio (grey), Total Tau (relative FLuc RLUs, green) and 4R Tau (relative NLuc RLUs, yellow) as a function of increasing compound concentration. (a-d, f) Data show the mean ± SD of a representing experiment of three independent experiments with three technical replica. Selected ANOVA analysis results of Bonferroni MCT are shown. (e) Modulation of the *MAPT* alternative splicing and isoform pattern on a post-transcriptional level in $MAPT^{\text{EXSISERS}}$ hiPSC derived smNPCs upon 0.1 µM TSA, 0.8 µM SAHA, 0.01 µM Panobinostat or 0.4 µM Mocetinostat exposure over 72 h. *MAPT* excluding exon 10 (3R, light blue) and including exon 10 (4R, yellow) mRNA expression. Selected unpaired t-test analysis results of Bonferroni MCT are shown. (f) Cell viability as normalised calcein-orange-red signal after Panobinostat (pink), TSA (blue), 5-ITU (red), Mocetinostat (green) and SAHA (orange) treatment as a function of increasing compound concentration. The black dashed line indicates the vehicle control. Data is normalised to each vehicle control. p-value: * < 0.05, ** < 0.01, *** < 0.001, **** < 0.0001 (detailed statistical results are provided in Supp. Tab. A.4 and Supp. Tab. A.6).

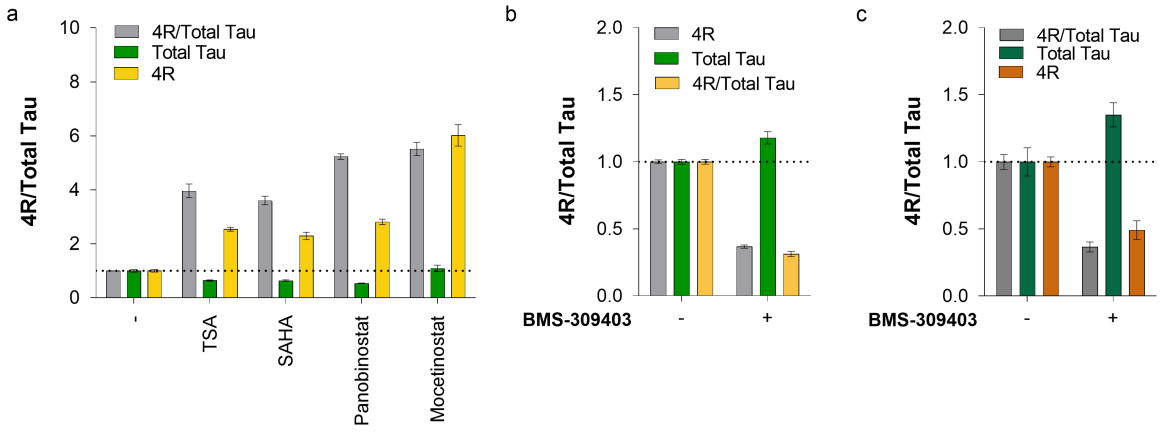

Figure 2.12: 4R Tau regulation corresponding to qRT-PCR data. (a) Bar chart of 4R (relative NLuc RLUs) and Total Tau (relative FLuc RLUs) shown as 4R/Total Tau ratio (bright grey), Total Tau (bright green) and 4R Tau (yellow) as a function of 0.1 µM TSA, 0.8 µM SAHA, 0.01 µM Panobinostat or 0.4 µM Mocetinostat exposure over the time course of 72 h normalised to vehicle control in *MAPT*$^{\text{EXSISERS}}$ hiPSC derived smNPCs. Bar chart of 4R (relative NLuc RLUs) and Total Tau (relative FLuc RLUs) shown as 4R/Total Tau ratio (light grey, dark grey), Total Tau (light green, dark green) and 4R Tau (yellow, orange) as a function of 1 µM BMS-309403 over 72 h normalised to vehicle control in (b) *MAPT*$^{\text{EXSISERS}}$ and (c) *MAPT*$^{\text{IVS10+16EXSISERS}}$ hiPSC derived smNPCs. The black dashed line indicates the vehicle control all values are normalised to.

upon 0.2 µM SAHA exposure with a normalised FLuc RLU of 1.39 ± 0.08 (p-value: * < 0.05, one-way ANOVA with Bonferroni MCT, Fig. 2.11b). Total Tau exposure significantly decreased compared to vehicle control upon 0.8 µM or higher SAHA exposure (normalised FLuc RLU 0.64 ± 0.13, p-value: ** < 0.01, one-way ANOVA with Bonferroni MCT, Fig. 2.11b), coinciding with decreasing cell viability upon higher SAHA exposure (Fig. 2.11f). 4R Tau expression was significantly increased by 0.01 µM Panobinostat exposure (normalised NLuc RLU 2.82 ± 0.10, p-value: * < 0.05, one-way ANOVA with Bonferroni MCT, Fig. 2.11c). Total Tau expression was significantly increased upon 0.001 µM Panobinostat exposure (normalised FLuc RLU 1.69 ± 0.08, p-value: ** < 0.01, one-way ANOVA with Bonferroni MCT, Fig. 2.11c), but decreased with concentrations higher than 0.01 µM. Mocetinostat exposure of 0.4 µM over a time course of 72 h showed an significant increase in 4R Tau expression in MAPT$^{\text{EXSISERS}}$ hiPSC derived smNPCs (normalised NLuc RLU 6.02 ± 0.40, p-value: * < 0.05, one-way ANOVA with Bonferroni MCT, Fig. 2.11d). Total Tau expression was significantly lower than vehicle control upon Mocetinostat concentrations greater than 0.8 µM (normalised FLuc RLU 0.65 ± 0.07, p-value: ** < 0.01, one-way ANOVA with Bonferroni MCT, Fig. 2.11d).
On an mRNA level I was able to show an significant upregulation of *MAPT* mRNA including exon 10, reflecting the 4R Tau isoforms, upon treatment with specific concentrations of compound (Fig. 2.11e). The greatest increase in *MAPT* mRNA including exon 10, was detected upon 0.8 µM Mocetinostat (relative *MAPT* exon 10 including mRNA expression 2.76 ± 0.56, two-tailed p-value: * < 0.05, unpaired t-test, Fig. 2.11e). Bioluminescence data corresponding to the post-transcriptional level are shown in Fig. 2.12a, emblematising the alternative splicing modulation by all compounds in *MAPT*$^{\text{EXSISERS}}$ hiPSC derived smNPCs.
Cell viability of *MAPT*$^{\text{EXSISERS}}$ hiPSC derived smNPCs was reduced by Panobinostat treatment of a concentration of 0.01 µM and greater (relative calcein-orange-red signal 0.31 ± 0.05, Fig. 2.11f). TSA showed reduction of cell viability to under 50% of the vehicle control upon treatment

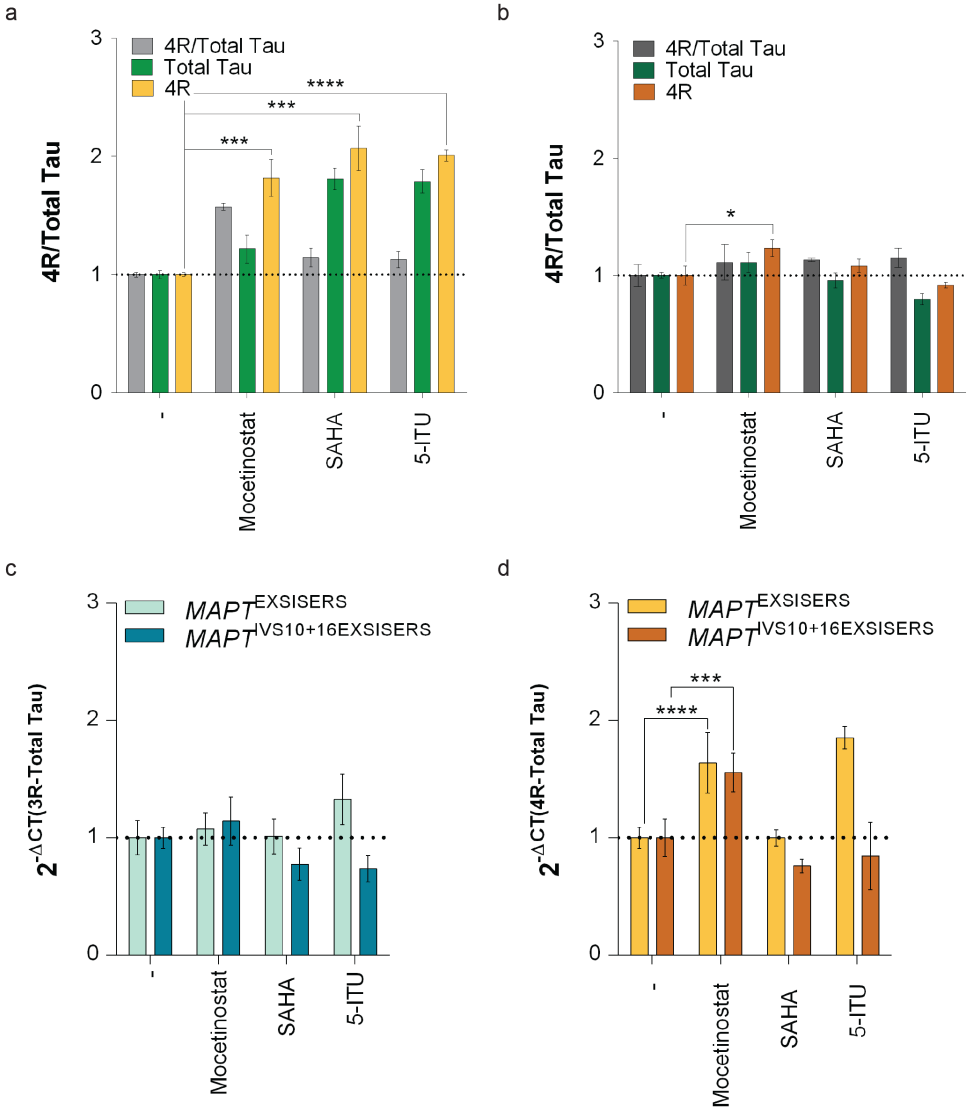

Figure 2.13: Neuronal *MAPT* alternative splicing modulation by HDACi. Bar chart of 4R (relative NLuc RLUs) and Total Tau (relative FLuc RLUs) shown as 4R/Total Tau ratio (light grey, dark grey), Total Tau (light green, dark green) and 4R Tau (yellow, orange) as a function of 0.1 µM of HDAC inhibitor Mocetinostat or SAHA or DYRK1A/GSK3β inhibitor 5-ITU exposure over the time course of differentiation in (a) $MAPT^{\text{EXSISERS}}$ and (b) $MAPT^{\text{IVS10+16EXSISERS}}$ hiPSC derived neurons (d41). Post-transcriptional *MAPT* alternative splicing modulation with mRNA corresponding to (c) 3R Tau (light blue, dark blue) and (d) 4R Tau (yellow, orange) in $MAPT^{\text{EXSISERS}}$ and $MAPT^{\text{IVS10+16EXSISERS}}$ neurons (d41) upon compound exposure relative to vehicle. The black dashed line indicates the vehicle control, all values are normalised to. Data show the mean ± SD of three technical replica (detailed statistical results are provided in Supp. Tab. A.3 and Supp. Tab. A.6).

with concentrations of 0.1 µM and greater (relative calcein-orange-red signal 0.40 ± 0.09, Fig. 2.11f). All other compounds showed a 50% reduction of cell viability with 1 µM treatment. Promising alternative splicing modulation effects shown in hiPSC derived smNPCs raise the question, whether modulation shows an cell type independent regulation. Hence, I differentiated $MAPT^{\text{EXSISERS}}$ and $MAPT^{\text{IVS10+16EXSISERS}}$ into neurons, while concurrently treating the cells with respective compounds. Treatment of $MAPT^{\text{EXSISERS}}$ neurons with HDAC inhibitors Mocetinostat (normalised NLuc RLU 1.81 ± 0.16, two-tailed p-value: *** < 0.001, unpaired

t-test) and SAHA (normalised NLuc RLU 2.10 ± 0.19, two-tailed p-value: *** < 0.001, unpaired t-test) showed a significant increase in 4R Tau isoforms at day 41 of differentiation on a post-translational level (Fig. 2.13a). Treatment of $MAPT^{\text{IVS10+16EXSISERS}}$ hiPSC derived neurons with HDAC inhibitor Mocetinostat or SAHA showed no comparable 4R Tau isoform increase (Fig. 2.13b). Contrary to the regulation of 4R Tau isoform expression, $MAPT^{\text{IVS10+16EXSISERS}}$ showed a comparable increase in 4R corresponding mRNA compared to $MAPT^{\text{EXSISERS}}$ upon Mocetinostat treatment (Fig. 2.13d). No significant increase in exon 10 including mRNA was observed upon SAHA nor 5-ITU treatment coinciding with post-translational results of Tau regulation in $MAPT^{\text{IVS10+16EXSISERS}}$ (Fig. 2.13b, d). On the other hand, treatment of $MAPT^{\text{EXSISERS}}$ with Mocetinostat (relative $MAPT$ exon 10 including mRNA expression 1.63 ± 0.26, p-value: *** < 0.001, two-way ANOVA with Bonferroni MCT) or 5-ITU (relative $MAPT$ exon 10 including mRNA expression 1.85 ± 0.10, p-value: **** < 0.0001, two-way ANOVA with Bonferroni MCT) resulted in a matching increase in 4R responding mRNA on a post-transcriptional level compared to the post-translational level. mRNA corresponding to 3R Tau isoforms did not show any significant regulation upon any compound treatment in both cell lines (Fig. 2.13c).

2.5 4R Tau expression decreased by FABPi

Nominated 4R Tau downregulating compounds of initial screening results of the Repurposing Library were also sought to be verified by screening these selected compounds again under resembling screening condition (Fig. 2.10, App. Fig. A.14). We were able to show 4R Tau expression decrease upon BMS-909403 treatment. Even though, 4R Tau downregulation was less pronounced than indicated by the initial screening data, 4R Tau was significantly decreased (normalised NLuc RLU 0.37 ± 0.01, p-value: ** < 0.01, one-way ANOVA with Bonferroni MCT, App. Fig. A.14). Following up, to analyse 4R Tau regulation further, I conducted a dose response of BMS-309403 in $MAPT^{\text{EXSISERS}}$ and $MAPT^{\text{IVS10+16EXSISERS}}$ hiPSC derived smNPCs (Fig. 2.14). 4R Tau was reduced compared to vehicle control in $MAPT^{\text{EXSISERS}}$ upon BMS-309403 exposure of 0.1 µM and higher, with the most significant decrease at a compound exposure of 1 µM (normalised NLuc RLU 0.37 ± 0.01, p-value: ** < 0.01, one-way ANOVA with Bonferroni MCT, Fig. 2.14a). Total Tau expression was not significantly changed upon

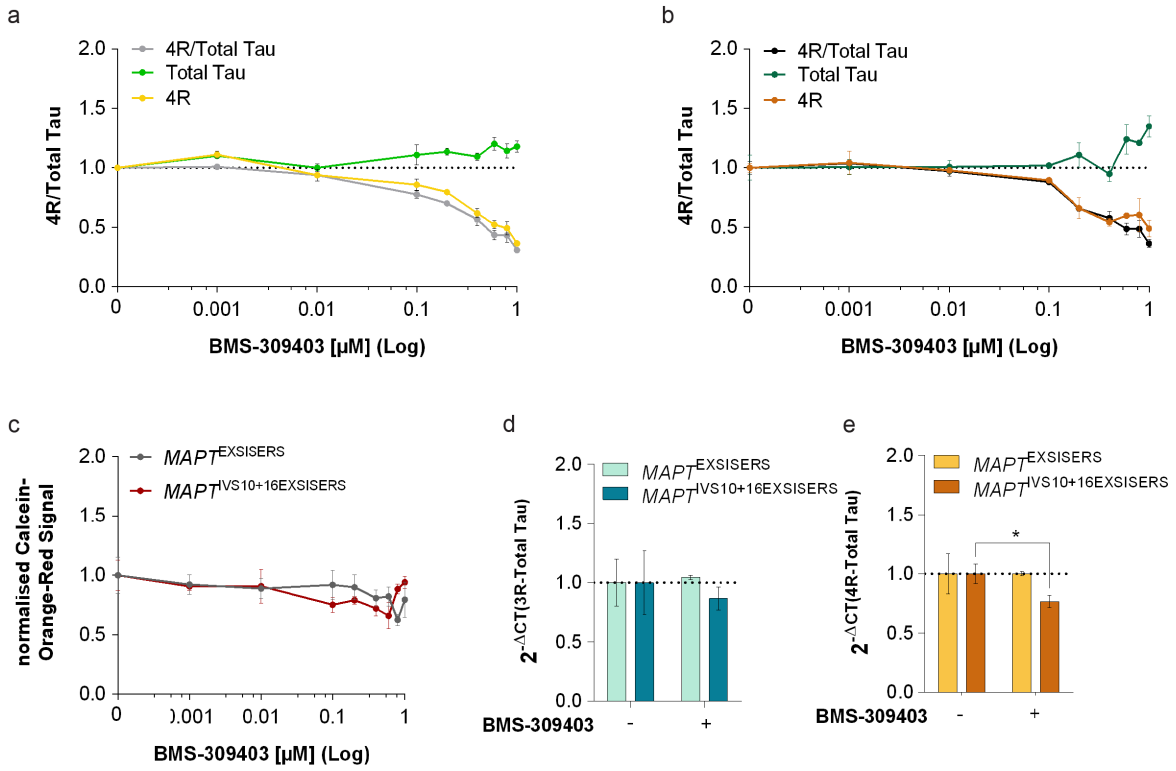

Figure 2.14: 4R Tau isoform downregulation. Dose response as a linear-log plot of BMS-309403 in (a) $MAPT^{\text{EXSISERS}}$ and (b) $MAPT^{\text{IVS10+16EXSISERS}}$ hiPSC derived smNPCs. Relative NLuc (4R) and FLuc (Total Tau) RLUs shown as 4R/Total Tau (grey, black), Total Tau (light green, dark green) and 4R (yellow, orange) as a function of increasing compound concentration. Data is normalised to each vehicle control. (c) Cell viability as normalised calcein-orange-red signal of $MAPT^{\text{EXSISERS}}$ (grey) and $MAPT^{\text{IVS10+16EXSISERS}}$ (red) as a function of increasing BMS-309403. Post-transcriptional (d) 3R Tau corresponding (light blue, dark blue) and (e) 4R Tau corresponding (yellow, orange) *MAPT* mRNA regulation upon 1 µM BMS-309403 treatment over 72 h. The black dashed line indicates the vehicle control, all values are normalised to. Data show the mean ± SD of three biological and technical replica. Selected ANOVA analysis results of Bonferroni MCT are shown: p-value: * < 0.05, ** < 0.01, *** < 0.001, **** < 0.0001 (detailed statistical results are provided in Tab. A.4 and Supp. Tab. A.6).

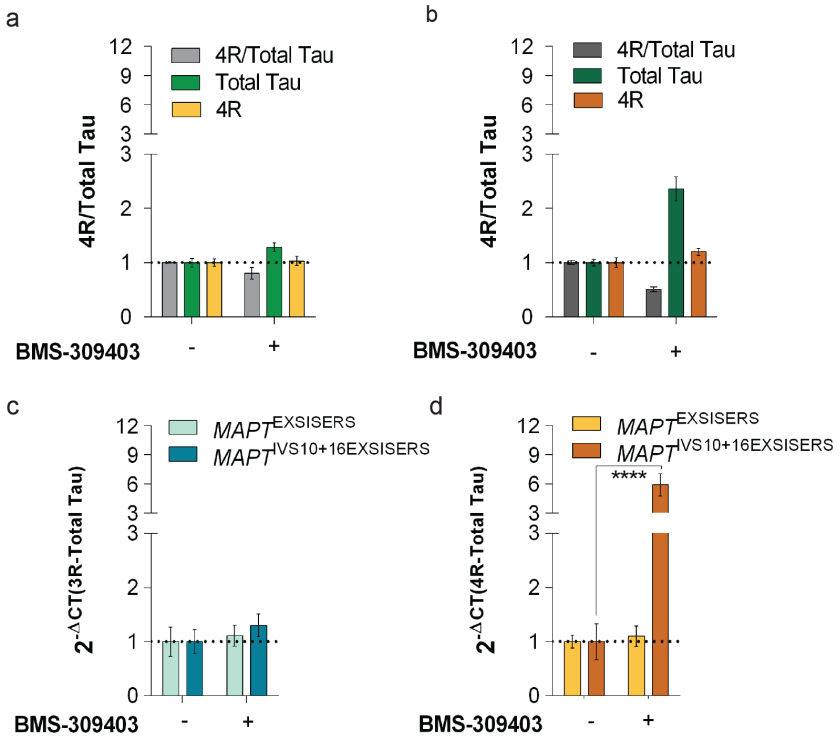

Figure 2.15: Neuronal *MAPT* alternative splicing modulation by FABPi. Bioluminescence measurement of 4R Tau (relative NLuc RLUs) and Total Tau (relative FLuc RLUs) for 4R/Total Tau ratio (bright grey, dark grey), Total Tau (light green, dark green) and 4R Tau (yellow, orange) as a function of 1 µM of FABP inhibitor BMS-309403 exposure of (a) $MAPT^{\text{EXSISERS}}$ and (b) $MAPT^{\text{IVS10+16EXSISERS}}$ hiPSC derived neurons (d41). Post-transcriptional *MAPT* alternative splicing modulation with mRNA corresponding to (c) 3R Tau and (d) 4R Tau in $MAPT^{\text{EXSISERS}}$ (mint green, yellow) and $MAPT^{\text{IVS10+16EXSISERS}}$ (dark green, orange) neurons d41 upon BMS-309403 exposure relative to vehicle control. The black dashed line indicates the vehicle control, all values are normalised to. Data show the mean ± SD of three technical replica. (detailed statistical results are provided in Supp. Tab. A.3 and Supp. Tab. A.6).

BMS-309403 treatment of any concentration. Similar regulation of 4R Tau was shown in $MAPT^{\text{IVS10+16EXSISERS}}$ hiPSC derived smNPCs (Fig. 2.14b). Greatest reduction of 4R Tau was shown upon 1 µM BMS-309403 with normalised NLuc RLU 0.49 ± 0.07. Total Tau was slightly increased upon 1 µM BMS-309403 (normalised FLuc RLU 1.35 ± 0.09). No significant impact on cell viability was detected by any BMS-309403 concentration in both $MAPT^{\text{EXSISERS}}$ and $MAPT^{\text{IVS10+16EXSISERS}}$ hiPSC derived smNPCs (Fig. 2.14c). As the EXSISERS detects changes in isoform expression on a post-translational level, I sought to investigate the alternative splicing modulation also on mRNA level. *MAPT* mRNA corresponding to the 4R Tau isoforms was significantly reduced by 0.77 ± 0.05 fold in $MAPT^{\text{IVS10+16EXSISERS}}$ upon FABP inhibitor BMS-309403 treatment, but had no impact on *MAPT* alternative splicing pattern in $MAPT^{\text{EXSISERS}}$ (two-tailed p-value: * < 0.05, unpaired t-test, Fig. 2.14d, e). Corresponding bioluminescence data specific for the 1 µM BMS-309403 treatment investigated on the post-transcriptional level are shown in Fig. 2.12b, c, emblematising an effect of BMS-309403 treatment on the Tau protein expression in $MAPT^{\text{EXSISERS}}$ and $MAPT^{\text{IVS10+16EXSISERS}}$ hiPSC derived smNPCs.

To evaluate the differences between the two cell models further, I analysed 41 days old hiPSC de-

rived neurons treated with BMS-309403 over the time course of 20 days. FABPi by BMS-309403 showed slight upregulation of the total Tau expression on a mRNA level in $MAPT^{\text{EXSISERS}}$ hiPSC derived neurons, the effect was significantly greater in $MAPT^{\text{IVS10+16EXSISERS}}$ (normalised FLuc RLU 2.36 ± 0.22, two-tailed p-value: *** < 0.001, unpaired t-test, Fig. 2.15c). 4R Tau was slightly increased on a post-translational level upon BMS-309403 exposure in $MAPT^{\text{IVS10+16EXSISERS}}$, but unchanged in $MAPT^{\text{EXSISERS}}$ 41 day old hiPSC derived neurons (Fig. 2.15a, c). FABP inhibitor BMS-309403 showed no impact on *MAPT* mRNA excluding exon 10 in $MAPT^{\text{EXSISERS}}$, but slight increase in $MAPT^{\text{IVS10+16EXSISERS}}$ 41 days old hiPSC derived neurons (Fig. 2.15b). *MAPT* mRNA including exon 10 on the other hand, showed a significant increase in expression in BMS-309403 treated $MAPT^{\text{IVS10+16EXSISERS}}$ hiPSC derived neurons (5.91 ± 1.14, p-value: **** < 0.0001, two-way ANOVA witch Bonferroni MCT, Fig. 2.15d).
BMS-309403 specifically decreases 4R Tau expression of physiological and pathological Tau. Modulation of *MAPT* mRNA including exon 10 upon BMS-309403 treatment was observed in $MAPT^{\text{IVS10+16EXSISERS}}$ but not in $MAPT^{\text{EXSISERS}}$.

2.6 Bioinformatic pathway analysis

The physical and functional associations of TSA, SAHA, Mocetinostat, Panobinostat and BMS-309403 with Tau were assessed using the STITCH and Pathway Studio data base. With our obtained EXSISERS results as basis, I sought to conduct bioinformatic literature mining to propose possible pathways involved in *MAPT* alternative splicing and Tau isoform regulation. Bioinformatic analyses were conducted in collaboration with Dietrich Trümbach. We propose two different protein groups possibly involved in the *MAPT* alternative splicing and, or Tau isoform regulation: HDACs and FABPs (Fig. 2.16). Unbiased bioinformatic analysis identified two clusters of interaction, coinciding with the 4R Tau modulation properties. TSA, SAHA, Mocetinostat and Panobinostat as regulators impact the MAPT alternative splicing process, as much as 4R Tau isoform regulation. This indicates a possible involvement of HDAC in the process. Other proteins show direct interaction by some of the compounds identified to increase 4R Tau expression. Non of those show interaction with all compounds. Nevertheless, especially HDAC3 is apparent to interact with all identified compounds with 4R Tau upregulating properties. This hints towards a connection of HDAC3 in the process of alternative splicing modulation of *MAPT* in a physiological and pathological manner. HDAC6 as the only HDAC has documentation of interacting with Tau. Our EXSISERS based bioinformatic analysis suggest undocumented connections in need to be further investigated.
The second cluster identified by the unbiased bioinformatic pathway analysis is comprised of FABP4, FABP5 and PPARγ. FABP4 and FABP5 are indicated to be inhibited by BMS-309403. The 4R Tau downregulating properties of BMS-309403 in a physiological and pathological state suggest a so far not documented involvement of FABPs in the process of 4R Tau modulation. Connections specifically to *MAPT* and Tau were not detected, emphasising the novelty of gained knowledge.
Unbiased data mining gives reason to believe, that HDACs and FABPs are connected in the process of *MAPT* alternative splicing.

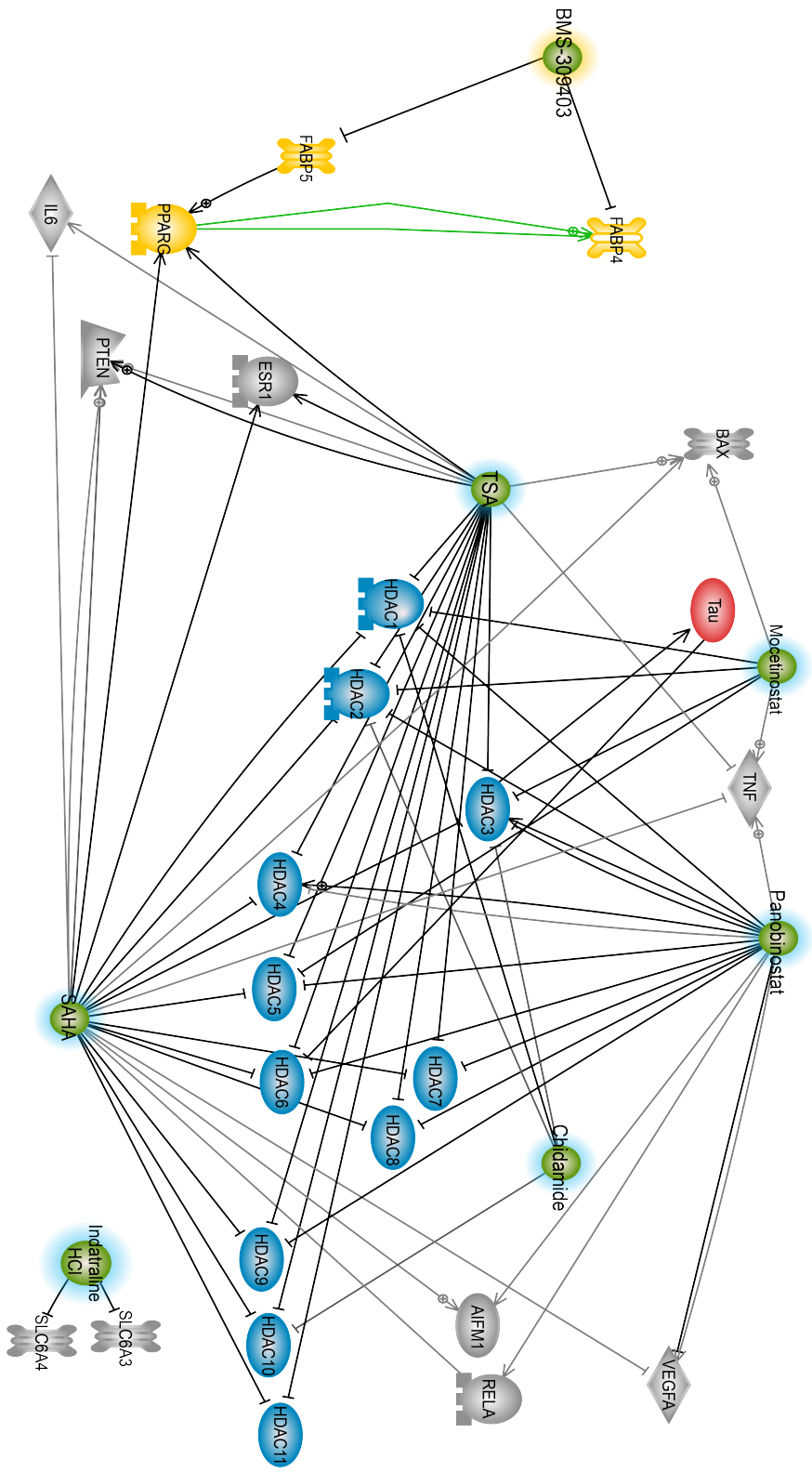

Figure 2.16: Pathway analysis. The pathways involved in *MAPT* alternative spicing and 4R Tau isoform regulation were deducted by *in silico* literature mining. Network consolidation was performed by verification of all connections in the published literature. The compounds identified to modulate 4R Tau isoform expression are shown in green. The histone deacetylase (HDAC) cluster is shown in blue, the fatty acid binding protein (FABP) cluster in yellow. Shown interactions are combined from analysis conducted using the STITCH and Pathway Studio data base, original data sets are show in Supp. Fig. A.19 and Supp. Fig. A.20. The original bioinformatic analysis was performed by Dietrich Trümbach.

3 Discussion

Alterations in *MAPT* exon 10 splicing are prone to result in an excess of 4R Tau. This excess, a result of increased *MAPT* exon 10 inclusion, defines Tau as a pathological feature of several neurodegenerative diseases, tauopathies as FTLD and AD. The high occurrence of aberrant *MAPT* exon 10 alternative splicing associated to tauopathies emphasises the necessity to understand not only the pathological but also the physiological mechanisms of *MAPT* alternative splicing. Nevertheless, deciphering the alternative splicing mechanisms encountered several limits, with a discrepancy in splicing mechanisms involved between rodents and humans as much as vulnerable isoform detection in hiPSCs. Prior work struggled to implement disease models with pronounced Tau pathology and species-specific alternative splicing machineries, with a lot of preclinical work not able to be translated into clinical significant results.
In this work, I closed the gap of insufficient *MAPT* exon 10 alternative splicing models by generating the $MAPT^{\text{EXSISERS}}$ and $MAPT^{\text{IVS10+16EXSISERS}}$ hiPSC as human based models. The hiPSC based models allowed the monitoring of *MAPT* exon 10 based alternative splicing modulation in a HTS manner and longitudinal monitoring. With this cell models in place, I was able to decipher the complexity of *MAPT* exon 10 alternative splicing and translational regulation of the mature *MAPT* mRNA further. These results indicate a recruitment of a different spliceosome machinery in the pathological Tau environment, an involvement of HDACs in *MAPT* alternative splicing processes in a physiological state as much as an involvement of FABPs in the translational regulation of mature *MAPT* mRNA.

3.1 Longitudinal Tau isoform monitoring

A recurring problem is the lack of animal models exhibiting neuropathological profiles matching pathological changes found in the human brain. Further accompanied by the different splice mechanisms in place in rodents, compared to humans. We took advantage of the latest development of biotechnology for alternative splicing monitoring combined with the benefits of hiPSC research.
Adaptation of the highly sensitive EXSISERS to study the alternative splicing of exon 10 of *MAPT* by applying the CRISPR/Cas9 system to generate a $MAPT^{\text{EXSISERS}}$ for physiological Tau studies and $MAPT^{\text{IVS10+16EXSISERS}}$ for tauopathy associated pathological Tau was successful. With generation of the two EXSISERS hiPSC models, I was able to show a successful introduction and monitoring of Tau isoforms, already in immature hiPSCs and smNPCs, but also showed a longitudinally monitored Tau isoform expression in neuron cultures up to day 100. A clear difference of the tauopathy associated IVS10+16 c > t point mutation was shown with expected 4R Tau upregulation, when introduced in an hiPSC line with a healthy genetic background also reflected by the EXSISERS. Hence, adaptation of the EXSISERS as a human based disease modelling strategy was proven. Furthermore, while detection of isoform resembling mRNA was reported to be able to detect in healthy hiPSCs and derivates, detection on a post-translational level was unreliable and methods so far too insensitive to pick up the low levels of isoform expression in the immature hiPSC and derived neurons [221]. Similar results were shown in our longitudinal studies, post-transcriptional detection of 3R and 4R isoform

resembling mRNA did not match the immunoblotting results, showing mainly the fetal 0N3R isoform, but relative to non 4R Tau isoform expression. EXSISERS allowed detection of the post-translational expression of the 4R Tau isoforms and total Tau by luminescence showed matching longitudinal regulation, proving the improvement of isoform studies by EXSISERS. Also giving reason for a adaptive system responding according to the endogenous expression pattern in hiPSCs and derivates.

3.2 Early 4R Tau dependent maturation in neurons

Development of the MAPT$^{\text{EXSISERS}}$ and *MAPT*$^{\text{IVS10+16EXSISERS}}$ models allowed us to investigate physiological and pathological Tau in not only an alternative splicing setting, but also on a morphological level. By investigation of the neuron complexity I identified a significant difference between 41 days old *MAPT*$^{\text{EXSISERS}}$ and *MAPT*$^{\text{IVS10+16EXSISERS}}$. *MAPT*$^{\text{IVS10+16EXSISERS}}$ exhibiting the tauopathy associated point mutation IVS10+16 c > t showed a complexer neuritic tree compared to *MAPT*$^{\text{EXSISERS}}$ and parental cell line, with no difference in total length between the two parental cell lines. Suggesting a maturity effect by increased 4R Tau expression. During neurogenesis, neurons emerge from stem cells, differentiating to neuronal precursors, to immature neurons, with little to no dendritic trees [243]. In the process of maturation, neurons develop a more and more complex dendritic tree, with higher degree of branches. Furthermore, with increasing maturity, proliferation decreases, eventually entering a state of post mitotic cell state [243]. 4R Tau was shown to suppress proliferation, promoting neuronal differentiation, further strengthening the maturity phenotype detected in MAPT$^{\text{IVS10+16EXSISERS}}$ hiPSC derived neurons [244–246]. Further indication of 4R Tau based maturation in a hiPSC derived neuron setting, was given, when investigating neuronal excitability of patient hiPSC derived neurons bearing the tauopathy associated intronic IVS10+16 c > t point mutation [247]. Neuronal excitability being an indicator of neuron maturity. Investigation of our cell model has advantage over the patient derived neurons, as our system shows clear IVS10+16 c > t mutation associated maturation effect, on an otherwise genetically unobtrusive background.
The decrease in total length detected in *MAPT*$^{\text{EXSISERS}}$ compared to both parental lines may be caused by the extensive experimental interventions involved in the EXSISERS KI pipeline. Parental lines investigated in this context were not isogenic hiPSCs controls, as the process of passing through the KI pipeline is laborious and extraordinarily expensive, which is not possible to circumvent based on technical limitations. Due to this, the difference between EXSISERS KI cell line *MAPT*$^{\text{EXSISERS}}$ and the parental cell line HPSI0614i-uilk_2 is rather cause of the KI pipeline than a general KI effect. Small difference in overall neuron differentiation efficiency and complexity between these two cell lines strengthen this observation. *MAPT*$^{\text{IVS10+16EXSISERS}}$ compared to the parental cell line HPSI0514i-vuna_3 showed greater differences in total length and overall complexity. Considering the pipeline having a decreasing effect on total length, increase observed in *MAPT*$^{\text{IVS10+16EXSISERS}}$ is most likely result of the intronic IVS10+16 c > t point mutation. *MAPT*$^{\text{IVS10+16EXSISERS}}$ showing an increase in maturity when compared to either *MAPT*$^{\text{EXSISERS}}$ and the parental cell lines.
Hence, complexity, and subsequent maturity is based on an increased 4R Tau isoform expression, present in the *MAPT*$^{\text{IVS10+16EXSISERS}}$, observed on post-transcriptional and post-translational level.

3.3 *MAPT*$^{\text{EXSISERS}}$ for HTS

Pharmacological screening of ~1,500 FDA approved compounds in *MAPT*$^{\text{EXSISERS}}$ hiPSC derived smNPCs showed applicability of the EXSISERS in stem cell derivates for HTS on a technical basis. Detection of the already published 4R isoform increasing compounds Digoxin and Digitoxigenin was possible. Nevertheless, the contradictory results from primary screen to verification, as much as partial rerun of the library screen, indicated a malfunction of the library screen in general. Absolute NLuc and FLuc RLUs of the screen were 10-fold lower than the absolute RLUs measured in the Broad Repurposing Library screen of over 5,000 compounds. Additionally, differences in NLuc and FLuc brightness were not reflected in the measured absolute RLUs screening the small library, also hinting towards a malfunction. Screening of the Broad Repurposing Library on the other hand, using the same conditions and reporter cell line, showed expected relation between absolute NLuc and FLuc values reflecting the different brightnesses of the two luciferases, indicating a working screen on a technical site. Furthermore, a magnificent increase in all absolute RLUs neglecting hit nomination below the noise threshold was shown. Applicability of the EXSISERS on a hiPSC background was also strengthened by positive verification of mostly all nominated primary screening hits. Targets of nominated primary screening hits with 4R Tau increasing properties cluster all as HDAC inhibitors, validated the screening results further. Nominated primary hits for 4R Tau isoform downregulation were more diverse in their targets, not following a specific pattern. Diversity in targets of primary 4R Tau isoform depressing hits and subsequent failed validation of all but one hit, may also be result of detection limitations. Strong downregulation of 4R Tau is necessary to have a lasting impact on the sensitive luciferase system. Discrepancy between the primary screen of the Broad Repurposing Library and subsequent verification assessment may also be based on a timing issue. Downregulation of 4R Tau and luciferase stability is time dependent, hence, downregulation is harder to detect confidently. Thus, EXSISERS and luciferase systems are more precise in nomination of upregulating modulators, modulators depressing the EOI resulting in a referring protein isoform are to be screened with intense care, to verify and isolate the hits.

3.4 HDAC mediated *MAPT* exon 10 alternative splicing

HDACs in a tight regulation with HATs are epigenetic modifiers directly or indirectly mediating neuronal-specific, immune-specific and tissue-specific gene expressions, so far known to be mediated mainly by histone acetylation [161]. SAHA, TSA and Panobinostat are known pan-HDAC inhibitors and Mocetinostat a Class I and IV HDAC inhibitor. Within my work, I observed greater *MAPT* exon 10 inclusion in *MAPT*$^{\text{EXSISERS}}$ hiPSC derived smNPCs and neurons upon SAHA, TSA, Panobinostat or Mocetinostat mediated HDACi. Robust dose response fitting of the detected drugs is pivotal for the definition of accurate drug vulnerabilities. We identified a novel alternative splicing pathway, not described before. Pharmacological screening identified a HDAC dependent 4R Tau regulation, able to be verified in *MAPT*$^{\text{EXSISERS}}$ smNPCs and 41 days old neurons. Considering the target documentation of the verified HDAC inhibitors, alternative splicing may involve one or more of the Class I and/or IV HDACs.
Bioinformatic analysis showed connection of all compounds with HDACi properties to Class I HDAC, HDAC3, also showing interaction with Tau. With its predominant location in the nucleus and the observed effect by Mocetinostat HDAC3 shows great indication of connection to the physiological *MAPT* exon 10 alternative splicing process. Further investigations are crucial for a clear identification. All other HDACs identified in the bioinformatic pathway analysis

showed no connection to all compounds nor Tau. Possibility is given, that I identified a novel pathway, with no previous literature recognition. Hence, a further investigation identifying the precise pathway, connecting *MAPT* alternative splicing and HDACs, is indispensable.

3.4.1 Alteration in spliceosome recruitment in tauopathies

Post-transcriptional and post-translational expression of the mRNA or protein corresponding to the 4R Tau isoforms in $MAPT^{\text{EXSISERS}}$ hiPSC derived smNPCs showed a reciprocal regulation on both levels, manifesting the hypothesis of HDAC related alternative splicing regulation of *MAPT* exon 10. Cell viability reduction by increasing concentration of any HDAC inhibitor may be attributed to the non-selective inhibition of HDAC activity, also impairing other cell relevant processes. TSA previously reported to inhibit cell proliferation, cell cycle arrest and subsequent cell apoptosis, greatly diminishing cell viability with increasing concentration, indicates high stress upon HDACi [248–250]. Elevated total Tau expression in 41 days old $MAPT^{\text{EXSISERS}}$ hiPSC derived neurons compared to smNPCs may be based on the overall difference in maturity. Over the time course of differentiation Tau is ascending, a pattern also detected in both EXSISERS models when differentiated into neurons over a timespan of 100 days. Similar modulation of *MAPT* alternative splicing and Tau isoform modulation by the HDAC inhibitors was shown in 41 day old $MAPT^{\text{EXSISERS}}$ hiPSC derived neurons, with physiological Tau expression pattern. Thus, indicating a clear alternative splicing modulation in a direct or indirect manner by Class I and IV HDACi, indifferent in both maturity stages. Only exception in pattern similarity between post-transcriptional and post-translational regulation by HDACi was shown by treatment with the pan-HDAC inhibitor SAHA. Despite visible increase in 4R Tau expression based on NLuc read out, no elevation in exon 10 including *MAPT* mRNA was shown. Different regulation of the well studied HDAC inhibitor may be excluded, due to shown alternative splicing modulation by HDACi. Indifferent expression of exon 10 including *MAPT* mRNA may rather be a result of a technical error. Regardless of presented results by samples obtained in the same differentiation, samples were harvested from two different wells to obtain enough sample material for further experimental evaluation. Technical errors may have occurred treating the cells, used for post-transcriptional modulation by SAHA mediated HDACi. Impact of SAHA on NLuc modulating the substrate catalysation is not to be considered possible. For that to be true, SAHA is necessary to substitute as a substrate of NLuc, competitively binding NLuc instead of furimazine. Considering the chemical structure of furimazine and SAHA, SAHA does not qualify as substrate substitute to block furimazine binding. Similarity in chemical structure between the HDAC inhibitors investigated, specifically comparing TSA and SAHA, underline the technical error. Blockage of furimazine binding to NLuc would be similar by TSA and SAHA. Furthermore, SAHA catalysation would not result in light emission, detectable in conducted bioluminescence measurement. Strengthening the technical issue reasoning, absent exon 10 inclusion coincides with absent NLuc expression, hence, no bioluminescence measurement. Furthermore, SAHA mediated HDACi in $MAPT^{\text{EXSISERS}}$ hiPSC derived smNPCs showed alternative splicing modulation reciprocally translated in protein isoform expression, similar to patterns observed for all other HDAC inhibitors investigated in hiPSC derived smNPCs and neurons.
Contrary to $MAPT^{\text{EXSISERS}}$ hiPSC derived neurons, $MAPT^{\text{IVS10+16EXSISERS}}$ showed no modulation of 4R Tau by HDACi. Post-translational indifference by any of the HDAC inhibitor treatments in $MAPT^{\text{IVS10+16EXSISERS}}$ hiPSC derived neurons may be caused by recruitment of different splicing factors usually involved in physiological *MAPT* expression. Hence, due to

the destabilisation of the stem loop by the point mutation, a different splice machinery may be in place. Indication on a different splice machinery in place gives the loss of the strong ISS placed in the stem loop, destabilised by the intronic point mutation IVS10+16 c > t. The ISS interferes with the pairing of snRNA U1, weakening exon 10 inclusion under physiological conditions. By IVS10+16 c > t, the ISS is disrupted, increasing *MAPT* exon 10 inclusion with stronger snRNA U1 binding [74].
Indifferent response by compound treatment may also be based on a general higher expression of 4R Tau and therefore a saturation in 4R Tau expression in $MAPT^{\text{IVS10+16EXSISERS}}$ hiPSC derived neurons. Plateau in 4R Tau corresponding mRNA was also detected in the longitudinal monitoring of Tau isoform expression in $MAPT^{\text{IVS10+16EXSISERS}}$, strengthening the hypothesis of plateau reached, with no further impact on expression by exon 10 alternative splicing modulating compounds.
Several protein-protein interactions were observed between HDACs and SRSF in connection of splice factor deacetylation [174]. *MAPT* exon 10 inclusion in $MAPT^{\text{EXSISERS}}$ hiPSC derived smNPCs and neurons may be affiliated with the acetylation of splice factors involved in *MAPT* exon 10 inclusion. Furthermore, acetylation was shown to stabilise hnRNPs. HnRNPE2 and hnRNPE3 are already indicated to take part in the regulation of *MAPT* exon 10 inclusion [70, 71]. Hence, stabilisation of hnRNPE2 and hnRNPE3 by acetylation may cause increase in *MAPT* exon 10 inclusion in $MAPT^{\text{EXSISERS}}$ hiPSC derived smNPCs and neurons. Alternative splicing modulation of MAPT exon 10 by hnRNPE3 is mediated by binding to the 5'-ccc-3' sequence located in the ISE downstream of exon 10. Steric competitive binding of hnRNPE3 to the ISE may also be cause of undetected changes in *MAPT* exon 10 alternative splicing modulation in $MAPT^{\text{IVS10+16EXSISERS}}$ hiPSC derived neurons. Competitive binding may only occur with an intact ISS. *MAPT* exon 10 inclusion upon HDACi may occur due to a advantage of hnRNPs promoting exon 10 inclusion by protein stabilisation in comparison to hnRNPs and splice factors binding to the ISS. Thus, stabilisation of hnRNPE2 and hnRNPE3 by acetylation upon HDACi may contribute to the increased *MAPT* exon 10 inclusion under physiological conditions, but may also explain ineffective splice modulation by HDACi in a pathological state. Moreover, in FTLD-Tau pathology context, interaction of hnRNPE2 with exon 10 was shown, also strengthening the hypothesis of higher binding of hnRNPE2 and hnRNPE3 to the ISE in case of disturbed ISS [72].

3.4.2 HDACi as neurodegenerative disease treatment

Previously reported interest in the investigation of HDACi in context of neurodegenerative disease therapy and specifically AD, affirms given relevance of HDAC in tauopathy pathology. Focus being mainly the clearance of Aβ plaques in AD pathology, without investigating Tau pathology, despite Tau dysfunction and aggregation occurring decades prior to clinical symptom onset. Moreover, isolated investigation of only Aβ or Tau in a therapeutic context moving into clinical trials is not advisable, considering the significant crosstalk between Aβ and Tau [251, 252]. Recent investigation implemented Aβ involvement in Tau uptake in neurons, with a more severe pathology as a result [253]. Several lines of evidence support the direct interaction between Aβ and Tau, even though the molecular mechanism of crosstalk is still mostly elusive. We present further reason for investigation, for successful implementation of pharmacological therapy opportunities for AD and other tauopathies. Investigation of TSA and SAHA showed beneficial effect by HDACi in AD models, with Aβ clearance and memory improvement, but failed in transition from mouse model to human clinical trial [184, 191]. We show an involvement

of Class I and/or Class IV HDACs in the context of *MAPT* exon 10 alternative splicing. Contradictory to reported beneficial effect, recommanding HDACi as a potential therapeutic target for AD and other neurodegenerative diseases with Tau pathology, I showed increase in 4R Tau isoforms upon HDACi. Selective alternative splicing modulation in favour of *MAPT* exon 10 inclusion and subsequent 4R Tau isoform increase is to be viewed critically in the context of tauopathy development. For one, alternative splicing modulation shifting to a 4R Tau isoform increase contributes to the already pathological state of Tau imbalance, increasing rather than decreasing the difference in expression for Class I and II tauopathies. HDACi may only be considered as therapy for Class III tauopathies with increased 3R Tau expression, counteracting the imbalance by shifting alternative splicing into favouring *MAPT* exon 10 inclusion. With the pathological hallmark of hyperphosphorylation in mind, 4R Tau has a higher tendency of hyperphosphorylation and subsequent accumulation in NFTs [36, 37, 109]. By alteration of the alternative splicing machinery in place, responsible for *MAPT* exon 10 in- or exclusion in favour of inclusion of exon 10, hyperphosphorylation may also be an issue, rather implementing than rescuing tauopathy pathology. Hence, when considering HDACi as a therapeutic approach for AD and other tauopathies, alternative splicing and potential alterations in spliceosome recruitment for *MAPT* exon 10 splicing shall be considered and not neglected in *in vivo* studies leading to clinical trials.

3.5 FABP5i mediated *MAPT* translational initiation regulation

Several severe tauopathies are characterised by the dysregulation of *MAPT* alternative splicing in favour of inclusion of exon 10 resulting in an imbalance between 3R and 4R Tau. Hence, understanding the regulation of *MAPT* from its gene expression up to its post-translational modulation is crucial to find a target for potential therapy.
Post-transcriptional regulation of *MAPT* mRNA was mainly investigated in context of microRNA interference in Tau expression [254, 255]. By identification of BMS-309403 as a 4R Tau isoform modulator, I shed some new light on a different translational regulation pathway.
Post-transcriptional *MAPT* regulation in hiPSC derived smNPCs upon BMS-309403 showed a clear difference between the two investigated cell models. $MAPT^{\text{EXSISERS}}$ showed no post-transcriptional regulation upon BMS-309403 treatment. Yet, *MAPT* exon 10 including mRNA was decreased in $MAPT^{\text{IVS10+16EXSISERS}}$ hiPSC derived smNPCs upon treatment. Interestingly, while I detected a different post-transcriptional expression of *MAPT* exon 10 including mRNA, post-translational regulation was similar in both cell models. 4R Tau isoforms showed a dose-dependent downregulation without significantly impacting the total Tau expression. Corresponding to the detected differences in alternative splicing regulation upon HDACi in $MAPT^{\text{IVS10+16EXSISERS}}$ hiPSC derived neurons, BMS-309403 also indicates a recruitment of a different spliceosome. Alternative splicing may be altered by BMS-309403 due to its action as FABP inhibitor. BMS-309403 targets FABP3, 4, 5, but based on the expression pattern in the brain, FABP3 and FABP5 and their downstream targets may be considered to influence Tau modulation upon BMS-309403 mediated FABPi. PPARγ was shown to link the transcriptional and alternative splicing regulation by interaction with a splicing factor [256]. Thus, increased *MAPT* exon 10 including mRNA may be due repressed interaction of PPARγ with certain splicing factors upon BMS-309403 treatment. Possible interaction partners of splicing factors involved in the exclusion of *MAPT* exon 10 may be SRSF3, SRSF4, SRSF6, SRSF7 and SRSF11 [35]. The specific interaction, including other factors involved in the altered spliceosome interacting with PPARγ require further investigation. General involvement of PPARs in the alternative

splicing process of Tau may be unlikely, reason being an unchanged *MAPT* alternative splice pattern upon BMS-309403 in $MAPT^{\text{EXSISERS}}$ hiPSC derived smNPCs.
Discrepancy in the post-transcriptional but not on post-translational level in $\text{MAPT}^{\text{EXSISERS}}$ and $MAPT^{\text{IVS10+16EXSISERS}}$ hiPSC derived smNPCs by BMS-309403 manifests a modulation of BMS-309403 on a translational regulation level. Several indications of FABPs and PPARs in context of translational initiation were made. PPARβ/δ was shown to regulate the human *sirtuin-1 (SIRT1)* gene known for its capacity to deacetylate AMPK. By deacetylation, AMPK activity increases [257]. Activation of AMPK showed decreased activation of several protein kinases in the mammalian target of the mTOR/Akt pathway as evidenced by reduced phosphorylation of PKB and eukaryotic initiation factor eukaryotic initiation factor 4E (eIF4E)-binding protein [258].
FABP5 may also regulate mRNA translational independent of the PPAR pathway. FABP5 KD showed an PPAR independent pathway, including an increase in phosphorylated AMPK [259]. Increased phosphorylation and therefore, activated AMPK may be the regulating pathway in which, translational initiation of *MAPT* is altered upon BMS-309403 treatment. This suggests that higher amount of phosphorylated AMPK inhibits the mTOR/Akt pathway mediated translational initiation by inhibiting mTOR Complex 1 (mTORC1). Inhibition is mediated by phosphorylation of raptor upstream of the eIF4E complex formation for translational initiation [259, 260]. Recent data investigating the regulation of hypoxia-inducible factor-1 α connected FABP5 to translational regulation [261]. Strengthening the hypothesis of a novel signalling pathway involving FABP5 in the regulation of translational regulation independent of PPARs. Differences in observed post-transcriptional and post-translational regulation of the alternative splicing and isoform expression may therefore be connected to an inhibition of the mTOR/Akt pathway mediated translational initiation and elongation.
BMS-309403 treatment of hiPSC derived neurons showed an upregulation of *MAPT* exon 10 including mRNA in $MAPT^{\text{IVS10+16EXSISERS}}$ but no indication of 4R Tau corresponding mRNA in $MAPT^{\text{EXSISERS}}$. A trend towards increasing *MAPT* exon 10 excluding mRNA was shown upon BMS-309403 treatment in $MAPT^{\text{IVS10+16EXSISERS}}$. In doing so, on a protein level total Tau was increased but 4R Tau expression remained similar to the vehicle control. No modulation of alternative splicing nor protein expression in comparison to the vehicle control was shown in $MAPT^{\text{EXSISERS}}$. Even though, a slight trend towards increased total Tau may be apparent. Coinciding with the results in hiPSC derived smNPCs, neurons bearing the intronic IVS10+16 c > t point mutation show no correlation between the mRNA levels and protein levels of the respective isoforms. Contradictory to the post-transcriptional regulation in $MAPT^{\text{IVS10+16EXSISERS}}$ hiPSC derived smNPCs, regulation of *MAPT* exon 10 including mRNA in neurons was upregulated. Differences may be attributed to an effect of BMS-309403 on differentiation in itself, potentially affecting $MAPT^{\text{IVS10+16EXSISERS}}$ more significantly than $MAPT^{\text{EXSISERS}}$. Complexity and hence, increased maturity of the $MAPT^{\text{IVS10+16EXSISERS}}$ hiPSC derived neurons in itself were also shown by Sholl analysis. BMS-309403 possibly enhances the observed maturity further. Impact of BMS-309403 on mRNA translational regulation was evident in smNPCs and neurons. HiPSCs and derived neurons remain rather immature in their epigenetic profile. The epigenetic imprint is lost during the reprogramming process. $MAPT^{\text{IVS10+16EXSISERS}}$ by bearing the IVS10+16 c > t point mutation already show a greater maturity compared to $MAPT^{\text{EXSISERS}}$. This difference makes them potentially more sensitive to the impact of BMS-309403 on differentiation. This might be due to already shifted cell homeostasis. Hypothesis of BMS-309403 affecting the differentiation state of hiPSC derived neurons is strengthened by the observation of increased total Tau expression with also elevated 4R Tau isoform expression, considering the

relation between BMS-309403 and vehicle in $MAPT^{\text{IVS10+16EXSISERS}}$ hiPSC derived smNPCs and neurons. The effect was not as evident in $MAPT^{\text{EXSISERS}}$ hiPSC derived neurons, only showing a trend towards increased total Tau expression upon BMS-309403 treatment.
Hence, indifferent post-transcriptional level upon BMS-309403 in $MAPT^{\text{EXSISERS}}$ hiPSC derived smNPCs and neurons strengthens the evidence of hypothesised alteration in spliceosome recruitment in $MAPT^{\text{IVS10+16EXSISERS}}$, while suggesting a PPAR involvement in alternative splicing in pathogenic Tau. Furthermore, BMS-309403 showed impact on the mRNA translation regulation in both cell lines in favour of reduced 4R Tau isoform expression, indicating FABP5 as possible mediator of *MAPT* translational regulation in physiological and pathological state. Although the detailed molecular mechanism of FABP contribution to the translational regulation of Tau remains an open question, investigation of the alternative splicing on a post-translational level using the EXSISERS helped to give indication on translational regulation of *MAPT*. This gives a basis to decipher the aberrant regulation of pathological Tau further. With our system I was able to show a novel level of regulation involved in pathological *MAPT* not possible to show with the methods commonly used for protein detection. Previous HTSs investigating the *MAPT* alternative splicing modulation, on the basis of minigenes, were able to detect Digitoxigenin and Digoxin. Minigene investigations also showed 4R Tau upregulation, but were restricted to the alternative splicing modulator identification [242]. This expanse the advantages of using the EXSISERS over minigenes as a reporter based model to decipher the regulation of *MAPT* and Tau regulation in a physical and pathological state.

4 Conclusion and Outlook

With adaptation of the EXSISERS system for hiPSC application, I sought to establish a human cell model for *MAPT* exon 10 alternative splice modulation. Using the cell model for HTS helped to identify underlying process in place regulating the isoform expression in a physiological and pathological state. I established a pipeline for CRISPR/Cas9 mediated KI of the EXSISERS for alternative splicing modulation investigation in a HTS manner. In this context, I adapted the pipeline to fit the requirements of hiPSCs and *MAPT* studies. Pipeline adjustments were made, to conquer cell line specific silencing effects of the EF1α promoter driving the PuroR cassette. Two EXSISERS hiPSC lines were generated one representing the physiological state, the other bearing the tauopathy associated intronic point mutation IVS10+16 c > t.
Adaptation of the EXSISERS into hiPSC was verified by longitudinal isoform monitoring under physiological and pathological Tau conditions represented by our two EXSISERS hiPSC models. I observed direct correlation between mRNA and protein levels, with increased 4R Tau expression corresponding with the pathological state. Observed morphological differences in neuron complexity in hiPSC derived neurons were identified in neurons bearing the tauopathy associated intronic point mutation IVS10+16 c > t, causing a 4R Tau mediated maturity effect. Modulation of *MAPT* exon 10 alternative splicing or translational regulation under the focus of complexity regulation may be an aspect of future work. Analysis may give indication on the potential of pharmacological modulating the morphology with beneficial effects for further therapeutic applications.
By HTS I identified several HDAC inhibitors and BMS-309403 as modulators of 4R Tau expression. HDACi modulated *MAPT* exon 10 alternative splicing under physiological conditions, not detected under pathological conditions. An alteration in spliceosome recruitment between the physiological and pathological condition was indicated to be causative. We hypothesise an involvement of HDACs in physiological *MAPT* alternative splicing, abolished under pathological conditions. More investigations shall be conducted to decipher the specific Class I or Class IV HDACs involved. Identification of the specific process may not only serve as a gain of knowledge in physiological *MAPT* exon 10 alternative splicing, but also give prospective on potential therapeutic targets to modulate alternative splicing benefiting the tauopathy pathology. Further investigation in the specificity of the HDACi shall be focus of future work. Furthermore, identification of the specific HDACs involved in the process demand the development of HDAC specific inhibitors. While bioinformatic analysis suggested involvement of HDAC3 in the process of *MAPT* exon 10 alternative splicing processes. The use of pan-HDAC inhibitors influences a great deal of processes, not only the pathway of interest. Considering the many functions of HDACs this may be rather detrimental than beneficial.
Difference in spliceosome recruitment was manifested in context of BMS-309403 treatment. Downregulation of *MAPT* exon 10 including mRNA upon BMS-309403 treatment was shown under pathological conditions in hiPSC derived smNPCs. Increase in *MAPT* exon 10 including mRNA was shown in hiPSC derived neurons bearing the tauopathy associated intronic point mutation IVS10+16 c > t. An effect of BMS-309403 on the neuron differentiation is not to be excluded. By exploiting the advantages of the EXSISERS in hiPSC derived smNPCs I identified a novel pathway regulating the physiological and pathological 4R Tau expression

specifically. BMS-309403 treatment showed an inhibitory effect on translational regulation, hinting towards a PPAR independent FABP pathway of translational regulation. In depth investigation to decode the underlying process of translational regulation needs to be conducted in future work. Transcriptome and proteome analysis will give rise to more information on target specificity and impact on overall cell homeostasis, crucial to be identified before moving forward with BMS-309403 as a potential pharmacologic therapy approach for 4R tauopathies. In this context, investigating the BMS-309403 inhibitory effects on *MAPT* translational regulation in patient derived hiPSCs and derivatives showing 4R tauopathy pathology may be considered to investigate the specificity and applicability of BMS-309403 as a pharmacological tauopathy treatment.

In conclusion, I successfully established hiPSC EXSISERS reporter lines to investigate physiological and pathological Tau in a HTS manner. The use of the EXSISERS enabled the identification of further components involved in the *MAPT* exon 10 alternative splicing process up to this point elusive. Involvement of HDACs in the alternative splicing process of *MAPT* exon 10 including mRNA was identified under physiological conditions, while indicating an alteration in spliceosome recruitment in pathological conditions. BMS-309403 was shown to exclusively interfere with *MAPT* exon 10 including mRNA translation. Therefore, this work presents novel indications in *MAPT* exon 10 alternative splicing and translational regulation.

5 Material and Methods

5.1 Materials

5.1.1 Chemicals

Table 5.1: Chemicals

Chemicals	Catalogue No.	Supplier
5-ITU	I100	Sigma-Aldrich
β-ME (cell culture suitable)	31350010	Thermo Fisher Scientific
Accutase	A6964	Sigma-Aldrich
Acedic Acid	W200603	Sigma-Aldrich
Acetopromazine maleate salt	A7111	Sigma-Aldrich
Agar	05040	Sigma-Aldrich
Agarose	870055	Biozym, Germany
Alcuronium chloride	A0325200	Sigma-Aldrich
Alfacalcidol	MCE-HY-10003	Biozol Diagnostics
Alfuzosin HCl	S1409	Selleckchem Chemicals
Alprenolol hydrochloride	S5802	Selleckchem Chemicals
Amoxicillin	S3015	Selleckchem Chemicals
Azaguanine-8	S4194	Selleckchem Chemicals
BMS-309403	HY-101903	MedChemExpress
bovine serum albumin (BSA)	A7906	Sigma-Aldrich
Bradford Reagent	B6916	Sigma-Aldrich
Budesonide	SC-202980	Santa Cruz
Buflomedil HCl	S2607	Selleckchem Chemicals
Chidamide	HY-13592	MedChemExpress
Collagenase type IV	17104-019	Thermo Fisher Scientific
DAPI-Solution	62248	Thermo Fisher Scientific
Digitoxigenin	D9404	Sigma-Aldrich
Digoxin	S4290	Selleckchem Chemicals
DMSO, >= 99.5% (DMSO)	D5879-100ML	Sigma-Aldrich
Dorsomorphin dihydrochloride	3093/10	Tocris Bioscience
Doxycycline Hydrochloride	D3447-500MG	Sigma-Aldrich
DPBS, w/o Ca^{2+}, w/o Mg^{2+}	14190169	Thermo Fisher Scientific
Ethanol (EtOH) absol. P.A 2,5L M983	Merck 1009832500	Merck Millipore
Ethidium bromid (EtBr)	2218.2	Carl Roth GmbH
Ethylenediamintetraacetic acid (EDTA)	EDS-1KG	Sigma-Aldrich
Eptapirone (F-11440)	HY-19946	MedChemExpress
Fomepizole	222569	Sigma-Aldrich

Chemicals	Catalogue No.	Supplier
Formalin, 10%	F5554	Sigma-Aldrich
Gatifloxacin	S1340	Selleckchem Chemicals
Indatraline HCl	1588	Tocris Bioscience
ITSA-1	HY-100508	MedChemExpress
Lacidipine	S1994	Selleckchem Chemicals
Methanol (MtOH)	1.06009.2500	Merck Millipore
Metergoline	0590	Tocris Bioscience
Meticrane	M6902	Sigma-Aldrich
Metronidazole	Cay9002409	Cayman Chemicals
Milk powder	70166-500G	Sigma-Aldrich
Mocetinostat	HY-12164	MedChemExpress
Moclobemide	M3071	Sigma-Aldrich
Nazartinib	HY-12872	MedChemExpress
Nystatine	S1934	Sellckchem Chemicals
PLB	E1941	Promega
Purmorphamin (PMA)	4551	R&D Systems
Sodium chlorid (NaCl)	D6750	Sigma-Aldrich
Pancuronium bromide	P1918	Sigma-Aldrich
Panobinostat	HY-10224	MedChemExpress
Pentylenetetrazole	P6500	Sigma-Aldrich
Pivmecillinam HCl	S5473	Selleckchem Chemicals
Propafenone HCl	S2500	Selleckchem Chemicals
PT-2385	HY-12867	MedChemExpress
RGFP966	HY-13909	MedChemExpress
Salbutamol	Cay21003	Cayman Chemicals
Salbutamol Sulfate	S2507	Selleckchem Chemicals
Santacruzamate A	HY-N0931	MedChemExpress
Sibutramine HCl	AMO-M5958	Biozol Diagnostics
Spiramycin	S4082	Selleckchem Chemicals
Temozolomide	T2577	Sigma-Aldrich
Testosterone propionate	T1875	Sigma-Aldrich
TSA	A8183	APExBio
Tris hydroxymethyl-aminoethan (Tris)	93352	Sigma-Aldrich
Triton X-100	T9284	Sigma-Aldrich
Tubastatin A	HY-13271A	MedChemExpress
Tween 20	P1379	Sigma-Aldrich
Yeast extract	Y1625	Sigma-Aldrich
Ziprasidone HCl	S1444	Selleckchem Chemicals

5.1.2 Cell culture media, supplements and small molecules

Table 5.2: Cell Culture Media, Supplements and Small Molecules

Media	Catalogue No.	Supplier
Advanced DMEM	12491023	Thermo Fisher Scientific
Ascorbic acid 2-phosphate	A8960-5G	Sigma-Aldrich
B-27™ Supplement (50X), minus vitamin A	12587010	Thermo Fisher Scientific
B-27™ Supplement (50X)	11530536	Thermo Fisher Scientific
CloneR™ Supplement (10x)	05888	STEMCELL Technologies
CHIR99021	4423/10	Tocris Bioscience
Cryostor® cell cryopreservation media CS10	C2874-100ML	Sigma-Aldrich
Essential 8™ Flex (E8™ Flex)	A2858501	Thermo Fisher Scientific
GlutaMAX™ Supplement	13462629	Sigma-Aldrich
Human BDNF, research grade	130-093-811	Miltenyi Biotec GmbH
Human FGF8b, premium grade	130-095-740	Miltenyi Biotec GmbH
Human GDNF, research grade	130-096-291	Miltenyi Biotec GmbH
Insulin Solution, Human recombinant	I9278-5ML	Sigma-Aldrich
jetOPTIMUS® DNA Tranfection Reagent	117	Polyplus transfection
KnockOut Serum Replacement	10828028	Thermo Fisher Scientific
DMEM/F12 GlutaMAX™	10565018	Thermo Fisher Scientific
DMEM/F12, HEPES	11330032	Thermo Fisher Scientific
N-2 Supplement (100X)	17502048	Thermo Fisher Scientific
Neurobasal™ Medium	21103049	Thermo Fisher Scientific
MEM non essential amino acids, 100mL	11140035	Thermo Fisher Scientific
NT-3, recombinant human	4500310	PeproTech
Opti-MEM™-I	31985-047	Thermo Fisher Scientific
Penicillin Streptomycin	15140122	Thermo Fisher Scientific
STEMdiff™ Trilineage Differentiation Kit	05230	STEMCELL Technologies
StemMACS™ LDN193189	130-103-925	Miltenyi Biotec GmbH
StemMACS™ Passaging Solution XF	130-104-688	Miltenyi Biotec GmbH
StemMACS™ SB431542	130-106-275	Miltenyi Biotec GmbH
Thiazovivin	42022010MG	Merck Millipore
Y-27632.dihydrochloride	ALX-270-333-M005	Enzo Life Sciences
X-tremeGENE HP DNA Transfection Reagent	6366236001	Sigma-Aldrich

5.1.3 Coating

Table 5.3: Cell Culture Coatings

Coating	Catalogue No.	Supplier
Geltrex™ LDEV-Free, hESC-Qualified, Reduced Growth Factor Basement Membrane Matrix	A1413302	Thermo Fisher Scientific
Laminin from Engelbreth-holm-swarm murin	L2020-1MG	Sigma-Aldrich
Matrigel™, growth factor reduced	354230	Corning
Poly-L-Ornithine hydrobromide (P/O) Mol WT*300 00-70000	P3655	Sigma-Aldrich

5.1.4 Cell lines

Table 5.4: List of cell lines

Cell line	Catalogue No.	Supplier
HPSI0514i-vuna_3	77650602	HipSci
HPSI0614i-uilk_2	77650606	HipSci
HPSI0913i-diku_1	77650088	HipSci
HPSI1013i-yemz_1	77650060	HipSci
HPSI1113i-qolg_1	77650145	HipSci

5.1.5 Antibodies

Table 5.5: Primary Antibodies

Primary Antibody	Dilution	Catalogue No.	Supplier
β-Actin	1:10,000 (WB)	GTX26276	GeneTex
3R Tau (8E6/C11)	1:1000 (WB)	05-803	Sigma-Aldrich
4R Tau (1E1/A4)	1:200 (WB)	05-804	Sigma-Aldrich
AT8 Phospho-Tau (Ser202, Thr205)	1:250 (ICC)	MN1020	Thermo Fisher Scientific
AT100 Phospho-Tau (Thr212, Ser214)	1:250 (ICC)	MN1060	Thermo Fisher Scientific
AT180 Phospho-Tau (Thr231)	1:250 (ICC)	MN1040	Thermo Fisher Scientific
CRISPR-Cas9 (6G12)	1:1000 (WB)	NBP2-52398	R&D Systems
HA tag	1:1000 (WB)	H3663	Sigma-Aldrich
M2 anti-FLAG	1:1000 (WB)	F3165	Sigma-Aldrich
MAP2	1:1000 (ICC)	AB5622	Millipore

Primary Antibody	Dilution	Catalogue No.	Supplier
MC1	1:50 (ICC)		gift by Amir Tayaranian Marvian
NANOG	1:200 (ICC)	AF1997	R&D Systems
NCAM	1:500 (ICC)	ab204446	Abcam
Nestin (10C2)	1:250 (ICC)	MA1110	Thermo Fisher Scientific
NeuN	1:1000 (ICC)	ab104224	abcam
NLuc (965853)	(ICC)	MAB100261SP	R&D Systems
Oct3/4 (C30A3)	1:400 (ICC)	2840S	Cell Signaling
OLLAS (L6)	1:1000 (WB)	MA5-16125	Thermo Fisher Scientific
Pan Tau (PC1C6)	1:200 (WB)	MAB3420	Merck
Pax6	1:200 (ICC)	Ab78545	Abcam
Sox1	1:500 (ICC)	Ab87775	Abcam
SOX2	1:500 (ICC)	Sc17320	Santa Cruz
SOX17	1:500 (ICC)	AF1924	R&D Sysrems
TBXT	1:500 (ICC)	ab209665	Abcam
TUBB3	1:500 (ICC)	T50762000UL	Sigma-Aldrich

Table 5.6: Secondary Antibodies

Secondary Antibody	Conjugate	Dilution	Catalogue No.	Supplier
Donkey-anti-mouse	Alexa 594	1:500 (ICC)	A21203	Thermo Fisher Scientific
Donkey-anti-goat	Alexa 488	1:500 (ICC)	A11055	Thermo Fisher Scientific
Donkey-anti-rabbit	Alexa 594	1:500 (ICC)		Thermo Fisher Scientific
Goat-anti-mouse	HRP	1:10000 (WB)	115-035-146	Dianova
Goat-anti-rabbit	HRP	1:10000 (WB)	111-035-003	Dianova
Goat-anti-rabbit	Alexa 488	1:500 (ICC)	A11008	Thermo Fisher Scientific

5.1.6 Equipment

Table 5.7: List of Equipment

Instrument	Supplier
Centro LB 960 Plate Reader	Berthold Technologies
ELx405 Select Deep Well Washer	BioTek
EnVision 2105 multimode plate reader	Perkin Elmer

Instrument	Supplier
EVOS™ FL Auto Cell Imaging System	Invitrogen™
Fusion FX7/SL advanced imaging system	Vilber Lourmat
Gel-Documentation System E.A.S.Y. Win32	Herolab, Germany
Milli-Q Integral Water Purification System	Merck Millipore
MultiFlo FX Multimode-Dispenser	BioTek
Mr. Frosty™ Freezing Container	Thermo Fisher Scientific
NanoDrop Spectrophotometer ND-1000	Peqlab, Germany
ZEISS Axiovert 200	Zeiss, Germany
ZEISS Axio Imager.M2	Zeiss, Germany

5.1.7 Software

Table 5.8: List of Software

Software	Supplier
Adobe Illustrator®	Adobe
Genenious Prime 2021.2.2	Biomatters
GraphPad Prism 6	Graphpad Software, Inc.
ImageJ	NIH
Neurolucida	MBF Bioscience
R	R Core Team
Stereo Investigator	MBE Bioscience

5.1.8 Commercial kits

Table 5.9: List of Commercial Kits

Kit	Catalogue No.	Supplier
Alexa Flour 555 Conjugation Kit (Fast)-Lightning Link	ab269820	Abcam
CellTrace™ Calcein Red-Orange AM	C34851	Invitrogen™
LongAmp Taq 2X Master Mix	M0287	NEB
Luna Universal One-Step RT-qPCR Kit	E3005	NEB
Luna Universal Probe One-Step RT-qPCR Kit	E3006	NEB
Nano-Glo Dual-Luciferase Reporter Assay	N1620	Promega
NEBuilder HiFi DNA Assembly Master Mix	E2621	NEB
Monarch DNA Gel Extraction Kit	T1020	NEB
Monarch PCR & DNA Cleanup Kit	T1030	NEB
MycoAlert™ Mycoplasma Detection Kit	LT07-218	Lonza

Kit	Catalogue No.	Supplier
P2 Primary Cell 4D-Nucleofector X Kit	V4XP-2024	Lonza
P3 Primary Cell 4D-Nucleofector X Kit	V4XP-3024	Lonza
Pierce BCA Protein Assay	23225	Thermo Fisher Scientific
Primary Cell Optimization 4D-Nucleofector X Kit	V4XP-9096	Lonza
Q5 High-Fidelity 2X Master Mix	M0492	NEB
QIAamp DNA Mini Kit	51306	Qiagen
QIAprep Spin Maxiprep Kit	12163	Qiagen
QIAprep Spin Miniprep Kit	27104	Qiagen
QIAquick Gel Extraction Kit	28706	Qiagen
QuikChange Site-Directed Mutagenesis Kit	200523	Agilent Technologies
SuperSignal West Femto Chemilumineszenz-Substrat	34095	Thermo Fisher Scientific
Wizard SV Genomic DNA Purification System	A2360	Promega

5.1.9 Consumables

Table 5.10: List of Consumables

Description	Catalogue No.	Supplier
10x Tris/Glycine Buffer	1610771	Bio-Rad
Assay Plate, 96 well, black with clear flat bottom	3603	costar
Aqua-Poly/Mount	18606	Polysciences
Cell scraper	83.1830	Sarstedt
Clear Flat Bottom Ultra-Low Attachment Multiple Well Plates	3471	costar
Criterion XT 4-12% Bis-Tris Gels	3450124	Bio-Rad
GeneRuler 100bp DNA Ladder	SM0243	Thermo Fisher Scientific
GeneRuler 1kb DNA Ladder	SM0311	Thermo Fisher Scientific
Immobilon-P PVDF Membrane	IPVH00010	Merck Millipore
Masterblock, 96 well, 2 mL	780271	Greiner Bio One
Multi-well plate, 6 well	353046	Falcon
Multi-well plate, 48 well	353078	Falcon
Multi-well plate, 24 well	353047	Falcon
Multi-well plate, 96 well	9407473	Nunc
Protein Marker VI (10-245)	A8889	PanReac AppliChem
Spectra™ Multicolor High Range Protein Ladder	26626	Thermo Fisher Scientific
Whatman® cellulose chromatography papers	WHA3030672	Sigma-Aldrich
XT MOPS Running Buffer	1610788	Bio-Rad
XT Reduction Agent	1610792	Bio-Rad
XT Sample Buffer	1610791	Bio-Rad

5.1.10 Solutions and buffers

Table 5.11: Composition of Solutions and Buffers

Instrument	Supplier
1x TBS-T	100 mL 10x Tris buffered saline (TBS) 1 mL Tween20 Add to 1 L with H_2O
Blocking Buffer (ICC)	DPBS 1% FBS 0.5% Triton X-100
Blocking Buffer (WB)	5% (w/v) skim milk powder 1x TBS-T buffer
Blotting Buffer (WB)	200 mL Tris/Glycin (TG) Buffer (10x) 400 mL MtOH Add H_2O to 2 L
LB-Agar Plates	10 g Tryptone 5 g Yeast extract 10 g NaCl 15 g Agar Add H_2O to 1 L
LB medium	10 g Tryptone 5 g Yeast extract 10 g NaCl Add H_2O to 1 L Adjust to pH 7.0
Running Buffer (WB)	50 mL XT MOPS Buffer (20x) Add with H_2O to 1 L
TAE Buffer	40 mM Tris 20 mM acetic acid 1 mM EDTA

5.1.11 Enzymes

Table 5.12: List of Enzymes

Enzyme	Catalogue No.	Supplier
λ Protein Phosphatase	P0753	NEB
BbsI-HF	R3539	NEB
DpnI	R0176	NEB
EcoRI-HF	R3101	NEB
EcoRV-HF	R3195	NEB
NotI-HF	R3189	NEB
PacI	R0547	NEB
T4 DNA Ligase	M0202	NEB

5.1.12 DNA vectors

Table 5.13: List of DNA Vectors

DNA Vector	Supplier
pBS_EXSISERS$_{MAPT\text{Ex10:NLuc}}$	available at IDG
pBS_EXSISERS$_{MAPT\text{IVS10+16Ex10:NLuc}}$	available at IDG
pBS_EXSISERS$_{MAPT\text{Ex11:FLuc}}$	available at IDG
pmaxGFP™	Lonza
pMB_Cas9_$MAPT_{\text{sgRNA:Ex10}}$	available at IDG
pMB_Cas9_$MAPT_{\text{sgRNA:Ex11}}$	available at IDG
pCAG_Cre_c-Myc_NLS	available at IDG, generated by Dong-Juinn Jeffery Truong
pCAG_iFLP	available at IDG, generated by Dong-Juinn Jeffery Truong

5.2 Methods

5.2.1 Molecular methods

5.2.1.1 Restriction enzyme digest

Vectors for either subsequent T4 Ligation (5.2.1.3) or Gibson cloning (5.2.1.4) were linearised by restriction enzyme digest (RD). All used enzymes are listed in Table 5.12. In short, vectors were digested in a single enzyme or double enzyme reaction. Appropriate buffer, incubation temperature and heat inactivation temperature was individually adjusted as indicated by the manufacturer.

5.2.1.2 Oligo annealing

Cloning of targeting vectors carrying the sgRNA and prime editing guide RNA (pegRNA), respectively, was performed by oligo annealing and subsequent T4 Ligation, as described in detail in the following and 5.2.1.3. Protospacer sequences for respective sgRNAs were ordered as forward and reverse oligos, whereby, the forward (5'-3') oligo presented the sgRNA protospacer sequence. Oligos had a 100% homology, except for BbsI restriction site overhangs, as listed in 5.26. Annealing of the homologous oligos was initiated by incubation at 96 °C for 10 min. 10 µL of each oligo and 80 µL of TE buffer were set into one reaction. Subsequently the reaction was slowly cooled down by turning off the heat block, ensuring proper annealing of the oligos. Annealed oligos were either subsequently used for T4 Ligation (5.2.1.3) or stored at -20 °C for later use.

5.2.1.3 T4 Ligation

T4 Ligation was performed, following the provided protocol by NEB. In case of sgRNA cloning, increase in ligation efficiency was achieved by redigestion of the ligation reaction with BbsI. Hence, 1 µL of BbsI-HF was directly added to the ligation reaction and incubated for 10 min at 37 °C. Undigested vector still carrying the BbsI restriction recognition site are therefore linearised and can not be transformed into chemically competent *E.coli*, leaving only correctly

ligated vectors for transformation. BbsI restriction digest was stopped by heat inactivation of the enzyme at 65 ℃ for 10 min.

5.2.1.4 Gibson assembly

Gibson Assembly for cloning of donor plasmids for hiPSC genetargeting, was performed using the DNA HiFi Assembly Kit, following the manufacturers protocol. In short, vector backbones were linearised by restriction digest, as described in 5.2.1.1 and subsequent purification of respective fragment by gel extraction. Gel-extraction was performed after gel electrophoresis, as described in 5.2.1.5. Inserts were were amplified by PCR with primers presenting the respective overhang for successful Gibson cloning. Reactions were incubated indifferently at 50 ℃ for 1 h in a thermocycler. Subsequently, Gibson reaction was transformed into chemically competent cells, as described in 5.2.7.4.

5.2.1.5 DNA Gel Electrophoresis

DNA of PCR fragments and RD products were separated by size and visualisation by EtBr under UV light. In general, gels were run at 120 Volt (V) for 45 min. Pictures were taken using the ... documentation system. In case of gel extraction, appropriate fragments were cut out of the gel under UV light and purified using the Monarch Gel Extraction Kit following the manufacturers protocol.

5.2.1.6 Preperation of genomic DNA

Genomic DNA of hiPSCs and derivates was purified using the QIAamp DNA Mini Kit, following the Blood or Body Fluid Spin Protocol. All genomic DNA was diluted in nuclease free H_2O and stored at 4 ℃.

5.2.1.7 Preperation of RNA

RNA was isolated from hiPSCs and derivates growing in a monolayer to 70%-80% confluency in a multi well 6 well plate format using the RNeasy Mini Kit, following the manufacturers protocol. RNA was subsequently used for qRT-PCR as discribed in 5.2.1.8

5.2.1.8 qRT-PCR

qRT-PCRs were conducted using either the Luna Universal Probe One-Step RT-qPCR Kit or the Luna Universal One-Step RT-qPCR Kit, depending on the probe and primers used. Primers used for SYBR™ Green based qRT-PCR are listed in 5.14, following the manufacturers protocol of the Luna Universal One Step RT qPCR Kit. TaqMan™ Probes used in combination with the Luna Universal Probe One Step RT qPCR Kit are listed in 5.15. Expressionlevels of target genes were normalised to stable expressed housekeeping genes, by determination of the best keeper, based on [262]. All qRT-PCRs were performed using the QuantStudio™ 7 Flex Real-Time PCR System.

Table 5.14: Primer Sequences for smNPCs Characterisation by qRT-PCR

Name	Sequence 5'-3'
c-MYC_FW	TCAAGAGGCGAACACACAAC
c-MYC_RV	GGCCTTTTCATTGTTTTCCA
GPBP1_FW	ATCATTCGGTCTTCAACCTTCC
GPBP1_RV	ATCCTCAGTTAAGGGAGCACA
KLF4_FW	GCCACCCACACTTGTGATTA-
KLF4_RV	CGTCCCAGTCACAGTGGTAA
LIN28_FW	CATCTCCATGATAAACCGAGAGG
LIN28_RV	GTTACCCGTATTGACTCAAGGC
NANOG_FW	AAGGTCCCGGTCAAGAAACAG
NANOG_RV	CTTCTGCGTCACACCATTGC
OCT4_FW	AGTGAGAGGCAACCTGGAGA
OCT4_RV	GCCGGTTACAGAACCACACT
POU5F1_FW	GTGTTCAGCCAAAAGACCATCT
POU5F1_RV	GGCCTGCATGAGGGTTTCT
PSMC1_FW	CACACTCAGTGCCGGTTAAAA
PSMC1_RV	GTAGACACGATGGCATGATTGT
RPL22_FW	CACGAAGGAGGAGTGACTGG
RPL22_RV	TGTGGCACACCACTGACATT
SOX2_FW	AGTCTCCAAGCGACGAAAAA
SOX2_RV	GCAAGAAGCCTCTCCTTGAA
TBP_FW	AAAGAACGCTGTACTCAGTGTG
TBP_RV	CCCCGGTTGAGGGCTTTTA
UBQLN1_FW	TGCAGGTCTGAGTAGCTTGG
UBQLN1_RV	AACTGTCTCATCAGGTCAGGAT

Table 5.15: TaqMan™ Probes for qRT-PCR

Name	Target
Hs00902192_m1	MAPT exon 9-11 junction
Hs00902312_m1	MAPT exon 9-10 junction
Hs00902194_m1	MAPT exon 12-13 junction
Hs99999903_m1	β-actin
Hs04260367_gH	POU5F1
Hs02758991_g1	GAPDH
Hs01086177_m1	FABP4
Hs02339439_g1	FABP5
Hs01115513_m1	PPARγ
Hs00187320_m1	HDAC3

5.2.1.9 Preparation of protein

Protein was isolated from either cells growing in a monolayer to 70%-80% confluency in a multi-well 6 well plate format or from a pool of 2-4 forebrain organoids collected in a 1.5 mL tube. Isolation was performed using 1x PLB, diluted in DPBS. Media was aspirated and cells and forebrain organoids washed once with DPBS prior to adding appropriate volumes of 1x PLB to the well and the 1.5 mL tube, respectively. Cell and forebrain organoid were lysed by incubation in 1x PLB for 10 min at room temperature (RT). Subsequently, the cell lysate was transferred to a pre-cooled 1.5 mL tube. Lysates were centrifugated at 10,000 x rcf, for 4 min. The supernatant was transferred to a new pre-cooled 1.5 mL tube and either stored at -20 ℃ or subsequently used for WB (5.2.1.11) or Luciferase assay (5.2.1.12).

5.2.1.10 Bradford protein assay

The protein concentration was assessed by Bradford protein assay. A BSA standard curve with known concentrations served as a reference to determine the cell lysates protein concentration. The assessment was performed in a multi-well 96 well plate format, working in duplicates for standards and samples. The BSA standards were prepared in 1x PLB. For sample concentration determination, samples were diluted 1:5 in H_2O to ensure sample concentration detection within the standard curve range. 5 µL of each standard concentration and sample was added to a well, respectively. 250 µL of Bradford reagent was added to each well used and gently mixed prior to incubation for 5-45 min at RT. Subsequently, absorbance was measured at a wavelength of 595 nm.

5.2.1.11 Immunoblotting

WBs were performed to detect specific proteins of interest and analyse their expression levels. Protein of cells grown in a multi-well 6 well plate formate was prepared using 1x PLB, as described in 5.2.1.9. The cell lysates were separated by sodium dodecyl sulfate (SDS)-PAGE. A 4-12% gradient SDS polyacrylamide gel was used for sufficient separation of the proteins. Gels were run in 1x XT MOPS Running Buffer for 2 h at 150 V at RT. Proteins were then transferred to a PVDF membrane in TG Buffer at 15 V at 4 ℃, overnight and subsequently blocked with 5% (w/v) milk powder dissolved in 5 x TBS-T. After blocking, the membranes were exposed to the respective primary antibody listed in Table 5.5 and incubated overnight at 4 ℃, agitating. Membranes were then washed three times while shaken in 5 x TBS-T for 5 min. An incubation in the secondary antibody conjugated with HRP for 1 h at RT, shaking, followed. Respective dilutions of secondary antibody were made up in 5% (w/v) milk powder dissolved in 5 x TBS-T. The SuperSignal™ West Pico Chemiluminescent Substrate Kit was used according the manufacturer's protocol to visualize the proteins on a Fusion FX7/SL advanced imaging system. Membranes were washed in 5 x TBS-T prior to stripping. Membrane incubation in stripping buffer for 15 min at RT, gently shaking, was followed by a short washing step with 5 x TBS-T. Subsequently, membrane was blocked with 5% (w/v) milk powder dissolved in 5 x TBS-T, shortly washed with 5x TBS-T and exposed to the next primary antibody, overnight at 4 ℃, agitating. For development of membrane, the steps were followed as described above. For a following quantitative analysis, the membranes were again washed three times with 5 x TBS-T for 10 min and incubated in the housekeeping protein antibody overnight at 4 ℃, agitating. The development of the membrane was carried out as previously mentioned, the following day.

All antibodies used to detect the proteins of interest are listed in Table 5.5 and 5.6 . Dilutions were made in 5% (w/v) milk powder dissolved in 5 x TBS-T.

5.2.1.12 Dual luciferase assay

Dual Luciferase assays were conducted using the Nano-Glo Dual Reporter Assay System. Cells used for assays were either seeded in a multi-well 6 well plate or black with clear flat bottom 96 well plate formate. Protein of cells grown in a multi-well 6 well format was prepared using 1x PLB, as described in 5.2.1.9. 30 µL of protein lysate per well were transferred to a black with clear flat bottom 96 well plate for measurement. All measurements based on 1x PLB were conducted in three technical replica per biological replicate. Equal amount of ONE-Glo™ EX reagent was added to the protein lysate. Subsequently, the plate was agitated to ensure sufficient mixing. Samples were incubated for 10 min at RT, prior to FLuc measurement. Measurement was conducted with an integration time of 1 sec and 5 sec, respectively. FLuc activity was stopped and NLuc substrate was supplied by adding 30 µL NanoDLR™ Stop & Glo reagent to the wells. For sufficient FLuc quenching, plate was agitated to ensure proper buffer mixing. Plates were incubated for 10 min at RT, prior to NLuc measurement. Measurement was conducted with an integration time of 1 sec and 5 sec, respectively. For HTS, cells were directly grown in a black with clear flat bottom 96 well plate. Cells were lysed directly in the well with 30 µL ONE-Glo™ EX reagent, after aspirating the media leaving only 30 µL media in each well. From this step forward, HTS plates were handled equally to 1x PLB samples, following the steps as described above.

5.2.1.13 Cell viability

The cell viability of cells upon compound treatment was assessed using the CellTrace™ Calcein Red-Orange acetoxymethyl (AM) dye. Cells were seeded on a clear multi-well 96 well plate format, 24 h prior to compound treatment. A 1:100 dilution in appropriate media was made of Calcein Orange-Red AM dye and subsequently added in a ratio of 1:10 (end concentration of 0.25 µM) to the cells, 72 h post compound treatment. Cells were incubated for 30 min, 37 ℃ and invariant 5% CO_2 saturation. Afterwards, media was aspirated and DPBS added to the wells prior to measurement. Fluorescence measurement was conducted with an excitation of 577 nm, an emission of 620 nm and a cut-off of 590 nm.

5.2.2 Tissue culture methods

Cell culture work was performed under a Type A2 Biological Safety Cabinet. Growing cells were invariantly incubated at 37 ℃ and invariant 5% CO_2 saturation.

5.2.2.1 hiPSCs and derivates

All hiPSCs used in this thesis were kindly donated by Prof Dr Günther Heuting, German Center for Neurodegenerative Diseases, Munich, in collaboration with the high throughput (HIT) Tau Consortium.

5.2.2.1.1 Thawing of hiPSCs and derivates

HiPSCs were brought into culture from cryopreservation by thawing the cell in a 37 ℃ water bath, cell containing CryoStore CS media was transferred drop wise to a 15 mL falcon tube, containing 2 mL of E8™ Flex media, supplemented with 10 µM Rho-associated coiled-coil containing protein kinase (ROCK) inhibitor Y-27632-dihydrochloride. Cells were pelleted by centrifugation, 200 x rcf, 5 min at RT. Supernatant was aspirated and cells resuspended in 2 mL fresh E8™ Flex media, supplemented with 10 µM ROCK inhibitor Y-27632-dihydrochloride. Subsequently, cells were seeded into a multi-well 6-well plate, coated with 1% (v/v) Geltrex™ and incubated at 37 ℃ and constant 5% CO_2 saturation overnight. Cells were released from ROCK inhibitor Y-27632-dihydrochloride 24 h after thawing by aspirating the media, washing cells once with DPBS and newly added E8™ Flex media. Thawing smNPCs followed the same procedure, changes were made using smNPC maintenance media for cultivation. Composition of smNPC maintenance media is listed in Table 5.19.

5.2.2.1.2 Maintenance of hiPSCs and derivates

HiPSCs were primarily cultured in 6-well multi-well plate format, coated with 1% (v/v) Geltrex™. Plates were coated at least 1 h prior to use by adding 1 mL 1:100 diluted Geltrex™ coating and 0.5 mL DMEM/F12, GlutaMAX™ supplement to each well of a multi-well 6-well plate. Dilutions were made in DMEM/F12-GlutaMAX™ supplement. Plates for coating were incubated at 37 ℃ with invariant 5% CO_2 saturation. Geltrex™ volume was adjusted accordingly, depending on the culture plate format used.
HiPSCs were subcultivated at 70%-80% confluency, whereby, colony size was always morphologically assessed under the microscope, prohibiting colony merging. For subcultivation, media was aspirated from the wells and cells were washed once with RT DPBS. Cells were detached from the surface by adding 1 mL Passaging Solution XF to each well and subsequent incubation at RT for 5 min. Afterwards, Passaging Solution was aspirated and 1 mL E8™ Flex media was added. Cells were harvested in cell clumps, by gently pipetting the media up and down. Subsequently, cells were transferred to a 15 mL falcon containing 2 mL E8™ Flex media. Seeding of cells for expansion and maintenance was done by adding 4-8 drops of cell containing media to a well of a 6 well multi-well plate. Split ratio was adjusted according to the proliferation rate of each cell line, to ensure proper colony growth without merging nor too small colony size, decreasing cell survival and favouring random differentiation. Cells were left to grow in the 37 ℃ CO_2 incubator with invariant 5% CO_2 saturation. Medium was changed every other day, or after three days in case of performed double feeds.
SmNPCs were cultured primarily in a multi-well 6-well plate format, either coated with 1% (v/v) Geltrex™ or 15 µg/mL P/O and 10 µg/mL Laminin, depending on the smNPC differentiation. Cells were supplied with N2B27 media (Table 5.18) or smNPC maintenance media, composition listed in Table 5.19. Whereby, cells were subcultivated at a 70%-80% confluency. Media was aspirated and cells were washed once with DPBS prior to adding 1 mL Accutase solution to the wells to detach the cells from the surface. Accutase was incubated for 10 min at 37 ℃. Accutase reaction was terminated by transfer of detached cells to a 15 mL falcon, containing 6 mL DMEM/F-12, GlutaMAX™. Subsequently, smNPCs were sedimented by centrifugation, 5 min, 200 x rcf. Cell pellet was resuspended in 2 mL appropriate media and cells counted using a Neubauer improved, precision disposable plastic haemocytometer C-chip™. Appropriate cell numbers were seeded, according to the multi-well plate format used for maintenance, and cells

were left to grow in a 37 ℃ CO_2 incubator with invariant 5% CO_2 saturation.

5.2.2.1.3 Cryopreservation of hiPSCs and derivatives

HiPSCs and smNPCs were preserved in liquid nitrogen. When cells were grown to 70%-80% confluency, media was aspirated and cells washed once with DPBS. To detach cells, 1 mL of Passaging Solution XF and Accutase Solution were added, respectively. HiPSCs were incubated for 5 min, at RT, before aspirating the Passaging Solution XF and adding 1 mL E8™ Flex to the wells. HiPSCs were gently broken down to small cell clumps by pipetting up and down and subsequently transferred to a 15 mL falcon, containing 2 mL E8™ Flex media. SmNPCs were detached by accutase incubation for 10 min at 37 ℃. Accutase reaction was stopped by transferring the cells to a 15 mL falcon containing 6 mL DMEM/F-12, GlutaMAX™. Cells were sedimented by centrifugation, 200 x rcf for 5 min. Cell pellets of hiPSCs and smNPCs, respectively, were resuspended in CryoStore CS Media and 1 mL of resuspended cells subsequently transferred to a sterile cryogenic storage vial. Freezing container, Mr. Frosty, was used for slowly freezing down cells to -80 ℃ overnight. The vials were transferred to liquid nitrogen for long-time storage.

5.2.2.1.4 Germlayer differentiation of hiPSCs

Pluripotency of the EXSISERS hiPSC reporter lines was verified by differentiation of the reporter and parental cell line in all three germ layers. Trilineage differentiation was conducted using the StemDiff Trilineage Differentiation Kit, following the manufacturer's protocol. Verification of germ layer specific marker expression was performed by fixation of the cells and subsequent ICC, as described in 5.2.2.3.

5.2.2.1.5 smNPC differentiation by EB formation

SmNPC differentiation by EB formation was performed based on Reinhardt *et al.* [263], in short: hiPSC colonies were lifted from 1% (v/v) Geltrex™ coated plates using Collagenase type IV. Colonies were transferred into a suspension plate containing the first smNPC initiation media (Table 5.16).

Table 5.16: Composition of EB based first smNPC initiation media

Media/Supplement	Final Concentration
Knock-Out Serum (KSR)	1x
CHIR99021	3 µM
Dorsomorphine	1 µM
PMA	0.5 µM
SB431542	10 µM
Thiazovivin	2 µM

Two days after, formed EBs were transferred into a new well of a multi-well 6-well plate

containing the second smNPC initiation media, composed of N2B27 Basis Media (Table 5.17), supplemented with 1 µM, 10 µM SB431542, 3 µM CHIR99021 and 0.5 µM PMA.

Table 5.17: Composition of N2B27 basis media. Media basis for smNPC initiation media via EB formation and smNPC maintenance of smNPCs derived from hiPSC via EB formation.

Media/Supplement	**Final Concentration**
DMEM/F-12, GlutaMAX™ Supplement	1:1
N-2 Supplement	1x
Minimum Essential Medium (MEM) non essential amino acids	1x
Insulin	5 µg/mL
β-ME	100 µM
Neurobasal™ Medium	1:1
B27™ Supplement (50x), minus vitamin A	1x
GlutaMAX™ Supplement	1x
Penicillin/Streptomycin	1x

On day four of smNPC initiation, EBs were transferred into new N2B27 basis media, supplemented with 3 µM CHIR99021 and 0.5 µM PMA and 50 mM ascorbic acid. Plating of formed EBs onto 1% (v/v) Geltrex™ coated multi-well 6 well plates was performed on day 6 of differentiation. EBs were broken down by pipetting up and down and subsequently seeded onto the wells, containing N2B27 media (Table 5.18).

Table 5.18: Composition of N2B27 media for smNPC maintenance of smNPCs derived via an EB stadium

Media/Supplement	**Final Concentration**
DMEM/F-12, GlutaMAX™ Supplement	1:1
N-2 Supplement	1x
MEM non essential amino acids	1x
Insulin	5 µg/mL
β-ME	100 µM
Neurobasal™ Medium	1:1
B27™ Supplement (50x), minus vitamin A	1x
GlutaMAX™ Supplement	1x
Penicillin/Streptomycin	1x
CHIR99021	3 µM
PMA	0.5 µM
Ascorbic acid	50 mM

smNPCs were either frozen down for later use, following the protocol described in 5.2.2.1.3 or expanded and maintained, as described in 5.2.2.1.2. Media was changed any other day.

5.2.2.1.6 adherent smNPC differentiation

HiPSCs were plated on appropriate multi-well plates, coated with 1% (v/v) Geltrex™, 24 h prior to neural initiation. For neural initiation, E8™ Flex medium was aspirated and 2 mL smNPC maintenance media (Table 5.19) was added to the cells, supplemented with additional 100 ng/µL FGF8b. Cells were incubated at 37 ℃ and invariant 5% CO_2 saturation, and media was changed every day. On day 14 of neural initiation the neuroepithelial sheed was replated to an appropriate multi-well plate, coated with 15 µg/mL P/O and 10 µg/mL Laminin. Replating was performed using a cell scraper. Media was changed the following day to remove dead cells. Subsequently, media was changed every day until day 21 of smNPC differentiation. On day 21 of differentiation, cells were either frozen down for later use, following the protocol described in 5.2.2.1.3, or reseeded on 15 µg/mL P/O and 10 µg/mL Laminin coated plates for maintenance, as described in 5.2.2.1.2.

Table 5.19: Composition of smNPC maintenance media.

Media/Supplement	Final Concentration
DMEM/F-12, GlutaMAX™ Supplement	1:1
N-2 Supplement	1x
MEM non essential amino acids	1x
Insulin	5 µg/mL
β-ME	100 µM
Neurobasal™ Medium	1:1
B27™ Supplement (50x)	1x
GlutaMAX™ Supplement	1x
Penicillin/Streptomycin	1x
LDN	100 nM
SB431542	10 µM

5.2.2.1.7 hiPSC derived neurons

HiPSCs were differentiated into smNPCs, following the protocol described in 5.2.2.1.6. Subsequently, smNPCs were plated on multi-well 6 well plates, coated with 15 µg/mL P/O and 10 µg/mL Laminin, 24 h prior to neuron differentiation initiation. Media was aspirated and cells washed once with DPBS. Cells were detached by accutase incubation for 10 min at 37 ℃. Accutase reaction was stopped by transferring the cells into a 15 mL falcon, containing 6 mL DMEM/F-12, GlutaMAX™. Cells were sedimented by centrifugation, 200 x rcf for 5 min, and cell pellets resuspended in 2 mL smNPC maintenance media (Table 5.19) supplemented with 100 µM ROCK-inhibitor Y-27632 dihydrochloride and subsequently counted using a Neubauer improved, precision disposable plastic haemocytometer C-chip™. Appropriate cell densities were seeded on plates, coated with 15 µg/mL P/O and 10 µg/mL Laminin, and cultured in smNPC maintenance media, supplemented with 100 µM ROCK-inhibitor Y-27632 dihydrochloride for 24 h at 37 ℃ and invariant 5% CO_2 saturation. The following day, media was aspirated and neuron differentiation initiated by adding neuronal induction media. Media was changed any

other day. Long-term cultures of over 100 days were maintained in neuronal induction media. In case of detachment of neuronal network, cells were reseeded onto new 15 µg/mL P/O and 10 µg/mL Laminin coated plates. Neuronal network was dissociated into single cells by accutase. Hereby, cells were carefully washed once with DPBS and cells incubated with accutase for 15 min at 37 ℃ and invariant 5% CO_2 saturation. Accutase reaction was stopped by transferring the cell solution to a 15 mL falcon, containing 3 mL neuronal induction media, supplemented with 100 µM ROCK-inhibitor Y-27632 dihydrochloride. Cells were released from ROCK-inhibitor Y-27632 dihydrochloride by a media change 24 h after reseeding.

Table 5.20: Composition of neuronal induction media.

Media/Supplement	**Final Concentration**
DMEM/F-12, GlutaMAX™ Supplement	1:1
N-2 Supplement	1x
MEM non essential amino acids	1x
Insulin	5 µg/mL
β-ME	100 µM
Neurobasal™ Medium	1:1
B27™ Supplement	1x
GlutaMAX™ Supplement	1x
Penicillin/Streptomycin	1x
BDNF	20 ng/mL
Ascorbic acid	200 µM

5.2.2.1.8 FBO differentiation

FBO differentiation was performed as described by Qian *et al.* [264]. In short, hiPSCs were cultivated to reach a colony size of 1 µm, prior to starting forebrain (FB) organoid differentiation. Once colony size was reached, colonies were detached from the surface by collagenase type IV treatment, lifting the whole colony to enable EB formation. Lifted colonies are transferred to a 15 mL conical tube and allowed to settle to the bottom of the tube. Supernatant was aspirated from the top of the tube, without disturbing the colonies. Settled colonies were gently washed with 5 mL E8™ Flex media. Supernatant was once again aspirated prior to adding the first culture media for forebrain organoid initiation to the tube (Table 5.21). Colonies were subsequently transferred to a multi-well 6 well plate. From this stage onwards, plates were indifferently incubated on a orbital shaker at 37 ℃ and invariant 5% CO_2 saturation, to prohibit aggregation of EBs and FBOs , respectively. After 24 h media was changed, as following: Plates were gently swirled to allow EBs to gather in the centre of the well. The EBs were settled on the bottom of the wells, by tilting the plate. Media was gently aspirated, without disturbing the EBs. Fresh media was added by pipetting the media slowly into the well. On day 3 and 4 of FBO initiation, FB first culture media was refreshed.

Table 5.21: Composition of FB first culture media.

Media/Supplement	Final Concentration
DMEM/F12, HEPES	
KSR	20%
GlutaMAX™ Supplement	1x
MEM non essential amino acids	1x
β-ME	100 µM
Penicillin/Streptomycin	1x
Dorsomophin	2 µM
A-83	2 µM

On day 5 and 6, a partial media change with FB second culture media (Table 5.22) was made. EBs were embedded in Matrigel™ on day 7. Therefore, Matrigel™ was gently thawed on ice and EBs transferred to a 15 mL conical tube. Supernatant of settled EBs was aspirated and replaced with 1 mL FB second culture media. 20-30 EBs were transferred to a microcentrifuge tube and mixed with Geltrex™ by pipetting up and down multiple times. Using a cut tip, the mixture was spread onto the centre of an ultra-low-attachment six well plate to embed the EBs. Matrigel™ should fully envelop the EBs, yet, ensuring separation of the EBs, to avoid fusion. Matrigel™ 'Cookies' were incubated at 37 ℃ for at least 30 min to solidify. Subsequently, 3 mL FB second culture media was gently added. 'Cookies' were not incubated on an orbital shaker until from this day onwards until day 14. Media was changed every other day. On day 14, growing FBOs were dissociated from Matrigel™ by pipetting the 'Cookie' up and down with a 5 mL pipette.

Table 5.22: Composition of FB organoid second culture media.

Media/Supplement	Final Concentration
DMEM/F-12,HEPES	
N-2 Supplement	1x
GlutaMAX™ Supplement	1x
MEM non essential amino acids	1x
Penicillin/Streptomycin	1x
CHIR99021	1 µM
SB431542	1 µM

From day 14 onwards, organoids were cultured in FB third culture media (Table 5.23) and media changed every other day. From day 35 onwards, to generate an extracellular matrix, Geltrex™ at a dilution of 1:100 was added to the FB third culture media.

Table 5.23: Composition of FB organoid third culture media.

Media/Supplement	Final Concentration
DMEM/F-12, HEPES	
N-2 Supplement	1x
B27™ Supplement	1x
GlutaMAX^{RM} Supplement	1x
MEM non essential amino acids	1x
β-ME	100 µM
Penicillin/Streptomycin	1x
Insulin	2.5 µg/mL

Neuronal maturation of FBOs was initated at day 70 of differentiation, by replacing FB third culture media with FB fourth culture media. Media was changed every other day.

Table 5.24: Composition of FB organoid fourth culture media.

Media/Supplement	Final Concentration
DMEM/F-12, HEPES	
B27™ Supplement	1x
GlutaMAX™ Supplement	1x
MEM non essential amino acids	1x
Penicillin/Streptomycin	1x
Ascorbic acid	0.2 µM
cyclic adenosine monophosphate (cAMP)	0.5 µM
GDNF	20 ng/mL
BDNF	20 ng/mL

5.2.2.1.9 Mycoplasma testing

HiPSC were tested frequently for mycoplasma contamination and after initial thawing in our laboratory using the MycoAlert™ mycoplasma detection kit, as described by the manufacturer. Values were determined with a Centro LB 960 plate reader.

5.2.2.1.10 Karyotyping of hiPSC

Karyotyping of *MAPT*$^{\text{EXSISERS}}$ and *MAPT*$^{\text{IVS10+16EXSISERS}}$ hiPSCs was performed in collaboration with the Klinikum rechts der Isar, Munich. Cells were checked for karyotype abnormalities based on G-banding.

5.2.2.2 Cell counting

Determination of cell number was performed using a Neubauer improved, precision disposable plastic haemocytometer C-chip™. 10 µL of cell suspension of known volume was transferred to the C-chip™ and cells counted for at least two of four outer squares (top-left, top-right, bottom-left, bottom-right). Cell number was calculated as follows:

$$\frac{Total\ Number\ of\ Cells * 10,000}{Number\ of\ Counted\ Squares} = \frac{Cell\ Number}{mL} \quad . \tag{5.1}$$

5.2.2.3 Immunocytochemistry

HiPSC pluripotency, germ layer identity, smNPC identity and hiPSC derived cortical neuron identity were verified by immunocytochemistry.Cells were either grown on glass slides in a multi-well 24 well plate format, or in a multi-well 96 well plate format for subsequent ICC. Cells were pre-fixated with 10% formaline, by adding 50% (v/v) 10% formaline directly to the culture media. Cells were incubated for 10 min at 37 °C and 5% CO_2. Subsequently, formaline-media mixture was aspirated from the cells and 10% formaline was added and cells incubated for 30 min at 37 °C and 5% CO_2. Afterwards, cells were washed three times with DPBS and either stored at 4 °C, in DPBS, or subsequently stained with the appropriate antibodies. For improvement of antibody penetration, cells were incubated in 0.5% Triton X-100, 1% (v/v) FBS diluted in DPBS for 10 min at RT. The primary antibody was added to cells in 0.5% (v/v) Triton X-100, 1% FBS diluted in DPBS and incubated for 2 h at RT or overnight at 4 °C. Afterwards, cells were washed three times with DPBS prior to appropriate secondary antibody incubation for 1 h at RT. Nuclei were visualised by 4', 6-Diamidin-2-phenylindol (DAPI). Imaging was performed using epifluorescence microscopy with corresponding filter sets. Primary Antibodies are listed in Table 5.5, secondary antibodies in Table 5.6.
FBOs were fixated by 10% paraformaldehyd (PFA). FBO were incubated in PFA for 30 min at RT prior to aspirating the PFA and washing the FBO once with DPBS. FBOs were subsequently transferred into 30% sucrose and incubated overnight at 4 °C. The next day, FBOs were embedded for subsequent cryo-sectioning. Sections of FBOs were used for subsequent ICC.

5.2.3 Generation of *MAPT*$^{\text{EXSISERS}}$ hiPSC Lines

5.2.3.1 Vectorpreperation of *MAPT*$^{\text{EXSISERS}}$

Donorvectors for $MAPT^{\text{EXSISERSEx10:NLuc\_PuroR}}$ and $MAPT^{\text{EXSISERSEx11:FLuc\_PuroR}}$ cassettes, including respective homology-arms (HAs), were prepared by Gibson Assembly, following the protocol described in detail in 5.2.1.4. pBS vectors presenting only the EXSISERS$^{\text{NLuc_PuroR}}$ and EXSISERS$^{\text{FLuc_PuroR}}$ cassettes, respectively, were kindly gifted by Dong-Jiunn Jeffery Truong. Cassettes and backbone were linearised by RD with BbsI-HF and HAs added. Prior to cloning, regions of interest were confirmed by Sanger sequencing, to ensure 100% homology between the endogenous locus and designed HAs for each cell line. After successful sequencing, asymmetric HAs were amplified by PCR from target genomic DNA (gDNA) of subjected cell lines, including Gibson overhangs for either the pBS backbone or the respective cassette. Wherby,

the HAs of the $MAPT^{\text{EXSISERSEx10:NLuc\_PuroR}}$ donor were 1.5 kbp (5'HA) and 3 kbp (3'HA) in size. In case of the $MAPT^{\text{EXSISERSEx11:FLuc\_PuroR}}$ donor the 5'-HA was 1.5 kbp and the 3'-HA 3.0 kbp long. Respective primer sequences used for fragment amplification are listed in Table 5.25.
The $MAPT^{\text{EXSISERSEx10:NLuc\_PuroR}}$ is composed of an N- and C-terminal part of gp41-intein, flanking the whole cassette, two α helices (AP6 and P5) flanking the intein parts on the inside of the cassette, an OLLAS-tag, the NLuc of *Oplophorus Gracilirostris*, two FRT F3 sites, flanking an EF1α promoter driven PuroR cassette, for positive clone selection in hiPSCs. The $MAPT^{\text{EXSISERSEx11:FLuc\_PuroR}}$ cassette is comprised of an N- and C-terminal part of Nrdj-intein, the FLuc of *Photinus Pyralis*, a FLAG-tag and two Lox5171 sites flanking a PuroR cassette, driven by an EF1α promoter.

Table 5.25: EXSISERS Primer Sequences for Gibson Assembly. Primer Sequences for donor vector cloning of $MAPT^{\text{EXSISERSEx10:NLuc\_PuroR}}$ and $MAPT^{\text{EXSISERSEx11:FLuc\_PuroR}}$

Name	Sequence 5'-3'	Properties
HsMAPT10_5'HA-1.5kbp_FW	GTGGTTTCCACCCAGCATTCTCAA	Exon 10 5'-HA
HsMAPT10_5'HA-1.5kbp_RV	GCACCTGGGTCTTAAGGTCCAGGCAGCCAC ACTTGGACTGGACGTTG	Exon 10 5'-HA
HsMAPT10_3'HA-3.0kbp_FW	CGCCAACGATATCCTGACCCACAACTCAAAG GATAATATCAAACACGTCCCGGG	Exon 10 3'-HA
HsMAPT10_3'HA-3.0kbp_RV	CACGCTGTAGGGACTCCACAG	Exon 10 3'-HA
HsMAPT10_IVS_3'HA-3.0kbp_FW	CACCTGTTCTACGCCAACGATATCCTGACCC ACAACTCAAAGGATAATATCAAACACGTCCC GGGAGG	Exon 10 IVS10+16 3'-HA
HsMAPT10_IVS_3'HA-3.0kbp_RV	GAGCCTCGGGTGCCCAGTC	Exon 10 IVS10+16 3'-HA
HsMAPT11_5'HA-1.5kbp_FW	GGCGAATTGGAGCTGAAGACCTCACGAGTTA CCTCACC	Exon 11 5'-HA
HsMAPT11_5'HA-1.5kbp_RV	GATCTCGCTGCTGCCCACGAGACACTTGGAG GTCACCTTGCTC	Exon 11 5'-HA
HsMAPT11_3'HA-3.0kbp_FW	GCCAACGACATCCTGGTGCACAACTGTGGC TCATTAGGCAACATCC	Exon 11 3'-HA
HsMAPT11_3'HA-3.0kbp_RV	GAACAAAAGCTGGGTACGAAGACGCAGAAG AAGGGTCCCTCTC	Exon 11 3'-HA

MAPT IVS10+16 c > t mutation introduction to the $MAPT^{\text{EXSISERSIVS10+16Ex10:NLuc\_PuroR}}$ donor was generated by double digest of the $MAPT^{\text{EXSISERSEx10:NLuc\_PuroR}}$ donor with EcoRV-HF and SalI-HF (see Table 5.12 for more details on the enzymes). Primer presenting the point mutation were used for fragment amplification, to exchange the cut out fragment with the mutation presenting one via Gibson Assembly.
The respective sgRNAs (listed in Table 5.26) targeting either $MAPT^{\text{Ex10}}$ or $MAPT^{\text{Ex11}}$, were expressed under the U6 promoter (RNA Polymerase (Pol) III), encoded on the same pMB backbone as the Cas9, which was expressed under the regulation of the hybrid chicken β-actin promoter (CBA) promoter (CBh). Oligos for sgRNAs introduction into the plasmid were design with overhangs matching the BbsI-HF restriction site. Oligos were annealed by oligo annealing,

described in 5.2.1.2 and subsequently cloned into the pMB backbone downstream of the U6 promoter by T4 ligation, described in detail in 5.2.1.3.

Table 5.26: sgRNA for *MAPT*$^{\text{EXSISERS}}$ genetargeting

Name	Sequence 5'-3'	Properties
gHsMAPT-CdEx10-1_FW	CACCGCCAGTCCAAGTGTGGCTCAA	*MAPT* Ex10 Targeting
gHsMAPT-CdEx10_RV	AAACTTGAGCCACACTTGGACTGGC	*MAPT* Ex10 Targeting
gHsMAPT-CdEx11_FW	CACCGTTGCCTAATGAGCCACACT	*MAPT* Ex11 Targeting
gHsMAPT-CdEx11_RV	AAACAGTGTGGCTCATTAGGCAAC	*MAPT* Ex11 Targeting

5.2.3.2 Genome targeting *MAPT*$^{\text{EXSISERS}}$ of hiPSC

The *MAPT* EXSISERS was introduced in the hiPSC lines HPSI0514i-vuna_3 and HPSI0614i-uilk_2. Generation of the EXSISERS hiPSC lines was conducted in four major gene-targeting steps: 1. KI of *MAPT*$^{\text{EXSISERSEx11:FLuc\_PuroR}}$, 2. excision of PuroR$^{\text{EXSISERSEx11}}$ by Cre, 3. KI of *MAPT*$^{\text{EXSISERSEx10:NLuc\_PuroR}}$ and 4. excision of PuroR$^{\text{EXSISERSEx10}}$ by FLP. Whereby, all targeting was conducted by delivering respective vector DNA to the cells by nucleofection, described in detail in 5.2.7.3. In case of *MAPT*$^{\text{EXSISERSEx11:FLuc\_PuroR}}$ and *MAPT*$^{\text{EXSISERSEx10:NLuc\_PuroR}}$ KIs targeted hiPSCs were left to recover for 72 h after nucleofection, prior to applying selectional pressure by adding 1 µg puromycin to the cells. Selectional pressure was lifted after 72 h, entering a second recovery phase. HiPSC colonies were left to grow to reach a appropriate size for picking. One colony was defined to be emerged from one single cell. Single colonies were picked under a light microscope, placed under a Type A2 Biological Safety Cabinet. Whereby, colonies were gently scraping off of the surface with a 200 µL pipette tip, without disturbing the colony and transferred to a well of a multi-well 24 well plate, containing 500 µL E8™ Flex media, supplemented with 100 µM ROCK-inhibitor Y-27632 dihydrochloride. Picked colonies were expanded to an multi-well 6 well format, genotyped and cryopreserved prior to respective excise of the PuroR cassette from the locus. Excision of the *MAPT*$^{\text{EXSISERSEx11:FLuc\_PuroR}}$ and *MAPT*$^{\text{EXSISERSEx10:NLuc\_PuroR}}$ PuroR cassette was accomplished by Cre and FLP, respectively. After nucleofection for PuroR excision, cells were left to recover until reaching a confluency of 70%-80% prior to clonolising them by limited dilution. Hereby, cells were washed once with DPBS, pior to adding 1 mL accutase solution to the wells to detach the cells from the surface and incubated for 10 min at 37 °C. The reaction was stopped by transferring the single cell solution to a 15 mL falcon, containing 2 mL E8™ Flex media, supplemented with 1x CloneR Supplement. Subsequently, hiPSCs were sedimented by centrifugation, 5 min, 200 x rcf. Cell pellet was resuspended in 2 mL E8™ Flex media, supplemented with 1x CloneR Supplement and cells counted using a Neubauer improved, precision disposable plastic haemocytometer C-chip™. Limited dilutions were prepared, in a concentration of 0.8 cells/well. Single cells were seeded in multi-well 96 well plates, containing E8™ Flex media, supplemented with 1x CloneR Supplement and subsequently incubated at 37 °C and invariant 5% CO_2 saturation. Media was renewed 72 h after seeding. After further 72 h of incubation, media was changed to E8™ Flex media, without any supplement. Colonies emerged from only one cell were expanded and maintained as described in 5.2.2.1.2. When reached a sufficient cell number, single clones were genotyped.

5.2.3.3 Genotyping of *MAPT*^{EXSISERS} hiPSC lines

Clones of the hiPSC *MAPT*$^{\text{EXSISERS}}$ reporter line, generated as described in 5.2.3.2, were continuously genotyped after ever targeting step. Cells were expanded as single clones and gDNA was isolated from cells grown in either a multi-well 6 well or 24 well plate format, as described in 5.2.1.6. In general, primers were designed to pick up WT and KI alleles in one PCR reaction. Sequences of the referred primers are listed in Table 5.27. In case of *MAPT*$^{\text{EXSISERSEx10:NLuc\_PuroR}}$, genotyping was performed using three primers in one PCR reaction. One forward primer, binding upstream of the 5'-HA of the cassette (HsMAPT_Ex10_FW) and two reverse primers, binding inside of the 3'- HA (HsMAPT_Ex10_WT_RV) and inside of the *MAPT*$^{\text{EXSISERSEx10:NLuc\_PuroR}}$ insertion (HsMAPT_Ex10_KI_RV), respectively. A fragment size of 2086 bps indicates a WT allele, a fragment size of 2700 bps a successful *MAPT*$^{\text{EXSISERSEx10:NLuc\_PuroR}}$ KI. Following the excision of the selection cassette, single clones were genotyped by a PCR with primers HsMAPT_Ex10_Locus_FW and HsMAPT_Ex10_Locu
s_RV, binding right outside of the 5' and 3'-HA. A fragment size of 6.4 kbp indicates a successful excision of the PuroR selection cassette, however a fragment size of 8.7 kbp indicates a remaining PuroR selection cassette. A fragment size of 5.0 kbp indicates a WT allele.

Table 5.27: Genotyping of *MAPT*$^{\text{EXSISERS}}$

Name	Sequence 5'-3'	Properties
HsMAPT_Ex10_FW	GTCTGAGGCTTGAGAATGAAC	HsMAPT Exon 10 NLuc
HsMAPT_Ex10_WT_RV	CTACATTCACCCAGAGGTC	HsMAPT Exon 10 NLuc
HsMAPT_Ex10_KI_RV	CGAAGTAGTCGATCATGTTTG	HsMAPT Exon 10 NLuc
HsMAPT_Ex10_Locus_FW	CTACCAAGTATAGGTATACAGG	HsMAPT Exon 10 Locus
HsMAPT_Ex10_Locus_RV	CTAGAGCAAAGACCATCAGTA	HsMAPT Exon 10 Locus
HsMAPTEx11_FW	CATCCACTCCTCTCCTTTC	HsMAPT Exon 11 FLuc
HsMAPTEx11_WT_RV	CTTTCCAGCCCCTTCTGAAG	HsMAPT Exon 11 FLuc
HsMAPTEx11_KI_RV	GCTTGAAGTCGTACTCGTTG	HsMAPT Exon 11 FLuc
HsMAPT_Ex11_Locus_FW	GACTGAGATCAGCTGGCAGC	HsMAPT Exon 11 Locus
HsMAPT_Ex11_Locus_RV	CTGCCGATGGTGAAGTGTCTC	HsMAPT Exon 11 Locus

MAPT$^{\text{EXSISERSEx11:FLuc\_PuroR}}$ genotyping was performed using primer HsMAPTEx11_FW, HsMAPTEx11_KI_RV and HsMAPTEx11_WT_RV. Whereby, the forward primer was binding outside of the 5'-HA and the reverse primers, inside of the *MAPT*$^{\text{EXSISERSEx11:FLuc\_PuroR}}$ cassette and the 3'-HA, respectively, picking up WT and KI alleles in the same reaction. A fragment size of 2.6 kbp indicates a successful KI of the *MAPT*$^{\text{EXSISERSEx11:FLuc\_PuroR}}$ cassette, a fragment size of 1.7 kbp indicates a WT allele. Following the excision of the selection cassette, single clones were genotyped by a PCR with primers HsMAPT_Ex11_Locus_FW and HsMAPT_Ex11_Locus_RV, binding right outside of the 5' and 3'-HA. A fragment size of 5.0 kbp indicates a successful excision of the PuroR selection cassette, however a fragment size of 7.3 kbp indicates a remaining PuroR selection cassette. A fragment size of 2.6 kbp indicates a WT allele.

Table 5.28: PCR Mix for Q5 Hot Start Pol 2x Master Mix

Component	Volume
Q5 Hot Start 2x Master Mix	12.5 µL
forward primer (10 µM)	1.25 µL
reverse primer I (10 µM)	1.25 µL
(reverse primer II (10 µM)	1.25 µL
DNA template	10 ng
Nuclease free H_2O	add to 25 µL

Table 5.29: PCR Cycling for Q5 HotStart Pol *MAPT*$^{\text{EXSISERSEx10:NLuc\_PuroR}}$ Genotyping

Step	Temperature	Duration	Cycles
Initial denaturation	98 °C	3 min	1
Denaturation	98 °C	10 sec	
Annealling	59 °C	40 sec	35
Elongation	72 °C	1 min 48 sec	
Final Elongation	72 °C	2 min	1
Cooling	4 °C	∞	

Table 5.30: PCR Cycling for Q5 HotStart Pol *MAPT*$^{\text{EXSISERSEx11:FLuc\_PuroR}}$ Genotyping

Step	Temperature	Duration	Cycles
Initial denaturation	98 °C	3 min	1
Denaturation	98 °C	10 sec	
Annealling	63 °C	40 sec	35
Elongation	72 °C	1 min 50 sec	
Final Elongation	72 °C	2 min	1
Cooling	4 °C	∞	

Table 5.31: PCR Mix for LongAmp Hot Start Pol 2x Master Mix

Component	Volume
LongAmp Hot Start 2x Master Mix	12.5 µL
forward primer (10 µM)	1.25 µL
reverse primer I (10 µM)	1.25 µL
DNA template	100 ng
Nuclease free H_2O	add to 25 µL

Table 5.32: PCR Cycling for *MAPT*$^{\text{EXSISERS}}$. Genotyping of *MAPT* Exon 10 PuroR Excision

Step	Temperature	Duration	Cycles
Initial denaturation	94 °C	3 min	1
Denaturation	94 °C	10 sec	
Annealling	50 °C	40 sec	35
Elongation	65 °C	9 min	
Final Elongation	65 °C	10 min	1
Cooling	4 °C	∞	-

Table 5.33: PCR Cycling for *MAPT*$^{\text{EXSISERS}}$. Genotyping of *MAPT* Exon 11 PuroR Excision

Step	Temperature	Duration	Cycles
Initial denaturation	94 °C	3 min	1
Denaturation	94 °C	10 sec	
Annealling	60 °C	40 sec	35
Elongation	65 °C	12 min	
Final Elongation	65 °C	10 min	1
Cooling	4 °C	∞	

5.2.4 *MAPT* alternative splicing stimulation

5.2.4.1 *MAPT* alternative splicing modulation in hiPSC derived smNPCs

4R Tau isoform expression was stimulated by 5-ITU. Whereby, smNPCs were seeded either on a multi-well 6 well plate or a black with clear flat bottom multi-well 96 well plate 24 h prior to 5-ITU treatment. Cells were treated with 5-ITU over a period of 24 h, 48 h and 72 h, with concentrations of 0.1 µM, 0.25 µM, 0.5 µM and 1 µM. Protein was isolated for each of this concentrations and time point for further isoform investigation. In case of multi-well 96 well format seeded cells, cells were directly lysed in the plate and used for luciferase assay based isoform analyses (see subsubsection 5.2.1.12 for details).
Pharmacological compound screen primary hits were tested in *MAPT*$^{\text{EXSISERS}}$ hiPSC derived smNPCs, seeded in a density of 35,000 cells/well of black with clear flat bottom multi-well 96 well plates, respectively, coated with 15 µg/mL P/O and 10 µg/mL Laminin 24 h prior to compound exposure. For Prestwick Library hits, compound treatment was performed in a titration manner, with the highest concentration being 10 µM and a dilution factor of 2. In case of confirmed primary hits of the Broad Repurpose Library screen, by reproduction of the initial test results (1 µM, 72 h), a dose response was conducted. Compound concentration were 0.001, 0.01, 0.1, 0.2, 0.4, 0.6, 0.8 and 1.0 µM. Cells were exposed to referring concentrations for 72 h without any compound renewal prior to bioluminescence measurement (5.2.1.12). Compound treatment for subsequent protein and RNA isolation, was performed using following concentrations: 1 µM and 0.1 µM TSA, 0.8 µM and 1 µM SAHA, 1 µM BMS-309403, 0.01 µM and 1 µM Panobinostat, 0.4 µM and 1 µM Mocetinostat and 1 µM 5-ITU. Cells were incubated for 72 h

prior to protein and RNA isolation, without any renewal of media. All compound concentations were set up, not exceeding 1% (v/v) DMSO, also serving as vehicle control.

5.2.4.2 *MAPT* alternative splicing modulation in hiPSC derived neurons

hiPSC derived neurons (as described in 5.2.2.1.7) were cultivated with compounds starting from day 21 of differentiation. Whereby, 1% (v/v) DMSO containing neuronal induction media (Tab. 5.20) was always freshly supplemented with a set concentration of compound: 0.001 µM Panobinostat, 0.01 µM Mocetinostat, 0.01 µM TSA, 0.01 µM SAHA, 1 µM BMS-309403 or 0.01 µM 5-ITU. Neurons were differentiated until day 37 of differentiation. Subsequently, cells were seeded on 15 µg/mL P/O and 10 µg/mL Laminin coated glass slides at a density of 20.000 cells/well. Neurons were either transfected 3 days post seeding, as described in 5.2.7.2, and fixated 24 h post transfection or fixated on day 41 of differentiation without transfection, for ICC.

5.2.4.3 *MAPT* alternative splicing modulation in hiPSC derived FBOs

For FBOs, treatment was performed by transferring two FBOs at day 22 of differentiation into a multi-well 24 well plate with 500 mL FBO third culture media (Table 5.23) and incubating them at 37 ℃ and 5% CO_2 agitating. On day 24 of differentiation, FBOs were treated with 5-ITU in a concentration of 0.25 µM, 0.5 µM and 1 µM diluted in 1% (v/v) DMSO FBOs third culture media for 72 h and 10 days, working in three biological replicates. Whereby, partial media change was performed, letting the FBOs sink to the bottom of the plate, aspirating 100 µL old media and replacing it with either 5% (v/v) DMSO compound containing FBO third culture media (day 1 of treatment), or 1% (v/v) DMSO compound containing FBO third culture media (any other day). For bioluminescence measurement, FBOs were lysed by aspirating most of the media, 60 µL remaining, and adding equal amounts of ONE-Glo-Buffer to each well. 20 µL of the lysate were then transferred to a black with clear flat bottom multi-well 96 well plate in technical triplicates for dual luciferase assay.

5.2.5 High throughput pharmacological compound screen

The high throughput pharmacological compound screens of the FDA approved compound screen (Prestwick Library) and the Repurposing Library (Broad Library) were performed in collaboration with the Assay Development and Environmental Health Platform, Institute for Molecular Toxicology, Helmholtz Centre for Environmental Health, Munich.
For screening, hiPSC $MAPT^{EXSISERS}$ derived smNPCs, following the adherent smNPCs differentiation protocol (5.2.2.1.6), were invariantly cultured in smNPC maintenance media (Table 5.19). The cells were seeded at a density of 45,000 cells/well of black with clear flat bottom 96 well plates, coated with 15 µg/mL P/O and 10 µg/mL Laminin. Coating of plates and cell seeding was performed using the ELx405 select deep well microplate washer and MultiFlo FX Multimode-Dispenser. SmNPCs were seeded 24 h prior to compound transfer abstain from ROCK-inhibitor Y-27632-dihydrochloride. Whereby, compounds were set in with a concentration of 1 µM and incubated with smNPCs for 72 h prior to Dual Luciferase Assay to screen for altered Tau protein expression, described in detail in 5.2.1.12. 1 µM 5-ITU and 1% (v/v) DMSO were added to each plate as a positive and negative control, respectively. The Prestwick Library

was screened in one day, the Broad Library screen was conducted in 4 consecutive days. The assay quality was assessed by application of the SW and C_V and subsequently hits identified. The SW, setting the range between $control_n$ as the lowest and $control_p$ as the highest signal, is

$$SW = \frac{(\mu_p - \mu_n) - 3(\sigma_p + \sigma_n)}{\sigma_p} \quad , \tag{5.2}$$

where μ is the mean of $control_p$ and $control_n$ and σ the respective standard derivation. SW > 2 are recommended, SW > 1 are acceptable and SW < 1 not considered as a Hit [265]. The $\%C_V$ was calculated to allow comparison of the ratio measurements of the Dual Luciferase Assay, meeting the minimum quality requirements. Therefore, as a quality control for ratio based screens, set in the HTS Assay Validation guidelines [266], the $\%C_V$ was calculated, as follows:

$$\%C_V = 100 * \frac{\mu}{\sigma} \quad , \tag{5.3}$$

where μ is the mean and σ the respective standard derivation of either $control_n$ ($\%C_{V\,min}$) or $control_p$ ($\%C_{V\,max}$). To meet the quality requirements, the $\%C_{V\,max}$ and $\%C_{V\,min}$ have to be $<$ 20% for each plate.
The Hit threshold was calculated for each plate, as follows:

$$Hit\ threshold > \tilde{x} - (3 * \sigma) \quad , \tag{5.4}$$

whereby, $\tilde{x}$ is the median and σ the standard derivation of all ratios of all cells treated with compounds, excluding the negative and positive control.
The %Activity was calculated as described below,

$$\%Activity = \frac{100 * \lambda_c}{\mu_p} \quad , \tag{5.5}$$

where λ_c is the NLuc/FLuc ratio of respective well treated with compound (c) and μ_p is the mean of the positive control, located on the same plate as the compound.

5.2.5.1 Stability of screening system

The stability of potential screening system was tested by Tau expression stimulation with 5-ITU prior to FDA approved chemical compound screen (5.2.5). DMSO was established as a negative

control, whereby DMSO concentration never exceeded 1% (v/v) of the total media volume. Calculation of the Z'-factor, as a measure of statistical effect size, was conducted, using the following equation,

$$Z' - factor = 1 - \frac{3(\sigma_p + \sigma_n)}{|\mu_p - \mu_n|} \quad , \tag{5.6}$$

where μ is the mean of positive (p) and negative (n) control and σ the respective standard derivation. Acceptance criteria being Z'-factors ≥ 0.5 indicate an excellent assay, a Z'-factor of 1 an ideal one. Z'-factors between 0 and 0.5 indicate a doable assay, and a Z'-factor < 0 too much overlap between positive and negative control, considered unacceptable [265].

5.2.6 Neuritic tree quantification

hiPSCs were differentiated as described in 5.2.2.1.7. For transient GFP expression, hiPSC derived neurons were transfected as described in 5.2.7.2. NeuN served as a marker to identify GFP-NeuN positive cells. Neuritic trees were manually measured using the Meander Scan. All measurements were conducted using a ZEISS Axio Imager.M2 stereomicroscope. Cell bodies and neurites were distinguished. Sholl Analysis was conducted for every individual neuron using the Neurolucida Explorer, whereby, the radius was set to 2 µm, with a line width of 1 µm. Efficiency of hiPSC derived neuron differentiation was acquired using Stereo Investigator with a ZEISS Axio Imager.M2 stereomicroscope, counting up to 25 grids of each cover slip of a size of 100 µm x 100 µm at a 45x magnification. NeuN and DAPI positive cells were counted within the counting frame.

5.2.7 DNA delivery

5.2.7.1 HEK293T transfection

HEK293Ts were seeded in a multi-well 48 well or 96 well plate format 24 h prior to transfection. DNA was diluted in RT Opti-MEM-I and appropriate amount of X-tremeGENE HP reagent was added. DNA-transfection cocktail was incubated for 20 min at RT before added drop-wiseto wells. For CRISPR/Cas9 approaches, cells were incubated for 48 h or 72 h, prior to DNA isolation, protein preparation and subsequent analysis.

5.2.7.2 hiPSC derived neuron transfection

HiPSC derived neurons (day 37 of differentiation) were seeded in a density of 20,000 cells/well on 15 µg/mL P/O and 10 µg/mL Laminin coated glass slides in a multi-well 24 well plate format, 4 days prior to transfection. JetOPTIMUS® DNA transfection reagent was used, following the manufacturers protocol. A DNA amount of 0.25 µg of pmaxGFP™ was transfected per well. Media of transfected cells was changed 4 h post transfection. Cells were pre-fixated 24 h post transfection by adding 20% (v/v) formalin, 10% to each well, still containing media. Cells were incubated at 37 °C and invariant 5% CO_2. Subsequently, media was aspirated and formaline,

10% was added and incubated for 30 min at RT. Cells were washed three times with DPBS prior to dendritic tree quantification, described in 5.2.6.

5.2.7.3 Nucleofection

Nucleofection of hiPSCs was conducted using the 4D Nucleofector X Unit. Once cells reached 70%-80% confluence, medium was aspirated and cells washed once with RTDPBS. 1 mL accutase solution was added to a 6 well and cells were incubated for 10 min at 37 ℃ and invariant 5% CO_2 saturation. Accutase was stopped by transferring the single cell solution to a 15 mL falcon tube containing 3 mL E8™ Flex media, supplemented with 100 µM ROCK-inhibitor Y-27632 dihydrochloride and counted using a Neubauer improved, precision disposable plastic haemocytometer C-chip™. 0.8-1 million single cells were pelleted by centrifugation, 200 x rcf, 5 min, per nucleofection reaction. The cell pellet was resuspended in either P2 or P3 Primary Cell solution and supplement, following the manufacturers protocol of referring kit for a 100 µL cuvette. Cell solution was transferred to a 100 µL cuvette, provided with the kit, and DNA was added to the cells. Vector DNA was diluted in DPBS, to a total volume of 24 µL. For KI approaches a total of 4 µg of DNA was set in (3 µg donor vector, 1 µg Cas9_i53 vector), in case of Puromycin cassette excision 1 µg vector DNA. Nucleofection was conducted using either program CB-150 or CM-150. After run program, 1 mL RT E8™ Flex media, supplemented with 100 µM ROCK-inhibitor Y-27632 dihydrochloride, was added to the 100 µL cuvette and left for recovery at 37 ℃ and invariant 5% CO_2 saturation for 5 min, prior to seeding cells in two wells of a multi-well 6 well plate containing 2 mL E8™ Flex media, supplemented with 100 µM ROCK-inhibitor Y-27632 dihydrochloride. Cells were incubated at 37 ℃ and invariant 5% CO_2 saturation for 24 h prior to a media change, releasing the cells from 100 µM ROCK-inhibitor Y-27632 dihydrochloride.

5.2.7.4 Transformation of chemically competent cells

Chemically competent *E.coli* were gently thawed on ice. 50 mL of cells were used per transformation reaction and transferred to a clean prechilled 1.5 mL tube. DNA was added to the chemically competent cells and mixed by gently flicking the tube twice. Cell-DNA mix was incubated on ice for 30 min prior to performing a heat shock in a 42 ℃ water bath for 45 sec. Chemically competent cells were transferred back to ice for 2 min and 500 µL super optimal broth with catabolite repression (SOC) media was added. Cells were incubated at 37 ℃ for 45 min, shaking (350 x rpm). Transformation mix was plated to LB-Agar plates with Ampicilin (Amp) for selection and incubated at 37 ℃, overnight.

5.2.8 Data analysis

5.2.8.1 GraphPad Prism 8

Statistics of Western blots and dual luciferase assays were utilized by GraphPad Prism 8. The respective statistical tests that were applied were either one-way ANOVA or two-way ANOVA depending on the dataset analysed. All experiments were conducted in at least three biological replica, if not otherwise indicated. As MCT, for further analyses, served Bonferroni tests for statistically analysed data.

5.2.8.2 ImageJ

Quantification of the protein bands of WB, were performed by using ImageJ. Background subtraction made sure, that the values measured were not biased by background noise. Measured values of β-actin were subtracted from the values measured for the respective samples, to eliminate loading faults. Further analyses were taken out by Microsoft Excel (Microsoft Corporation, Redmond, USA).

5.2.8.3 Geneious

All vector designs for genome targeting approaches were done using Geneious. Sanger Sequencing results for genome editing verification were analysed using Geneious.

5.2.8.4 Neurolucida

Measurement of the neuritic tree of hiPSC derived neurons was performed using the the Neurolucida software in combination with **Stereo Name**. The automated scanning procedure of the Meander Scan was used to track the neuritic trees, as described in .

5.2.8.5 Stereo Investigator

Neuron differentiation efficiency of hiPSC derived neurons was assessed by counting NeuN and DAPI positive cells using the Stereo Investigator software in combination with the optical fraction scan. The automated scanning procedure was set to a counting frame of 100 µm x 100 µm and a grid of 25 counting frames/cover slip.

5.2.8.6 STITCH

Bioinformatic predictions of protein and chemical interactions were predicted using the STITCH database interaction networks of chemicals and proteins [267]. Adaptations and main work was performed by Dietrich Trümbach. Data Mining included all interaction partners, showing more than two predicted interactions.

5.2.8.7 Pathway Studio

Bioinformatic prediction of pathways involved in the HDAC mediated alternative splicing modulation were performed using the pathway finder database. Adaptations and main work was performed by Dietrich Trümbach. Data Mining included all interaction partners, showing more than two predicted interactions.

A Appendix

Table A.1: List of Two-way ANOVA analyses: Time-Genotype

Figure	**Time**		**Genotype**	
	F (DF_n, DF_d)	p-value	F (FD_n, FD_d)	p-value
Fig. 2.3 c	F (8,32) =7.156	$p < 0.0001$	F (1,4) = 47.93	$p = 0.0023$
Fig. 2.3 d	F (5,24) = 18.42	$p < 0.0001$	F (1,24) = 224.1	$p < 0.0001$
Fig. 2.3 f	F (5,24) = 14.43	$p < 0.0001$	F (5,24) = 95.96	$p < 0.0001$

Table A.2: List of Two-way ANOVA analyses: Time-Concentration

Figure	**Time**		**Concentration**	
	F (DF_n, DF_d)	p-value	F (FD_n, FD_d)	p-value
Fig. 2.6 c	F (2,20) = 18.98	$p < 0.0001$	F (4,10) = 23.84	$p < 0.0001$
Fig. 2.6 e	F (1,16) = 531.3	$p < 0.0001$	F (3,16) = 34.25	$p < 0.0001$

Table A.3: List of Two-way ANOVA analyses: Genotype-Treatment

Figure	**Genotype**		**Treatment**	
	F (DF_n, DF_d)	p-value	F (FD_n, FD_d)	p-value
Fig. 2.14 d	F(1,8) = 0.7914	$p = 0.3996$	F(1,8) = 0.1865	$p = 0.6773$
Fig. 2.14 e	F(1,8) = 4.355	$p = 0.0704$	F(1,8) = 4.125	$p = 0.0767$
Fig. 2.13 b	F(1,16) = 9.175	$p = 0.0080$	F(3,16) = 2.015	$p = 0.1525$
Fig. 2.13 d	F(1,16) = 23.47	$p = 0.0002$	F(3,16) = 22.72	$p < 0.0001$
Fig. 2.15 b	F(1,8) = 0.0305	$p = 0.8561$	F(1,8) =0.5622	$p = 0.4748$
Fig. 2.15 d	F(1,8) = 82.70	$p < 0.0001$	F(1,8) = 33.00	$p = 0.0004$

Table A.4: List of One-way ANOVA analyses

Figure	Compound	Isoform	Concentration	
			F (DF_n, DF_d)	p-value
Fig. 2.11 a	TSA	4R/Total Tau	F(1.303,2.606)=474.3	p=0.0005
		Total Tau	F(1.923,3.847)=773.7	p<0.0001
		4R	F(1.469,2.938)=129.1	p=0.0015
Fig. 2.11 b	SAHA	4R/Total Tau	F(1.196,2.393)=376.6	p=0.0011
		Total Tau	F(1.921,3.841)=261.5	p<0.0001
		4R	F(1.377,2.753)=112.6	p=0.0024
Fig. 2.11 c	Panobinostat	4R/Total Tau	F(1.165,2.330)=224.5	p=0.0022
		Total Tau	F(1.160,2.320)=995.9	p=0.0004
		4R	F(1.615,3.230)=96.17	p=0.0014
Fig. 2.11 d	Mocetinostat	4R/Total Tau	F(1.563,3.126)=734.8	p<0.0001
		Total Tau	F(1.515,3.030)=1183	p<0.0001
		4R	F(1.630,3.260)=818.5	p<0.0001
Fig. 2.11 f	Panobinostat		F(1.515,3.029)=74.96	p=0.0028
	TSA		F(1.253,2.505)=19.55	p=0.0305
	5-ITU		F(1.882,3.764)=39.41	p=0.0031
	SAHA		F(1.856,3.712)=17.73	p=0.0129
	Mocetinostat		F(1.239,2.479)=4.241	p=0.1536
Fig. 2.14 a	BMS-309403	4R/Total Tau	F(1.952,3.904)=369.7	p<0.0001
EXSISERS		Total Tau	F(1.332,2.663)=4.251	p=0.1457
		4R	F(1.846,3.692)=273.9	p=0.0001
Fig. 2.14 b	BMS-309403	4R/Total Tau	F(1.376,2.752)=31.95	p=0.0131
IVS10+16EXSISERS		Total Tau	F(1.425,2.850)=1.511	p=0.3362
		4R	F(1.765,3.530)=167.8	p = 0.0003
Fig. 2.14 c EXSISERS	BMS-309403		F(1.779,3.559)=0.6710	p=0.5498
IVS10+16EXSISERS	BMS-309403		F(1.142,2.283)=4.404	p=0.1571
Fig. A.15 a	TSA	4R/Total Tau	F(1.883,3.767)=202.7	p=0.0002
		Total Tau	F(1.248,2.496)=213.8	p=0.0017
		4R	F(1.037,2.074)=44.66	p=0.0197
Fig. A.15 b	SAHA	4R/Total Tau	F(1.168,2.337)=95.45	p=0.0060
		Total Tau	F(1.450,2.901)=76.74	p=0.0033
		4R	F(1.457,2.914)=133.1	p=0.0015
Fig. A.15 c	Panobinostat	4R/Total Tau	F(1.129,2.259)=1190	p=0.0004
		Total Tau	F(1.980,3.961)=231,9	p<0.0001
		4R	F(1.421,2.841)=139.8	p=0.0015
Fig. A.15 d	Mocetinostat	4R/Total Tau	F(1.203,2.407)=257.9	p=0.0016
		Total Tau	F(1.794,3.588)=165.9	p=0.0003
		4R	F(1.851,3.703)=95.22	p=0.0007
Fig. A.15 f	Panobinostat		F(1.586,3.172)=16.60	p=0.0218
	TSA		F(1.255,2.510)=53.53	p=0.0092

Figure	Compound	Isoform	Concentration	
			F (DF_n, DF_d)	p-value
	5-ITU		F(1.653,3.305)=18.65	p=0.0165
	SAHA		F(1.298,2.596)=6.864	p=0.0921
	Mocetinostat		F(1.188,2.376)=24.65	p=0.0264
Fig. A.16 a	TSA	4R/Total Tau	F(1.676,3.351)=719.9	p<0.0001
		Total Tau	F(1.251,2.502)=567.7	p=0.0005
		4R	F(1.302,2.603)=69.44	p=0.0058
Fig. A.16 b	SAHA	4R/Total Tau	F(1.419,2.838)=415.6	p=0.0003
		Total Tau	F(1.704,3.409)=85.46	p=0.0013
		4R	F(1.874,3.749)=209.9	p=0.0001
Fig. A.16 c	Panobinostat	4R/Total Tau	F(1.497,2.995)=561.6	p=0.0001
		Total Tau	F(1.661,3.323)=265.4	p=0.0002
		4R	F(1.237,2.475)=71.45	p=0.0068
Fig. A.16 d	Mocetinostat	4R/Total Tau	F(1.643,3.286)=420,4	p=0.0001
		Total Tau	F(1.562,3.125)=1149	p<0.0001
		4R	F(1.321,2.642)=174.1	p=0.0017
Fig. A.16 f	Panobinostat		F(1.129,2.258)=4.108	p=0.1677
	TSA		F(1.118,2.235)=44.75	p=0.0161
	5-ITU		F(1.882,3.764)=39.41	p=0.0031
	SAHA		F(1.740,3.480)=8.949	p=0.0435
	Mocetinostat		F(1.151,2.302)=17.84	p=0.0402
Fig. A.17 a	CHIR99021	4R/Total Tau	F(1.114,2.229)=17.10	p=0.0446
		Total Tau	F(1.480,2.960)=31.35	p=0.0108
		4R	F(1.511,3.021)=52.38	p=0.0048
Fig. A.17 b	CHIR99021		F(1.889,3.779)=21.56	p=0.0087
Fig. A.17 c	CHIR99021	4R/Total Tau	F(1.324,2.648)=12.74	p=0.0450
		Total Tau	F(1.976,3.951)=15.24	p=0.0139
		4R	F(1.686,3.371)=13.96	p=0.0242
Fig. A.17 d	CHIR99021		F(1.198,2.395)=0.9574	p=0.4382
Fig. A.17 e	CHIR99021	4R/Total Tau	F(1.828,3.656)=20.15	p=0.0109
		Total Tau	F(1.802,3.604)=22.84	p= 0.0093
		4R	F(1.982,3.963)=20.33	p=0.0083
Fig. A.17 f	CHIR99021		F(1.188,2.376)=6.364	p = 0.1091
Fig. A.18 a	BMS-309403	4R/Total Tau	F(1.887,3.774)=369.0	p<0.0001
EXSISERS		Total Tau	F(1.373,2.745)=12.22	p=0.0443
		4R	F(1.894,3.787)=115.8	p=0.0004
Fig. A.18 b	BMS-309403	4R/Total Tau	F(1.128,2.256)=20.28	p=0.0365
IVS10+16EXSISERS		Total Tau	F(1.628,3.256)=0.4247	p=0.6498
		4R	F(1.454,2.908)=14.50	p=0.0320
Fig. A.18 c	BMS-309403	4R/Total Tau	F(1.072,2.144)=19.60	p=0.0418
EXSISERS		Total Tau	F(1.925,3.851)=19.31	p=0.0100
		4R	F(1.117,2.234)=19.96	p=0.0379

Figure	Compound	Isoform	Concentration	
			F (DF_n, DF_d)	p-value
Fig. A.18 d	BMS-309403	4R/Total Tau	F(1.734,3.468)=38.76	p=0.0044
IVS10+16EXSISERS		Total Tau	F(1.593,3.186)=2.296	p=0.2361
		4R	F(1.338,2.677)=14.12	p=0.0390
Fig. A.18 e EXSISERS	BMS-309403		F(1.704,3.407)=9.742	p=0.0401
IVS10+16EXSISERS	BMS-309403		F(1.895,3.790)=5.435	p=0.0776
Fig. A.18 f EXSISERS	BMS-309403		F(1.667,3.334)=11.30	p=0.0338
IVS10+16EXSISERS	BMS-309403		F(1.827,3.653)=11.62	p=0.0267
Fig. A.7 a			F(3,4)=18.44	p=0.0083

Table A.5: List of Kolmogorov-Smirnov-tests analyses

Figure	*p*-value	KSD
Fig. 2.5 a	p < 0.0001	KSD = 0.7551
Fig. A.7 b	p < 0.0001	KSD = 0.4561
Fig. A.7 d	p = 0.0168	KSD = 0.3415
Fig. A.7 f	p < 0.0001	KSD = 0.5850

Table A.6: List of unpaired two-tailed t-test analyses

Figure	Compound	Isoform	*p*-value	t	df
Fig. 2.5 b			p<0.0001	t=5.966	df=78
Fig. 2.11 e	TSA				
	0.1 µM	3R	p=0.0599	t=2.603	df=4
	0.1 µM	4R	p=0.0171	t=3.933	df=4
	SAHA				
	0.8 µM	3R	p=0.1692	t=1.675	df=4
	0.8 µM	4R	p=0.0012	t=8.186	df=4
	1 µM	3R	p=0.0908	t=2.218	df=4
	1 µM	4R	p=0.0014	t=7.913	df=4
	Panobinostat				
	0.01 µM	3R	p=0.0186	t=3.830	df=4
	0.01 µM	4R	p=0.0025	t=6.737	df=4
	Mocetinostat				
	0.4 µM	3R	p=0.0090	t=4.746	df=4
	0.4 µM	4R	p=0.0063	t=5.242	df=4
Fig. 2.14 d EXSISERS			p=0.8054	t=0.2632	df=4

Figure	Compound	Isoform	*p*-value	t	df
IVS10+16EXSISERS			p=0.3196	t=1.136	df=4
Fig. 2.14 e EXSISERS			p=0.7344	t=0.3638	df=4
IVS10+16EXSISERS			p=0.0150	t=4.088	df=4
Fig. 2.13 a	Mocetinostat	4R/Total Tau	p<0.0001	t=27	df=4
		Total Tau	p=0.0375	t=3.064	df=4
		4R	p=0.0009	t=8.983	df=4
	SAHA	4R/Total Tau	p=0.0353	t=3.126	df=4
		Total Tau	p=0.0002	t=13.15	df=4
		4R	p<0.0001	t=35.57	df=4
	5-ITU	4R/Total Tau	p=0.0384	t=3.039	df=4
		Total Tau	p=0.0001	t=14.35	df=4
		4R	p=0.0006	t=9.733	df=4
Fig. 2.13 c	Mocetinostat	4R/Total Tau	p=0.3462	t=1.067	df=4
		Total Tau	p=0.0933	t=2.194	df=4
		4R	p=0.0205	t=3.720	df=4
	SAHA	4R/Total Tau	p=0.0785	t=2.351	df=4
		Total Tau	p=0.3276	t=1.114	df=4
		4R	p=0.2270	t=1.426	df=4
	5-ITU	4R/Total Tau	p=0.1069	t=2.073	df=4
		Total Tau	p=0.0023	t=6.902	df=4
		4R	p=0.1679	t=1.682	df=4
Fig. 2.15 a	BMS-309403	4R/Total Tau	p=0.0368	t=3.082	df=4
		Total Tau	p=0.0125	t=4.134	df=4
		4R	p=0.6563	t=0.4799	df = 4
Fig. 2.15 c	BMS-309403	4R/Total Tau	p=0.0001	t=15.50	df=4
		Total Tau	p=0.0005	t=10.27	df=4
		4R	p=0.0347	t=3.145	df=4
Fig. A.7 c			p=0.0010	t=3.405	df=78
Fig. A.7 e			p<0.0001	t=4.571	df=78

Table A.7: Selected Broad Repurposing Library analysis. Initial Broad Repurposing Library analysis of all compounds tested in the hit verification process. Wherby, values of NLuc, FLuc, their ratio (NLuc/FLuc), %Activity (calculated by equation 5.5) and HT (calculated by equation 5.4) are listed.

Compound	NLuc	FLuc	NLuc/FLuc	%Activity	HT
BMS-309403	190	2908	0.06533	5.02	236.98
Chidamide	8430	2982	2.82696	222.62	282.20
CHIR99021	824	1538	0.53576	110.45	315.95
Eptapirone	67	3236	0.02070	1.57	282.20
Indatraline HCl	4334	5507	0.78700	67.56	196.29

Compound	NLuc	FLuc	NLuc/FLuc	%Activity	HT
Mocetinostat	6298	942	6.68577	464.79	237.26
Nazartinib	208	2346	0.08866	6.45	236.98
Panobinostat	8026	3182	2.52231	198.23	282.20
PT-2385	236	2275	0.10374	7.17	236.98
SAHA	4016	776	5,17526	404.10	315.04
TSA	4177	699	5.97568	415.46	237.26

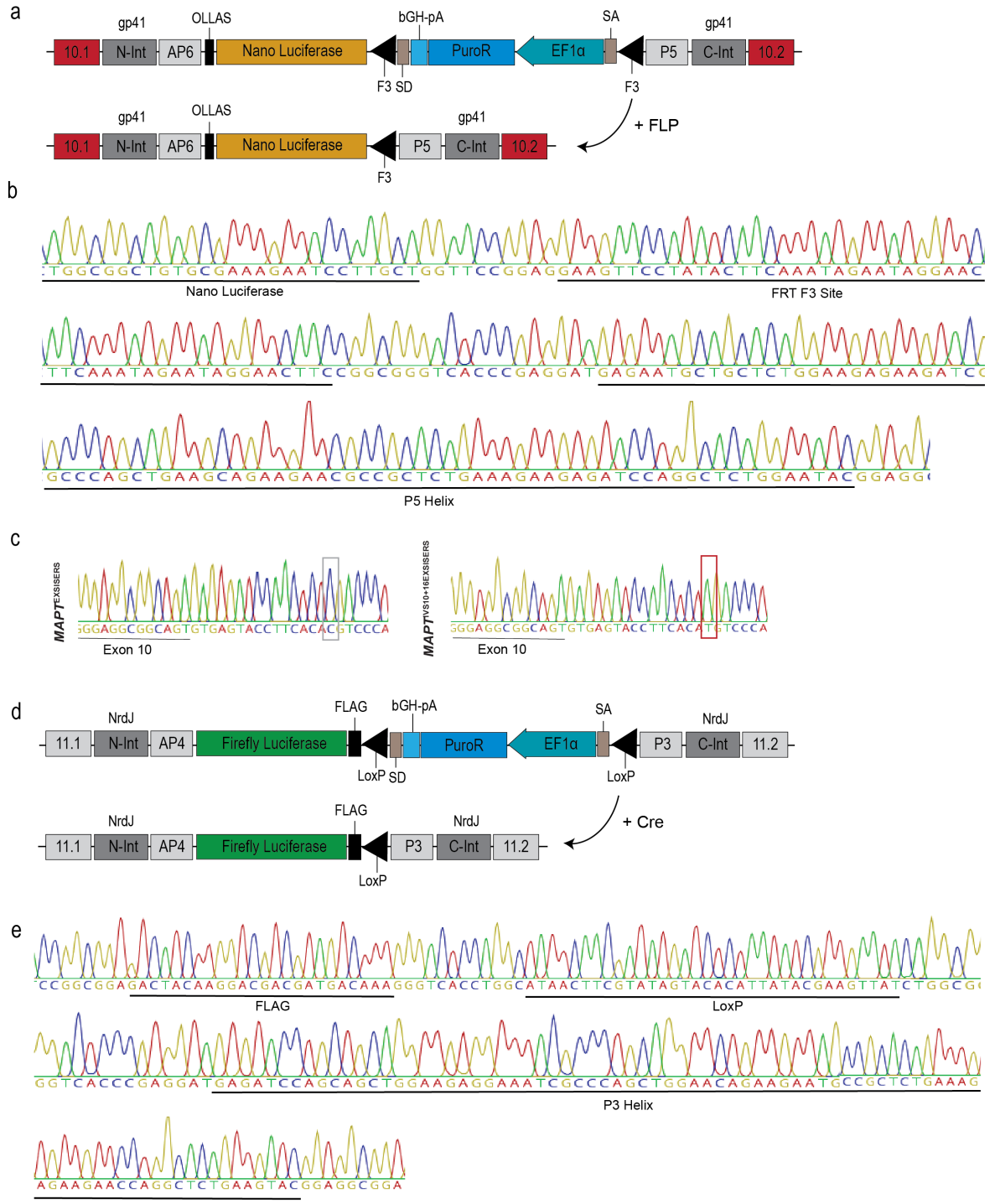

Figure A.1: Generation of *MAPT*$^{\text{EXSISERS}}$ hiPSC Line. (a) Schematic description of the CRISPR/Cas9 mediated KI of the EXSISERS into *MAPT* exon 10 (red, 10.1 and 10.2), with NLuc as a reporter for the Tau 4R isoforms (yellow) and excision of the F3 sites (black) flanked selection cassette, PuroR (blue), by FLP. PuroR selection cassette expression was regulated by the EF1α promoter (cyan). Post-translational intein-mediated excision of the *MAPT*$^{\text{EXSISERSEx10:NLuc}}$ is enabled by gp41-inteins, N-terminus (N-Int) and C-terminus (C-Int) of the KI cassette. α-helices (AP6 and P5, bright grey) enhance the intein-mediated reporter excision. The OLLAS epitope tag was included in *MAPT*$^{\text{EXSISERSEx10:NLuc}}$. (b) Molecular analysis of the homozygously tar-

Figure A.1 ***(continued)*:** geted hiPSC $MAPT^{\text{EXSISERS}}$ clone to confirm excision of the F3 site flanked election cassette. (c) Molecular confirmation of introduction of the of the tauopathy associated point mutation IVS10+16 c>t in the hiPSC $MAPT^{\text{IVS10+16EXSISERS}}$ line by Sanger Sequencing. The red box indicates the position of the transition from c>t. (d) Schema describing the CRISPR/Cas9 mediated KI of the EXSISERS into *MAPT* exon 11 (grey, 11.1 and 11.2) with FLuc as a reporter for Total Tau (green) and excision of the LoxP sites flanked selection cassette, PuroR, (blue) by Cre. PuroR selection cassette expression was regulated by the EF1α promoter (cyan). Post-translational intein-mediated self-excision of the $MAPT^{\text{EXSISERSEx11:FLuc}}$ is enabled by NrdJ-inteins, N-terminus (N-Int) and C-terminus (C-Int) of the KI cassette. α-helices (AP6 and P5, bright grey) enhance the intein-mediated reporter excision. The FLAG epitope tag was included in $MAPT^{\text{EXSISERSEx11:FLuc}}$. (e) Molecular analysis of the homozygously targeted hiPSC $MAPT^{\text{EXSISERS}}$ clone to confirm excision of the LoxP site flanked selection cassette.

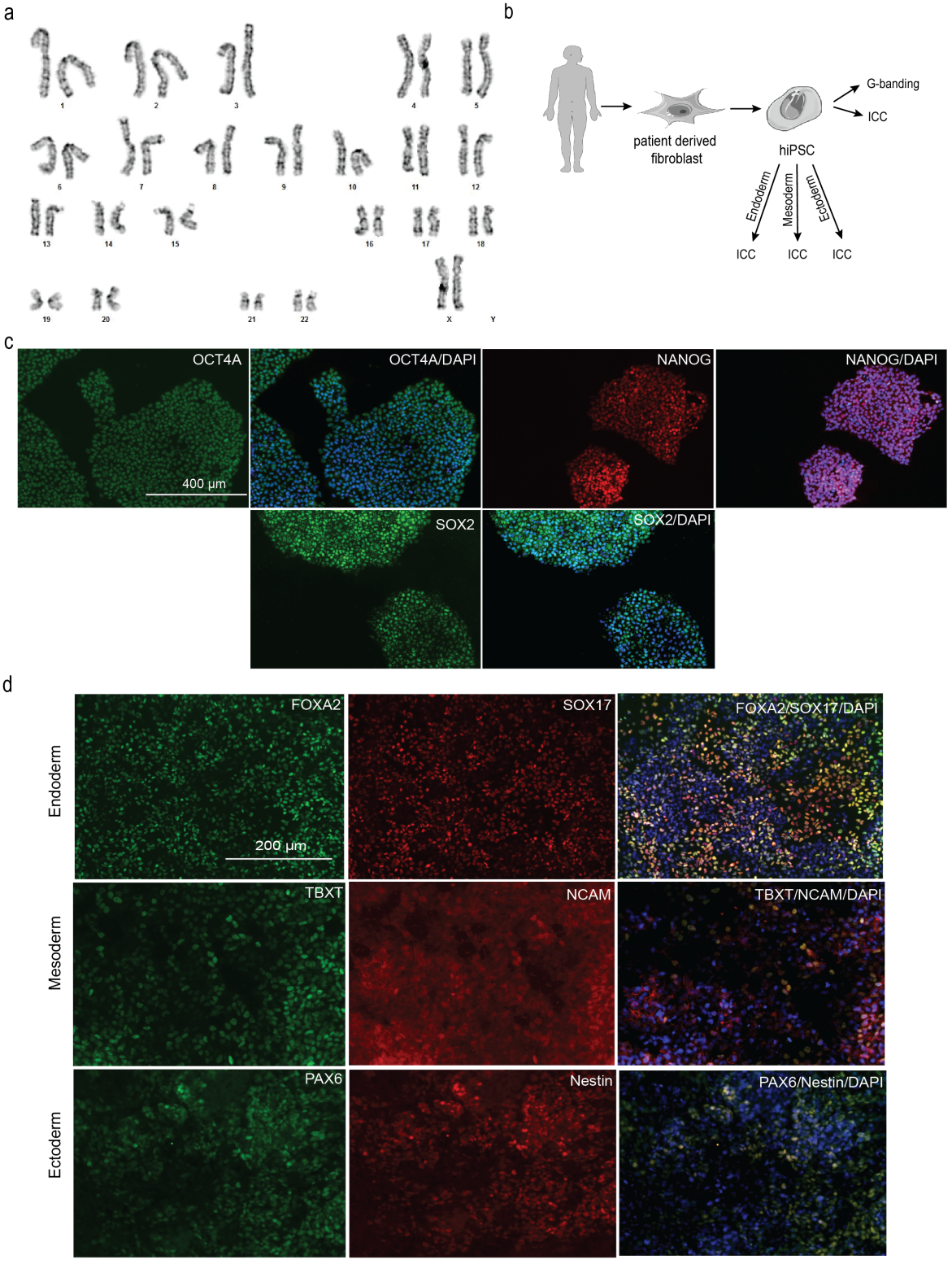

Figure A.2: Pluripotency of *MAPT*$^{\text{IVS10+16EXSISERS}}$ hiPSC Line. (a) Normal genetically female karyotype of the *MAPT*$^{\text{IVS10+16EXSISERS}}$ hiPSC line. (b) Schematic description of pluripotency assessment. HiPSCs were used for analyses of the karyotype, pluripotency marker expression and germ layer differentiation after CRISPR/Cas9 mediated KI of the EXSISERS into the *MAPT* locus. Germ layer specificity was analysed

Figure A.2 ***(continued)*:** by marker expression. (c) Immunofluorescence analysis of $MAPT^{\text{IVS10+16EXSISERS}}$ hiPSC line staining positive for pluripotency associated markers OCT4A, NANOG and SOX2. (d) Differentiation of the $MAPT^{\text{IVS10+16EXSISERS}}$ hiPSC line into all three germ layers. Immunofluorescence analysis of endoderm specific markers FOXA2 (green) and SOX17 (red), mesoderm specific markers TBXT (green) and NCAM (red) and ectoderm specific markers paired box 6 (green) and Nestin (red).

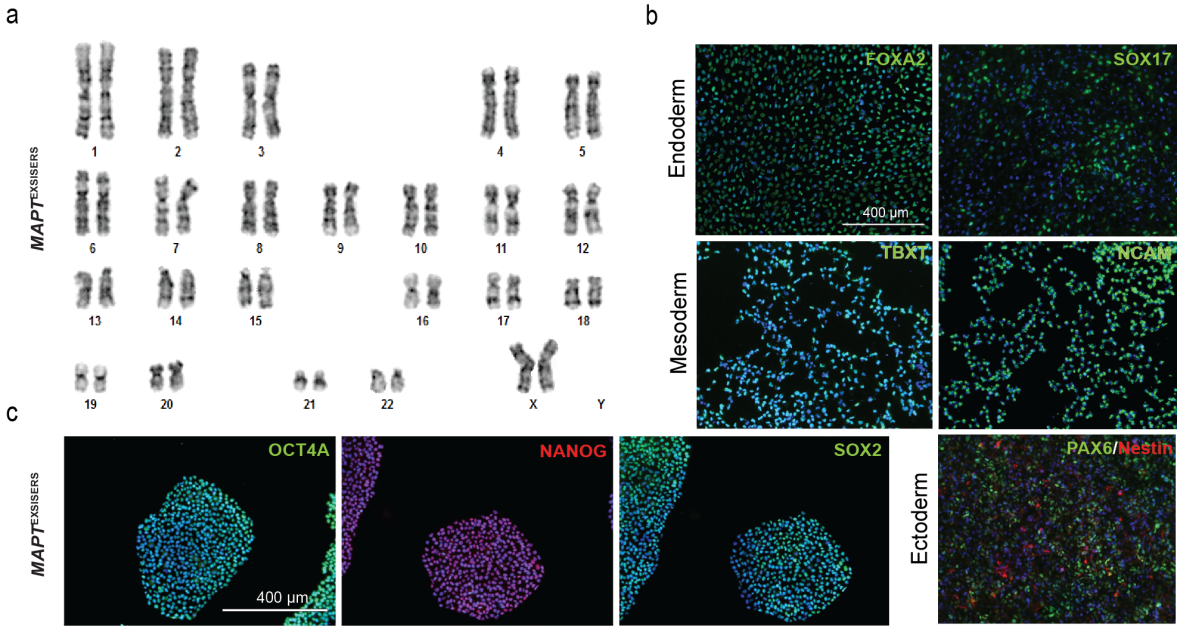

Figure A.3: Pluripotency of $MAPT^{\text{EXSISERS}}$ hiPSC Line. (a) Normal genetically female karyotype of the $MAPT^{\text{EXSISERS}}$ hiPSC line. (b) Differentiation of the $MAPT^{\text{EXSISERS}}$ hiPSC line into all three germ layers. Immunofluorescence analysis of endoderm specific markers FOXA2 (green) and SOX17 (green), mesoderm specific markers TBXT (green) and NCAM (green) and ectoderm specific markers PAX6 (green) and Nestin (red). (c) Immunofluorescence analysis of $MAPT^{\text{EXSISERS}}$ hiPSC line staining positive for pluripotency associated markers Oct3/4 (green), NANOG (red) and SOX2 (green).

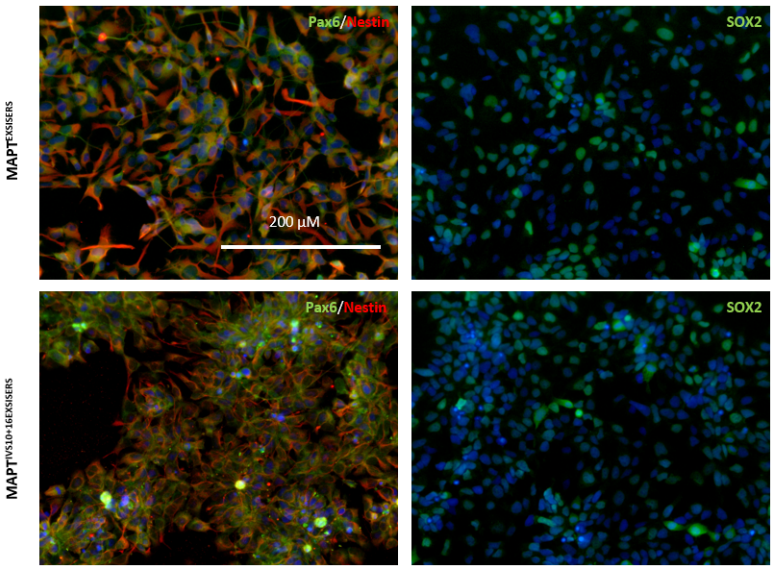

Figure A.5: Confirmation of smNPC identity. ICC of Pax6, Nestin and SOX2 to confirm hiPSC derived smNPC identity of $MAPT^{\text{EXSISERS}}$ and $MAPT^{\text{IVS10+16EXSISERS}}$ following the adherent smNPC protocol.

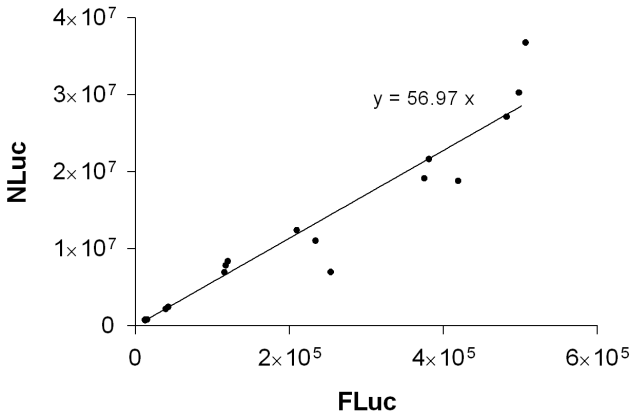

Figure A.4: Bioluminescence assessment of NLuc and FLuc. Assessment of absolute RLU relation between NLuc and FLuc under the set assay conditions in HEK293T cells. 56.97 FLuc are needed to match the brightness of one NLuc protein.

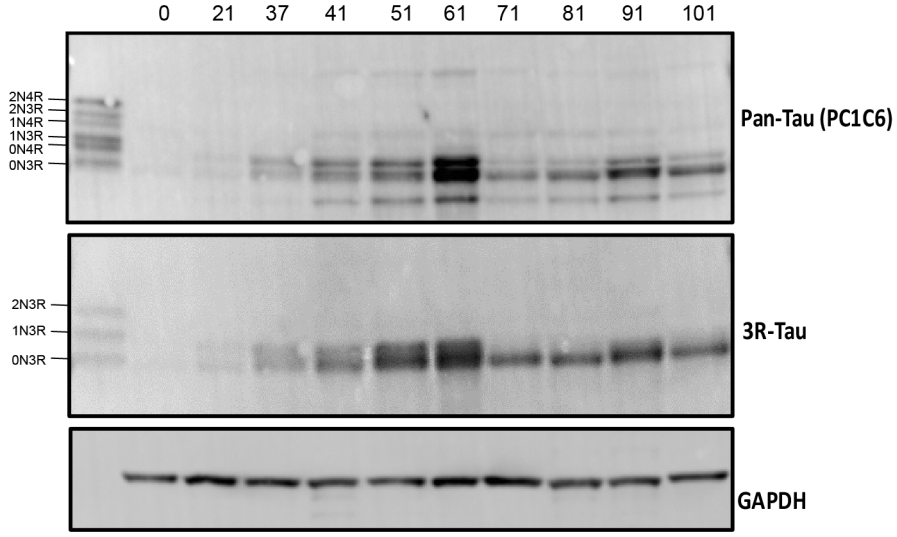

Figure A.6: Longitudinal Tau expression in $MAPT^{\text{IVS10+16EXSISERS}}$. Longitudinal Tau expression of $MAPT^{\text{IVS10+16EXSISERS}}$ hiPSC derived neurons over a time course of 100 days. The Tau ladder gives indication on the six Tau isoforms expressed in the mature human brain., blotting for pan-Tau and the 3R isoforms, GAPDH served as a loading control.

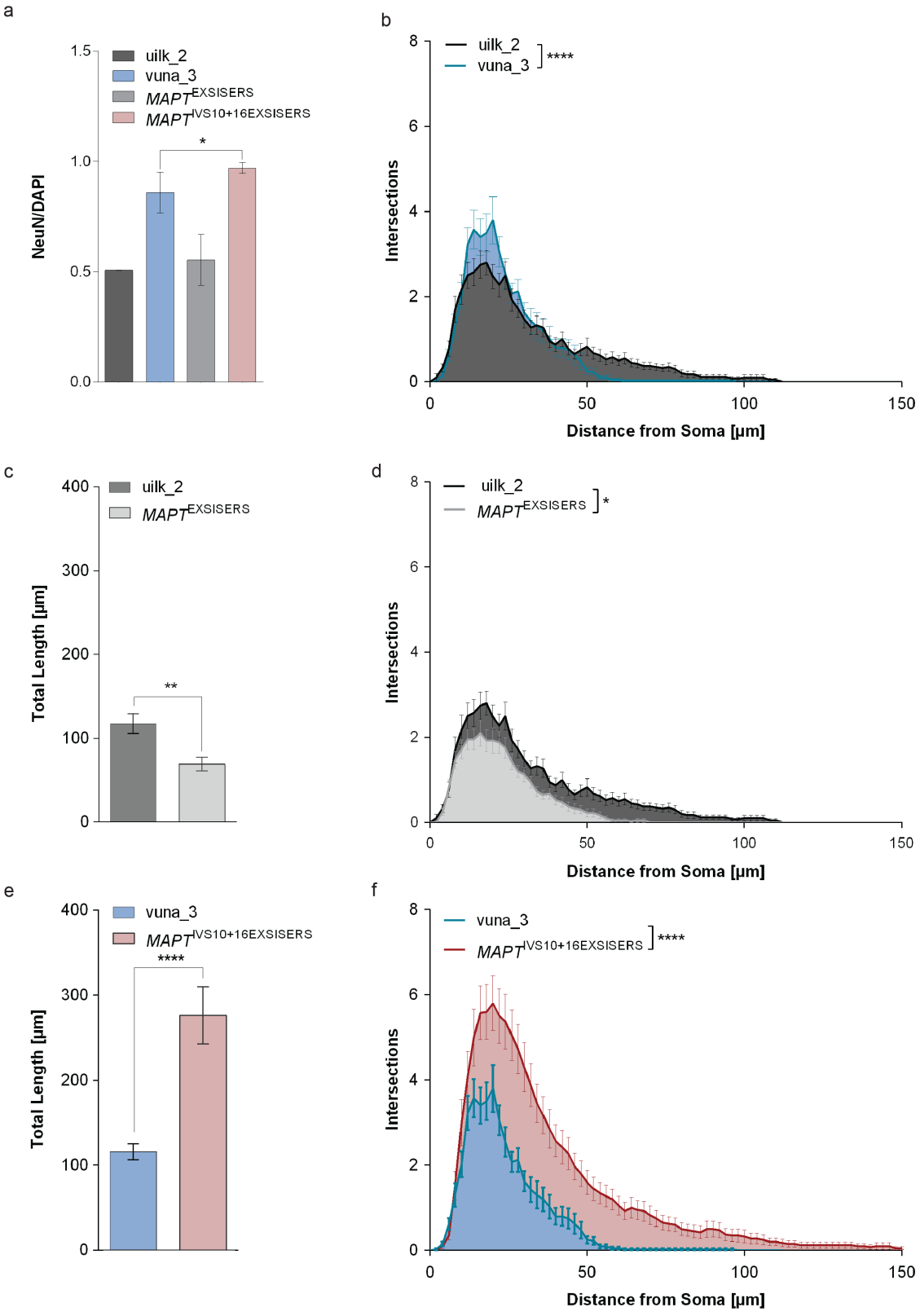

Figure A.7: Neuritic tree analysis. (a) Neuron differentiation efficiency and (b) Sholl analysis of hiPSC derived neurons day 41 of differentiation) of the parental cell lines HPSI0614i-uilk_2 (dark grey) and HPSI0514i-

Figure A.7 ***(continued)*:** vuna_3 (bright blue). (c) Total tree length and (d) Sholl analysis of hiPSC derived neurons HPSI0614i-uilk_2 (dark grey) and $MAPT^{\text{EXSISERS}}$ (bright grey). (e) Total tree length and (f) Sholl analysis of HPSI0514i-vuna_3 (bright blue) and $MAPT^{\text{IVS10+16EXSISERS}}$ (red). Data show the mean ± SEM of 40 measured neurons per cell line. Selected statistical tests (unpaired two-tailed t-test (a,c,d), Kolmogorov-Smirnov-Test (b, d, f)) are shown: p-value: * < 0.05, ** < 0.01, *** < 0.001, **** < 0.0001 (detailed statistical results are provided in Table A.6 and A.5.

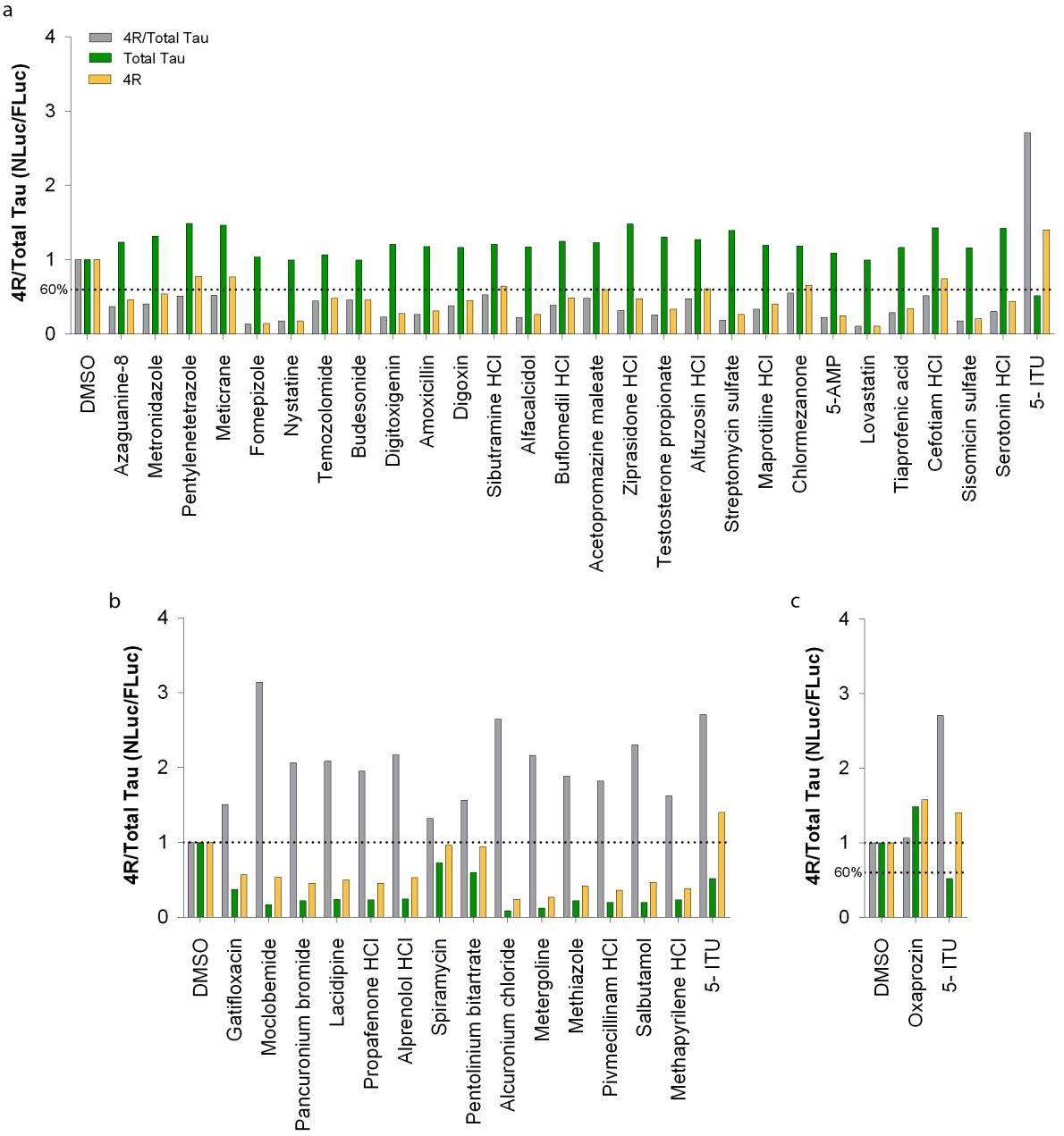

Figure A.8: Prestwick Library - Potential Compounds of *MAPT* Alternative Splicing Modulation. 4R/Total Tau ratio (grey), Total Tau (green) and 4R (yellow) of the RLUs of NLuc and FLuc, normalised to vehicle for all compounds selected for potential *MAPT* alternative splicing modulation identified in primary Prestwick library screen, (a) by exon 10 exclusion, (b) by exon 10 inclusion, (c) general upregulation of Tau expression. A threshold (dotted line) of $< 60\%$ 4R expression compared to the vehicle control was applied for exon 10 exclusion, $> 100\%$ for exon 10 inclusion and overall upregulation $> 100\%$ of the vehicle control for 4R and Total Tau for general upregulation.

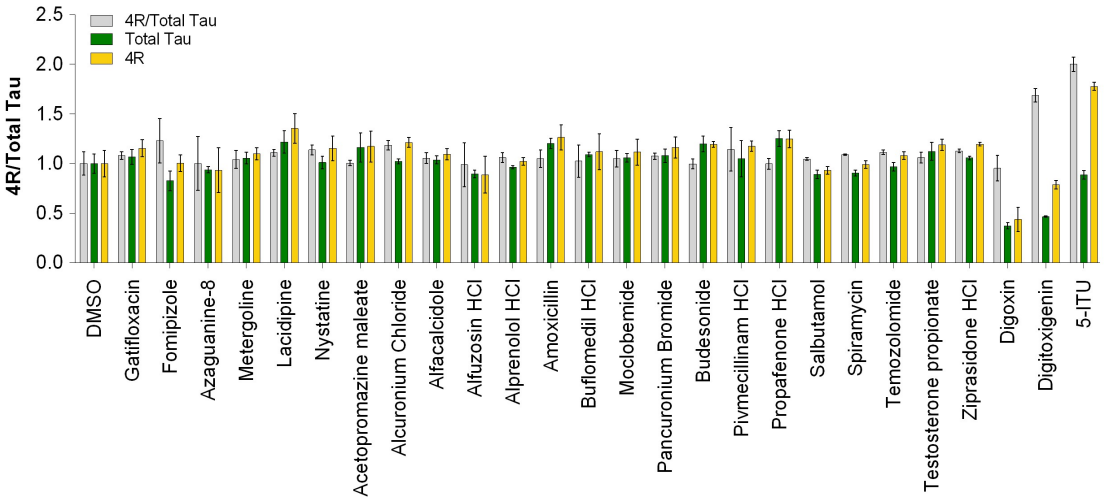

Figure A.9: Prestwick Library - Nominated Hit Verification. Out of 1280 compounds identified in the primary screen 25 compounds were subject for further analysis. 4R/Total Tau ratio (grey), Total Tau (green) and 4R (yellow) as a function of 1 µM of referring compound normalised to vehicle. Data are the mean ± SD of three technical and biological replica.

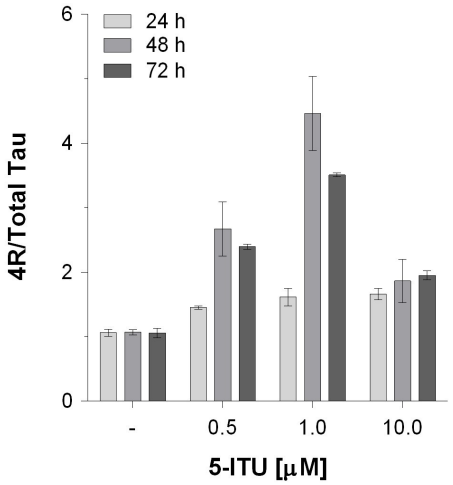

Time	Concentration	*Z'-factor*
48 h	1.0 µM	0.26
	10.0 µM	-0.43
72 h	1 µM	0.87
	10.0 µM	0.52

Figure A.10: EXSISERS stability assessment. Stability assessment under screening conditions by upregulation of the 4R Tau isoforms by DYRK1A/GSK3β inhibitor 5-Iodotubercidin (5-ITU). $MAPT^{\text{EXSISERS}}$ hiPSC derived smNPCs were exposed to 0.5, 1.0 and 10 µM 5-ITU over a time period of 24 h, 48 h and 72 h. Selected Z'-factors are listed (calculated as described by equation 5.6) with considerate 4R/Total Tau ratio of the RLUs of nano luciferase (NLuc) and firefly luciferase (FLuc) normalised to vehicle.

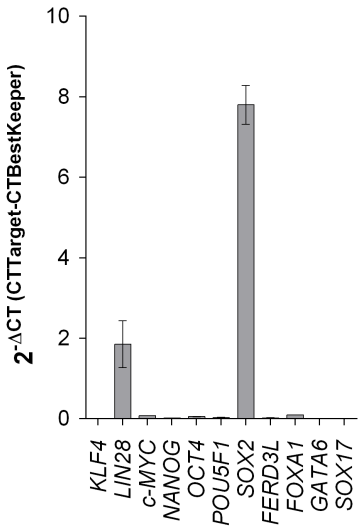

Figure A.11: Primary Prestwick Library Screen. Gene expression in $MAPT^{\text{EXSISERS}}$ hiPSC derived smNPCs used for Prestwick library screen. *KLF4*, *LIN28*, *c-MYC*, *NANOG*, *Oct3/4*, *POU5F1* and *SOX2* being markers for stemness, markers for early differentiation are *FERD3L*, *FOXA1*, *GATA binding protein 6* and *SOX17*. Values of target genes were normalised to the best keeper, calculated based on [262]. Data are the mean ± SD of three technical replica.

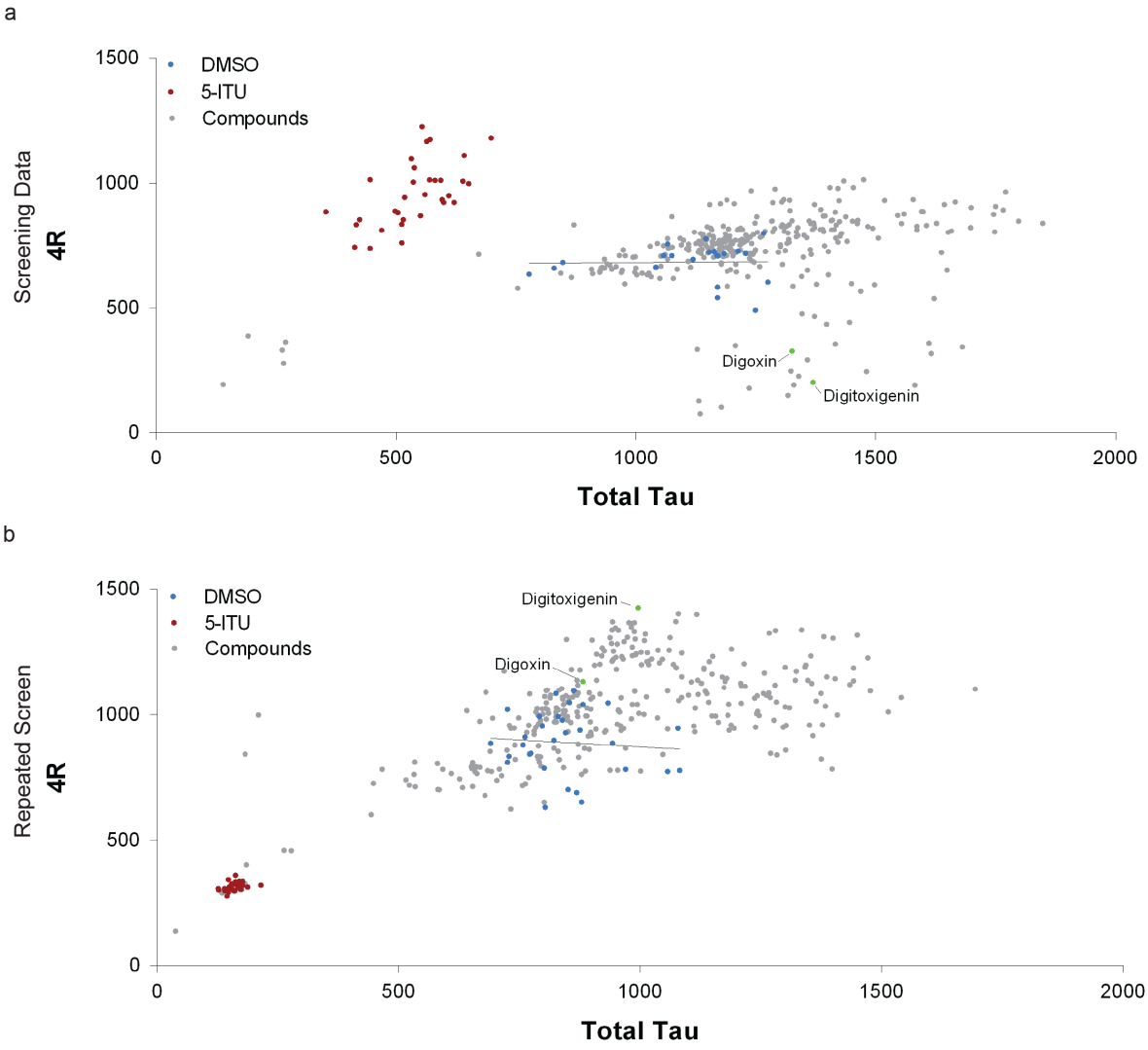

Figure A.12: Prestwick Library- FDA02 Rerun. Out of the 1280 initially screened compounds, 320 compounds were reassessed under the same screening conditions in $MAPT^{\text{EXSISERS}}$ hiPSC derived smNPCs. (a) Scatter blot of absolute NLuc and FLuc RLUs for 4R and Total Tau expression of the (a) initial screen and (b) repeated screen. Whereby, $MAPT^{\text{EXSISERS}}$ hiPSC derived smNPCs were exposed to the library for 72 h prior to bioluminescence imaging. 5-ITU (red), a DYRK1A/GSK3β inhibitor, served as a positive control for Tau 4R upregulation, DMSO as vehicle (blue). The linear regression of the vehicle is shown by a line (black). Responding values of Digoxin and Digitoxigenin are shown in green.

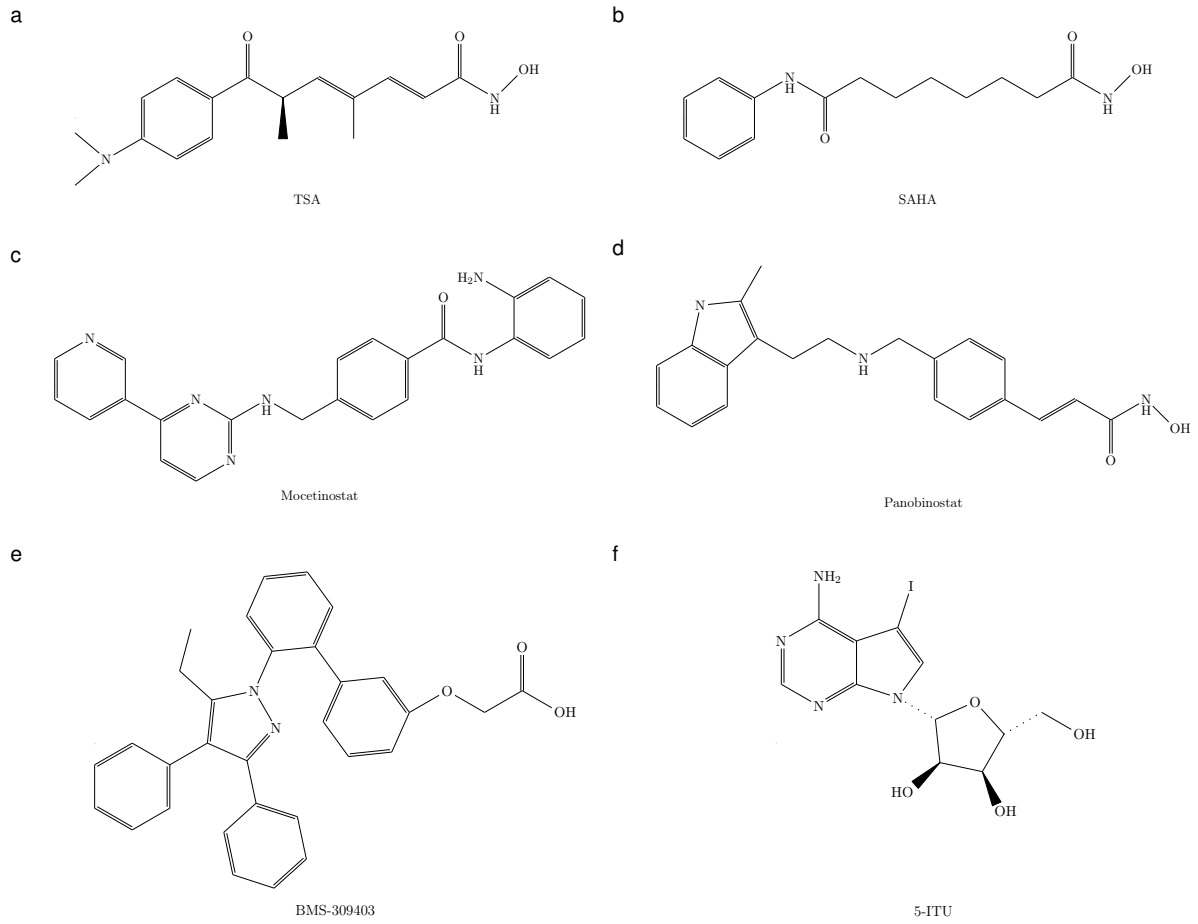

Figure A.13: Chemical structure of identified 4R Tau modulators. Chemical structure of 4R Tau upregulating compound (a) TSA, (b) SAHA, (c) Mocetinostat, (d) Panobinostat. (e) Chemical structure of the 4R Tau downregulating compound BMS-309403. (f) Chemical structure of the DYRK1A/GSK3β inhibitor 5-ITU, with 4R Tau upregulating properties.

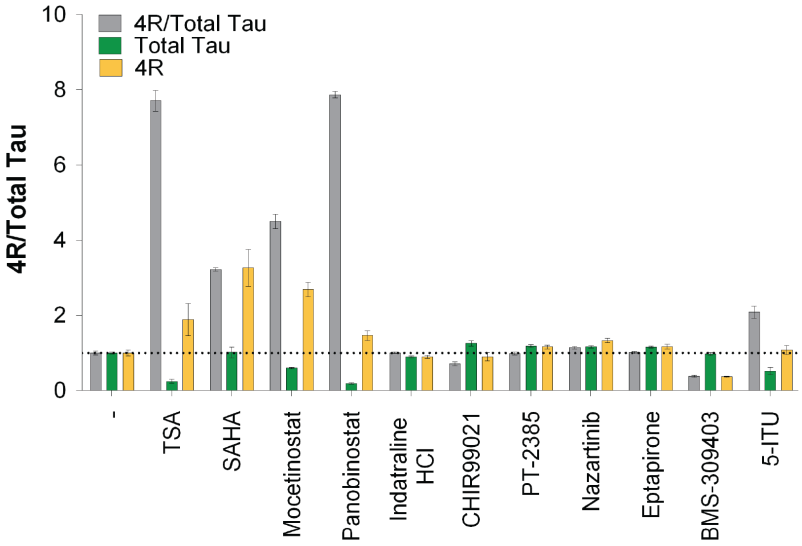

Figure A.14: Broad Repurposing Library Screen - 1 µM validation Bar chart of verification of nominated primary hits normalised to vehicle. Shown are the 4R/Total Tau ratio (grey), Total Tau (green) and 4R (yellow) of relative NLuc (4R Tau) and FLuc (Total Tau) RLUs. The black dashed line indicates the vehicle control, all values are normalised to. Data are the mean ± SD of three technical replica.

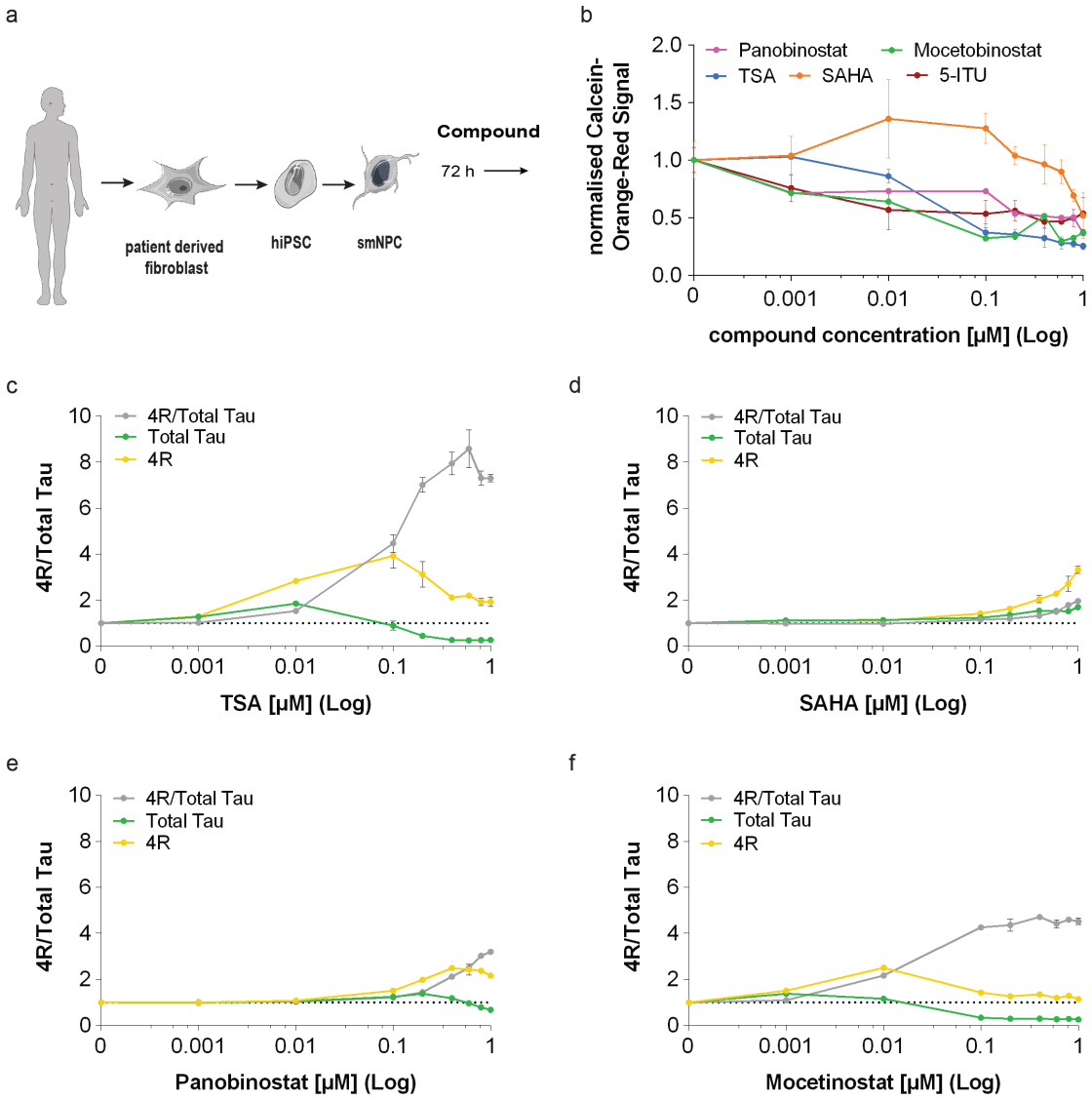

Figure A.15: *MAPT* Alternative Splicing Modulators- Independent experiment 2. (a) Schematic description of compound treatment in hiPSC derived smNPCs (b) Cell viability as relative calcein-orange-red signal after TSA (orange), SAHA (blue), CHIR99021 (grey), 5-ITU (black), Mocetinostat (purple) and Panobinostat (red) treatment as a function of increasing compound concentration normalised to vehicle. Dose response as a linear-log plot of (c) TSA, (d) SAHA, (e) Panobinostat and (f) Mocetinostat in $MAPT^{\text{EXSISERS}}$hiPSC derived smNPCs after compound treatment of 72 h. (c-f) Relative NLuc and FLuc RLUs for 4R Tau (yellow), Total Tau (green) and 4R/Total Tau (grey). Data is normalised to each vehicle control. (b-f) Data show the mean ± SD of a representing experiment of three biological replica (see 2.3 and A.16). Selected ANOVA analysis results of Bonferroni MCT are shown: p-value: * < 0.05, ** < 0.01, *** < 0.001, **** < 0.0001 (detailed statistical results are provided in Supp. Tab. A.4.

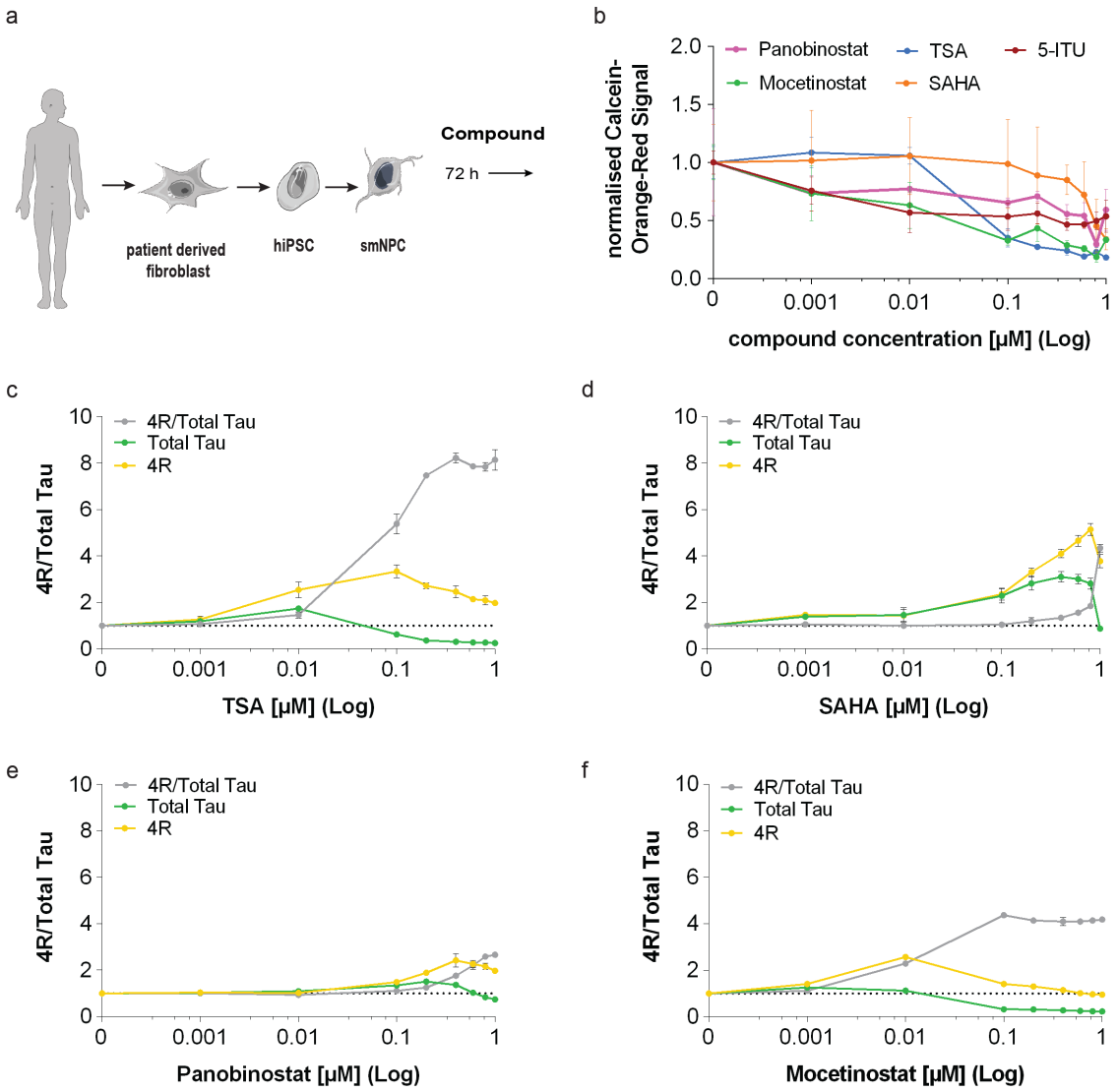

Figure A.16: *MAPT* Alternative Splicing Modulators- Independent experiment 3.(a) Schematic description of compound treatment in hiPSC derived smNPCs (b) Cell viability as relative calcein-orange-red signal after TSA (orange), SAHA (blue), CHIR99021 (grey), 5-ITU (black), Mocetinostat (purple) and Panobinostat (red) treatment as a function of increasing compound concentration normalised to vehicle. Dose response as a linear-log plot of (c) TSA, (d) SAHA, (e) Panobinostat and (f) Mocetinostat in $MAPT^{\text{EXSISERS}}$hiPSC derived smNPCs after compound treatment of 72 h. (c-f) Relative NLuc and FLuc RLUs for 4R Tau (yellow), Total Tau (green) and 4R/Total Tau (grey). Data is normalised to each vehicle control. (b-f) Data show the mean ± SD of a representing experiment of three biological replica (see 2.3 and A.15). Selected one-way ANOVA analysis results of Bonferroni MCT are shown: p-value: * < 0.05, ** < 0.01, *** < 0.001, **** < 0.0001 (detailed statistical results are provided in Supp. Tab. A.4.

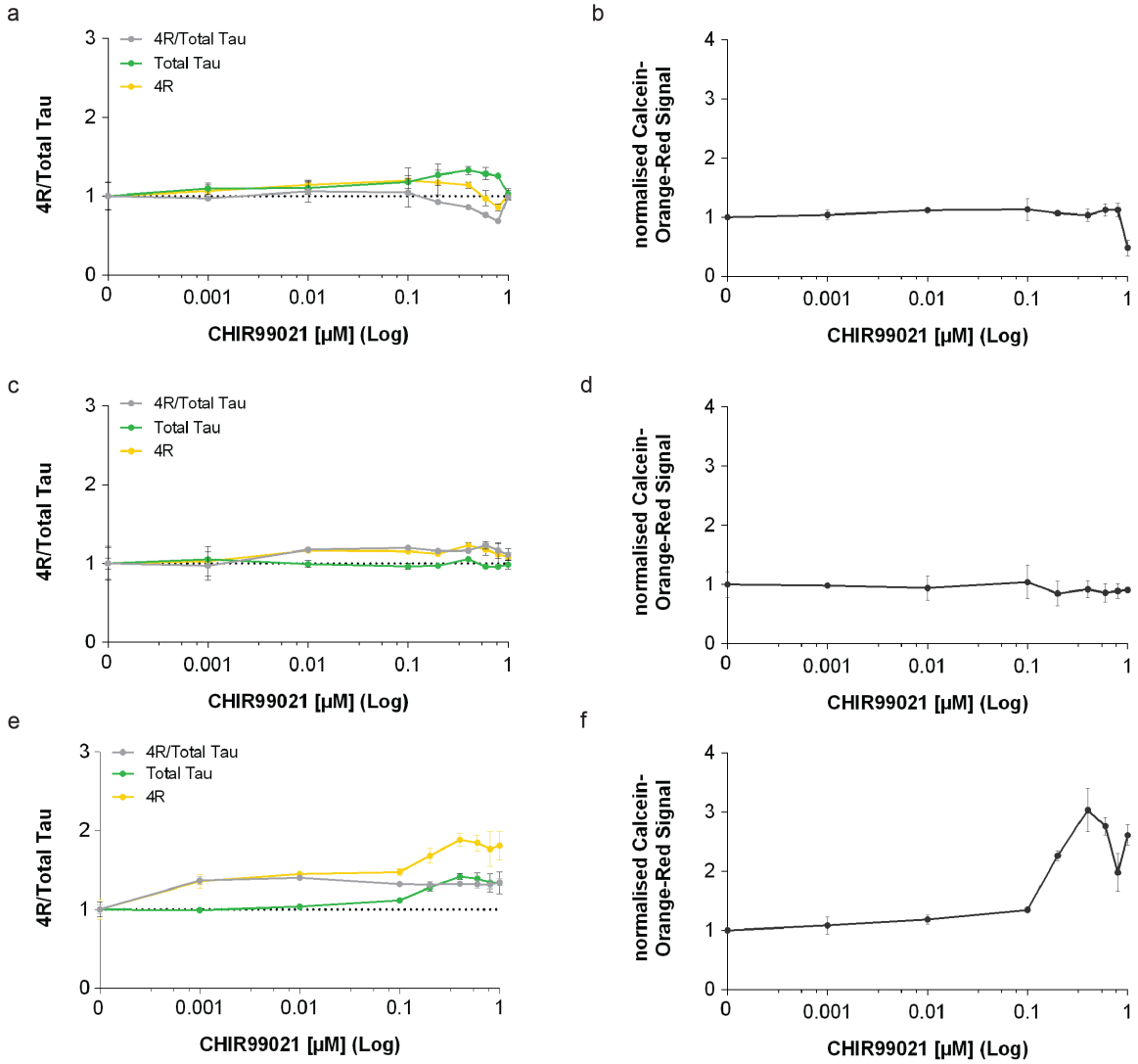

Figure A.17: *MAPT* Alternative Splicing Modulators - CHIR99021. (a,c,e) Three independent experiment of *MAPT* alternative splicing modulation by CHIR99021 $MAPT^{\text{EXSISERS}}$ hiPSC derived smNPCs as a function of increasing compound concentration, showing the relative 4R/Total Tau ratio (grey), Total Tau (green) and 4R values (yellow) normalised to the vehicle control. (b,d,f) Three independent cell viability assays in $MAPT^{\text{EXSISERS}}$ hiPSC derived smNPCs as a function of increased CHIR99021 concentration. Data show the mean ± SD of three technical replica. Selected ANOVA analysis results of Bonferroni MCT are shown: p-value: * < 0.05, ** < 0.01, *** < 0.001, **** < 0.0001 (detailed statistical results are provided in Supp. Tab. A.4.

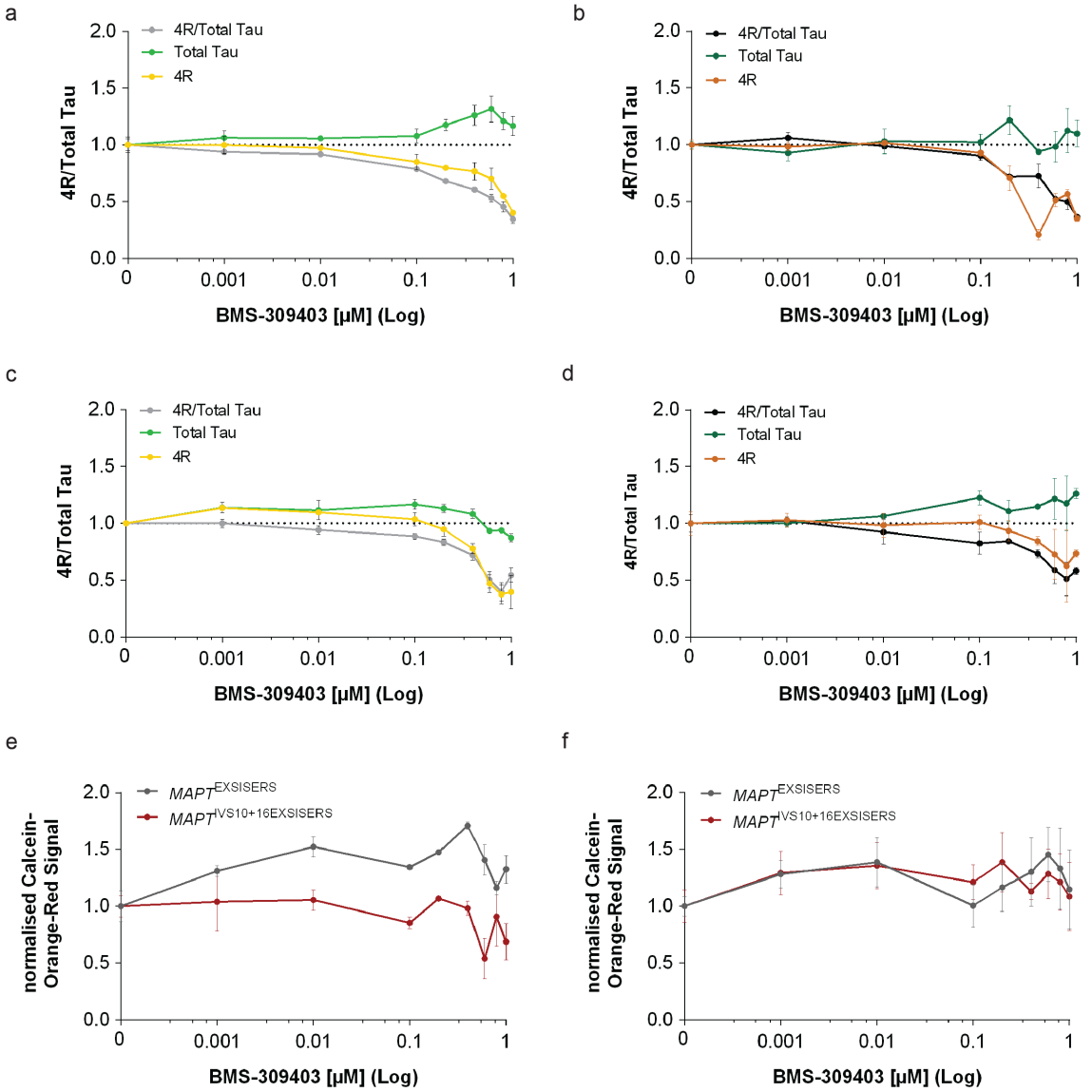

Figure A.18: *MAPT* Alternative Splicing Modulators - BMS-309403. Second and third independent experiment of *MAPT* alternative splicing modulation by BMS-309403 in (a+c) $MAPT^{EXSISERS}$ *and (b+d)* $MAPT^{IVS10+16EXSISERS}$ as a function of increasing compound concentration, showing the 4R/Total Tau ratio (grey, black), Total Tau (bright green, dark green) and 4R values (yellow, orange) normalised to the respective vehicle control. (e+f) Second and third independent cell viability assay in $MAPT^{EXSISERS}$ (grey) and $MAPT^{IVS10+16EXSISERS}$ (red) as a function of increased BMS-309403 concentration. Data show the mean ± SD of three technical replica. Selected ANOVA analysis results of Bonferroni MCT are shown: p-value: * < 0.05, ** < 0.01, *** < 0.001, **** < 0.0001 (detailed statistical results are provided in Supp. Tab. A.4.

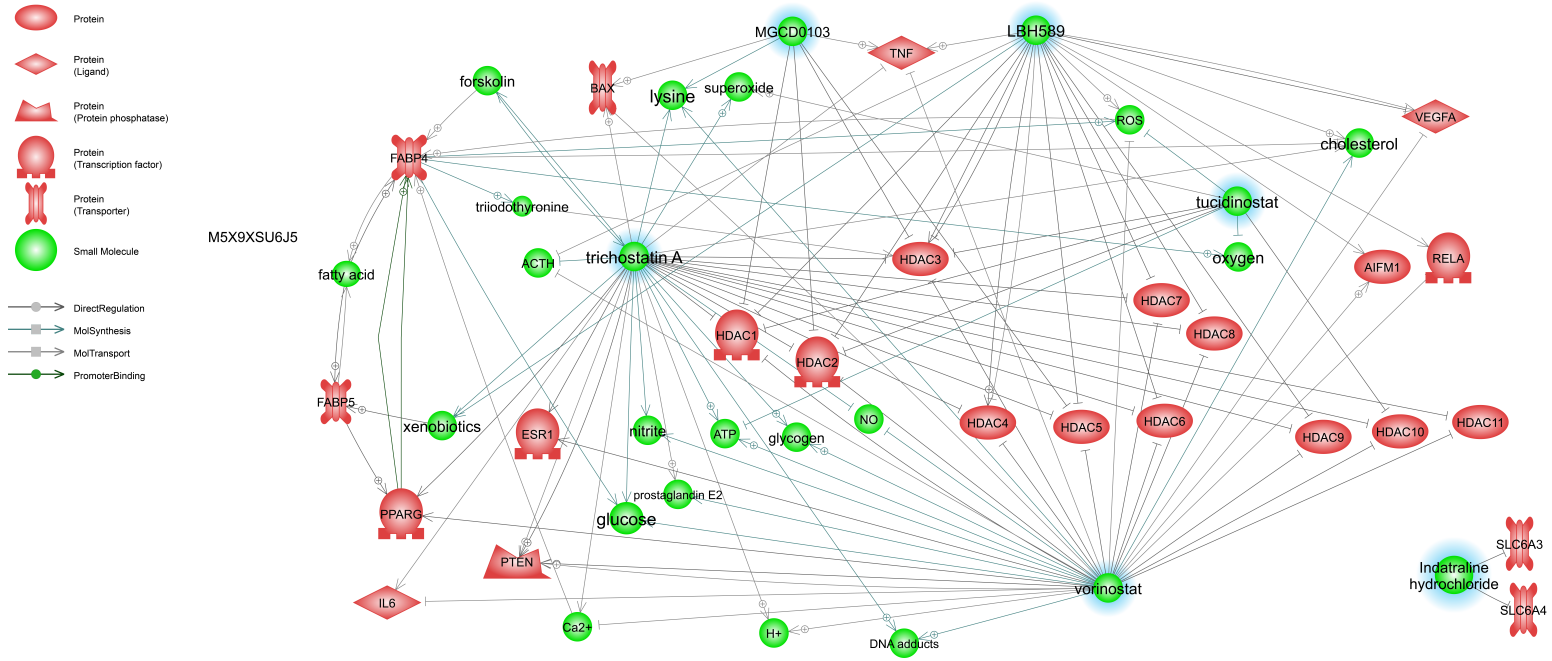

Figure A.19: Pathway Studio Data Mining. The pathways involved in *MAPT* alternative spicing and 4R Tau isoform regulation were deducted by *in silico* literature mining using the Pathway Studio database. The network was consolidated by verification of all connections in the published literature. The bioinformatic analysis was performed by Dietrich Trümbach.

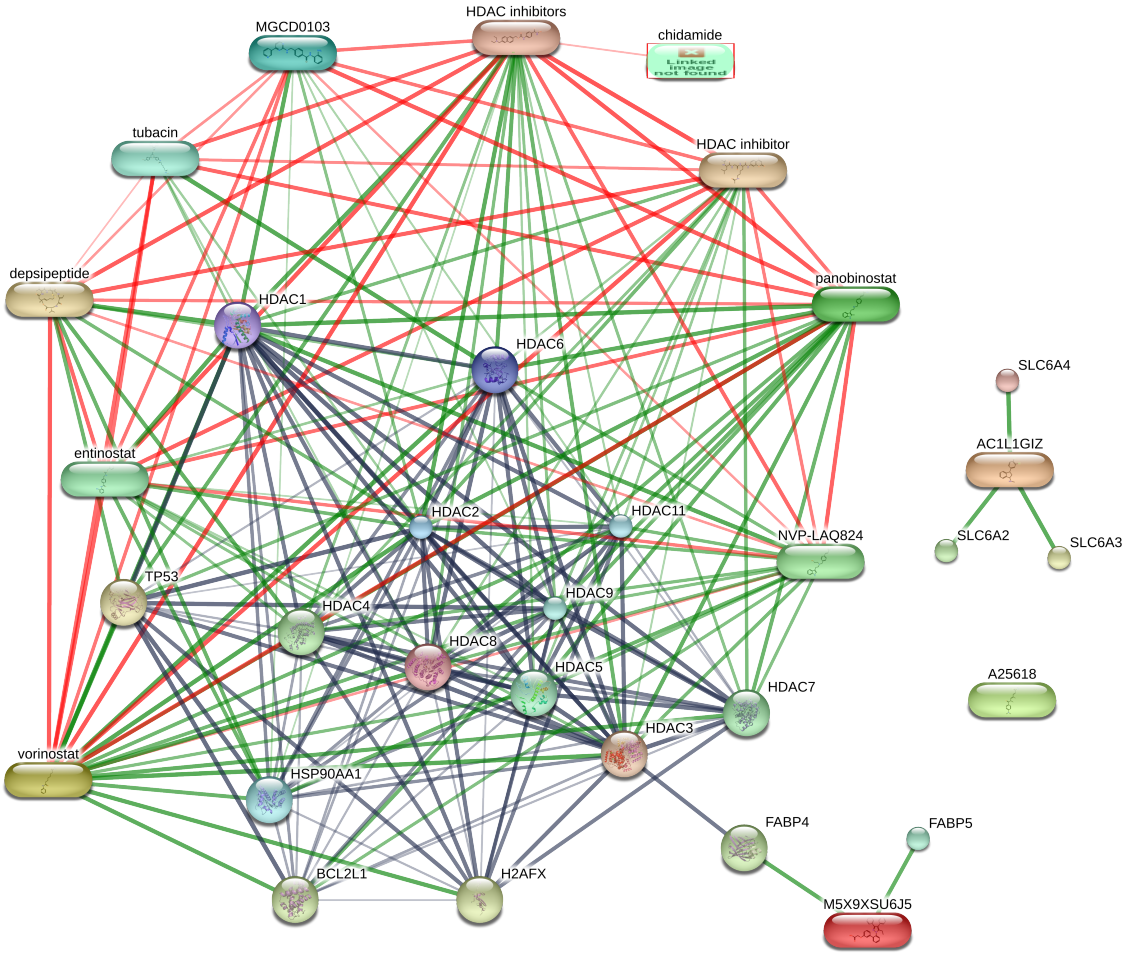

Figure A.20: Stitch Data Mining. The pathways involved in *MAPT* alternative spicing and 4R Tau isoform regulation were deducted by *in silico* literature mining using the Stitch database [267]. The network was consolidated by verification of all connections in the published literature. The bioinformatic analysis was performed by Dietrich Trümbach.

List of Figures

List of Tables

Acronyms

β-ME	β-mercaptoethanol
3R	three repeat
4E-BP	eIF4E binding protein
4R	four repeat
5-ITU	5-Iodotubercidin
FABPi	FABP inhibition
FTLD-Tau	FTLD-Tau
HDACi	HDAC inhibition
PPARi	PPAR inhibition
smNPC	small molecule neuronal precursor cell
E.coli	*Escherichia coli*
Aβ	amyloid β
AD	Alzheimer's Disease
ADAM10	a disintegrin and metalloproteinase 10
ADP	adenosindiphosphat
Akt	protein kinase B
Alp1	alkaline phosphatase
ALS	amyotrophic lateral sclerosis
AM	acetoxymethyl
AMP	adenosinmonophosphat
Amp	Ampicilin
AMPK	AMP-activated protein kinase
ANOVA	analysis of variance
AP2	apetala 2
APA	alternative polyadenylation
APOEϵ4	apolipoprotein ϵ 4
APP	amyloid precursor protein
Arg	arginin
ATCC®	American Type Culture Collection
ATP	adenosintriphosphat
BACE	β-site amyloid precursor protein-cleaving enzyme-1
BDNF	brain-derived neurotrophic factor
bGH pA	Bovine growth hormone polyA
BMS	Bristol-Myers Squibb
bps	base pairs
Br	bromide
BS	BlueSkript
BSA	bovine serum albumin
C_V	coefficient of variation

Ca^{2+}	Calcium
CAG	CMV enhancer CBA promoter and rabbit β-globin acceptor site
CaKMII	Ca^{2+}/calmodulin-dependent protein kinase II
cAMP	cyclic adenosine monophosphate
Cas9	CRISPR-associated protein 9
CBA	chicken β-actin promoter
CBD	corticobasal degeneration
CBh	hybrid CBA promoter
Cdk	cytokine
cDNA	complimentary DNA
CK1	casein kinase 1
Cl	chloride
CMV	Cytomegalievirus
CN	cortical neuron
CNS	central nervous system
CoREST	corepressor of REST
Cre	Cre recombinase
CRISPR	clustered regularly interspaced short palindromic repeats
d	day
DAPI	4', 6-Diamidin-2-phenylindol
DAT	dopamin transporter
DMEM	dulbecco's modified eagle medium
DMSO	dimethyl sulfoxide
DNA	desoxyribonucleic acid
dNTP	deoxy nucleotides
DPBS	phosphate buffered saline Dulbecco
DS	double split
DSB	double strand break
DYRK1A	dual specificity tyrosine phosphorylation regulated kinase 1A
E8™ Flex	Essential 8™ Flex
EB	embryonic body
EDTA	ethylenediamintetraacetic acid
EF1α	eukaryotic translation elongation factor 1 α
EGFR	epidermal growth factor receptor
eIF	eukaryotic initiation factor
eIF4E	eukaryotic initiation factor 4E
EOI	exon of interest
ESC	embryonic stem cell
Esrrb	estrogen-related receptor β
EtBr	ethidium bromid
EtOH	ethanol
EXSISERS	Exon Specific Isoform Expression Reporter System
FABP	fatty acid binding protein
FABP4	fatty acid binding protein 4

FACS	Fluirescence-activated cell sorting
FB	forebrain
FBO	forebrain organoid
FBS	fetal brovine serum
Fbx15	F-box protein 15
FDA	U.S. Food and Drug Administration
FERD3L	Fer3-like protein
FFAR	free fatty acid receptor
FGF	fibroblast growth factor
FL	full length
FLP	flippase
FLuc	firefly luciferase
FOXA1	forkhead box protein A1
FOXA2	forkhead box protein A2
FRT	FLP recognition target
FTD	frontotemporal dementia
FTLD	frontotemporal lobar degeneration
GAPDH	glycerinaldehyd-3-phosphat-dehydrogenase
GATA6	GATA binding protein 6
GCF	GC-rich sequence DNA-binding factor
gDNA	genomic DNA
GDNF	glial cell-derived neurotrophic factor
GFP	green fluorescent protein
GSK3β	glykogensynthasekinase-3 β
GTP	guanosintriphosphat
h	hour
HA	homology-arm
HA tag	hemagglutinin epitope tag
HAT	histone acetyltransferase
HCl	hydrochloride
HD	Huntington's disease
HDAC	histone deacetylase
HDR	homology directed repair
HEK293T	human embryonic kidney cells
HeLa	Henrietta Lacks
HEPES	4-(2-hydroxyethyl)-1-piperazineethanesulfonic acid
het	heterozygous
HF	high fidelity
hiPSC	human induced pluripotent stem cell
HipSci	Human Induced Pluripotent Stem Cell Initiative
HIT	high throughput
hnRNP	heterogeneous nuclear ribonucleoprotein
hom	homozygous
HRP	horseradish peroxidase

Hs	*Homo sapiens*
HT	Hit threshold
HTS	high throughput screening
ICC	immunocytochemistry
IRES	internal ribosome-entry sequence
ISE	intron splicing enhancer
ISS	intron splicing silencer
IVS	intervening sequence
kbp	kilo base pairs
KD	knock down
kDa	kilo Dalton
KI	knock-in
KLF4	kruppel-like factor 4
KSD	Kolmogorov-Smirnov Distance
KSR	Knock-Out Serum
KXGS	K259Q, K290Q, K321Q, K353Q
L	litre
LB	lysogeny broth
Lys	lysine
M	molar
m^7G	7-methyl guanosine
MAP	microtubule associated protein
MAPK	mitogen-activated protein kinase
MAPT	microtubule associated protein Tau
MARK	microtubule affinity-regulating kinases
MB	MasterBlaster
MBD	microtubules binding domain
MBF1	multiprotein-bridging factor 1
MCT	multiple comparison test
MEM	Minimum Essential Medium
MiDAC	mitotic deacetylase complex
min	minute
mL	mililitre
mM	milimolar
MOPS	3-(N-morpholino)propanesulfonic acid
mRNA	messenger RNA
MS	multiple sclerosis
mtau	murine Tau
MTF1	metal regulatory transcription factor 1
MtOH	Methanol
mTOR	mammalian target of rapamycin
mTORC1	mTOR Complex 1
n	negative
NaCl	sodium chlorid

NAD	nicotinamide adenine dinucleotide
NaOH	sodium hydroxide
NCAM	neural cell adhesion molecule
NCoR	nuclear receptor corepressor
NEB	New England Biolabs GmbH
NEP	neprilysin
NeuN	neuronal nuclear protein
NFT	neurofibrillary tangle
ng	nano gramm
NHEJ	non-homologous end joining
NLS	nuclear localisation signal
NLuc	nano luciferase
nm	nano meter
nM	nano molar
NMR	nuclear magnetic resonance
NR	nuclear receptor
Nrf1	nuclear respiratory factor 1
nRLU	normalised RLU
NuRD	nucleosome remodeling and deacetylase complex
Oct3/4	octamer binding transcription factor 4
OLLAS	*E.coli* OmpF linker and mouse langerin fusion sequence
OmpF	outer membrane protein F
ONC	overnight culture
OSKM	Oct3/4-SOX2-KLF4-c-Myc
p	positive
P/O	Poly-L-Ornithine hydrobromide
pTau	phosphorylated Tau
PABP	poly(A)-binding protein
PAM	Protospacer adjacent motif
PAX6	paired box 6
PCR	polymerase chain reaction
PD	Parkinson's Disease
pegRNA	prime editing guide RNA
PFA	paraformaldehyd
PHF	paired helical filament
PiD	Pick's Disease
PKA	protein kinase A
PKB	protein kinase B
PKC	protein kinase C
PLB	passive lysis buffer
PMA	Purmorphamin
PNS	peripheral nervous system
Pol	Polymerase
POU5F1	POU Class 5 Homeobox 1

PP	protein phosphortase
PPAR	peroxisome proliferator-activated receptor
PPARα	PPARα
PPARβ/δ	PPARβ/δ
PPARγ	PPARγ
PPi	diphosphat
PS1	prenesillin 1
PS2	prenesillin 2
PSP	progressive supranuclear palsy
PTEN	phosphatase and tensin homolog
PUFA	polyunsaturated fatty acids
PuroR	puromycin resistance
PVDF	polyvinylidene difluoride
qRT-PCR	quantitative real-time PCR
RAF	rapidly growing fibrosarcoma
rcf	relative centrifugal force
RD	restriction enzyme digest
RE	repressor element
REST	RE1-silencing restriction factor
RLU	relative light unit
RNA	ribonucleic acid
RNP	ribonucleoprotein
ROCK	Rho-associated coiled-coil containing protein kinase
rpm	rounds per minute
RT	room temperature
RXR	retinoid X receptor α
S6K	S6 kinase
SAHA	suberoylanilide hydroxamic acid
Sall4	Sal-like protein 4
SD	standard diviation
SDS	sodium dodecyl sulfate
sec	second
SEM	standard error of mean
Ser	serine
SERT	serotonin transporter
sgRNA	single guide RNA
SIN3A	SIN3 transcriptional regulator family member A
SIRT1	sirtuin-1
SMC3	structural maintenance of chromosomes 3
smFISH	single-molecule fluorescent *in situ* hybridization
SMRT	retinoid and thyroid receptors
SNP	single nucleotide polymorphism
snRNA	small nuclear RNA
snRNP	small nuclear RNP

SOC	super optimal broth with catabolite repression
SOX17	sex determining region Y-box 17
SOX2	sex determining region Y-box 2
Sp	*Streptococcus pyogenes*
SP1	specificity protein 1
SpCas9	*Streptococcus pyogenes* Cas9
SR	Ser and Arg-rich
SRSF	SR splice factor
SSEA1	stage-specific embryonic antigen 1
SW	Signal Window
Taq	*Thermus Aquaticus*
TAR	transactive response
Tau	tubulin associated unit
TBS	Tris buffered saline
TBS-T	Tris buffered saline-Tween 20
TBXT	T-Box transcription factor T
TG	Tris/Glycin
Thr	threonine
Tris	Tris hydroxymethyl-aminoethan
TSA	Trichostatin A
TTBK	Tau-tubulin kinase
TUBB3	β-Tubulin III
Tyr	tyrosine
Ucp1	uncoupling protein 1
UTR	untranslated region
UV	ultra violet
v	volume
V	Volt
w	weight
WB	Western Blot
WT	wild type

Bibliography

1. Truong, D.-J. J. *et al.* Non-invasive and high-throughput interrogation of exon-specific isoform expression. en. *Nature Cell Biology,* 1–12 (June 2021).
2. Collaborators, G. 2. D. F. Estimation of the global prevalence of dementia in 2019 and forecasted prevalence in 2050: an analysis for the Global Burden of Disease Study 2019. *The Lancet Public Health* (Jan. 2022).
3. Ross, C. A. & Poirier, M. A. Protein aggregation and neurodegenerative disease. eng. *Nature Medicine* **10 Suppl,** S10–17 (July 2004).
4. Soto, C. Unfolding the role of protein misfolding in neurodegenerative diseases. en. *Nature Reviews Neuroscience* **4,** 49–60 (2003).
5. Goedert, M. NEURODEGENERATION. Alzheimer's and Parkinson's diseases: The prion concept in relation to assembled Aß, tau, and a-synuclein. eng. *Science (New York, N.Y.)* **349,** 1255555 (2015).
6. Soto, C. & Pritzkow, S. Protein misfolding, aggregation, and conformational strains in neurodegenerative diseases. en. *Nature Neuroscience* **21,** 1332–1340 (2018).
7. Skillbäck, T., Farahmand, B., Bartlett, J. W., Rosén, C., Mattsson, N., Nägga, K., Kilander, L., Religa, D., Wimo, A., Winblad, B., Rosengren, L., Schott, J. M., Blennow, K., Eriksdotter, M. & Zetterberg, H. CSF neurofilament light differs in neurodegenerative diseases and predicts severity and survival. eng. *Neurology* **83,** 1945–1953 (Nov. 2014).
8. Zetterberg, H., Skillbäck, T., Mattsson, N., Trojanowski, J. Q., Portelius, E., Shaw, L. M., Weiner, M. W., Blennow, K. & Alzheimer's Disease Neuroimaging Initiative. Association of Cerebrospinal Fluid Neurofilament Light Concentration With Alzheimer Disease Progression. eng. *JAMA neurology* **73,** 60–67 (Jan. 2016).
9. Pereira, J. B., Janelidze, S., Ossenkoppele, R., Kvartsberg, H., Brinkmalm, A., Mattsson-Carlgren, N., Stomrud, E., Smith, R., Zetterberg, H., Blennow, K. & Hansson, O. Untangling the association of amyloid-ß and tau with synaptic and axonal loss in Alzheimer's disease. eng. *Brain: A Journal of Neurology* **144,** 310–324 (Feb. 2021).
10. Du, X., Wang, X. & Geng, M. Alzheimer's disease hypothesis and related therapies. eng. *Translational Neurodegeneration* **7,** 2 (2018).
11. Mattson, M. P. Pathways towards and away from Alzheimer's disease. en. *Nature* **430,** 631–639 (Aug. 2004).
12. Mayeux, R. & Stern, Y. Epidemiology of Alzheimer disease. eng. *Cold Spring Harbor Perspectives in Medicine* **2,** a006239 (Aug. 2012).
13. Overk, C. R. & Masliah, E. Pathogenesis of synaptic degeneration in Alzheimer's disease and Lewy body disease. *Biochemical Pharmacology* **88,** 508–516 (Apr. 2014).
14. Cras, P., Kawai, M., Lowery, D., Gonzalez-DeWhitt, P., Greenberg, B. & Perry, G. Senile plaque neurites in Alzheimer disease accumulate amyloid precursor protein. en. *Proceedings of the National Academy of Sciences* **88,** 7552–7556 (Sept. 1991).

15. Perl, D. P. Neuropathology of Alzheimer's Disease. en. *Mount Sinai Journal of Medicine: A Journal of Translational and Personalized Medicine* **77,** 32–42 (2010).

16. Armstrong, R. A. The molecular biology of senile plaques and neurofibrillary tangles in Alzheimer's disease. eng. *Folia Neuropathologica* **47,** 289–299 (2009).

17. Costantini, C., Ko, M. H., Jonas, M. C. & Puglielli, L. A reversible form of lysine acetylation in the ER and Golgi lumen controls the molecular stabilization of BACE1. eng. *The Biochemical Journal* **407,** 383–395 (Nov. 2007).

18. Kang, E. L., Cameron, A. N., Piazza, F., Walker, K. R. & Tesco, G. Ubiquitin regulates GGA3-mediated degradation of BACE1. eng. *The Journal of Biological Chemistry* **285,** 24108–24119 (July 2010).

19. Kang, E. L., Biscaro, B., Piazza, F. & Tesco, G. BACE1 Protein Endocytosis and Trafficking Are Differentially Regulated by Ubiquitination at Lysine 501 and the Di-leucine Motif in the Carboxyl Terminus *. English. *Journal of Biological Chemistry* **287,** 42867–42880 (Dec. 2012).

20. Thal, D. R., Rüb, U., Orantes, M. & Braak, H. Phases of A beta-deposition in the human brain and its relevance for the development of AD. eng. *Neurology* **58,** 1791–1800 (June 2002).

21. Grothe, M. J., Barthel, H., Sepulcre, J., Dyrba, M., Sabri, O., Teipel, S. J. & Alzheimer's Disease Neuroimaging Initiative. In vivo staging of regional amyloid deposition. eng. *Neurology* **89,** 2031–2038 (Nov. 2017).

22. Chen, G.-F., Xu, T.-H., Yan, Y., Zhou, Y.-R., Jiang, Y., Melcher, K. & Xu, H. E. Amyloid beta: structure, biology and structure-based therapeutic development. eng. *Acta Pharmacologica Sinica* **38,** 1205–1235 (Sept. 2017).

23. Tabaton, M. & Piccini, A. Role of water-soluble amyloid-beta in the pathogenesis of Alzheimer's disease. eng. *International Journal of Experimental Pathology* **86,** 139–145 (June 2005).

24. Johnson, K. A., Schultz, A., Betensky, R. A., Becker, J. A., Sepulcre, J., Rentz, D., Mormino, E., Chhatwal, J., Amariglio, R., Papp, K., Marshall, G., Albers, M., Mauro, S., Pepin, L., Alverio, J., Judge, K., Philiossaint, M., Shoup, T., Yokell, D., Dickerson, B., Gomez-Isla, T., Hyman, B., Vasdev, N. & Sperling, R. Tau positron emission tomographic imaging in aging and early Alzheimer disease. eng. *Annals of Neurology* **79,** 110–119 (Jan. 2016).

25. Brion, J.-P. Neurofibrillary Tangles and Alzheimer's Disease. *European Neurology* **40,** 130–140 (1998).

26. Kempf, A. M. S. J. *Neurofibrillary tangles in Alzheimer's disease: elucidation of the molecular mechanism by immunohistochemistry and tau protein phospho-proteomics* Nov. 4, 2016.

27. Hoogenraad, C. C. & Bradke, F. Control of neuronal polarity and plasticity – a renaissance for microtubules? *Trends in Cell Biology* **19,** 669–676 (Dec. 2009).

28. Voelzmann, A., Hahn, I., Pearce, S. P., Sánchez-Soriano, N. & Prokop, A. A conceptual view at microtubule plus end dynamics in neuronal axons. *Brain Research Bulletin* **126,** 226–237 (Sept. 2016).

29. Lindwall, G. & Cole, R. D. Phosphorylation affects the ability of tau protein to promote microtubule assembly. eng. *The Journal of biological chemistry* **259,** 5301–5 (8 Apr. 1984).

30. Mandelkow, E. M., Biernat, J., Drewes, G., Gustke, N., Trinczek, B. & Mandelkow, E. Tau domains, phosphorylation, and interactions with microtubules. *Neurobiology of Aging* **16,** 355–362 (May 1995).

31. Ramkumar, A., Jong, B. Y. & Ori-McKenney, K. M. ReMAPping the microtubule landscape: How phosphorylation dictates the activities of microtubule-associated proteins. *Developmental Dynamics* **247,** 138–155 (Oct. 2017).

32. Weingarten, M. D., Lockwood, A. H., Hwo, S. Y. & Kirschner, M. W. A protein factor essential for microtubule assembly. *Proceedings of the National Academy of Sciences* **72,** 1858–1862 (May 1975).

33. Goedert, M., Spillantini, M., Jakes, R., Rutherford, D. & Crowther, R. Multiple isoforms of human microtubule-associated protein tau: sequences and localization in neurofibrillary tangles of Alzheimer's disease. *Neuron* **3,** 519–526 (Oct. 1989).

34. Goedert, M., Spillantini, M. G., Potier, M. C., Ulrich, J. & Crowther, R. A. Cloning and sequencing of the cDNA encoding an isoform of microtubule-associated protein tau containing four tandem repeats: differential expression of tau protein mRNAs in human brain. *The EMBO Journal* **8,** 393–399 (Feb. 1989).

35. Park, S. A., Ahn, S. I. & Gallo, J.-M. Tau mis-splicing in the pathogenesis of neurodegenerative disorders. eng. *BMB Reports* **49,** 405–413 (2016).

36. Spires-Jones, T. L., Stoothoff, W. H., de Calignon, A., Jones, P. B. & Hyman, B. T. Tau pathophysiology in neurodegeneration: a tangled issue. en. *Trends in Neurosciences* **32,** 150–159 (Mar. 2009).

37. Lee, V. M.-Y., Goedert, M. & Trojanowski, J. Q. Neurodegenerative Tauopathies. *Annual Review of Neuroscience* **24,** 1121–1159 (2001).

38. Caffrey, T. M., Joachim, C., Paracchini, S., Esiri, M. M. & Wade-Martins, R. Haplotype-specific expression of exon 10 at the human MAPT locus. en. *Human Molecular Genetics* **15,** 3529–3537 (Dec. 2006).

39. Majounie, E., Cross, W., Newsway, V., Dillman, A., Vandrovcova, J., Morris, C. M., Nalls, M. A., Ferrucci, L., Owen, M. J., O'Donovan, M. C., Cookson, M. R., Singleton, A. B., de Silva, R. & Morris, H. R. Variation in tau isoform expression in different brain regions and disease states. en. *Neurobiology of Aging* **34,** 1922.e7–1922.e12 (July 2013).

40. Trabzuni, D., Wray, S., Vandrovcova, J., Ramasamy, A., Walker, R., Smith, C., Luk, C., Gibbs, J. R., Dillman, A., Hernandez, D. G., Arepalli, S., Singleton, A. B., Cookson, M. R., Pittman, A. M., de Silva, R., Weale, M. E., Hardy, J. & Ryten, M. MAPT expression and splicing is differentially regulated by brain region: relation to genotype and implication for tauopathies. en. *Human Molecular Genetics* **21,** 4094–4103 (Sept. 2012).

41. Cleveland, D. W., Hwo, S. Y. & Kirschner, M. W. Purification of tau, a microtubule-associated protein that induces assembly of microtubules from purified tubulin. eng. *Journal of Molecular Biology* **116,** 207–225 (Oct. 1977).

42. Fulga, T. A., Elson-Schwab, I., Khurana, V., Steinhilb, M. L., Spires, T. L., Hyman, B. T. & Feany, M. B. Abnormal bundling and accumulation of F-actin mediates tau-induced neuronal degeneration in vivo. eng. *Nature Cell Biology* **9,** 139–148 (Feb. 2007).

43. Strang, K. H., Golde, T. E. & Giasson, B. I. MAPT mutations, tauopathy, and mechanisms of neurodegeneration. *Laboratory Investigation* **99,** 912–928 (Feb. 2019).

44. Liu, F. & Gong, C.-X. Tau exon 10 alternative splicing and tauopathies. *Molecular Neurodegeneration* **3,** 8 (July 2008).

45. Stefansson, H., Helgason, A., Thorleifsson, G., Steinthorsdottir, V., Masson, G., Barnard, J., Baker, A., Jonasdottir, A., Ingason, A., Gudnadottir, V. G., Desnica, N., Hicks, A., Gylfason, A., Gudbjartsson, D. F., Jonsdottir, G. M., Sainz, J., Agnarsson, K., Birgisdottir, B., Ghosh, S., Olafsdottir, A., Cazier, J.-B., Kristjansson, K., Frigge, M. L., Thorgeirsson, T. E., Gulcher, J. R., Kong, A. & Stefansson, K. A common inversion under selection in Europeans. eng. *Nature Genetics* **37,** 129–137 (Feb. 2005).

46. Zody, M. C., Jiang, Z., Fung, H.-C., Antonacci, F., Hillier, L. W., Cardone, M. F., Graves, T. A., Kidd, J. M., Cheng, Z., Abouelleil, A., Chen, L., Wallis, J., Glasscock, J., Wilson, R. K., Reily, A. D., Duckworth, J., Ventura, M., Hardy, J., Warren, W. C. & Eichler, E. E. Evolutionary toggling of the MAPT 17q21.31 inversion region. en. *Nature Genetics* **40,** 1076–1083 (Sept. 2008).

47. Martin, E. R. *et al.* Association of single-nucleotide polymorphisms of the tau gene with late-onset Parkinson disease. eng. *JAMA* **286,** 2245–2250 (Nov. 2001).

48. Pastor, P. *et al.* MAPT H1 Haplotype is Associated with Late-Onset Alzheimer's Disease Risk in APOEϵ4 Noncarriers: Results from the Dementia Genetics Spanish Consortium. *Journal of Alzheimer's Disease* **49,** 343–352 (2015).

49. Pastor, P., Ezquerra, M., Perez, J. C., Chakraverty, S., Norton, J., Racette, B. A., McKeel, D., Perlmutter, J. S., Tolosa, E. & Goate, A. M. Novel haplotypes in 17q21 are associated with progressive supranuclear palsy. *Annals of Neurology* **56,** 249–258 (2004).

50. Verpillat, P., Camuzat, A., Hannequin, D., Thomas-Anterion, C., Puel, M., Belliard, S., Dubois, B., Didic, M., Michel, B.-F., Lacomblez, L., Moreaud, O., Sellal, F., Golfier, V., Campion, D., Clerget-Darpoux, F. & Brice, A. Association between the extended tau haplotype and frontotemporal dementia. eng. *Archives of Neurology* **59,** 935–939 (June 2002).

51. Houlden, H., Baker, M., Morris, H., MacDonald, N., Pickering-Brown, S., Adamson, J., Lees, A., Rossor, M., Quinn, N., Kertesz, A., Khan, M., Hardy, J., Lantos, P., George-Hyslop, P. S., Munoz, D., Mann, D., Lang, A., Bergeron, C., Bigio, E., Litvan, I., Bhatia, K., Dickson, D., Wood, N. & Hutton, M. Corticobasal degeneration and progressive supranuclear palsy share a common tau haplotype. *Neurology* **56,** 1702–1706 (June 2001).

52. Myers, A., Kaleem, M., Marlowe, L., Pittman, A., Lees, A., Fung, H., Duckworth, J., Leung, D., Gibson, A., Morris, C., de Silva, R. & Hardy, J. The H1c haplotype at the MAPT locus is associated with Alzheimer's disease. *Human Molecular Genetics* **14,** 2399–2404 (July 2005).

53. Pittman, A. M., Myers, A. J., Duckworth, J., Bryden, L., Hanson, M., Abou-Sleiman, P., Wood, N. W., Hardy, J., Lees, A. & de Silva, R. The structure of the tau haplotype in controls and in progressive supranuclear palsy. eng. *Human Molecular Genetics* **13,** 1267–1274 (June 2004).

54. Rademakers, R., Melquist, S., Cruts, M., Theuns, J., Del-Favero, J., Poorkaj, P., Baker, M., Sleegers, K., Crook, R., De Pooter, T., Bel Kacem, S., Adamson, J., Van den Bossche, D., Van den Broeck, M., Gass, J., Corsmit, E., De Rijk, P., Thomas, N., Engelborghs, S., Heckman, M., Litvan, I., Crook, J., De Deyn, P. P., Dickson, D., Schellenberg, G. D., Van Broeckhoven, C. & Hutton, M. L. High-density SNP haplotyping suggests altered regulation of tau gene expression in progressive supranuclear palsy. eng. *Human Molecular Genetics* **14,** 3281–3292 (Nov. 2005).

55. Allen, M. *et al.* Association of MAPT haplotypes with Alzheimer's disease risk and MAPT brain gene expression levels. eng. *Alzheimer's Research & Therapy* **6,** 39 (2014).

56. Zhang, C.-C., Zhu, J.-X., Wan, Y., Tan, L., Wang, H.-F., Yu, J.-T. & Tan, L. Meta-analysis of the association between variants in MAPT and neurodegenerative diseases. eng. *Oncotarget* **8,** 44994–45007 (July 2017).

57. Nilsen, T. W. & Graveley, B. R. Expansion of the eukaryotic proteome by alternative splicing. *Nature* **463,** 457–463 (Jan. 2010).

58. Pan, Q., Shai, O., Lee, L. J., Frey, B. J. & Blencowe, B. J. Deep surveying of alternative splicing complexity in the human transcriptome by high-throughput sequencing. *Nature Genetics* **40,** 1413–1415 (Nov. 2008).

59. Wang, E. T., Sandberg, R., Luo, S., Khrebtukova, I., Zhang, L., Mayr, C., Kingsmore, S. F., Schroth, G. P. & Burge, C. B. Alternative isoform regulation in human tissue transcriptomes. *Nature* **456,** 470–476 (Nov. 2008).

60. Sanchez, L. Sex-determining mechanisms in insects. *The International Journal of Developmental Biology* **52,** 837–856 (2008).

61. Makeyev, E. V., Zhang, J., Carrasco, M. A. & Maniatis, T. The MicroRNA miR-124 Promotes Neuronal Differentiation by Triggering Brain-Specific Alternative Pre-mRNA Splicing. *Molecular Cell* **27,** 435–448 (Aug. 2007).

62. Boutz, P. L., Stoilov, P., Li, Q., Lin, C.-H., Chawla, G., Ostrow, K., Shiue, L., Ares, M. & Black, D. L. A post-transcriptional regulatory switch in polypyrimidine tract-binding proteins reprograms alternative splicing in developing neurons. *Genes & Development* **21,** 1636–1652 (July 2007).

63. Sugnet, C. W., Kent, W. J., Ares, M. & Haussler, D. *Transcriptome and genome conservation of alternative splicing events in humans and mice* in *Biocomputing 2004* (Dec. 2003).

64. Braunschweig, U., Gueroussov, S., Plocik, A. M., Graveley, B. R. & Blencowe, B. J. Dynamic Integration of Splicing within Gene Regulatory Pathways. *Cell* **152,** 1252–1269 (Mar. 2013).

65. De Conti, L., Baralle, M. & Buratti, E. Exon and intron definition in pre-mRNA splicing. eng. *Wiley interdisciplinary reviews. RNA* **4,** 49–60 (Feb. 2013).

66. Schmucker, D., Clemens, J. C., Shu, H., Worby, C. A., Xiao, J., Muda, M., Dixon, J. E. & Zipursky, S. Drosophila Dscam Is an Axon Guidance Receptor Exhibiting Extraordinary Molecular Diversity. *Cell* **101,** 671–684 (June 2000).

67. Kelemen, O., Convertini, P., Zhang, Z., Wen, Y., Shen, M., Falaleeva, M. & Stamm, S. Function of alternative splicing. *Gene* **514,** 1–30 (Feb. 2013).

68. Daguenet, E., Dujardin, G. & Valcárcel, J. The pathogenicity of splicing defects: mechanistic insights into pre- mRNA processing inform novel therapeutic approaches. *EMBO reports* **16,** 1640–1655 (Nov. 2015).

69. Qian, W. & Liu, F. Regulation of alternative splicing of tau exon 10. eng. *Neuroscience Bulletin* **30,** 367–377 (Apr. 2014).

70. Broderick, J., Wang, J. & Andreadis, A. Heterogeneous nuclear ribonucleoprotein E2 binds to tau exon 10 and moderately activates its splicing. eng. *Gene* **331,** 107–114 (Apr. 2004).

71. Wang, Y., Gao, L., Tse, S.-W. & Andreadis, A. Heterogeneous nuclear ribonucleoprotein E3 modestly activates splicing of tau exon 10 via its proximal downstream intron, a hotspot for frontotemporal dementia mutations. eng. *Gene* **451,** 23–31 (Feb. 2010).

72. D'Souza, I. & Schellenberg, G. D. Determinants of 4-repeat tau expression. Coordination between enhancing and inhibitory splicing sequences for exon 10 inclusion. eng. *The Journal of Biological Chemistry* **275,** 17700–17709 (June 2000).

73. Umeda, T., Yamashita, T., Kimura, T., Ohnishi, K., Takuma, H., Ozeki, T., Takashima, A., Tomiyama, T. & Mori, H. Neurodegenerative Disorder FTDP-17–Related Tau Intron 10 +16C>T Mutation Increases Tau Exon 10 Splicing and Causes Tauopathy in Transgenic Mice. en. *The American Journal of Pathology* **183,** 211–225 (July 2013).

74. Qian, W., Liang, H., Shi, J., Jin, N., Grundke-Iqbal, I., Iqbal, K., Gong, C.-X. & Liu, F. Regulation of the alternative splicing of tau exon 10 by SC35 and Dyrk1A. eng. *Nucleic Acids Research* **39,** 6161–6171 (Aug. 2011).

75. Chen, C., Jin, N., Qian, W., Liu, W., Tan, X., Ding, F., Gu, X., Iqbal, K., Gong, C.-X., Zuo, J. & Liu, F. Cyclic AMP-dependent protein kinase enhances SC35-promoted Tau exon 10 inclusion. eng. *Molecular Neurobiology* **49,** 615–624 (Feb. 2014).

76. Gu, J., Shi, J., Wu, S., Jin, N., Qian, W., Zhou, J., Iqbal, I.-G., Iqbal, K., Gong, C.-X. & Liu, F. Cyclic AMP-dependent protein kinase regulates 9G8-mediated alternative splicing of tau exon 10. eng. *FEBS letters* **586,** 2239–2244 (July 2012).

77. Ding, S., Shi, J., Qian, W., Iqbal, K., Grundke-Iqbal, I., Gong, C.-X. & Liu, F. Regulation of alternative splicing of tau exon 10 by 9G8 and Dyrk1A. eng. *Neurobiology of Aging* **33,** 1389–1399 (July 2012).

78. Chen, K.-L., Yuan, R.-Y., Hu, C.-J. & Hsu, C. Y. Amyloid-ß peptide alteration of tau exon-10 splicing via the GSK3ß-SC35 pathway. eng. *Neurobiology of Disease* **40,** 378–385 (Nov. 2010).

79. Shi, J., Zhang, T., Zhou, C., Chohan, M. O., Gu, X., Wegiel, J., Zhou, J., Hwang, Y.-W., Iqbal, K., Grundke-Iqbal, I., Gong, C.-X. & Liu, F. Increased dosage of Dyrk1A alters alternative splicing factor (ASF)-regulated alternative splicing of tau in Down syndrome. eng. *The Journal of Biological Chemistry* **283,** 28660–28669 (Oct. 2008).

80. Deribe, Y. L., Pawson, T. & Dikic, I. Post-translational modifications in signal integration. en. *Nature Structural & Molecular Biology* **17,** 666–672 (June 2010).

81. Buée, L., Bussière, T., Buée-Scherrer, V., Delacourte, A. & Hof, P. R. Tau protein isoforms, phosphorylation and role in neurodegenerative disorders. eng. *Brain Research. Brain Research Reviews* **33,** 95–130 (Aug. 2000).

82. Hanger, D. P., Anderton, B. H. & Noble, W. Tau phosphorylation: the therapeutic challenge for neurodegenerative disease. eng. *Trends in Molecular Medicine* **15,** 112–119 (Mar. 2009).

83. Sergeant, N., Bretteville, A., Hamdane, M., Caillet-Boudin, M.-L., Grognet, P., Bombois, S., Blum, D., Delacourte, A., Pasquier, F., Vanmechelen, E., Schraen-Maschke, S. & Buée, L. Biochemistry of Tau in Alzheimer's disease and related neurological disorders. eng. *Expert Review of Proteomics* **5,** 207–224 (Apr. 2008).

84. Hasegawa, M., Morishima-Kawashima, M., Takio, K., Suzuki, M., Titani, K. & Ihara, Y. Protein sequence and mass spectrometric analyses of tau in the Alzheimer's disease brain. en. *Journal of Biological Chemistry* **267,** 17047–17054 (1992).

85. Lovestone, S. & Reynolds, C. H. The phosphorylation of tau: a critical stage in neurodevelopment and neurodegenerative processes. eng. *Neuroscience* **78,** 309–324 (May 1997).

86. Morishima-Kawashima, M., Hasegawa, M., Takio, K., Suzuki, M., Yoshida, H., Titani, K. & Ihara, Y. Proline-directed and Non-proline-directed Phosphorylation of PHF-tau (*). en. *Journal of Biological Chemistry* **270,** 823–829 (Jan. 1995).

87. Paudel, H. K. & Li, W. Heparin-induced Conformational Change in Microtubule-associated Protein Tau as Detected by Chemical Cross-linking and Phosphopeptide Mapping*. en. *Journal of Biological Chemistry* **274,** 8029–8038 (Mar. 1999).

88. Roder, H. M., Fracasso, R. P., Hoffman, F. J., Witowsky, J. A., Davis, G. & Pellegrino, C. B. Phosphorylation-dependent Monoclonal Tau Antibodies Do Not Reliably Report Phosphorylation by Extracellular Signal-regulated Kinase 2 at Specific Sites*. en. *Journal of Biological Chemistry* **272,** 4509–4515 (1997).

89. Martin, L., Latypova, X. & Terro, F. Post-translational modifications of tau protein: Implications for Alzheimer's disease. en. *Neurochemistry International* **58,** 458–471 (Mar. 2011).

90. Dickey, C. A., Kamal, A., Lundgren, K., Klosak, N., Bailey, R. M., Dunmore, J., Ash, P., Shoraka, S., Zlatkovic, J., Eckman, C. B., Patterson, C., Dickson, D. W., Nahman, N. S., Hutton, M., Burrows, F. & Petrucelli, L. The high-affinity HSP90-CHIP complex recognizes and selectively degrades phosphorylated tau client proteins. eng. *The Journal of Clinical Investigation* **117,** 648–658 (Mar. 2007).

91. Biernat, J. & Mandelkow, E. M. The development of cell processes induced by tau protein requires phosphorylation of serine 262 and 356 in the repeat domain and is inhibited by phosphorylation in the proline-rich domains. eng. *Molecular Biology of the Cell* **10,** 727–740 (Mar. 1999).

92. Cohen, T. J., Guo, J. L., Hurtado, D. E., Kwong, L. K., Mills, I. P., Trojanowski, J. Q. & Lee, V. M. Y. The acetylation of tau inhibits its function and promotes pathological tau aggregation. eng. *Nature Communications* **2,** 252 (2011).

93. Kolarova, M., García-Sierra, F., Bartos, A., Ricny, J. & Ripova, D. Structure and pathology of tau protein in Alzheimer disease. eng. *International Journal of Alzheimer's Disease* **2012,** 731526 (2012).

94. Sohn, P. D., Tracy, T. E., Son, H.-I., Zhou, Y., Leite, R. E. P., Miller, B. L., Seeley, W. W., Grinberg, L. T. & Gan, L. Acetylated tau destabilizes the cytoskeleton in the axon initial segment and is mislocalized to the somatodendritic compartment. *Molecular Neurodegeneration* **11,** 47 (June 2016).

95. Tapia-Rojas, C., Cabezas-Opazo, F., Deaton, C. A., Vergara, E. H., Johnson, G. V. W. & Quintanilla, R. A. It's all about tau. eng. *Progress in Neurobiology* **175,** 54–76 (Apr. 2019).

96. Köpke, E., Tung, Y. C., Shaikh, S., Alonso, A. C., Iqbal, K. & Grundke-Iqbal, I. Microtubule-associated protein tau. Abnormal phosphorylation of a non-paired helical filament pool in Alzheimer disease. en. *Journal of Biological Chemistry* **268,** 24374–24384 (Nov. 1993).

97. Kowall, N. W. & Kosik, K. S. Axonal disruption and aberrant localization of tau protein characterize the neuropil pathology of Alzheimer's disease. en. *Annals of Neurology* **22,** 639–643 (1987).

98. Yanagisawa, M., Planel, E., Ishiguro, K. & Fujita, S. C. Starvation induces tau hyperphosphorylation in mouse brain: implications for Alzheimer's disease. *FEBS Letters* **461,** 329–333 (Nov. 1999).

99. Alzheimer, A. Über einen eigenartigen schweren Erkrankungsprozeß der Hirnrinde. *Neurologisches Centralblatt* **23: 1129–36** (1906).

100. Arendt, T., Stieler, J. T. & Holzer, M. Tau and tauopathies. en. *Brain Research Bulletin. Cytoskeletal proteins in health and neurodegenerative disease* **126,** 238–292 (Sept. 2016).

101. Mietelska-Porowska, A., Wasik, U., Goras, M., Filipek, A. & Niewiadomska, G. Tau Protein Modifications and Interactions: Their Role in Function and Dysfunction. en. *International Journal of Molecular Sciences* **15,** 4671–4713 (Mar. 2014).

102. Spillantini, M. G. & Goedert, M. Tau pathology and neurodegeneration. en. *The Lancet Neurology* **12,** 609–622 (June 2013).

103. Praticò, D. The Functional Role of microRNAs in the Pathogenesis of Tauopathy. en. *Cells* **9,** 2262 (Oct. 2020).

104. Holtzman, D. M., Carrillo, M. C., Hendrix, J. A., Bain, L. J., Catafau, A. M., Gault, L. M., Goedert, M., Mandelkow, E., Mandelkow, E.-M., Miller, D. S., Ostrowitzki, S., Polydoro, M., Smith, S., Wittmann, M. & Hutton, M. Tau: From research to clinical development. eng. *Alzheimer's & Dementia: The Journal of the Alzheimer's Association* **12,** 1033–1039 (2016).

105. Wang, Y. & Mandelkow, E. Tau in physiology and pathology. eng. *Nature Reviews. Neuroscience* **17,** 5–21 (2016).

106. Wischik, C. M., Novak, M., Thøgersen, H. C., Edwards, P. C., Runswick, M. J., Jakes, R., Walker, J. E., Milstein, C., Roth, M. & Klug, A. Isolation of a fragment of tau derived from the core of the paired helical filament of Alzheimer disease. eng. *Proceedings of the National Academy of Sciences of the United States of America* **85,** 4506–4510 (1988).

107. Vinters, H. V. Emerging Concepts in Alzheimer's Disease. *Annual Review of Pathology: Mechanisms of Disease* **10,** 291–319 (Jan. 2015).

108. Graham, W. V., Bonito-Oliva, A. & Sakmar, T. P. Update on Alzheimer's Disease Therapy and Prevention Strategies. *Annual Review of Medicine* **68,** 413–430 (2017).

109. Tobin, J. E. *et al.* Haplotypes and gene expression implicate the MAPT region for Parkinson disease: The GenePD Study. en. *Neurology* **71,** 28–34 (July 2008).

110. Saltiel, A. R. & Kahn, C. R. Insulin signalling and the regulation of glucose and lipid metabolism. eng. *Nature* **414,** 799–806 (Dec. 2001).

111. Hotamisligil, G. S. Inflammation and metabolic disorders. eng. *Nature* **444,** 860–867 (Dec. 2006).

112. Hara, T., Kimura, I., Inoue, D., Ichimura, A. & Hirasawa, A. Free fatty acid receptors and their role in regulation of energy metabolism. eng. *Reviews of Physiology, Biochemistry and Pharmacology* **164,** 77–116 (2013).

113. Richieri, G. V., Ogata, R. T., Zimmerman, A. W., Veerkamp, J. H. & Kleinfeld, A. M. Fatty acid binding proteins from different tissues show distinct patterns of fatty acid interactions. eng. *Biochemistry* **39,** 7197–7204 (June 2000).

114. Haunerland, N. H. & Spener, F. Fatty acid-binding proteins – insights from genetic manipulations. en. *Progress in Lipid Research* **43,** 328–349 (July 2004).

115. Chmurzynska, A. The multigene family of fatty acid-binding proteins (FABPs): Function, structure and polymorphism. en. *Journal of Applied Genetics* **47,** 39–48 (Mar. 2006).

116. Schachtrup, C., Emmler, T., Bleck, B., Sandqvist, A. & Spener, F. Functional analysis of peroxisome-proliferator-responsive element motifs in genes of fatty acid-binding proteins. eng. *The Biochemical Journal* **382,** 239–245 (Aug. 2004).

117. Motojima, K. Differential effects of PPARalpha activators on induction of ectopic expression of tissue-specific fatty acid binding protein genes in the mouse liver. eng. *The International Journal of Biochemistry & Cell Biology* **32,** 1085–1092 (Oct. 2000).

118. Tan, N.-S., Shaw, N. S., Vinckenbosch, N., Liu, P., Yasmin, R., Desvergne, B., Wahli, W. & Noy, N. Selective cooperation between fatty acid binding proteins and peroxisome proliferator-activated receptors in regulating transcription. eng. *Molecular and Cellular Biology* **22,** 5114–5127 (July 2002).

119. Storch, J. & Thumser, A. E. The fatty acid transport function of fatty acid-binding proteins. eng. *Biochimica Et Biophysica Acta* **1486,** 28–44 (June 2000).

120. Zimmerman, A. W. & Veerkamp, J. H. New insights into the structure and function of fatty acid-binding proteins. *Cellular and Molecular Life Sciences (CMLS)* **59,** 1096–1116 (July 2002).

121. Veerkamp, J. H. & Zimmerman, A. W. Fatty acid-binding proteins of nervous tissue. en. *Journal of Molecular Neuroscience* **16,** 133–142 (June 2001).

122. Wassall, S. R. & Stillwell, W. Polyunsaturated fatty acid–cholesterol interactions: Domain formation in membranes. en. *Biochimica et Biophysica Acta (BBA) - Biomembranes. Lipid Interactions, Domain Formation, and Lateral Structure of Membranes* **1788,** 24–32 (Jan. 2009).

123. Janssen, C. I. F. & Kiliaan, A. J. Long-chain polyunsaturated fatty acids (LCPUFA) from genesis to senescence: the influence of LCPUFA on neural development, aging, and neurodegeneration. eng. *Progress in Lipid Research* **53,** 1–17 (Jan. 2014).

124. Moullé, V. S. F., Cansell, C., Luquet, S. & Cruciani-Guglielmacci, C. The multiple roles of fatty acid handling proteins in brain. eng. *Frontiers in Physiology* **3,** 385 (2012).

125. Storch, J. & Corsico, B. The Emerging Functions and Mechanisms of Mammalian Fatty Acid–Binding Proteins. *Annual Review of Nutrition* **28,** 73–95 (Aug. 2008).

126. Liu, Y., Longo, L. D. & De León, M. In situ and immunocytochemical localization of E-FABP mRNA and protein during neuronal migration and differentiation in the rat brain. en. *Brain Research* **852,** 16–27 (Jan. 2000).

127. Liu, R.-Z., Mita, R., Beaulieu, M., Gao, Z. & Godbout, R. Fatty acid binding proteins in brain development and disease. eng. *The International Journal of Developmental Biology* **54,** 1229–1239 (2010).

128. De León, M., Welcher, A., Nahin, R., Liu, Y., Ruda, M., Shooter, E. & Molina, C. Fatty acid binding protein is induced in neurons of the dorsal root ganglia after peripheral nerve injury. en. *Journal of Neuroscience Research* **44,** 283–292 (1996).

129. Cheon, M. S., Kim, S. H., Fountoulakis, M. & Lubec, G. en. in (ed Lubec, G.) 225–234 (Springer, Vienna, 2003). ISBN: 9783709167212.

130. Murphy, E. J., Owada, Y., Kitanaka, N., Kondo, H. & Glatz, J. F. C. Brain Arachidonic Acid Incorporation Is Decreased in Heart Fatty Acid Binding Protein Gene-Ablated Mice. *Biochemistry* **44,** 6350–6360 (Apr. 2005).

131. Mollenhauer, B., Steinacker, P., Bahn, E., Bibl, M., Brechlin, P., Schlossmacher, M. G., Locascio, J. J., Wiltfang, J., Kretzschmar, H. A., Poser, S., Trenkwalder, C. & Otto, M. Serum Heart-Type Fatty Acid-Binding Protein and Cerebrospinal Fluid Tau: Marker Candidates for Dementia with Lewy Bodies. *Neurodegenerative Diseases* **4,** 366–375 (2007).

132. Teunissen, C. E., Veerhuis, R., Vente, J. D., Verhey, F. R. J., Vreeling, F., van Boxtel, M. P. J., Glatz, J. F. C. & Pelsers, M. A. L. Brain-specific fatty acid-binding protein is elevated in serum of patients with dementia-related diseases. *European Journal of Neurology* **18,** 865–871 (Dec. 2010).

133. Harari, O., Cruchaga, C., Kauwe, J. S. K., Ainscough, B. J., Bales, K., Pickering, E. H., Bertelsen, S., Fagan, A. M., Holtzman, D. M., Morris, J. C., Goate, A. M. & Alzheimer's Disease Neuroimaging Initiative. Phosphorylated tau-Aß42 ratio as a continuous trait for biomarker discovery for early-stage Alzheimer's disease in multiplex immunoassay panels of cerebrospinal fluid. eng. *Biological Psychiatry* **75,** 723–731 (May 2014).

134. Bjerke, M., Kern, S., Blennow, K., Zetterberg, H., Waern, M., Börjesson-Hanson, A., Östling, S., Kern, J. & Skoog, I. Cerebrospinal Fluid Fatty Acid-Binding Protein 3 is Related to Dementia Development in a Population-Based Sample of Older Adult Women Followed for 8 Years. eng. *Journal of Alzheimer's disease: JAD* **49,** 733–741 (2016).

135. Sepe, F. N., Chiasserini, D. & Parnetti, L. Role of FABP3 as biomarker in Alzheimer's disease and synucleinopathies. *Future Neurology* **13,** 199–207 (Nov. 2018).

136. Chawla, A., Repa, J. J., Evans, R. M. & Mangelsdorf, D. J. Nuclear Receptors and Lipid Physiology: Opening the X-Files. *Science* **294,** 1866–1870 (Nov. 2001).

137. Desvergne, B. & Wahli, W. Peroxisome Proliferator-Activated Receptors: Nuclear Control of Metabolism*. *Endocrine Reviews* **20,** 649–688 (Oct. 1999).

138. Straus, D. S. & Glass, C. K. Cyclopentenone prostaglandins: New insights on biological activities and cellular targets. en. *Medicinal Research Reviews* **21,** 185–210 (2001).

139. Nolte, R. T., Wisely, G. B., Westin, S., Cobb, J. E., Lambert, M. H., Kurokawa, R., Rosenfeld, M. G., Willson, T. M., Glass, C. K. & Milburn, M. V. Ligand binding and co-activator assembly of the peroxisome proliferator-activated receptor-? en. *Nature* **395,** 137–143 (Sept. 1998).

140. Berger, J. & Moller, D. E. The Mechanisms of Action of PPARs. *Annual Review of Medicine* **53,** 409–435 (2002).

141. Castrillo, A. & Tontonoz, P. Nuclear Receptors in Macrophages biology: At the Crossroads of Lipid Metabolism and Inflammation. *Annual Review of Cell and Developmental Biology* **20,** 455–480 (2004).

142. Tyagi, S., Gupta, P., Saini, A. S., Kaushal, C. & Sharma, S. The peroxisome proliferator-activated receptor: A family of nuclear receptors role in various diseases. eng. *Journal of Advanced Pharmaceutical Technology & Research* **2,** 236–240 (Oct. 2011).

143. Hotamisligil, G. S. & Bernlohr, D. A. Metabolic functions of FABPs—mechanisms and therapeutic implications. en. *Nature Reviews Endocrinology* **11,** 592–605 (Oct. 2015).

144. Watson, G. S., Cholerton, B. A., Reger, M. A., Baker, L. D., Plymate, S. R., Asthana, S., Fishel, M. A., Kulstad, J. J., Green, P. S., Cook, D. G., Kahn, S. E., Keeling, M. L. & Craft, S. Preserved cognition in patients with early Alzheimer disease and amnestic mild cognitive impairment during treatment with rosiglitazone: a preliminary study. eng. *The American Journal of Geriatric Psychiatry: Official Journal of the American Association for Geriatric Psychiatry* **13,** 950–958 (Nov. 2005).

145. Kaiser, C. C., Shukla, D. K., Stebbins, G. T., Skias, D. D., Jeffery, D. R., Stefoski, D., Katsamakis, G. & Feinstein, D. L. A pilot test of pioglitazone as an add-on in patients with relapsing remitting multiple sclerosis. English. *Journal of Neuroimmunology* **211,** 124–130 (June 2009).

146. Weinstein, D., Boyko, A., Pugliese, L., Tang, H., Lanfear, D., Zivadinov, R. & Finck, B. CHS-131, A Novel Once Daily Oral Treatment, Decreased Lesion Burden of Patients with Relapsing-Remitting Course of Multiple Sclerosis (RRMS) in a Randomized, Double-blind, Phase 2b, Multicenter Study (S50.002). en. *Neurology* **88** (Apr. 2017).

147. Geldmacher, D., Fritsch, T., McClendon, M. & Landreth, G. Pioglitazone in early Parkinson's disease: a phase 2, multicentre, double-blind, randomised trial. English. *The Lancet Neurology* **14,** 795–803 (Aug. 2015).

148. Nisbett, K. E. & Pinna, G. Emerging Therapeutic Role of PPAR-a in Cognition and Emotions. eng. *Frontiers in Pharmacology* **9,** 998 (2018).

149. Lecarpentier, Y., Claes, V., Duthoit, G. & Hébert, J.-L. Circadian rhythms, Wnt/beta-catenin pathway and PPAR alpha/gamma profiles in diseases with primary or secondary cardiac dysfunction. eng. *Frontiers in Physiology* **5,** 429 (2014).

150. Kitamura, Y., Shimohama, S., Koike, H., Kakimura, J. i., Matsuoka, Y., Nomura, Y., Gebicke-Haerter, P. J. & Taniguchi, T. Increased expression of cyclooxygenases and peroxisome proliferator-activated receptor-gamma in Alzheimer's disease brains. eng. *Biochemical and Biophysical Research Communications* **254,** 582–586 (Jan. 1999).

151. De la Monte, S. M. & Wands, J. R. Molecular indices of oxidative stress and mitochondrial dysfunction occur early and often progress with severity of Alzheimer's disease. eng. *Journal of Alzheimer's disease: JAD* **9,** 167–181 (July 2006).

152. Vallée, A. & Lecarpentier, Y. Alzheimer Disease: Crosstalk between the Canonical Wnt/Beta-Catenin Pathway and PPARs Alpha and Gamma. *Frontiers in Neuroscience* **10,** 459 (2016).

153. Combs, C. K., Johnson, D. E., Karlo, J. C., Cannady, S. B. & Landreth, G. E. Inflammatory mechanisms in Alzheimer's disease: inhibition of beta-amyloid-stimulated proinflammatory responses and neurotoxicity by PPARgamma agonists. eng. *The Journal of Neuroscience: The Official Journal of the Society for Neuroscience* **20,** 558–567 (Jan. 2000).

154. Sastre, M., Dewachter, I., Landreth, G. E., Willson, T. M., Klockgether, T., van Leuven, F. & Heneka, M. T. Nonsteroidal anti-inflammatory drugs and peroxisome proliferator-activated receptor-gamma agonists modulate immunostimulated processing of amyloid precursor protein through regulation of beta-secretase. eng. *The Journal of Neuroscience: The Official Journal of the Society for Neuroscience* **23,** 9796–9804 (Oct. 2003).

155. Camacho, I. E., Serneels, L., Spittaels, K., Merchiers, P., Dominguez, D. & Strooper, B. D. Peroxisome Proliferator-Activated Receptor ? Induces a Clearance Mechanism for the Amyloid-ß Peptide. en. *Journal of Neuroscience* **24,** 10908–10917 (Dec. 2004).

156. d'Abramo, C., Massone, S., Zingg, J.-M., Pizzuti, A., Marambaud, P., Dalla Piccola, B., Azzi, A., Marinari, U. M., Pronzato, M. A. & Ricciarelli, R. Role of peroxisome proliferator-activated receptor gamma in amyloid precursor protein processing and amyloid beta-mediated cell death. eng. *The Biochemical Journal* **391,** 693–698 (Nov. 2005).

157. Escribano, L., Simón, A.-M., Gimeno, E., Cuadrado-Tejedor, M., López de Maturana, R., García-Osta, A., Ricobaraza, A., Pérez-Mediavilla, A., Del Río, J. & Frechilla, D. Rosiglitazone Rescues Memory Impairment in Alzheimer's Transgenic Mice: Mechanisms Involving a Reduced Amyloid and Tau Pathology. en. *Neuropsychopharmacology* **35,** 1593–1604 (June 2010).

158. Ning, L., Rui, X., Bo, W. & Qing, G. The critical roles of histone deacetylase 3 in the pathogenesis of solid organ injury. en. *Cell Death & Disease* **12,** 734 (July 2021).

159. Xu, H., Wu, M., Ma, X., Huang, W. & Xu, Y. Function and Mechanism of Novel Histone Posttranslational Modifications in Health and Disease. en. *BioMed Research International* **2021,** e6635225 (Mar. 2021).

160. Campos, E. I. & Reinberg, D. Histones: annotating chromatin. eng. *Annual Review of Genetics* **43,** 559–599 (2009).

161. Abel, T. & Zukin, R. S. Epigenetic targets of HDAC inhibition in neurodegenerative and psychiatric disorders. eng. *Current Opinion in Pharmacology* **8,** 57–64 (Feb. 2008).

162. Watson, P. J., Fairall, L., Santos, G. M. & Schwabe, J. W. R. Structure of HDAC3 bound to co-repressor and inositol tetraphosphate. en. *Nature* **481,** 335–340 (Jan. 2012).

163. Xiong, B., Lu, S. & Gerton, J. L. Hos1 is a lysine deacetylase for the Smc3 subunit of cohesin. eng. *Current biology: CB* **20,** 1660–1665 (Sept. 2010).

164. Schmitz, J., Watrin, E., Lénárt, P., Mechtler, K. & Peters, J.-M. Sororin is required for stable binding of cohesin to chromatin and for sister chromatid cohesion in interphase. eng. *Current biology: CB* **17,** 630–636 (Apr. 2007).

165. Wendt, K. S., Yoshida, K., Itoh, T., Bando, M., Koch, B., Schirghuber, E., Tsutsumi, S., Nagae, G., Ishihara, K., Mishiro, T., Yahata, K., Imamoto, F., Aburatani, H., Nakao, M., Imamoto, N., Maeshima, K., Shirahige, K. & Peters, J.-M. Cohesin mediates transcriptional insulation by CCCTC-binding factor. en. *Nature* **451,** 796–801 (Feb. 2008).

166. Wen, Y. D., Perissi, V., Staszewski, L. M., Yang, W. M., Krones, A., Glass, C. K., Rosenfeld, M. G. & Seto, E. The histone deacetylase-3 complex contains nuclear receptor corepressors. eng. *Proceedings of the National Academy of Sciences of the United States of America* **97,** 7202–7207 (June 2000).

167. Fischle, W., Dequiedt, F., Hendzel, M. J., Guenther, M. G., Lazar, M. A., Voelter, W. & Verdin, E. Enzymatic activity associated with class II HDACs is dependent on a multiprotein complex containing HDAC3 and SMRT/N-CoR. eng. *Molecular Cell* **9,** 45–57 (Jan. 2002).

168. Guenther, M. G., Barak, O. & Lazar, M. A. The SMRT and N-CoR corepressors are activating cofactors for histone deacetylase 3. eng. *Molecular and Cellular Biology* **21,** 6091–6101 (Sept. 2001).

169. Ferrari, A., Longo, R., Fiorino, E., Silva, R., Mitro, N., Cermenati, G., Gilardi, F., Desvergne, B., Andolfo, A., Magagnotti, C., Caruso, D., Fabiani, E. D., Hiebert, S. W. & Crestani, M. HDAC3 is a molecular brake of the metabolic switch supporting white adipose tissue browning. en. *Nature Communications* **8,** 93 (July 2017).

170. Hnilicová, J., Hozeifi, S., Dušková, E., Icha, J., Tománková, T. & Stanek, D. Histone Deacetylase Activity Modulates Alternative Splicing. *PLoS ONE* **6,** e16727 (Feb. 2011).

171. Khan, D. H., Gonzalez, C., Cooper, C., Sun, J.-M., Chen, H. Y., Healy, S., Xu, W., Smith, K. T., Workman, J. L., Leygue, E. & Davie, J. R. RNA-dependent dynamic histone acetylation regulates MCL1 alternative splicing. eng. *Nucleic Acids Research* **42,** 1656–1670 (Feb. 2014).

172. Koumbadinga, G. A., Mahmood, N., Lei, L., Kan, Y., Cao, W., Lobo, V. G., Yao, X., Zhang, S. & Xie, J. Increased stability of heterogeneous ribonucleoproteins by a deacetylase inhibitor. eng. *Biochimica Et Biophysica Acta* **1849,** 1095–1103 (Aug. 2015).

173. Khan, D. H., Gonzalez, C., Tailor, N., Hamedani, M. K., Leygue, E. & Davie, J. R. Dynamic Histone Acetylation of H3K4me3 Nucleosome Regulates MCL1 Pre-mRNA Splicing. eng. *Journal of Cellular Physiology* **231,** 2196–2204 (Oct. 2016).

174. Rahhal, R. & Seto, E. Emerging roles of histone modifications and HDACs in RNA splicing. *Nucleic Acids Research* **47,** 4911–4926 (June 2019).

175. Hahnen, E., Hauke, J., Tränkle, C., Eyüpoglu, I. Y., Wirth, B. & Blümcke, I. Histone deacetylase inhibitors: possible implications for neurodegenerative disorders. eng. *Expert Opinion on Investigational Drugs* **17,** 169–184 (Feb. 2008).

176. Rouaux, C., Jokic, N., Mbebi, C., Boutillier, S., Loeffler, J.-P. & Boutillier, A.-L. Critical loss of CBP/p300 histone acetylase activity by caspase-6 during neurodegeneration. *The EMBO Journal* **22,** 6537–6549 (Dec. 2003).

177. Jiang, H., Nucifora, F. C., Ross, C. A. & DeFranco, D. B. Cell death triggered by polyglutamine-expanded huntingtin in a neuronal cell line is associated with degradation of CREB-binding protein. eng. *Human Molecular Genetics* **12,** 1–12 (Jan. 2003).

178. Saha, R. N. & Pahan, K. HATs and HDACs in neurodegeneration: a tale of disconcerted acetylation homeostasis. en. *Cell Death & Differentiation* **13,** 539–550 (Apr. 2006).

179. Kim, H. J., Rowe, M., Ren, M., Hong, J.-S., Chen, P.-S. & Chuang, D.-M. Histone deacetylase inhibitors exhibit anti-inflammatory and neuroprotective effects in a rat permanent ischemic model of stroke: multiple mechanisms of action. eng. *The Journal of Pharmacology and Experimental Therapeutics* **321,** 892–901 (June 2007).

180. Sinn, D.-I., Kim, S.-J., Chu, K., Jung, K.-H., Lee, S.-T., Song, E.-C., Kim, J.-M., Park, D.-K., Kun Lee, S., Kim, M. & Roh, J.-K. Valproic acid-mediated neuroprotection in intracerebral hemorrhage via histone deacetylase inhibition and transcriptional activation. eng. *Neurobiology of Disease* **26,** 464–472 (May 2007).

181. Wu, X., Chen, P. S., Dallas, S., Wilson, B., Block, M. L., Wang, C.-C., Kinyamu, H., Lu, N., Gao, X., Leng, Y., Chuang, D.-M., Zhang, W., Lu, R. B. & Hong, J.-S. Histone deacetylase inhibitors up-regulate astrocyte GDNF and BDNF gene transcription and protect dopaminergic neurons. eng. *The International Journal of Neuropsychopharmacology* **11,** 1123–1134 (Dec. 2008).

182. Chen, P. S., Wang, C.-C., Bortner, C. D., Peng, G.-S., Wu, X., Pang, H., Lu, R.-B., Gean, P.-W., Chuang, D.-M. & Hong, J.-S. Valproic acid and other histone deacetylase inhibitors induce microglial apoptosis and attenuate lipopolysaccharide-induced dopaminergic neurotoxicity. eng. *Neuroscience* **149,** 203–212 (Oct. 2007).

183. Hao, Y., Creson, T., Zhang, L., Li, P., Du, F., Yuan, P., Gould, T. D., Manji, H. K. & Chen, G. Mood Stabilizer Valproate Promotes ERK Pathway-Dependent Cortical Neuronal Growth and Neurogenesis. en. *Journal of Neuroscience* **24,** 6590–6599 (July 2004).

184. Peleg, S., Sananbenesi, F., Zovoilis, A., Burkhardt, S., Bahari-Javan, S., Agis-Balboa, R. C., Cota, P., Wittnam, J. L., Gogol-Doering, A., Opitz, L., Salinas-Riester, G., Dettenhofer, M., Kang, H., Farinelli, L., Chen, W. & Fischer, A. Altered histone acetylation is associated with age-dependent memory impairment in mice. eng. *Science (New York, N.Y.)* **328,** 753–756 (May 2010).

185. Volmar, C.-H., Salah-Uddin, H., Janczura, K. J., Halley, P., Lambert, G., Wodrich, A., Manoah, S., Patel, N. H., Sartor, G. C., Mehta, N., Miles, N. T. H., Desse, S., Dorcius, D., Cameron, M. D., Brothers, S. P. & Wahlestedt, C. M344 promotes nonamyloidogenic amyloid precursor protein processing while normalizing Alzheimer's disease genes and improving memory. en. *Proceedings of the National Academy of Sciences* **114,** E9135–E9144 (Oct. 2017).

186. Francis, Y. I., Fà, M., Ashraf, H., Zhang, H., Staniszewski, A., Latchman, D. S. & Arancio, O. Dysregulation of histone acetylation in the APP/PS1 mouse model of Alzheimer's disease. eng. *Journal of Alzheimer's disease: JAD* **18,** 131–139 (2009).

187. Fan, S.-J., Huang, F.-I., Liou, J.-P. & Yang, C.-R. The novel histone deacetylase 6 inhibitor, MPT0G211, ameliorates tau phosphorylation and cognitive deficits in an Alzheimer's disease model. eng. *Cell Death & Disease* **9,** 655 (May 2018).

188. Ricobaraza, A., Cuadrado-Tejedor, M., Marco, S., Pérez-Otaño, I. & García-Osta, A. Phenylbutyrate rescues dendritic spine loss associated with memory deficits in a mouse model of Alzheimer disease. en. *Hippocampus* **22,** 1040–1050 (2012).

189. Green, K. N., Steffan, J. S., Martinez-Coria, H., Sun, X., Schreiber, S. S., Thompson, L. M. & LaFerla, F. M. Nicotinamide Restores Cognition in Alzheimer's Disease Transgenic Mice via a Mechanism Involving Sirtuin Inhibition and Selective Reduction of Thr231-Phosphotau. en. *Journal of Neuroscience* **28,** 11500–11510 (Nov. 2008).

190. Selenica, M.-L., Benner, L., Housley, S. B., Manchec, B., Lee, D. C., Nash, K. R., Kalin, J., Bergman, J. A., Kozikowski, A., Gordon, M. N. & Morgan, D. Histone deacetylase 6 inhibition improves memory and reduces total tau levels in a mouse model of tau deposition. eng. *Alzheimer's Research & Therapy* **6,** 12 (2014).

191. Su, Q., Li, T., He, P.-F., Lu, X.-C., Yu, Q., Gao, Q.-C., Wang, Z.-J., Wu, M.-N., Yang, D. & Qi, J.-S. Trichostatin A ameliorates Alzheimer's disease-related pathology and cognitive deficits by increasing albumin expression and Aß clearance in APP/PS1 mice. *Alzheimer's Research & Therapy* **13,** 7 (Jan. 2021).

192. Kerridge, C., Belyaev, N. D., Nalivaeva, N. N. & Turner, A. J. The Aß-clearance protein transthyretin, like neprilysin, is epigenetically regulated by the amyloid precursor protein intracellular domain. eng. *Journal of Neurochemistry* **130,** 419–431 (Aug. 2014).

193. Zhang, Z.-Y. & Schluesener, H. J. Oral administration of histone deacetylase inhibitor MS-275 ameliorates neuroinflammation and cerebral amyloidosis and improves behavior in a mouse model. eng. *Journal of Neuropathology and Experimental Neurology* **72,** 178–185 (Mar. 2013).

194. Qing, H., He, G., Ly, P. T. T., Fox, C. J., Staufenbiel, M., Cai, F., Zhang, Z., Wei, S., Sun, X., Chen, C.-H., Zhou, W., Wang, K. & Song, W. Valproic acid inhibits Abeta production, neuritic plaque formation, and behavioral deficits in Alzheimer's disease mouse models. eng. *The Journal of Experimental Medicine* **205,** 2781–2789 (Nov. 2008).

195. Hu, J.-P., Xie, J.-W., Wang, C.-Y., Wang, T., Wang, X., Wang, S.-L., Teng, W.-P. & Wang, Z.-Y. Valproate reduces tau phosphorylation via cyclin-dependent kinase 5 and glycogen synthase kinase 3 signaling pathways. eng. *Brain Research Bulletin* **85,** 194–200 (May 2011).

196. Ricobaraza, A., Cuadrado-Tejedor, M., Pérez-Mediavilla, A., Frechilla, D., Del Río, J. & García-Osta, A. Phenylbutyrate ameliorates cognitive deficit and reduces tau pathology in an Alzheimer's disease mouse model. eng. *Neuropsychopharmacology: Official Publication of the American College of Neuropsychopharmacology* **34,** 1721–1732 (June 2009).

197. Noack, M., Leyk, J. & Richter-Landsberg, C. HDAC6 inhibition results in tau acetylation and modulates tau phosphorylation and degradation in oligodendrocytes. en. *Glia* **62,** 535–547 (2014).

198. Jeong, H., Shin, S., Lee, J.-S., Lee, S. H., Baik, J.-H., Lim, S. & Kim, Y. K. Pan-HDAC Inhibitors Promote Tau Aggregation by Increasing the Level of Acetylated Tau. *International Journal of Molecular Sciences* **20,** 4283 (Sept. 2019).

199. Puzzo, D., Gulisano, W., Palmeri, A. & Arancio, O. Rodent models for Alzheimer's disease drug discovery. eng. *Expert Opinion on Drug Discovery* **10,** 703–711 (July 2015).

200. Onos, K. D., Sukoff Rizzo, S. J., Howell, G. R. & Sasner, M. Toward more predictive genetic mouse models of Alzheimer's disease. en. *Brain Research Bulletin* **122,** 1–11 (Apr. 2016).

201. Hashimoto, S., Matsuba, Y., Kamano, N., Mihira, N., Sahara, N., Takano, J., Muramatsu, S.-i., Saido, T. C. & Saito, T. Tau binding protein CAPON induces tau aggregation and neurodegeneration. en. *Nature Communications* **10,** 2394 (June 2019).

202. Saito, T., Mihira, N., Matsuba, Y., Sasaguri, H., Hashimoto, S., Narasimhan, S., Zhang, B., Murayama, S., Higuchi, M., Lee, V. M. Y., Trojanowski, J. Q. & Saido, T. C. Humanization of the entire murine Mapt gene provides a murine model of pathological human tau propagation. eng. *The Journal of Biological Chemistry* **294,** 12754–12765 (Aug. 2019).

203. Spillantini, M. G. & Goedert, M. Tau protein pathology in neurodegenerative diseases. eng. *Trends in Neurosciences* **21,** 428–433 (Oct. 1998).

204. Brion, J. P., Smith, C., Couck, A. M., Gallo, J. M. & Anderton, B. H. Developmental changes in tau phosphorylation: fetal tau is transiently phosphorylated in a manner similar to paired helical filament-tau characteristic of Alzheimer's disease. eng. *Journal of Neurochemistry* **61,** 2071–2080 (Dec. 1993).

205. Sperling, R. A., Aisen, P. S., Beckett, L. A., Bennett, D. A., Craft, S., Fagan, A. M., Iwatsubo, T., Jack, C. R., Kaye, J., Montine, T. J., Park, D. C., Reiman, E. M., Rowe, C. C., Siemers, E., Stern, Y., Yaffe, K., Carrillo, M. C., Thies, B., Morrison-Bogorad, M., Wagster, M. V. & Phelps, C. H. Toward defining the preclinical stages of Alzheimer's disease: recommendations from the National Institute on Aging-Alzheimer's Association workgroups on diagnostic guidelines for Alzheimer's disease. eng. *Alzheimer's & Dementia: The Journal of the Alzheimer's Association* **7,** 280–292 (May 2011).

206. Yamanaka, S. Strategies and New Developments in the Generation of Patient-Specific Pluripotent Stem Cells. English. *Cell Stem Cell* **1,** 39–49 (June 2007).

207. Takahashi, K., Tanabe, K., Ohnuki, M., Narita, M., Ichisaka, T., Tomoda, K. & Yamanaka, S. Induction of Pluripotent Stem Cells from Adult Human Fibroblasts by Defined Factors. English. *Cell* **131,** 861–872 (Nov. 2007).

208. Yu, J., Vodyanik, M. A., Smuga-Otto, K., Antosiewicz-Bourget, J., Frane, J. L., Tian, S., Nie, J., Jonsdottir, G. A., Ruotti, V., Stewart, R., Slukvin, I. I. & Thomson, J. A. Induced Pluripotent Stem Cell Lines Derived from Human Somatic Cells. en. *Science* **318,** 1917–1920 (Dec. 2007).

209. Bar-Nur, O., Russ, H. A., Efrat, S. & Benvenisty, N. Epigenetic Memory and Preferential Lineage-Specific Differentiation in Induced Pluripotent Stem Cells Derived from Human Pancreatic Islet Beta Cells. English. *Cell Stem Cell* **9,** 17–23 (July 2011).

210. Ohi, Y., Qin, H., Hong, C., Blouin, L., Polo, J. M., Guo, T., Qi, Z., Downey, S. L., Manos, P. D., Rossi, D. J., Yu, J., Hebrok, M., Hochedlinger, K., Costello, J. F., Song, J. S. & Ramalho-Santos, M. Incomplete DNA methylation underlies a transcriptional memory of somatic cells in human iPS cells. en. *Nature Cell Biology* **13,** 541–549 (May 2011).

211. Kim, K., Zhao, R., Doi, A., Ng, K., Unternaehrer, J., Cahan, P., Hongguang, H., Loh, Y.-H., Aryee, M. J., Lensch, M. W., Li, H., Collins, J. J., Feinberg, A. P. & Daley, G. Q. Donor cell type can influence the epigenome and differentiation potential of human induced pluripotent stem cells. en. *Nature Biotechnology* **29,** 1117–1119 (Dec. 2011).

212. Biswas, M. H. U., Almeida, S., Lopez-Gonzalez, R., Mao, W., Zhang, Z., Karydas, A., Geschwind, M. D., Biernat, J., Mandelkow, E.-M., Futai, K., Miller, B. L. & Gao, F.-B. MMP-9 and MMP-2 Contribute to Neuronal Cell Death in iPSC Models of Frontotemporal Dementia with MAPT Mutations. English. *Stem Cell Reports* **7,** 316–324 (Sept. 2016).

213. Hallmann, A.-L., Araúzo-Bravo, M. J., Mavrommatis, L., Ehrlich, M., Röpke, A., Brockhaus, J., Missler, M., Sterneckert, J., Schöler, H. R., Kuhlmann, T., Zaehres, H. & Hargus, G. Astrocyte pathology in a human neural stem cell model of frontotemporal dementia caused by mutant TAU protein. en. *Scientific Reports* **7,** 42991 (Mar. 2017).

214. Imamura, K., Sahara, N., Kanaan, N. M., Tsukita, K., Kondo, T., Kutoku, Y., Ohsawa, Y., Sunada, Y., Kawakami, K., Hotta, A., Yawata, S., Watanabe, D., Hasegawa, M., Trojanowski, J. Q., Lee, V. M.-Y., Suhara, T., Higuchi, M. & Inoue, H. Calcium dysregulation contributes to neurodegeneration in FTLD patient iPSC-derived neurons. *Scientific Reports* **6** (Oct. 2016).

215. Iovino, M., Agathou, S., González-Rueda, A., Del Castillo Velasco-Herrera, M., Borroni, B., Alberici, A., Lynch, T., O'Dowd, S., Geti, I., Gaffney, D., Vallier, L., Paulsen, O., Káradóttir, R. T. & Spillantini, M. G. Early maturation and distinct tau pathology in induced pluripotent stem cell-derived neurons from patients with MAPT mutations. *Brain* **138,** 3345–3359 (Nov. 2015).

216. Sato, C., Barthélemy, N. R., Mawuenyega, K. G., Patterson, B. W., Gordon, B. A., Jockel-Balsarotti, J., Sullivan, M., Crisp, M. J., Kasten, T., Kirmess, K. M., Kanaan, N. M., Yarasheski, K. E., Baker-Nigh, A., Benzinger, T. L. S., Miller, T. M., Karch, C. M. & Bateman, R. J. Tau Kinetics in Neurons and the Human Central Nervous System. English. *Neuron* **98,** 861–864 (May 2018).

217. Silva, M. C., Cheng, C., Mair, W., Almeida, S., Fong, H., Biswas, M. H. U., Zhang, Z., Huang, Y., Temple, S., Coppola, G., Geschwind, D. H., Karydas, A., Miller, B. L., Kosik, K. S., Gao, F.-B., Steen, J. A. & Haggarty, S. J. Human iPSC-Derived Neuronal Model of Tau-A152T Frontotemporal Dementia Reveals Tau-Mediated Mechanisms of Neuronal Vulnerability. *Stem Cell Reports* **7,** 325–340 (Sept. 2016).

218. Verheyen, A., Diels, A., Reumers, J., Hoorde, K. V., den Wyngaert, I. V., van Outryve d'Ydewalle, C., Bondt, A. D., Kuijlaars, J., Muynck, L. D., Hoogt, R. D., Bretteville, A., Jaensch, S., Buist, A., Cabrera-Socorro, A., Wray, S., Ebneth, A., Roevens, P., Royaux, I. & Peeters, P. J. Genetically Engineered iPSC-Derived FTDP-17 MAPT Neurons Display Mutation-Specific Neurodegenerative and Neurodevelopmental Phenotypes. *Stem Cell Reports* **11,** 363–379 (Aug. 2018).

219. Verheyen, A., Diels, A., Dijkmans, J., Oyelami, T., Meneghello, G., Mertens, L., Versweyveld, S., Borgers, M., Buist, A., Peeters, P. & Cik, M. Using Human iPSC-Derived Neurons to Model TAU Aggregation. en. *PLOS ONE* **10,** e0146127 (Dec. 2015).

220. Sposito, T., Preza, E., Mahoney, C. J., Seto-Salvia, N., Ryan, N. S., Morris, H. R., Arber, C., Devine, M. J., Houlden, H., Warner, T. T., Bushell, T. J., Zagnoni, M., Kunath, T., Livesey, F. J., Fox, N. C., Rossor, M. N., Hardy, J. & Wray, S. Developmental regulation of tau splicing is disrupted in stem cell-derived neurons from frontotemporal dementia patients with the 10+16 splice-site mutation in MAPT. *Human Molecular Genetics* **24,** 5260–5269 (July 2015).

221. Ehrlich, M., Hallmann, A.-L., Reinhardt, P., Araúzo-Bravo, M. J., Korr, S., Röpke, A., Psathaki, O. E., Ehling, P., Meuth, S. G., Oblak, A. L., Murrell, J. R., Ghetti, B., Zaehres, H., Schöler, H. R., Sterneckert, J., Kuhlmann, T. & Hargus, G. Distinct Neurodegenerative Changes in an Induced Pluripotent Stem Cell Model of Frontotemporal Dementia Linked to Mutant TAU Protein. English. *Stem Cell Reports* **5,** 83–96 (July 2015).

222. Femino, A. M. Visualization of Single RNA Transcripts in Situ. *Science* **280,** 585–590 (Apr. 1998).

223. Raj, A., van den Bogaard, P., Rifkin, S. A., van Oudenaarden, A. & Tyagi, S. Imaging individual mRNA molecules using multiple singly labeled probes. *Nature Methods* **5,** 877–879 (Sept. 2008).

224. Katz, Y., Wang, E. T., Airoldi, E. M. & Burge, C. B. Analysis and design of RNA sequencing experiments for identifying isoform regulation. *Nature Methods* **7,** 1009–1015 (Nov. 2010).

225. Matsufuji, S., Matsufuji, T., Miyazaki, Y., Murakami, Y., Atkins, J. F., Gesteland, R. F. & Hayashi, S.-i. Autoregulatory frameshifting in decoding mammalian ornithine decarboxylase antizyme. *Cell* **80,** 51–60 (Jan. 1995).

226. Anderson, P. & Kedersha, N. RNA granules. *Journal of Cell Biology* **172,** 803–808 (Mar. 2006).

227. Baser, A., Skabkin, M., Kleber, S., Dang, Y., Balta, G. S. G., Kalamakis, G., Göpferich, M., Ibanez, D. C., Schefzik, R., Lopez, A. S., Bobadilla, E. L., Schultz, C., Fischer, B. & Martin-Villalba, A. Onset of differentiation is post-transcriptionally controlled in adult neural stem cells. *Nature* **566,** 100–104 (Jan. 2019).

228. O'Brien, J., Hayder, H., Zayed, Y. & Peng, C. Overview of MicroRNA Biogenesis, Mechanisms of Actions, and Circulation. *Frontiers in Endocrinology* **9** (Aug. 2018).

229. Lastella, P., Surdo, N. C., Resta, N., Guanti, G. & Stella, A. In silico and in vivo splicing analysis of MLH1 and MSH2 missense mutations shows exon- and tissue-specific effects. *BMC Genomics* **7** (Sept. 2006).

230. Baralle, M., Skoko, N., Knezevich, A., Conti, L. D., Motti, D., Bhuvanagiri, M., Baralle, D., Buratti, E. & Baralle, F. E. NF1mRNA biogenesis: Effect of the genomic milieu in splicing regulation of the NF1 exon 37 region. *FEBS Letters* **580,** 4449–4456 (July 2006).

231. Hsieh, Y.-C., Guo, C., Yalamanchili, H. K., Abreha, M., Al-Ouran, R., Li, Y., Dammer, E. B., Lah, J. J., Levey, A. I., Bennett, D. A., Jager, P. L. D., Seyfried, N. T., Liu, Z. & Shulman, J. M. Tau-Mediated Disruption of the Spliceosome Triggers Cryptic RNA Splicing and Neurodegeneration in Alzheimer's Disease. *Cell Reports* **29,** 301–316.e10 (Oct. 2019).

232. England, C. G., Ehlerding, E. B. & Cai, W. NanoLuc: A Small Luciferase is Brightening up the Field of Bioluminescence. *Bioconjugate chemistry* **27,** 1175–1187. ISSN: 1043-1802. `https://www.ncbi.nlm.nih.gov/pmc/articles/PMC4871753/` (2022) (May 2016).

233. Hall, M. P., Unch, J., Binkowski, B. F., Valley, M. P., Butler, B. L., Wood, M. G., Otto, P., Zimmerman, K., Vidugiris, G., Machleidt, T., Robers, M. B., Benink, H. A., Eggers, C. T., Slater, M. R., Meisenheimer, P. L., Klaubert, D. H., Fan, F., Encell, L. P. & Wood, K. V. Engineered luciferase reporter from a deep sea shrimp utilizing a novel imidazopyrazinone substrate. eng. *ACS chemical biology* **7,** 1848–1857. ISSN: 1554-8937 (Nov. 2012).

234. Aranko, A. S., Wlodawer, A. & Iwai, H. Nature's recipe for splitting inteins. *Protein Engineering Design and Selection* **27,** 263–271 (Aug. 2014).

235. Carvajal-Vallejos, P., Pallissè, R., Mootz, H. D. & Schmidt, S. R. Unprecedented Rates and Efficiencies Revealed for New Natural Split Inteins from Metagenomic Sources. *Journal of Biological Chemistry* **287,** 28686–28696 (Aug. 2012).

236. Shah, N. H. & Muir, T. W. Inteins: Nature's Gift to Protein Chemists. *Chemical science (Royal Society of Chemistry : 2010)* **5,** 446–461 (2014).

237. Yamazaki, T., Otomo, T., Oda, N., Kyogoku, Y., Uegaki, K., Ito, N., Ishino, Y. & Nakamura, H. Segmental Isotope Labeling for Protein NMR Using Peptide Splicing. *Journal of the American Chemical Society* **120,** 5591–5592 (June 1998).

238. Li, J., Sun, W., Wang, B., Xiao, X. & Liu, X.-Q. Protein trans-splicing as a means for viral vector-mediated in vivo gene therapy. eng. *Human Gene Therapy* **19,** 958–964 (Sept. 2008).

239. Ozawa, T., Takeuchi, M., Kaihara, A., Sato, M. & Umezawa, Y. Protein Splicing-Based Reconstitution of Split Green Fluorescent Protein for Monitoring Protein-Protein Interactions in Bacteria: Improved Sensitivity and Reduced Screening Time. *Analytical Chemistry* **73,** 5866–5874 (Dec. 2001).

240. Ozawa, T., Kaihara, A., Sato, M., Tachihara, K. & Umezawa, Y. Split Luciferase as an Optical Probe for Detecting Protein-Protein Interactions in Mammalian Cells Based on Protein Splicing. *Analytical Chemistry* **73,** 2516–2521 (June 2001).

241. Tan, L. P. & Yao, S. Q. Intein-mediated, in vitro and in vivo protein modifications with small molecules. eng. *Protein and Peptide Letters* **12,** 769–775 (Nov. 2005).

242. Stoilov, P., Lin, C.-H., Damoiseaux, R., Nikolic, J. & Black, D. L. A high-throughput screening strategy identifies cardiotonic steroids as alternative splicing modulators. en. *Proceedings of the National Academy of Sciences* **105,** 11218–11223 (Aug. 2008).

243. Overall, R. W. & Kempermann, G. The Small World of Adult Hippocampal Neurogenesis. *Frontiers in Neuroscience* **12** (Sept. 2018).

244. Sennvik, K., Boekhoorn, K., Lasrado, R., Terwel, D., Verhaeghe, S., Korr, H., Schmitz, C., Tomiyama, T., Mori, H., Krugers, H., Joels, M., Ramakers, G. J. A., Lucassen, P. J. & Van Leuven, F. Tau-4R suppresses proliferation and promotes neuronal differentiation in the hippocampus of tau knockin/knockout mice. eng. *FASEB journal: official publication of the Federation of American Societies for Experimental Biology* **21,** 2149–2161 (July 2007).

245. Dawson, H., Ferreira, A., Eyster, M., Ghoshal, N., Binder, L. & Vitek, M. Inhibition of neuronal maturation in primary hippocampal neurons from tau deficient mice. *Journal of Cell Science* **114,** 1179–1187 (Mar. 2001).

246. Fiock, K. L., Smalley, M. E., Crary, J. F., Pasca, A. M. & Hefti, M. M. Increased Tau Expression Correlates with Neuronal Maturation in the Developing Human Cerebral Cortex. *eneuro* **7,** ENEURO.0058–20.2020 (May 2020).

247. Kopach, O., Esteras, N., Wray, S., Rusakov, D. A. & Abramov, A. Y. Maturation and phenotype of pathophysiological neuronal excitability of human cells in tau-related dementia. *Journal of Cell Science* **133** (May 2020).

248. Ueki, N., Lee, S., Sampson, N. S. & Hayman, M. J. Selective cancer targeting with prodrugs activated by histone deacetylases and a tumour-associated protease. eng. *Nature Communications* **4,** 2735 (2013).

249. Wilson, P. M., Labonte, M. J., Martin, S. C., Kuwahara, S. T., El-Khoueiry, A., Lenz, H.-J. & Ladner, R. D. Sustained inhibition of deacetylases is required for the antitumor activity of the histone deactylase inhibitors panobinostat and vorinostat in models of colorectal cancer. eng. *Investigational New Drugs* **31,** 845–857 (Aug. 2013).

250. Chen, X., Xiao, W., Chen, W., Luo, L., Ye, S. & Liu, Y. The epigenetic modifier trichostatin A, a histone deacetylase inhibitor, suppresses proliferation and epithelial-mesenchymal transition of lens epithelial cells. eng. *Cell Death and Disease* **4,** e884 (Oct. 2013).

251. Scheff, S. W., Price, D. A., Schmitt, F. A., DeKosky, S. T. & Mufson, E. J. Synaptic alterations in CA1 in mild Alzheimer disease and mild cognitive impairment. *Neurology* **68,** 1501–1508 (Apr. 2007).

252. Scheff, S. W., Price, D. A., Schmitt, F. A. & Mufson, E. J. Hippocampal synaptic loss in early Alzheimer's disease and mild cognitive impairment. *Neurobiology of Aging* **27,** 1372–1384 (Oct. 2006).

253. Tripathi, T. & Khan, H. Direct Interaction between the beta-Amyloid Core and Tau Facilitates Cross-Seeding: A Novel Target for Therapeutic Intervention. *Biochemistry* **59,** 341–342 (Jan. 2020).

254. Mignon, L., Kordasiewicz, H., Lane, R., Smith, A., Miller, T., Narayanan, P., Swayze, E., Norris, D., Fitzsimmons, B. & Bennett, F. Design of the First-in-Human Study of IONIS-MAPTRx, a Tau-lowering Antisense Oligonucleotide, in Patients With Alzheimer Disease (S2.006). en. *Neurology* **90** (Apr. 2018).

255. Schoch, K. M., DeVos, S. L., Miller, R. L., Chun, S. J., Norrbom, M., Wozniak, D. F., Dawson, H. N., Bennett, C. F., Rigo, F. & Miller, T. M. Increased 4R-Tau Induces Pathological Changes in a Human-Tau Mouse Model. English. *Neuron* **90,** 941–947 (June 2016).

256. Kim, D.-J., Oh, B. & Kim, Y.-Y. Splicing factor ASF/SF2 and transcription factor PPAR-γ cooperate to directly regulate transcription of uncoupling protein-3. *Biochemical and Biophysical Research Communications* **378,** 877–882 (Jan. 2009).

257. Okazaki, M., Iwasaki, Y., Nishiyama, M., Taguchi, T., Tsugita, M., Nakayama, S., Kambayashi, M., Hashimoto, K. & Terada, Y. PPARβ/δ regulates the human SIRT1 gene transcription via Sp1. eng. *Endocrine Journal* **57,** 403–413 (2010).

258. Bolster, D. R., Crozier, S. J., Kimball, S. R. & Jefferson, L. S. AMP-activated Protein Kinase Suppresses Protein Synthesis in Rat Skeletal Muscle through Down-regulated Mammalian Target of Rapamycin (mTOR) Signaling. *Journal of Biological Chemistry* **277,** 23977–23980 (July 2002).

259. Senga, S., Kawaguchi, K., Kobayashi, N., Ando, A. & Fujii, H. A novel fatty acid-binding protein 5-estrogen-related receptor α signaling pathway promotes cell growth and energy metabolism in prostate cancer cells. *Oncotarget* **9,** 31753–31770 (Aug. 2018).

260. Gwinn, D. M., Shackelford, D. B., Egan, D. F., Mihaylova, M. M., Mery, A., Vasquez, D. S., Turk, B. E. & Shaw, R. J. AMPK Phosphorylation of Raptor Mediates a Metabolic Checkpoint. English. *Molecular Cell* **30,** 214–226 (Apr. 2008).

261. Seo, J., Jeong, D.-W., Park, J.-W., Lee, K.-W., Fukuda, J. & Chun, Y.-S. Fatty-acid-induced FABP5/HIF-1 reprograms lipid metabolism and enhances the proliferation of liver cancer cells. en. *Communications Biology* **3,** 1–14 (Oct. 2020).

262. Pfaffl, M. W., Tichopad, A., Prgomet, C. & Neuvians, T. P. Determination of stable housekeeping genes, differentially regulated target genes and sample integrity: BestKeeper – Excel-based tool using pair-wise correlations. *Biotechnology Letters* **26,** 509–515 (Mar. 2004).

263. Reinhardt, P., Glatza, M., Hemmer, K., Tsytsyura, Y., Thiel, C. S., Höing, S., Moritz, S., Parga, J. A., Wagner, L., Bruder, J. M., Wu, G., Schmid, B., Röpke, A., Klingauf, J., Schwamborn, J. C., Gasser, T., Schöler, H. R. & Sterneckert, J. Derivation and Expansion Using Only Small Molecules of Human Neural Progenitors for Neurodegenerative Disease Modeling. *PLoS ONE* **8** (ed Daadi, M.) e59252 (Mar. 2013).

264. Qian, X., Jacob, F., Song, M. M., Nguyen, H. N., Song, H. & Ming, G.-l. Generation of human brain region: specific organoids using a miniaturized spinning bioreactor. *Nature Protocols* **13,** 565–580 (Feb. 2018).

265. Iversen, P. W., Eastwood, B. J., Sittampalam, G. S. & Cox, K. L. A Comparison of Assay Performance Measures in Screening Assays: Signal Window, Z' Factor, and Assay Variability Ratio. *Journal of Biomolecular Screening* **11,** 247–252 (Feb. 2006).

266. Coussens, N. P. *et al.* Assay Guidance Manual : Quantitative Biology and Pharmacology in Preclinical Drug Discovery. *Clinical and Translational Science* **11,** 461–470 (June 2018).

267. Kuhn, M., von Mering, C., Campillos, M., Jensen, L. J. & Bork, P. STITCH: interaction networks of chemicals and proteins. *Nucleic Acids Research* **36,** D684–D688 (Jan. 2008).

Acknowledgements

Als Erstes möchte ich mir die Zeit nehmen meinem Doktorvater **Prof. Dr. Wolfgang Wurst** zu danken. Vielen Dank für die Aufnahme in deine Arbeitsgruppe und die Möglichkeit meine Doktorarbeit in dieser zu absolvieren. Danke auch, für deine Unterstützung in den kritischen Phasen der Doktorarbeit.

Meiner Prüfungskommission, **Prof. Dr. Angelika Schnieke** als Vorsitz, Prof. Dr. Wolfgang Wurst, sowie **Prof. Dr. Henriette Uhlenhaut** als Prüfer, möchte ich auch meinen Dank aussprechen.

Einen besonderen Dank möchte ich meinem Gruppenleiter **Dr. Florian Giesert** aussprechen. Ich schätze sehr mit wie viel Rat und Tat du mir bei den Höhen und Tiefen meiner Doktorarbeit beigestanden hast. Dein Humor und die Leichtigkeit haben auch die anspruchsvollen Zeiten mit Motivation gefüllt. Dabei wurde auch noch die größte gedachte Krise mit einer guten Portion Humor wieder in meinem Kopf gelindert. Dafür möchte ich dir hiermit nochmal ausdrücklich danken. Zusammenfassend: Vier Jahre, vier Jahre gefüllt von Erfolg, Krisen, Humor und Frust, fügen sich zusammen in 157 Seiten, wer hätte es gedacht: Was lange währt, wird endlich gut!

Dank möchte ich auch gegenüber meinen Thesis Committee Mitgliedern **Dr. Sigrid Schwarz** und **Prof. Dr. Konstanze Winklhofer** aussprechen. Die konstruktiven Ideen und motivierenden Worte haben die Richtung meiner Doktorarbeit ein gutes Stück gelenkt und auch drei Themenwechsel mit einem roten Faden versehen.

Dr. Dong-Juinn Jeffery Truong, danke, dass du mir auch grade in den Anfängen meiner Doktorarbeit eine große Hilfe warst. Ob bei der Etablierung des EXSISERS, oder deine Meinung zu bestimmten Resultaten, wenn ich nicht mehr wusste wo oben und unten ist. Danke! Ich räume hiermit ein, dass mein hiPSC-Zellkultur Advertisement noch Optimierung benötigt!

Dietrich Trümbach möchte ich auf diesem Wege meinen Dank aussprechen für die Durchführung der bioinformatischen Analysen, die ein großes Stück zur Interpretation meiner Screeningdaten beigetragen haben. Vielen Dank für deine Hilfsbereitschaft.

Der ganzen **Arbeitsgruppe Wurst** möchte ich für vier Jahre danken. Danke für jeden einzelnen von euch, der seinen Teil zur Arbeitsatmosphäre und zur Fertigstellung dieser Doktorarbeit beigetragen hat. Meine Zeit der Doktorarbeit in dieser Arbeitsgruppe zu absolvieren hat mir, wegen euch, viele schöne Momente bereitet. Ich möchte mir jedoch Zeit nehmen im Folgenden, manchen einen gesonderten Dank auszusprechen.

Die vielen Stunden in der Stammzellkultur wären undenkbar gewesen ohne dich, **Tanja Orschmann**. Ich möchte mich hier ganz ausdrücklich bei dir bedanken. Mit dir zusammen die Zellkultur und den kompletten Flur mit Musik zu beschallen, ob Disney Soundtracks oder Heavy Metal, ganz nach Laune, hat die Arbeit um Einiges bereichert. Vielen Dank für

deine ausdauernde Unterstützung bei der Versorgung der Zellen, deine immerwährende Hilfsbereitschaft, deine Aufmerksamkeit, wenn Not an der Frau war, oder ich endlich mal was essen sollte, wenn ich 8 Stunden ununterbrochen die Gänge lang wuselte für meine großen Screens. Einfach Danke!

Was wäre das Labor ohne unsere **Annerose Kurz-Drexler**. Vielen Dank, dass du so bist wie du bist, ob für den persönlichen Rat, den Ankerpunkt, für jedwede relevante Frage im Labor oder unsere gemeinsamen Fluchereien über nicht funktionierende Western Blots. Ich werde es vermissen und schätze die Zusammenarbeit mit dir sehr. Vielen Dank für die kleinen und großen Motivationsschübe, deine unendliche Hilfsbereitschaft, Positivität und die große Portion Menschlichkeit, die den Arbeitsalltag und das Durchhalten in der Doktorarbeit maßgeblich unterstützt haben.

Denise Herold möchte ich auf diesem Wege auch meinen Dank aussprechen, die grade in den letzten Zügen meiner Doktorarbeit eine große Hilfe war. Danke möchte ich dir aber ebenfalls sagen, für die Arbeitsatmosphäre die du geschaffen hast, die den Arbeitsalltag, die funktionierenden und nicht funktionierenden Genotypisierungen und alles drumherum mit viel Lachen und Humor ausgeschmückt haben.

Gefunden in den ersten Tagen der Doktorarbeit, kann ich mir die letzten vier Jahre nicht ohne uns vorstellen. Wir haben es geschafft! Danke, dass aus dem Büro Gewürfel solch eine Freundschaft entstanden ist. Vielen Dank für die gemeinsam durchlebten Höhen und Tiefen, ob im Labor oder im Privaten, **Kristina Niedermeier**. Unendlichen Dank für die vielen humorvollen Stunden, vermehrt in unserem zweiten Wohnzimmer, in denen wir uns gegenseitig motiviert haben, oder auch einfach mal den Frust rauslassen durften, wenn der Labor-Voodoo mal wieder gegen uns zu arbeiten schien. Unser gemeinsamer Dank darf da wohl an die Motivase ausgesprochen werden - Möge dies die Schokolade oder auch das Koffein gewesen sein. Daher bleibt zum Schluss nur noch eine Frage: "Coffee?!"

Ich möchte mir hier auch ausgiebig Zeit nehmen, um meinen **Freunden** einen allumfassenden Dank auszusprechen. Mit Worten ist die Unterstützung, die ich durch euch erfahren habe, nicht zu beschreiben. Einfach nur ein riesengroßes Danke, jeder einzelne von euch ist einfach wundervoll! Ob beim Bouldern, um mein Hintern aus der Zellkultur zu bekommen, ob bei der Motivation für die letzten Züge im Schreibmarathon, bei denen wir uns all zu oft fragten, ob es nicht besser *Confusion and Outlook* heißen sollte, den Wanderungen für den Schwung frische Luft, oder den eindringlichen Stimmen, die meinen Perfektionismus und meinen Willen fünf Meisterwerke gleichzeitig zu erbauen zähmten, ihr habt einen großen Teil zum Gelingen beigetragen! Ein ganz großes Danke, ihr seid Gold wert.

"Alleine!", oder vielleicht doch nicht? - Einen riesengroßen Dank möchte ich meiner **Familie** aussprechen, dafür, dass sie mir immer mit Vertrauen und Zuspruch unterstützend zur Seite stand. Worte beschreiben das Maß nur unzureichend. Danke, dass ihr mir auch geholfen habt, wenn ich den Stein selbst zum Erklimmen auserkoren habe und der Weg auch leichter hätte sein können. Angenommene kurvige Linie haben wir mit viel Kraft, Zuspruch und Anstrengung zu einer Geraden geformt. Danke für eure ausdauernde Kraft! Mit Höhe und Tiefen habt ihr stets drauf vertraut, dass ich schon weiß, welchen Kampf ich kämpfen mag. Ein ausgesprochen großes Dankeschön an euch alle, für den immensen Rückhalt den ihr mir über die Jahre geboten

habt, welche mir die irrwitzigsten Ideen, die mir in den Kopf kamen, ermöglichten. Ihr seid einfach wundervoll! - "Zusammen!"

Mischief managed!

Affidavit

Ich, Bianca Eßwein, erkläre an Eides statt, dass ich die bei der promotionsführenden Einrichtung Fakultät Wissenschaftszentrum Weihenstephan für Ernährung, Landnutzung und Umwelt der Technischen Universität München zur Promotionsprüfung vorgelegte Arbeit mit dem Titel: "*MAPT* exon 10 alternative splicing modulation in an hiPSC *MAPT*$^{\text{EXSISERS}}$ model" unter der Anleitung und Betreuung durch Herrn Professor Dr. Wolfgang Wurst ohne sonstige Hilfe erstellt und bei der Abfassung nur die gemäß § 6 Abs. 6 und 7 Satz 2 angegebenen Hilfsmittel benutzt habe. Ich habe keine Organisation eingeschaltet, die gegen Entgelt Betreuerinnen und Betreuer für die Anfertigung von Dissertationen sucht, oder die mir obliegenden Pflichten hinsichtlich der Prüfungsleistungen für mich ganz oder teilweise erledigt. Ich habe die Dissertation in dieser oder ähnlicher Form in keinem anderen Prüfungsverfahren als Prüfungsleistung vorgelegt. Teile der Dissertation wurden in *Nature Cell Biology* veröffentlicht.
Ich habe den angestrebten Doktorgrad noch nicht erworben und bin nicht in einem früheren Promotionsverfahren für den angestrebten Doktorgrad endgültig gescheitert. Ich habe keine Kenntnis über ein strafrechtliches Ermittlungsverfahren in Bezug auf wissenschaftsbezogene Straftaten gegen mich oder eine rechtskräftige strafrechtliche Verurteilung mit Wissenschaftsbezug.
Die öffentlich zugängliche Promotionsordnung der Technischen Universität Münchens ist mir bekannt, insbesondere habe ich die Bedeutung von § 27 PromO (Nichtigkeit der Promotion) und § 28 PromO (Entzug des Doktorgrades) zur Kenntnis genommen. Ich bin mir der Konsequenzen einer falschen Eidesstattlichen Erklärung bewusst.
Mit der Aufnahme meiner personenbezogenen Daten in die Alumni-Datei bei der Technischen Universität Münchens bin ich einverstanden.

Bianca Eßwein

Ort, Datum